

**A PALEOCLIMATIC AND PALEOHYDROLOGIC RECONSTRUCTION OF
PLEISTOCENE FOSSIL LAKE, OREGON**

By

© 2010

Julie Beth Retrum

B.A., University of Minnesota Morris, 2001

M.S., The University of Kansas, 2004

Submitted to the Department of Geology
and the Faculty of the Graduate School of The University of Kansas
in partial fulfillment of the requirements for the degree of
Doctor of Philosophy

Luis A González, Co-Chair

Stephen T. Hasiotis, Co-Chair

William C. Johnson

Jennifer A. Roberts

Gregory A. Ludvigson

Date Submitted: _____

The dissertation committee for Julie Beth Retrum certifies
that this is the approved version of the following dissertation:

**A PALEOCLIMATIC AND PALEOHYDROLOGIC RECONSTRUCTION OF
PLEISTOCENE FOSSIL LAKE, OREGON**

Committee:

Luis A González, Co-Chair

Stephen T. Hasiotis, Co-Chair

William C. Johnson

Jennifer A. Roberts

Gregory A. Ludvigson

Date Submitted: _____

ABSTRACT

Julie B. Retrum, Ph.D.
Department of Geology, September 2010
University of Kansas

Fossil Lake, Oregon, is a Pleistocene lacustrine basin (~ 650–13 ka) in the northwestern part of the Great Basin best known for its abundant and diverse vertebrate assemblage. Multi-proxy studies using lithostratigraphy, fossil ostracode faunal assemblages, and ostracode stable isotope geochemistry from cores taken at Fossil Lake record changes in paleoenvironment, paleoclimate, and paleohydrochemistry. From lithostratigraphic analysis, the depositional sequence was subdivided into eight lithosomes composed of fining-upward sequences, bounded by unconformities, indicating that the lake underwent several lake-level excursions. The two oldest lithosomes, ~ 646–610 ka, record deep lake environments deposited during wet conditions and correspond to marine oxygen isotope stages (MIS) 16 and 15. A major unconformity from ~ 610 ka until ~ 71 ka interrupts the record. Lithosomes III and IV, ~ 71–47 ka, were deposited during wet conditions that produced cool to cold, deep, alkaline lakes that were fresh to slightly saline and corresponds to MIS 4 and 3, respectively. Lithosome IV also records a short period of drier conditions with decreased lake level and increased methanogenesis rates that produced highly enriched $\delta^{13}\text{C}$ values in ostracodes. Lithosome V, VI, and VII, ~ 47–28 ka, were deposited during dry conditions that produced cold, shallow, alkaline lakes and correspond to MIS 3. Salinities ranged from saline to slightly saline in Lithosomes V and VI to relatively fresh in Lithosome VII. Wet conditions return abruptly in Lithosome VIII (~ 15 ka) that records a deep, cold lake environment and corresponds to MIS 2.

The repetitive cycles of flooding, lake stand, and desiccation indicates that Fossil Lake was highly susceptible to changes in precipitation and evaporation ratios, suggesting that climate forcing played a major role in the lake-level fluctuations. Over all, high and very high stands coincide with glacial cycles in MIS 16, 4, and 2.

DEDICATION

This dissertation is dedicated to Roger L. Kaesler, who taught me to never give up on my dreams and who gave me the opportunity, experience, and push I needed to fulfill those dreams.

ACKNOWLEDGMENTS

This research was not possible without the support, encouragement, and generosity of many people and institutions. I owe my biggest thanks to my three dissertation advisors, Roger Kaesler, whose support and belief in me was so great that he allowed me to design my own dissertation project, and Luis González and Steve Hasiotis, who without hesitation accepted me into their lab groups halfway through my dissertation and gave me endless amounts of time, support, guidance, encouragement, and advise. I must also thank Bill Johnson, whom I consider as my unofficial advisor, for access to his field and lab equipment that made much of this research possible and for his support, help, and guidance. I am especially grateful to each of these people for their patience, friendship, dedication, and the opportunity to work and learn from each of them. I owe a special thanks to James Martin for giving me the opportunity to work and learn from him while conducting fieldwork at Fossil Lake, providing me with samples, and assisting me with my fieldwork and research questions.

I would also like to thank many people for their assistance with fieldwork, equipment, samples, and data interpretations. I would like to thank Jon Smith for assistance with coring in the field, Greg Cane for assistance with stable isotope analyses, Alison Smith and James Van Alstine for assistance with ostracode identification, Lisa Park for assistance with general ostracode and ostracode taphonomic interpretations and for allowing me to spend a week working in her lab, Christoph Geiss for assistance with environmental magnetism interpretations, Stephen Kuehn for assistance with tephra samples, Tony Walton for assistance with zeolitic samples, Daniel Hirmas for assistance with soil samples, Mark Bowen for assistance with grain size analyses, and Michael Hillix and Cynthia Blanton for assistance with lab work. A special

thanks to my committee members, Jennifer Roberts, Edith Taylor, and Greg Ludvigson, who provided support and guidance and made improvements to my dissertation.

Lastly, I want to thank my family and friends. I big thank you to my parents and brother who have provided endless support and encouragement through the years and never complained when I had to miss family events. I also want to thank all my friends for offering encouragement and providing assistance, especially fellow graduate students Pete Schillig, Brian Platt, Jon Smith, Kim Metevier, Celina Suarez, Marina Suarez, April French, Cori Meyers, Erin Saupe-Finley, Wes Gapp, Karla Leslie, Arne Sturm, and Ezra Kulczycki.

This research was made possible by funding from Geological Society of America Student Research Grant, Sigma Xi Grants-in-Aid of Research, North American Micropaleontology Section Garry Jones Memorial Grant, University of Kansas Leaman Harris Award, University of Kansas Department of Geology, United States Bureau of Land Management, and the Institute of Rock Magnetism at the University of Minnesota.

TABLE OF CONTENTS

Abstract	iii
Dedication	v
Acknowledgments	vi
Chapter 1: Fossil Lake Introduction	1
Significance.....	2
Geologic Setting.....	3
References.....	5
Chapter 2: Depositional History of Fossil Lake from Lithostratigraphy and Magnetic Susceptibility Analysis	12
Introduction.....	12
Methods.....	12
Results.....	14
<i>Lithosome I (Unit 1)</i>	15
<i>Lithosome II (Units 2–4)</i>	15
<i>Lithosome III (Units 5–6)</i>	16
<i>Lithosome IV (Units 7–8)</i>	17
<i>Lithosome V (Units 9–10)</i>	18
<i>Lithosome VI (Units 11–12)</i>	18
<i>Lithosome VII (Units 13–14)</i>	19
<i>Lithosome VIII (Units 15–17)</i>	20
Discussion.....	20
Regional Comparison.....	25

Conclusions.....	27
References.....	28
Chapter 3: Fossil Lake Ostracode Faunal Assemblages	48
Introduction.....	48
Methods.....	49
Results.....	49
Discussion.....	52
<i>Ostracodes of Fossil Lake</i>	52
<i>Paleoclimate and Paleohydrology Interpretation</i>	53
Conclusions.....	58
References.....	59
Chapter 4: Carbon and Oxygen Stable Isotopes of Fossil Lake Ostracodes.....	68
Introduction.....	68
Methods.....	69
Results.....	70
Discussion.....	73
<i>Carbon stable isotopes</i>	73
<i>Oxygen stable isotopes</i>	75
<i>Cross Plots</i>	77
Conclusions.....	77
References.....	78

Chapter 5: Multiproxy Paleoclimatic and Paleochemical Reconstruction of Fossil Lake, Oregon, and Comparison to Pleistocene Global Climate Patterns and Great Basin

Paleolake Records 90

 Introduction..... 90

 Lithosome Interpretations 91

Lithosome I and II (~ 646–610 ka) 91

Lithosome III (~ 71 ka) 92

Lithosome IV–VII (~ 47–27.8 ka) 93

Lithosome VIII (~ 27.8–13 ka)..... 95

 Conclusions..... 96

 References..... 96

Chapter 6: Neochronological Experiments with the Freshwater Ostracode *Heterocypris*

***incongruens*: Implications for Reconstructing Aquatic Settings** 102

 Abstract..... 102

 Introduction..... 103

 The Organism..... 104

 Methods..... 105

 Experimental Results 106

Experiment 1: Crushed Kaolinite Sediment..... 106

Experiment 2: Heterogeneous very fine- to medium-grained sand 110

Experiment 3: Heterogeneous medium- to very coarse-grained sand..... 110

Trace Morphology After Sediment Desiccation..... 110

 Discussion..... 111

<i>Trace Behaviors</i>	111
<i>Preservation Potential</i>	114
<i>Paleontological Significance</i>	115
Conclusions.....	117
References.....	118
Chapter 7: Conclusions	131
Reference	132
Appendix A: Grain Size Distribution Data and Shepard Classifications	133
Appendix B: Magnetic Susceptibility and Frequency Dependence Data	156
Appendix C: Composite Depths for Lithostratigraphic Section and Stable Isotope Geochemistry	173
Appendix D: Ostracode Species and Taphonomic Feature Counts	191
Appendix E: EDX Elemental Profiles for Ostracode Coatings	204
Appendix F: Ostracode Stable Isotope Data	207

CHAPTER 1

FOSSIL LAKE INTRODUCTION

Fossil Lake, Oregon, is a Pleistocene lacustrine basin (~ 650–13 ka) in the northwestern part of the Great Basin that is best known for its abundant and diverse vertebrate assemblage including fish (Cope, 1883), birds (Shufeldt, 1913; Howard, 1946; Hargrave, 2009) and mammals (Elftman, 1931, Martin, 1996). Tens of thousands of specimens have been collected from Fossil Lake, representing hundreds of different species, making it an extremely important Quaternary paleontological locality in North America (Martin et al., 2005). The stratigraphy of Fossil Lake consists of rhythmic fining upward sequences that have been interpreted as the result of climatically induced lake level changes (Allison, 1979), but a high-resolution paleoenvironmental and paleoclimatic reconstructions are lacking. The purpose of this investigation is to provide a high-resolution reconstruction of the paleoenvironment and paleoclimate during Fossil Lake lake stands and quantify the changes in the lake's paleohydrologic history.

To reconstruct Fossil Lake's paleoenvironmental and paleoclimatic history, detailed lithostatigraphy, magnetic susceptibility, and ostracode biodiversity and geochemical analysis were conducted on cores extracted from the basin and their results and interpretations are presented individually in subsequent chapters. Chapter 2 introduces the method of collection for all cores and samples used in this study and presents lithostatigraphic, grain size, and magnetic susceptibility data from throughout the basin. Fossil ostracode assemblages and paleoecology are introduced in Chapter 3, while ostracode stable isotope geochemistry results are presented in Chapter 4. Chapter 5 provides is a synthesis of all of the data with comparisons to other Great

Basin lakes and Pleistocene global ice volume records. Chapter 6 describes ostracode traces observed from laboratory neochronological experiments and their preservation potential in the fossil record. Effort was made to look for ostracode locomotion or resting traces preserved in core or outcrop, or escape traces in tephra burial events at Fossil Lake, however, no ostracode traces were observed in either the lacustrine or tephra sediments.

Significance

The Great Basin is an internally drained hydrologic province that contained an abundant number of basins with pluvial lakes during the late Quaternary. The size of these lakes was sensitive to long term climatic changes resulting from precipitation and evaporation, making them valuable for paleoclimate reconstructions (e.g., Benson and Thompson, 1987; Benson et al., 1990; Cohen et al., 2000; Bright et al., 2006). Age control has been problematic in generating high-resolution paleoclimate records from the Great Basin pluvial lakes older than ~ 50 ka (limits of radiocarbon dating) because of the lack of dateable materials and because few locations have continuous depositional records (Cohen et al., 2000). The northwestern part of the Great Basin, where Fossil Lake lies, does not have the severe age control problems that the rest of the Great Basin exhibits because of its position downwind from the Cascade Range volcanoes. Tephra layers are common in these lacustrine deposits and allow for both intrabasinal and extrabasinal correlations (Negrini, 2002). Furthermore, a variety of techniques allow for absolute age dating of tephra well beyond the 50 ka limit of radiocarbon dating (Berger, 1991; Sarna-Wojcicki and Davis, 1991).

Determining the changes in paleohydrology, paleoclimate, and lake-level at Fossil Lake is significant because it will contribute a paleoclimatic record with some temporal constraints for

the extreme northwest corner of the Great Basin and allow for a study of the timing of climate change throughout the Great Basin during the Pleistocene. It will contribute a paleoclimate record for the middle Pleistocene with additional insights into the paleohydrology and paleoclimate of pluvial lake systems in the Great Basin, where only a few records have been studied. Understanding the paleoclimate and paleohydrology of Fossil Lake may provide insight into the biotic changes of the diverse vertebrate faunal assemblage preserved at Fossil Lake and to nearby archaeological sites.

Geologic Setting

The Fossil Lake subbasin is a small subdivision of the Fort Rock Basin, located in Lake County, south central Oregon. The Fort Rock Basin lies within a complex tectonic setting of echelon step-sense and oblique slip-sense extensional faulting with linking faults (Crider, 2001), that is generally thought to be at the northwest boundary of the continental extension of the Basin and Range (Thompson and Burke, 1974) (Fig. 1). The Columbia Intermontane province, dominated by volcanoes and volcanic deposits, lies just to the north of the basin and the Cascade Mountain range to the west.

The Fort Rock Basin trends nearly 65 km east-west can be subdivided into three smaller subbasins that connect at higher elevations, Fort Rock basin in the west, Silver Lake basin in the southwest, and Christmas Valley basin in the east (Fig. 2). Fossil Lake covers approximately 16 km² and lies within the Christmas Valley basin. During parts of the Pleistocene, as inferred by erosional and depositional shoreline features, the entire Fort Rock Basin was inundated forming Pluvial Fort Rock Lake (Allison, 1940; 1979; Friedel, 1993). At its greatest expansion, the lake was estimated to be as deep as 58 m (Allison 1979; Friedel, 1993). Additional lower elevation

shoreline features suggests that the lake waxed and waned a number of times likely the result of expansion or retraction of glacial ice sheets. It is unknown exactly when the Fort Rock Basin completely dried up, but extensive eolian processes followed desiccation. Active sand dunes still remain in the Fossil Lake area.

The geology of Fossil Lake was first discussed by Waring (1908) who stated that the region had been flooded by large Pleistocene lakes and by Smith (1926) who introduced the Fossil Lake Formation, composed of unknown thicknesses of horizontal lacustrine silts. A more comprehensive look at Fossil Lake geology was performed by Allison (1940; 1966; 1979) who used tephra deposits for correlation. More recently, a detailed geologic investigation of Fossil Lake lithostratigraphy and geochronology was conducted by Martin et al. (2005). They described 18 depositional units with eight rhythmic depositional packages of fining-upward sequences and five tephra deposits. A typical depositional package has a basal basalt conglomerate that grades into a tuffaceous and basaltic sandstone, which is overlain by a siltstone. Two major unconformities were recognized. Tephra deposits were electron microprobed and geochemically compared to known tephra. The five tephra deposits, in stratigraphic order, were correlated to the Rye Patch Dam tephra (~ 646 ka), Dibekulewe ash bed (~ 610 ± 20 ka), Tulelake pumice (~ 95 ± 23 ka), Mount St. Helens C ash (47 ± 2 ka), and Trego Hot Springs tephra (23.2 ± 0.3 ka BP) (Martin et al., 2005 and references within).

Currently Fossil Lake subbasin is an active deflation zone. Lacustrine sand and silts compose the basin floor and are continually weathered (Fig. 3). The eastern part of the basin is covered with active sand dunes. Interdunal areas expose lacustrine sediments. A small ephemeral playa still exists in the western part of the subbasin, but in recent years has rarely contained water. During wet years, small saline ponds form and are the watering hole for many

of the local fauna, including frogs, birds, and mammals. Evaporite crusts remain after the ponds dry up. Fossil Lake supports a sparse vegetation of sagebrush, rabbit brush, bunch grass, and salt grass. Higher elevations surrounding the basin support juniper trees and, to the northeast, a small forest of ponderosa pines.

Today the climate in the Fossil Lake area is semi-arid. The Silver Lake Ranger Station, located in the southeastern part of Fort Rock Basin, has recorded a mean annual precipitation of 24.79 cm for the time period of 1968 to 2005. Average temperature records for the same time period show a January mean maximum and minimum of 4.3 °C and -5.9 °C, respectively, and a July mean maximum and minimum of 28.8 °C and 6.8 °C, respectively. Climate in the basin is generally controlled by fronts derived from westerlies off the North Pacific Ocean. These fronts produce relatively mild temperatures. Less commonly, extreme temperatures occurred with continental air masses from the north and east that produce a very cold winter or very hot summer.

References

- Allison, I. S. 1940. Study of Pleistocene lakes of south central Oregon. Carnegie Institution of Washington Year Book 39, 299–300.
- Allison, I.S., 1966. Fossil Lake, Oregon: its geology and fossil faunas. Oregon State University Studies in Geology 9, pp. 48.
- Allison, I.S., 1979. Pluvial Fort Rock Lake, Lake County, Oregon. State of Oregon Department of Geology and Mineral Industries Special Paper 7, pp. 72.
- Benson, L.V., Currey, D.R., Dorn, R.I., Lajoie, K.R., Oviatt, C.G., Robinson, S.W., Smith, G.I., Scott, S., 1990. Chronology of expansion and contraction of four Great Basin lake

- systems during the past 35,000 years. *Palaeogeography, Palaeoclimatology, Palaeoecology* 78, 241–286.
- Benson, L.V., Thompson, R.S., 1987. Lake-level variation in the Lahontan Basin for the past 50,000 years. *Quaternary Research* 28, 69–85.
- Berger, G.W., 1991. The use of glass for dating volcanic ash by thermoluminescence. *Journal of Geophysical Research* 96, 19,705–19,720.
- Bright, J., Kaufman, D.S., Forester, R.M., Dean, W.E., 2006. A continuous 250,000 yr record of oxygen and carbon isotopes in ostracode and bulk-sediment carbonate from Bear Lake, Utah-Idaho. *Quaternary Science Reviews* 25, 2258–2270.
- Cohen, A.S., Palacios-Fest, M.R., Negrini, R.M., Wigand, P.E., Erbes, D.B., 2000. A paleoclimate record for the past 250,000 years from Summer Lake, Oregon, USA: II. Sedimentology, paleontology, and geochemistry. *Journal of Paleolimnology* 24, 151–182.
- Cope, E.D., 1883. On the fishes of the Recent and Pliocene lakes of the western part of the Great Basin, and of the Idaho Pliocene lake. *Proceedings of the Academy of Natural Sciences of Philadelphia* 35, 134–166.
- Crider, J.G., 2001. Oblique slip and the geometry of normal-fault linkage: mechanics and a case study from the Basin and Range of Oregon. *Journal of Structural Geology* 23, 1997–2009.
- Elftman, H.O., 1931. Pleistocene mammals of Fossil Lake, Oregon. *American Museum Novitates* 481, 1–21.

- Friedel, D.E., 1993. Chronology and climatic controls of late Quaternary lake-level fluctuations in Chewaucan, Fort Rock, and Alkali basins, south-central Oregon. Ph.D. Thesis, University of Oregon.
- Hargrave, J.E., 2009. Lithostratigraphy and fossil avifaunas of the Pleistocene Fossil Lake Formation, Fossil Lake, Oregon, and the Oligocene Etadunna Formation, Lake Palankarinna, Southern Australia. Ph.D. Thesis, University of Oklahoma.
- Howard, H., 1946. A review of the Pleistocene birds of Fossil Lake, Oregon. Carnegie Institution of Washington Publications 551, 143–195.
- Martin, J.E., 1996. First occurrence of *Cynomys* from west of the Rocky Mountains. *Journal of Vertebrate Paleontology* 16 (Supplement), 51A.
- Martin, J.E., Patrick, D., Kihm, A.J., Foit Jr., F.F., Grandstaff, D.E., 2005. Lithostratigraphy, tephrochronology, and rare earth element geochemistry of fossils at the classical Pleistocene Fossil Lake Area, South Central Oregon. *Journal of Geology* 113, 139–155.
- Negrini, R.M., 2002. Pluvial lake sizes in the northwestern Great Basin throughout the Quaternary period. *Smithsonian Contributions to the Earth Sciences* 33, 11–52.
- Sarna-Wojcicki, A.M., Davis, J.O., 1991. Quaternary Tephrochronology. In: Morrison, R.B. (Ed.), *Quaternary Nonglacial Geology: Conterminous U.S. The Geology of North America*, volume K-2. Geological Society of America, Boulder, Colorado, pp. 93–116.
- Shufeldt, R.W., 1913. Review of the fossil fauna of the desert region of Oregon, with a description of additional material collected there. *Bulletin of the American Museum of Natural History* 32, 123–178.
- Smith, W.D., 1926. Physical and economic geology of Oregon: the southeastern lake province. Oregon University, *Commonwealth Review of the University of Oregon* 8, 199–253.

Thompson, G.A., Burke, D.B., 1974. Regional geophysics of the Basin and Range Province.

Annual Review of Earth and Planetary Sciences 2, 213–238.

Waring, C.A., 1908. Geology and water resources of a portion of south-central Oregon. U. S.

Geological Survey Water-Supply Paper 220.

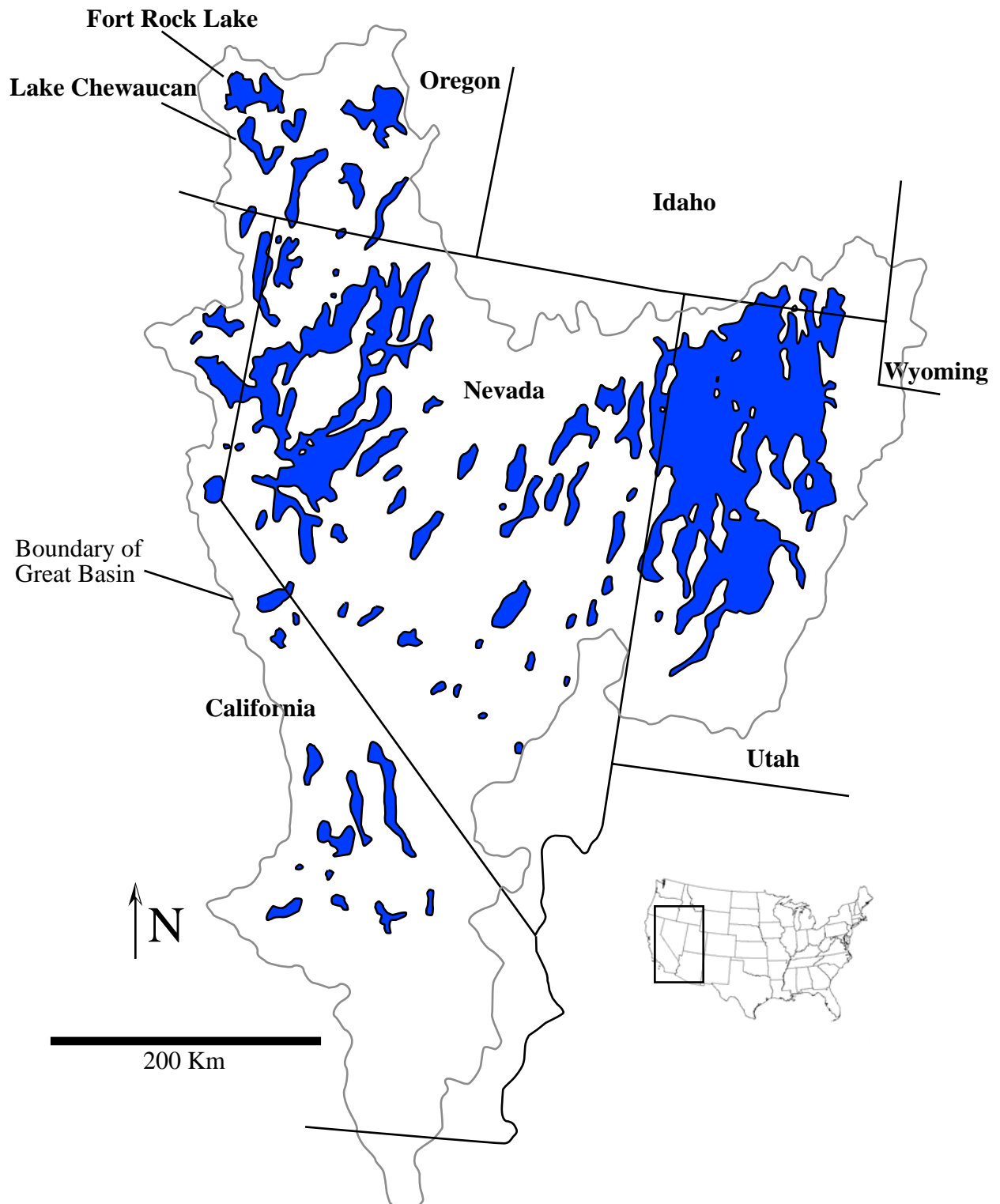


Fig. 1 Location of Pleistocene pluvial lakes in the Great Basin. Pluvial Fort Rock Lake is located in the northwest corner of the Great Basin.

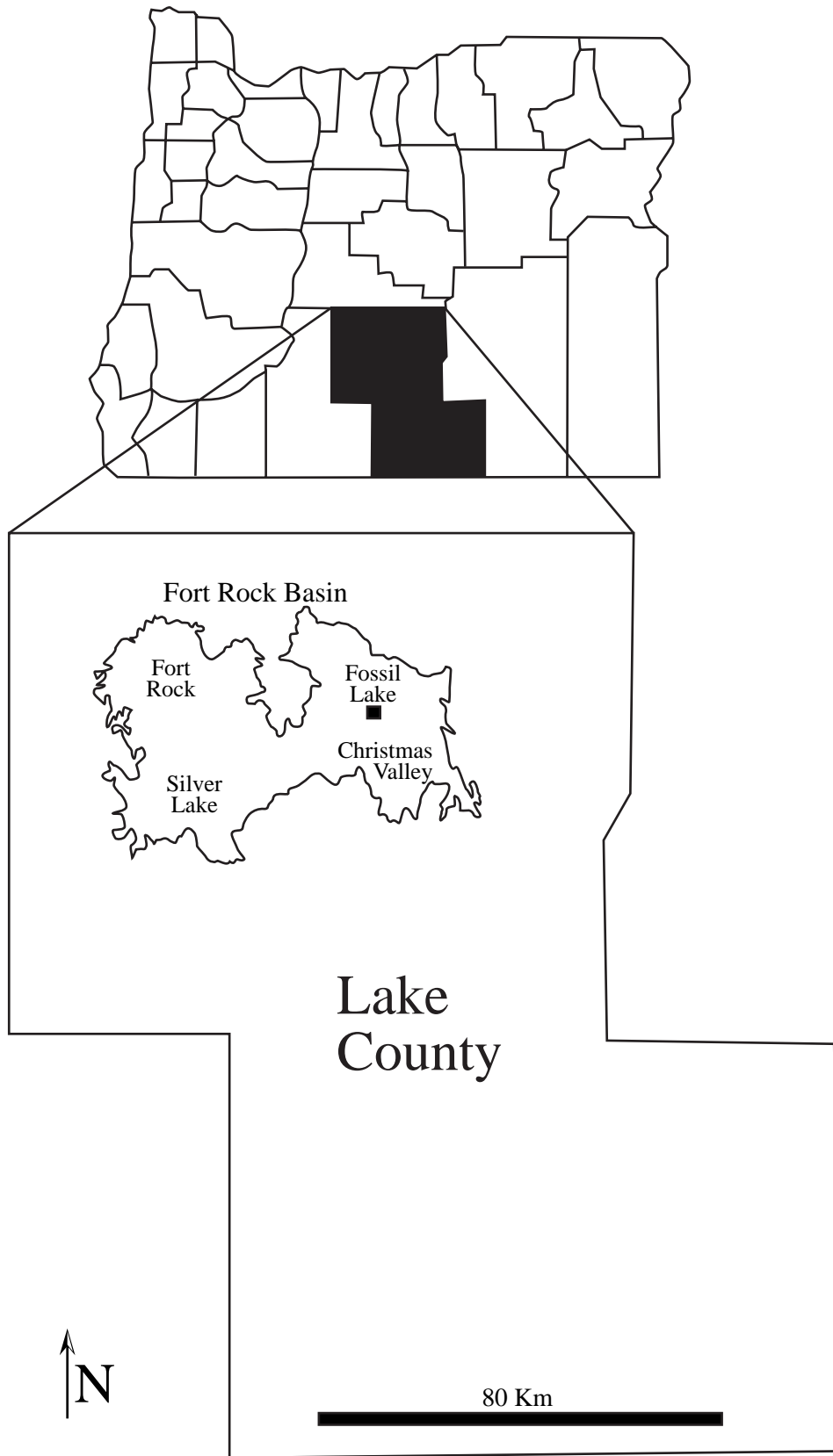


Fig. 2 Fort Rock Basin in Lake County, Oregon. The Fossil Lake subbasin is located in the east central part of the basin.



Fig. 3 Deflation surface at Fossil Lake, Oregon.

CHAPTER 2

DEPOSITIONAL HISTORY OF FOSSIL LAKE FROM LITHOSTRATIGRAPHY AND MAGNETIC SUSCEPTIBILITY ANALYSIS

Introduction

Previous lithostratigraphic studies at Fossil Lake have used extensive trenching and correlation of marker beds to assemble a composite lithostratigraphic section (Allison, 1966; Martin et al., 2005; Hargrave, 2009) because the topography of Fossil Lake is fairly flat and the only outcrops occur in microbuttes, < 2 m tall. Topography follows lithology, so few lithostratigraphic units are exposed at the surface. The purpose of this study is to: 1) expand upon previous Fossil Lake lithostratigraphy with data collected from five cores and two trenches, 2) examine depositional changes through north–south and east–west transects, and 3) reconstruct a depositional history for the basin.

Methods

Coring and trenching were used to examine changes in lithostratigraphy throughout the Fossil Lake basin. Coring sites were chosen based on driving accessibility of the coring rig and to produce east–west and north–south transects (Fig. 1). The east–west transect was taken in the northern part of the basin, and the north–south transect was taken in the western part of the basin. Cores were taken throughout the basin with a trailer-mounted Giddings® hydraulic coring machine. Drive segments were collected and preserved in 4.4-cm diameter, 152.4-cm long plastic liners. At most localities, coring ceased when the water table was reached, resulting in a saturated sediment sludge, though at core site 3, coring ceased above the water table due to a

lightning storm. A total of five cores were obtained, four cores in the northern part and one in the southern part of the basin. Cores were taken back to the University of Kansas Geography Soils Geomorphology Laboratory (SGL) where they were immediately frozen in an $\sim 18\text{ }^{\circ}\text{C}$ ($0\text{ }^{\circ}\text{F}$) commercial freezer to inhibit microbial growth until analysis.

In areas where the coring rig could not be taken, two trenches through two microbuttes and a series of small pits were excavated and examined throughout the basin to confirm the lithostratigraphy and examined sedimentary structures that would not be visible easily in the 4.4-cm diameter cores. The two trenches were described for color, lithology, tephra occurrence, sedimentary structures, and unconformities and sampled at 2-cm intervals for texture.

At SGL, cores were sliced longitudinally and the outer surface of the cores was removed to minimize the effects of sediment deformation and contamination at the core margins. Cores were measured and described for color, texture, lithology, tephra occurrence, sedimentary structures, and unconformities. The core were subsampled with 8 cc ($2 \times 2 \times 2\text{ cm}$) paleomagnetic sample cubes, approximately four 2-cm sample cubes per 10 cm. The cubes were air dried and capped. The sediment in these cubes was used for microscopic work, sediment magnetism, grain-size analysis, ostracode stratigraphy, and ostracode stable isotopes analyses. Each sample was examined microscopically to examine and inventory tephra, grain coatings, fossils, and sediment composition.

Sediment magnetism analyses were conducted first, using the unopened and unaltered 8 cc paleomagnetic sample cubes. Magnetic susceptibility was measured with a Bartington Model MS2 susceptibility bridge with dual-frequency sensor. Susceptibility, recorded in SI units ($10^{-8}\text{ m}^3\text{ kg}^{-1}$), was normalized by mass, and frequency dependence was computed from measurements at 0.465 and 4.65 kHz.

Samples for grain size were analyzed using a Malvern Mastersizer 2000 Hydro MU wet dispersion laser diffraction system. Pebble and gravel sized particles were removed prior to analyses and particle sizes were measured from 0.02 to 2000 μm . A subsample of approximately 0.1 g of sediment taken from sample cubes was placed in the analyzer's suspension liquid circulation system and sonicated for three minutes, a protocol that was established after multiple sample runs. Afterward, three measurement cycles were run and the data from the three runs were averaged. Sample data were plotted on a Shepard ternary diagram using the visual basic program SEDPLOT (Poppe and Eliason, 2008) and given a Shepard classification name (Shepard, 1954).

Previously reported radiocarbon ages were converted to absolute age (ka) using the calibration curve from Fairbanks et al. (2005).

Results

Lithostratigraphy of Fossil Lake is dominated by sandstones and siltstones, often punctuated with disconformities, and generally high magnetic susceptibility values (Fig. 2–6). All but one of Martin et al.'s (2005) lithostratigraphic units is represented in the cores (Fig. 7–13). Unit 18, a thin sandstone layer, is only found in a small area which was not accessible for coring. The base of the lacustrine deposits was not reached by core. Core 5, the southernmost, produced the longest core interval of 4.2 m and captured units 1–14. In the north, cores were shorter, rarely longer than 2.5 m, and did not reach the lower units, with the exception of core 4, which was taken in a topographic low where lower units were exposed at the surface.

Eight unconformity-bound lithosomes can be recognized from the cores that correspond to Martin et al.'s (2005) eight rhythmic depositional packages. Occasionally, unconformity

surfaces were not evident in the cores and lithologic criteria and absence of fossils that suggested shallow water processes were used for correlation. From oldest to youngest, these lithosomes include:

Lithosome I (Unit 1)

Lithosome I includes only one unit, a yellow claystone with silt interbeds, observed in core 5 and trench 1. The grain size analyses indicate that this unit and the other claystone units are a clayey siltstone. Microscopic examination, however, reveals predominantly clay particles, indicating sonication did not break up clay aggregates into clay particles, thus, biasing results towards a siltstone. Magnetic susceptibility is extremely low and frequency dependence is variable but generally high. The true thickness of this lithosome and depth of its basal unconformity are unknown because the base was not reached in core or field trenches. Only cyprinid fish fossils were observed in the core. A fining upward purplish tephra was observed in the field but was not present in core 5. Thickness of the tephra was up to 18 cm in field observations. Blocky ped structures and rhizoliths are common throughout the lithosome.

Lithosome II (Units 2–4)

Lithosome II overlies the disconformity at the top of the yellow claystone and is present in cores 4, 5, and trench 1. The base of Lithosome II is a thin basalt pebble conglomerate that grades into a gray-brown sandstone. In core 4 the sandstone contains silt interbeds. In core 5 and trench 1, the base of the sandstone contains reworked mud chips and clay intraclasts from the yellow claystone. Sand thickness ranges from 15.8 cm in the south to 22.0 cm in the north. The sandstone contains many ostracodes and gastropod shell fragments. A laterally

discontinuous fine-grain ash layer is found near the base of the sandstone. The ash layer had a maximum thickness of 3 cm in trench 1 but no discernable ash layer was observed in either of the cores. The sandstone grades upward into a brown siltstone with abundant ostracodes and gastropods and further grades into a white claystone with cyprinid fish fossils. Unit thicknesses range from 12.0–19.0 cm for the siltstone to 37.9–40.0 cm for the claystone. Blocky ped structures and rhizoliths are common in the white claystone. Total thickness for Lithosome II ranges from 74.0 cm in the north to 68.8 cm in the south. Magnetic susceptibility in the lithosome is low and slightly variable, and frequency dependence is generally high.

Lithosome III (Units 5–6)

Lithosome III overlies the disconformity at the top of the white claystone and is present in cores 3, 4, 5 and trench 1, but is incomplete in core 3, 4 and trench 1. The base of Lithosome III is a laterally discontinuous, thin basalt pebble to cobble conglomerate that grades into a gray-brown sandstone with brown silt interbeds. In core 4, 20.5 cm of reworked white claystone is deposited below the gray-brown sandstone. Ostracodes are common in the sandstone. At the base of the sandstone is a coarse-grained pumice tephra layer. In trench 1 and core 3, the pumice tephra layer is 2–4 cm thick with an additional 3–7 cm of reworked pumice above, but in cores 4 and 5, only reworked tephra is present. Magnetic susceptibility in the sandstone is variable and extremely high, corresponding to the presence of tephra, and frequency dependence is generally low. Total thickness of the sandstone is 39.2 cm in the northwest, 39–49.9 cm in the north central, and 21.1 cm in the south. The sandstone grades upward into a brown siltstone. In core 5, the base of the siltstone is thinly laminated, punctuated with rhizoliths. The siltstone unit contains abundant ostracodes and, near the top, granular structures and rhizoliths are common.

Magnetic susceptibility in the siltstone decreases from moderately high to moderately low, while frequency dependence gradually increases from low to high. Thickness of the siltstone ranges from 20.2 cm in the northwest to 46.9 cm in the south. Total thickness for Lithosome III is 70.1 cm in the south, whereas no complete sections were obtained in the north.

Lithosome IV (Units 7–8)

In Lithosome IV, a brown sandstone overlies the disconformity at the top of the brown siltstone, and is present in cores 2, 3, and 5. Thickness of the sandstone ranges from 22.3 cm in the northwest to 40 cm in the south. Abundant ostracodes, some recrystallized, are present in the unit. Magnetic susceptibility in the sandstone is high, but is not associated with a tephra deposit, and frequency dependence is low. The sandstone grades upward into a tan siltstone. In core 5, the tan siltstone is thinly laminated. A laterally discontinuous, fine-grained white ash layer in the siltstone gives it color. Associated with the deposition of the ash, are small biotite flakes. The white ash is reworked in the western part of the basin and no distinct layer was observed in any of the cores, however, biotite flakes were common. To the east, a 3–6 cm thick ash layer was observed. Abundant ostracodes are present in the siltstone and rhizoliths and granular structures are common in the upper portions. Magnetic susceptibility in the siltstone is variable but moderately low, and frequency dependence is generally high. Thickness of the siltstone ranges from ~ 9.6 cm in the northwest to 23.7 cm in the north central to 27.0 cm in the south. Total thickness for Lithosome IV is 31.9 cm in the northwest and 67.0 cm in the south.

Lithosome V (Units 9–10)

In Lithosome V, a brown sandstone overlies the disconformity at the top of the tan siltstone, and is present in cores 1, 2, 3, and 5, but is incomplete in core 1. In core 2, the brown sandstone overlies 16.3 cm of reworked tan silt. Thickness of the sandstone ranges from 3.3 cm in the northwest to 36.0 cm in the north central to 23.0 cm in the south. Ostracodes occur in the sandstone. Magnetic susceptibility in the sandstone is moderately high, but highly variable between cores, and frequency dependence is generally low. The sandstone grades upward into a brown siltstone that contains ostracodes and gastropods. The top of Lithosome V is scoured. Thickness of the siltstone ranges from ~ 1 cm in the northwest to 5.3–8.1 cm in the north central to 13.1 cm in the south. Magnetic susceptibility in the siltstone is moderately low, and frequency dependence is high. Total thickness for Lithosome V is 4.3 cm in the northwest, 44.1 in the north central, and 36.1 cm in the south.

Lithosome VI (Units 11–12)

In Lithosome VI, a brown sandstone overlies the disconformity at the top of the brown siltstone, and is present in cores 1, 2, 3, 5, and trench 2, but is incomplete in trench 2. Thickness of the sandstone ranges from 0.8 cm in the northwest to 57.8–87.3 cm in the north central to 13.5 cm in the south. Ostracodes, some bleached, commonly occur in the sandstone. Microscopic examination revealed reworked, white, coarse-grained tephra particles present near the top of the sandstone in cores 1 and 2. The sandstone grades upward into a brown siltstone that contains ostracodes. Thickness of the silt unit ranges from approximately 2.0 cm in the northwest to 6.1–6.9 cm in the north central to 7.9 cm in the south. Granular structures and rhizoliths are present at the top of the brown siltstone in core 5 and trench 2, while a scoured surface is present in cores

1, 2, and 3. Total thickness for Lithosome VI is 2.8 cm in the northwest, 64.7–93.4 cm in the north central, and 21.4 cm in the south. Magnetic susceptibility in the lithosome is moderately high and extremely variable and frequency dependence gradually increases from low to high.

Lithosome VII (Units 13–14)

In Lithosome VII, a brown sandstone overlies the unconformity at the top of the brown siltstone, and is present in cores 1, 2, 3, 5 and trench 2, but is incomplete in cores 2 and 5. Thickness of the sand unit ranges from 23.0 cm in the northwest to 25.4–33.3 cm in the north central to 76.0 cm in the northeast to 38.7 cm in the south. Microscopic examination revealed reworked white coarse-grained tephra particles present at the base of the sandstone in cores 1, 2, and trench 2. Ostracodes, some bleached, commonly occur in the sandstone. Magnetic susceptibility in the sandstone is moderately high and highly variable. An extremely large magnetic spike is recorded in core 5 that corresponds to coarse-grained sand. Frequency dependence in the sandstone is highly variable between cores, low in cores 3 and 5 but moderately high in cores 1 and 2. The sandstone grades upward into a brown siltstone with sand interbeds. Thickness of the siltstone ranges from 4.6 cm in the northwest to 15.9 cm in the north central to 38.5 cm in the northeast. Within the siltstone is a fine-grained white ash layer that reaches up to 10 cm thick. Often this ash is reworked and deposited as re-suspension layers. In trench 2, ash re-suspension layers are separated by siltstone with rhizoliths and granular structures. Ostracodes, some bleached, are occasionally present. Granular structures and rhizoliths are common in the brown siltstone. Magnetic susceptibility in the siltstone is highly variable, with high susceptibility corresponding to the presence of tephra. The frequency dependence of the siltstone is also variable and generally high, but samples with tephra have low

frequency dependence. Thickness of the Lithosome VII ranges from 27.6 cm in the northwest to 41.3 cm in the north central to 114.5 cm in the northeast.

Lithosome VIII (Units 15–17)

In Lithosome VIII, a well-sorted reddish-brown sandstone with planar- and cross-bedding overlies the disconformity at the top of the brown siltstone, and is present in cores 1, 3, and trench 2. An iron oxide stain on many of the sand grains gives this unit its reddish-brown color. Rare bleached ostracodes are present. Magnetic susceptibility and frequency dependence in the sandstone is highly variable ranging from moderately low to high. Thickness of the sandstone ranges from 69.3 cm in the northwest to 59.4 cm in the north central to 90.0 cm in the northeast. Overlying the sandstone is a laterally discontinuous brown siltstone that contains rhizoliths. The siltstone is missing in trench 2. Thickness of the sand unit ranges from 11.0 cm in the northwest to 6.0 cm in the north central. The siltstone grades upward into a white claystone. Blocky ped structures and rhizoliths are common in the claystone and only salmonid fossils are observed in cores. Thickness of the claystone ranges from 12.3 cm in the northwest to 43.5 cm in the north central to 1 cm in the northeast. Magnetic susceptibility gradually decreases while frequency dependence increases through the transition from siltstone to claystone. Thickness of the Lithosome VIII ranges from 92.6 cm in the northwest to 108.9 cm in the north central to 91 cm in the northeast.

Discussion

In a west to east transect of the northern part of the basin, cores and trenches only recovered the uppermost Lithosomes (Fig. 14). Lithosomes V and VI thin to < 5 cm in the

northwest core, indicating they were deposited near the lake margin or were more extensively eroded. Lithosome VII is thickest in the northeast trench indicating a longer deposition period, increased sedimentation, or less eroded.

In a north to south transect of the west part of the basin, all Lithosomes were recovered (Fig. 15). Lithosomes III and IV are thickest in the southern core and both contain laminated siltstones not seen in the northern cores, indicating calmer, deeper offshore deposition, less pedogenetic modification, or less eroded. Lithosomes V and VI thin to the northwest core, as seen in the west-east transect. Lithosome V, VI, and VII are thickest in the northeast core, indicating a longer deposition time period, increased sedimentation rates, or less eroded.

Using ash marker beds and unconformity surfaces, vertical magnetic susceptibility profiles, and vertical stable isotope profiles (Chapter 4), a composite lithostratigraphic section was constructed for Fossil Lake (Fig. 16). The section shows stacked fining upward lacustrine sequences capped by an unconformity surface.

The basal claystone with silt interbeds (Lithosome I) suggests an offshore lacustrine environment during relatively deep-water conditions with either fluctuating lake levels or episodic sediment flows. The fining upward tephra layer in the claystone correlates to the Rye Patch Dam tephra (Martin et al., 2005) and is 646 ka (Williams, 1994). The lack of tephra reworking or re-suspension deposits indicates that the tephra was deposited below storm wave-base level. The top of Lithosome I indicates that lake level dropped and was subaerially exposed and pedogenically modified, as indicated by blocky ped structures and rhizoliths and the presence of prairie dog fossils (*Cynomys* sp.) (Martin, 1996).

Deposition of Lithosome II commences with a large-scale flooding event that deposited a pebble conglomerate and clay intraclasts. The gray-brown sandstone with silt interbeds and the

laterally discontinuous ash with wave reworking and re-suspension layers imply deposition in a shallow lake environment with fluctuating lake levels. The ash has been correlated to the Dibekeluwe ash bed (Martin et al., 2005) and is dated at 610 ± 20 ka (Davis, 1978). The lake level rose throughout Lithosome II with deposition grading from sandstone to claystone. The claystone indicates deposition in deep water conditions. The presence of blocky ped structures and rhizoliths at the top of Lithosome II indicates the lake was subaerially exposed and pedogenically modified.

Another large-scale flooding event initiates Lithosome III deposition, marked by the presence of a pebble-cobble conglomerate. The lake remained shallow with small lake level fluctuations during the deposition of a gray-brown sandstone with silt interbeds and a pumice tephra with wave reworking. The pumice tephra has been correlated to the pumice tephra at Tulelake and is 95 ± 25 ka (Martin et al., 2005). This investigation was able to correlate the pumice tephra to tephra Bed 8 (Llao Rock Pumice Castle-like 1) at Summer Lake, Oregon, (Davis, 1985; Kuehn and Negrini, 2010; S. C. Kuehn, personal communication, 2010) and is 71 ± 5 ka (Bacon and Lanphere, 2006). The laminated siltstone above the sandstone indicates a shift to deeper water conditions and deposition below storm wave-base. The presence of granular structures and rhizoliths at the top of Lithosome III indicates the lake was subaerially exposed and pedogenically modified.

Lithosome IV, V, VI, and VII commence with the inundation of the basin. Thin, laterally discontinuous pebble conglomerate have been observed at the base of each of these lithosomes (Martin et al., 2005). Shallow-water conditions persisted for long periods of time as indicated by the thick basal sandstones. In Lithosome VI and VII bleached ostracodes are common in the sandstone, indicating very shallow-water depths and periodic subaerially exposure. Gradually,

the sandstones graded into siltstones as lake levels rose. In Lithosome IV, siltstone deposits are laminated in the south and contain salmonid fossils (J. E. Martin, personal communications, 2010), indicating deposition in a cold, deep-water setting. In Lithosome VI and VII, and VII, the thin siltstone layers, scouring surfaces, bleached ostracodes, and reworked ash suggest a shallow-water setting in dry conditions. The top of the all these lithosomes, except V, indicates lake level dropped and was subaerially exposed and pedogenically modified, as indicated by granular structures and rhizoliths. Lithosome V is capped by a scouring surface.

Two distinct and laterally expansive tephras are found in Lithosomes IV and VII. In Lithosome IV, the white ash layer correlates to the Marble Bluff Mt. St. Helens Set C ash (Martin et al., 2005) and is dated at 47 ± 2 ka (Berger and Busacca, 1995). In Lithosome VII, another thick white ash layer correlates to the Trego Hot Spring tephra (Martin et al., 2005) and is dated at 27.8 ± 0.4 ka (Benson et al., 1997). Two other tephras, previously unreported from Fossil Lake, occur at the top of Lithosome VI's sandstone and at the base of Lithosome VII in the northern part of the basin. Both of the tephras are reworked and no distinct layer exists and may represent lag deposits of the same tephra. Their stratigraphic position just below the Trego Hot Springs tephra indicates an age slightly older than ~ 28 ka.

The base of Lithosome VIII is a planar- and cross-bedded sandstone with sparse fossils and is indicative of eolian processes with possible intermittent shallow lake deposits. The presence of unbroken bleached ostracodes in the sandstone suggests that the ostracodes were not transported far and were sourced from a nearby water source. Fossil Lake was likely a playa environment during this time with episodic flooding events. Following the deposition of the sandstone, the basin filled rapidly reaching a lake high stand as indicated by claystone overlying eolian sands. The abundance of salmonid fossils in the claystone suggests that the lake was deep

and cold. A number of wave cut terraces and caves in the Fort Rock basin indicate a basin-wide lake that reached depths up to 58 m (Allison, 1979; Friedel, 1993). A radiocarbon age of 15.4 ± 0.9 ka was reported from charcoal in a wave-cut cave when the lake was 38 m deep (Bedwell, 1970). The top of Lithosome VIII indicates lake level dropped and was subaerially exposed and pedogenically modified, as indicated by blocky ped structures and rhizoliths.

The expansive lake deposits of Fossil Lake with repeated unconformities and little to no facies change make it impossible to determine the locations of either a shoreline or depocenter without further investigation. The vast diversity and number of terrestrial vertebrate and aquatic bird fossils throughout the basin suggest that palustrine or small shallow lake environments existed for some time each time Fossil Lake dried up.

Magnetic susceptibility is a concentration-dependent parameter of magnetic material present in the sediment. It can also be affected by magnetic grain size, shape, and mineralogy. Frequency dependence of susceptibility increases with the concentration of ultra-fine-grained magnetic material. In a rock-magnetism study completed for Summer Lake, Oregon, ~ 40 km south of Fossil Lake, lake sediments were found to be dominated by one mineral type, (titano)magnetite, suggesting susceptibility of fine-grained sediments was primarily a function of the concentration of magnetic minerals (Negrini et al., 2000). Results indicated higher magnetic concentrations related to deeper lake intervals and wetter conditions with increase sediment flux. Assuming Fossil Lake is also dominated by (titano)magnetite, similar trends are not seen in Fossil Lake sediments. Low magnetic susceptibility is associated with deeper water facies and high frequency dependence, and vice versa, suggesting susceptibility is influenced more by the grain size of the magnetic material than its concentration. Extremely high magnetic susceptibilities are associated with tephra depositional layers except for in Lithosome IV and

VII. In Lithosome IV, the high magnetic susceptibility proceeds and corresponds to a period of increased methanogenesis rates (Chapter 4) and indicates increased iron mobility in the substrate that is subsequently oxidized and precipitated at or near the sediment-water interface. In core 5, the high magnetic susceptibility in Lithosome VII is associated with coarse sand magnetic grains and may represent a flooding event.

Regional Comparison

A similar lithostratigraphic study, completed by Cohen et al. (2000) for nearby Summer Lake, Oregon, indicated that deposits at Summer Lake recorded a long Pleistocene history, ~250 to 16 ka, and were subdivided into eight lithosomes based on unconformity and paraconformity boundaries. Only one major unconformity was recorded, ~158 to 102 ka. Comparison and correlation to Fossil Lake lithostratigraphy is possible because diagnostic tephra layers are present in both basins. The Summer Lake section does not contain older lithosomes correlative to Lithosomes I or II, found at Fossil Lake (Fig. 17).

Fossil Lake's Lithosome III and IV can be correlated to Summer Lake's Lithosome V by the presence of Pumice Castle-like 1 tephra and Marble Bluff Mt. St. Helens set C ash. Summer Lake's Lithosome V is composed of a carbonate pebble conglomerate that is overlain by laminated and massive ostracodal muds with occasional micritic beds deposited below wave-base during a high stand and at its base is a tephra bed, dated at ~ 84 ka. A similar sequence of conglomerate grading to laminated siltstone or siltstone deposited in relatively deep-water conditions is seen in Fossil Lake's Lithosome III and IV, but the onset of Lithosome III is just prior to the Pumice Castle-like 1 tephra. The pumice tephra occurs approximately halfway through Summer Lake's Lithosome V, indicating that the Summer Lake basin flooded prior to

the onset of flooding in Fossil Lake. There is no evidence of subaerial exposure in Summer Lake's Lithosome V, however, at Fossil Lake, subaerial exposure and pedogenesis occur between Lithosomes III and IV, indicating that Fossil Lake was shallower and more susceptible to drying out.

Fossil Lake's Lithosomes V and VI likely correlate to Summer Lake's Lithosome VI and VII, based on their stratigraphic position between the Marble Bluff Mt. St. Helens set C ash and the Trego Hot Springs tephra. Summer Lake's Lithosome VI ranges in thickness from ~ 0.5 to 6 m and at its base is a pebble-rich sandy paraconformity directly below the Mt. St. Helens ash. Above the ash are massive ostracodal muds that change to oolitic mud near the top that were deposited in relatively shallow-water conditions above storm wave base. Summer Lake's Lithosome VII ranges in thickness from ~ 0.5 to 2.2 m and at its base is 2 cm thick oolitic sand. Above the oolitic sand are massive ostracodal muds with occasional sand laminae deposited in shallow-water conditions, above storm wave base. A similar shallow-water depositional setting is observed at Fossil Lake.

Fossil Lake's Lithosome VII and VIII can be correlated to Summer Lake's Lithosome VIII by the presence of Trego Hot Springs tephra. Summer Lake's Lithosome VIII ranges in thickness from ~ 1.8 to 4.3 m and at its base is a lag deposit of the Wono tephra, dated at ~ 32.6 ka. Above the tephra are massive ostracodal muds with sandier intervals that were deposited in relatively shallow water conditions. Multiple unconformities are present at one core locality. Little to no sedimentary record occurs after the deposition of the Trego Hot Springs Tephra, likely the result of erosion and deflation, but well-preserved and dated terraces surrounding the basin indicate a considerably deep lake existed from approximately 21–13 ka. Fossil Lake's Lithosome VII shows a similar depositional setting with a shallow lake environment ending with

the deposition of the Trego Hot Springs Tephra and cumulating in a considerably deep-water lake in Lithosome VIII. The lag deposit of tephra at the base of Fossil Lake's Lithosome VII and Summer Lake's Lithosome VIII may represent the same tephra deposit, the Wono tephra.

The lithostratigraphic sequences of Summer Lake and Fossil Lake show similar timing of high and low lake stands during the time period between ~ 71 and 27 ka (Fig. 17), with Summer Lake having nearly continuous sedimentation and two paraconformities and Fossil Lake having discontinuous sedimentation based on the presence of four unconformities. Minimum sedimentation rates were calculated for this time period from Fossil Lake's core 5 and composite depths from Summer Lake (Kuehn and Negrini, 2010). Fossil Lake has a minimum sedimentation rate of 0.064 mm/yr, whereas Summer Lake has a minimum sedimentation rate of 0.048 mm/yr, indicating Fossil Lake had considerably higher sedimentation during its episodic lake stands than at Summer Lake. Higher sedimentation rates at Fossil Lake may be the result of repeated flooding of the basin at the initiation of each lake stand.

Conclusions

Fossil Lake records a depositional history from ~ 646–610 ka and 71–13 ka, is repeatedly punctuated with unconformities. Three relative lake high stands occur at Fossil Lake, the earliest of which correspond to Lithosome I and II, ~ 646–610 ka. A major unconformity follows Lithosome II, spanning the interval ~ 610–71 ka. The second high stand interval corresponds to Lithosome III and IV, ~ 71–47 ka. Declining lake levels and dry conditions persisted during the deposition of Lithosomes V, VII, and VIII. The third high stand, and likely the deepest, corresponds to top of Lithosome VIII, ~ 25–13 ka. The base of Lithosome VIII was deposited in arid conditions as indicated by the presence of eolian cross bedded sands.

Fossil Lake and nearby Summer Lake have similar depositional histories for the past 71 ka. The onset of flooding occurs later in Fossil Lake, ~ 71 ka, as compared to Summer Lake, ~ 84 ka. The presence of soil horizons and multiple unconformities not seen in Summer Lake, suggest that Fossil Lake was shallower and more susceptible to drying out. Shallow remnant marshes or small shallow lakes environments, however, likely remained for short durations each time Fossil Lake dried up, as indicated by the diverse vertebrate faunal assemblage throughout the basin at Fossil Lake.

References

- Allison, I.S., 1966. Fossil Lake, Oregon: its geology and fossil faunas. Oregon State University Studies in Geology 9, pp. 48.
- Allison, I.S., 1979. Pluvial Fort Rock Lake, Lake County, Oregon. State of Oregon Department of Geology and Mineral Industries Special Paper 7, pp. 72.
- Bacon, C.R., Lanphere, M.A., 2006. Eruptive history and geochronology of Mount Mazama and the Crater Lake region, Oregon. Geological Society of America Bulletin 118, 1331–1359.
- Bedwell, S.F., 1970. Prehistory and environment of the Pluvial Fort Rock Lake area of south central Oregon. Ph.D. Thesis, University of Oregon.
- Benson, L.V., Smoot, J.P., Kashgarian, M., 1997. Radiocarbon ages and environments of deposition of the Wono and Trego Hot Springs Tephra layers in the Pyramid Lake subbasin, Nevada. Quaternary Research 47, 251-260.

- Berger, G.W., Busacca, A.J., 1995. Thermoluminescence dating of late Pleistocene loess and tephra from eastern Washington and southern Oregon and implications for the eruptive history of Mount St. Helens. *Journal of Geophysical Research* 100, 22,361–22,374.
- Cohen, A.S., Palacios-Fest, M.R., Negrini, R.M., Wigand, P.E., Erbes, D.B., 2000. A paleoclimate record for the past 250,000 years from Summer Lake, Oregon, USA: II. Sedimentology, paleontology, and geochemistry. *Journal of Paleolimnology* 24, 151–182.
- Davis, J.O., 1978. Quaternary tephrochronology of the Lake Lahontan area, Nevada and California. Nevada Archeological Survey, Research Paper 7, pp. 137.
- Davis, J.O., 1985. Correlation of late Quaternary tephra layers in a long pluvial sequence near Summer Lake, OR. *Quaternary Research* 23, 38–53.
- Fairbanks, R.G., Mortlock, R.A., Chiu, T.C., Li, C., Kaplan, A., Guilderson, T.P., Fairbanks, T.W., Bloom, A.L., 2005. Marine Radiocarbon Calibration Curve Spanning 0 to 50,000 Years B.P. Based on Paired $^{230}\text{Th}/^{234}\text{U}/^{238}\text{U}$ and ^{14}C Dates on Pristine Corals. *Quaternary Science Reviews* 24, 1781–1796.
- Friedel, D.E., 1993. Chronology and climatic controls of late Quaternary lake-level fluctuations in Chewaucan, Fort Rock, and Alkali basins, south-central Oregon. Ph.D. Thesis, University of Oregon.
- Hargrave, J.E., 2009. Lithostratigraphy and fossil avifaunas of the Pleistocene Fossil Lake Formation, Fossil Lake, Oregon, and the Oligocene Etadunna Formation, Lake Palankarinna, Southern Australia. Ph.D. Thesis, University of Oklahoma.

- Kuehn, S.C., Negrini, R.M., 2010. A 250 k.y. record of Cascade arc pyroclastic volcanism from late Pleistocene lacustrine sediments near Summer Lake, Oregon, USA. *Geosphere* 6, 397–429.
- Martin, J.E., 1996. First occurrence of *Cynomys* from west of the Rocky Mountains. *Journal of Vertebrate Paleontology* 16 (Supplement), 51A.
- Martin, J.E., Patrick, D., Kihm, A.J., Foit Jr., F.F., Grandstaff, D.E., 2005. Lithostratigraphy, tephrochronology, and rare earth element geochemistry of fossils at the classical Pleistocene Fossil Lake Area, South Central Oregon. *Journal of Geology* 113, 139–155.
- Negrini, R.M., Erbes, D.B., Faber, K., Herrera, A.M., Roberts, A.P., Cohen, A.S., Wigand, P.E., Foit, F.F., Jr., 2000. A paleoclimate record for the past 250,000 years from Summer Lake, Oregon, U.S.A. I. Chronology and magnetic proxies for lake level. *Journal of Palaeolimnology* 23, 125–149.
- Poppe, L.J., Eliason, A.H., 2008. A visual basic program to plot grain-size data on ternary diagrams. *Computers and Geosciences* 34, 561–565.
- Shepard, F.P., 1954. Nomenclature based on sand–silt–clay ratios. *Journal of Sedimentary Petrology* 24, 151–158.
- Williams, S.K., 1994. Late Cenozoic tephrastatigraphy of deep sediment cores from the Bonneville Basin, northwest Utah. *Geological Society of America Bulletin* 106, 1517–1530.

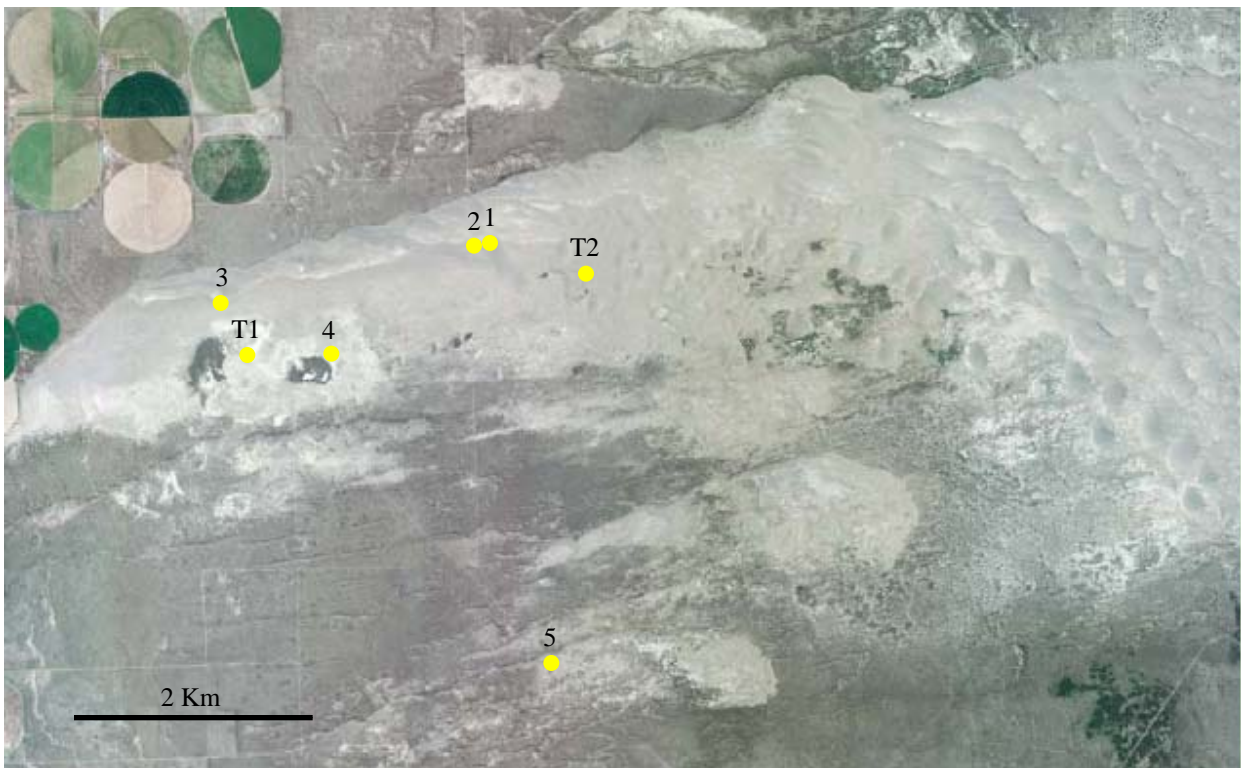


Fig. 1. Aerial photograph of Fossil Lake with core and trench locations.

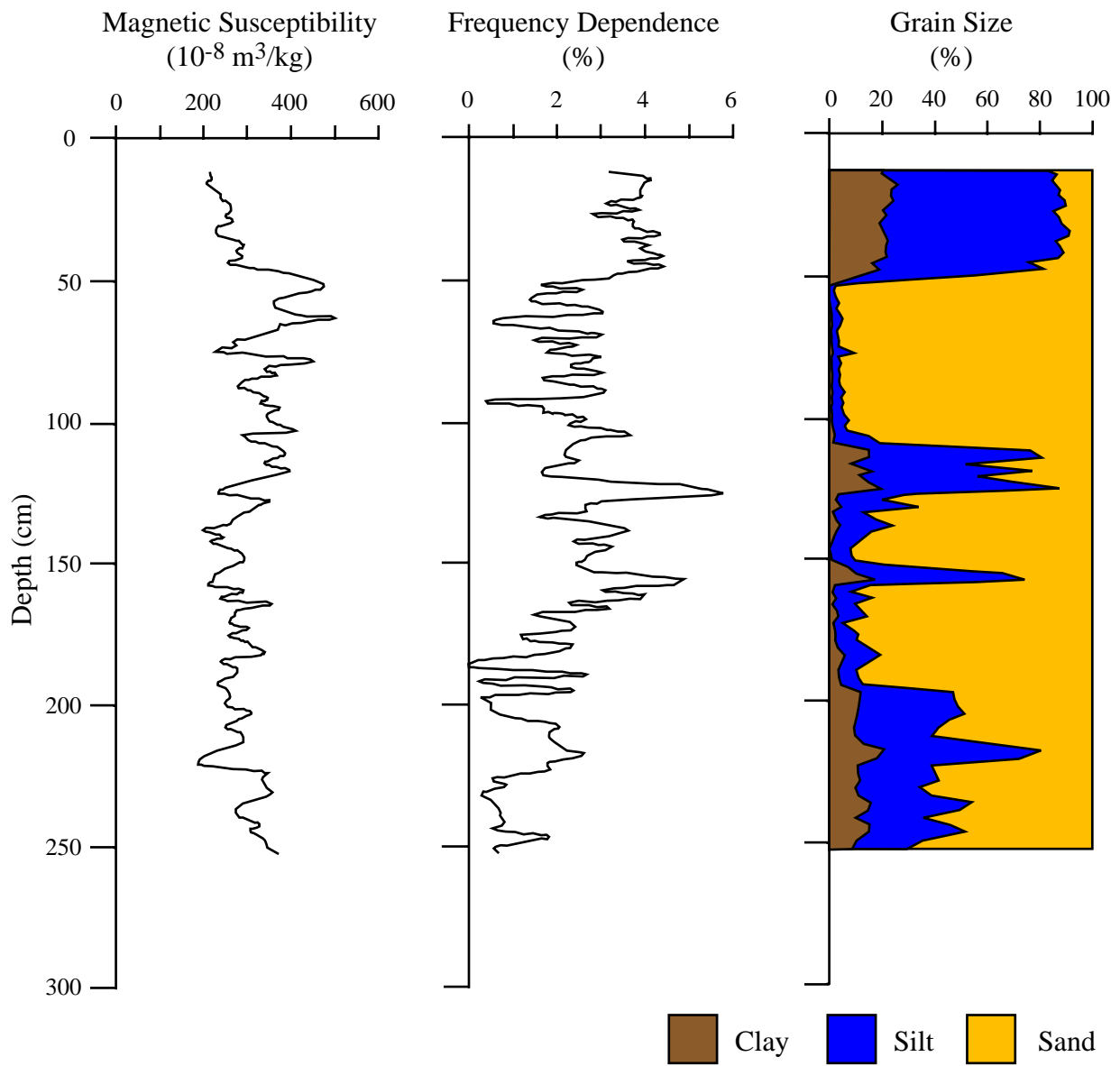


Fig. 2. Magnetic susceptibility, frequency dependence percentages and grain size percentages for core 1.

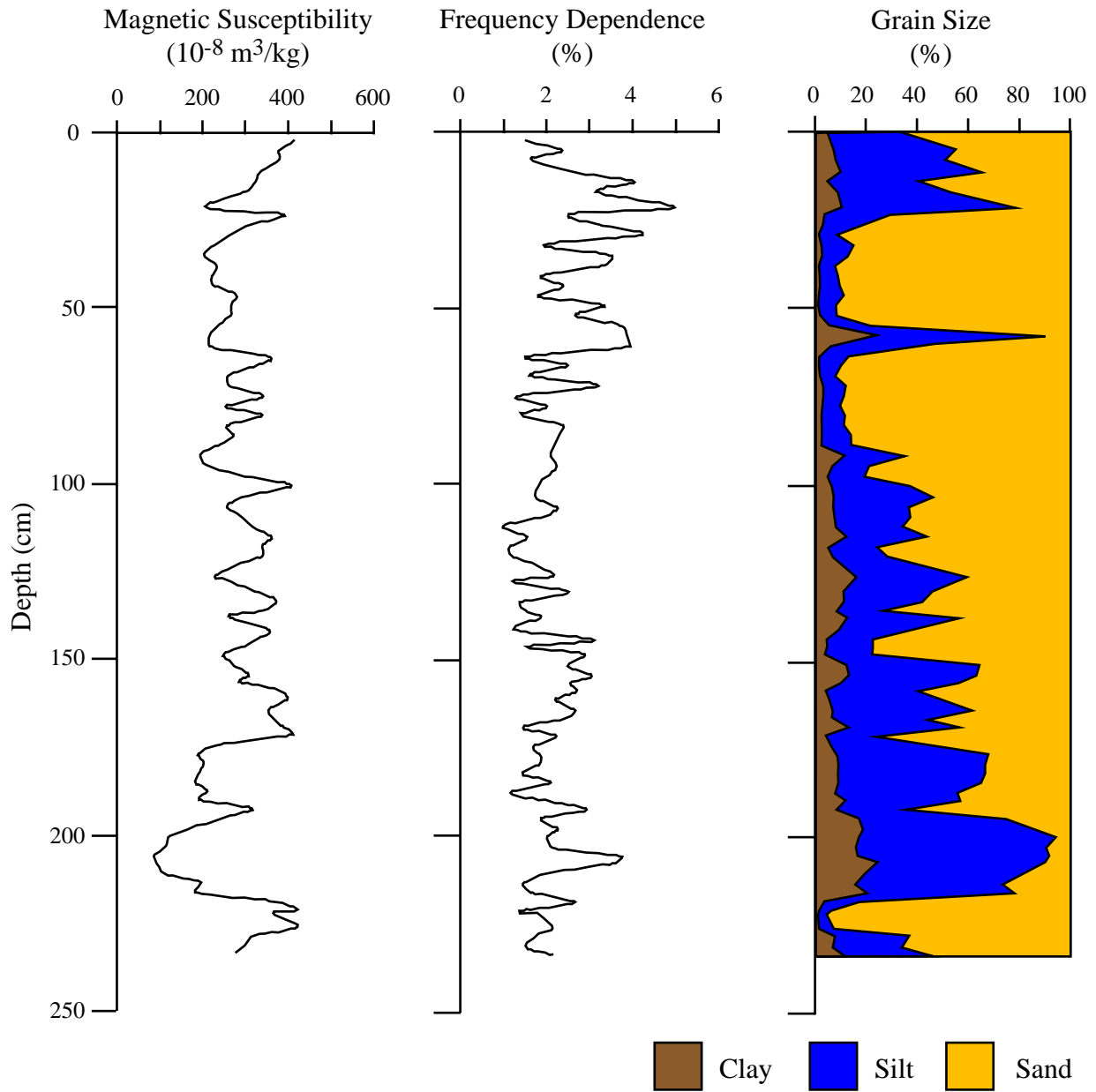


Fig. 3. Magnetic susceptibility, frequency dependence percentages and grain size percentages for core 2.

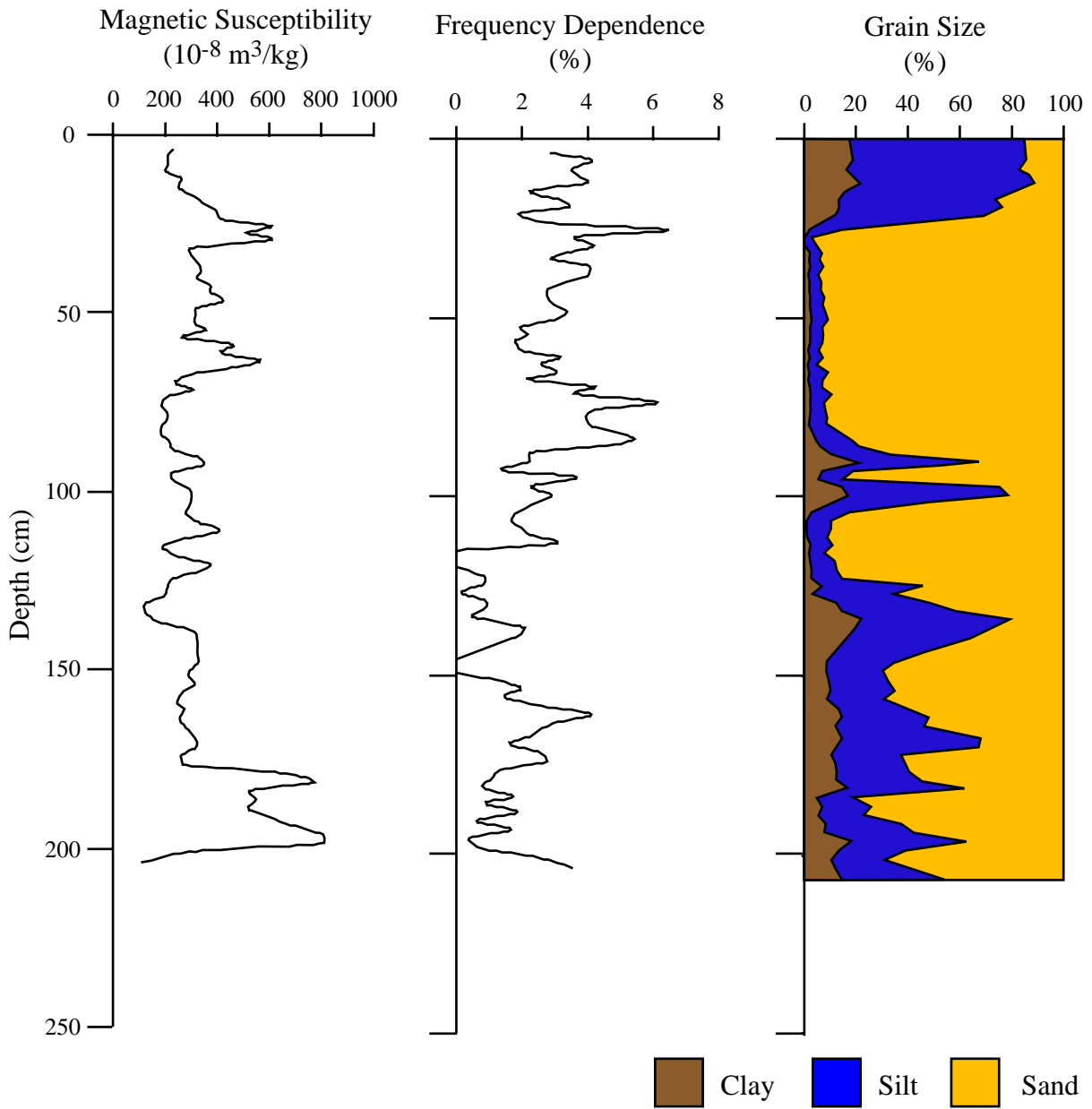


Fig. 4. Magnetic susceptibility, frequency dependence percentages and grain size percentages for core 3.

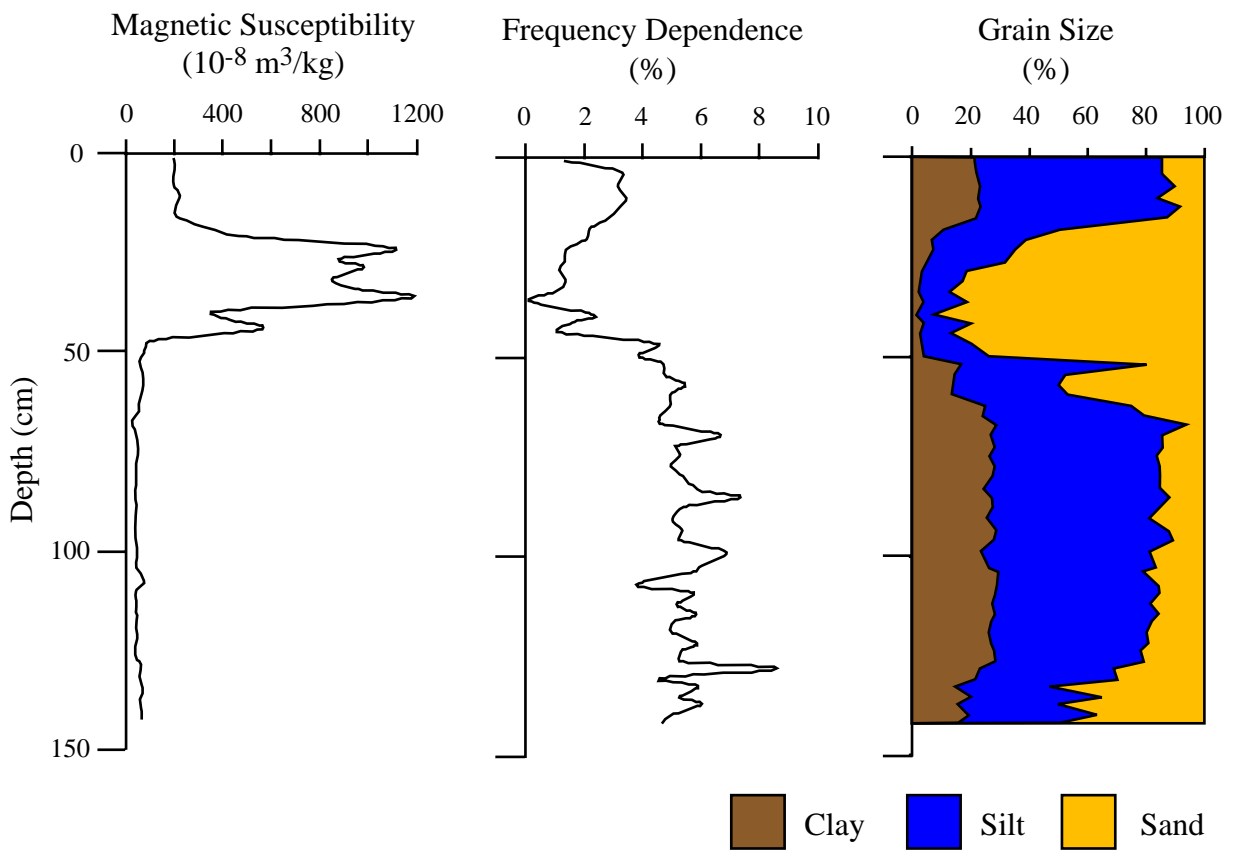


Fig. 5. Magnetic susceptibility, frequency dependence percentages and grain size percentages for core 4.

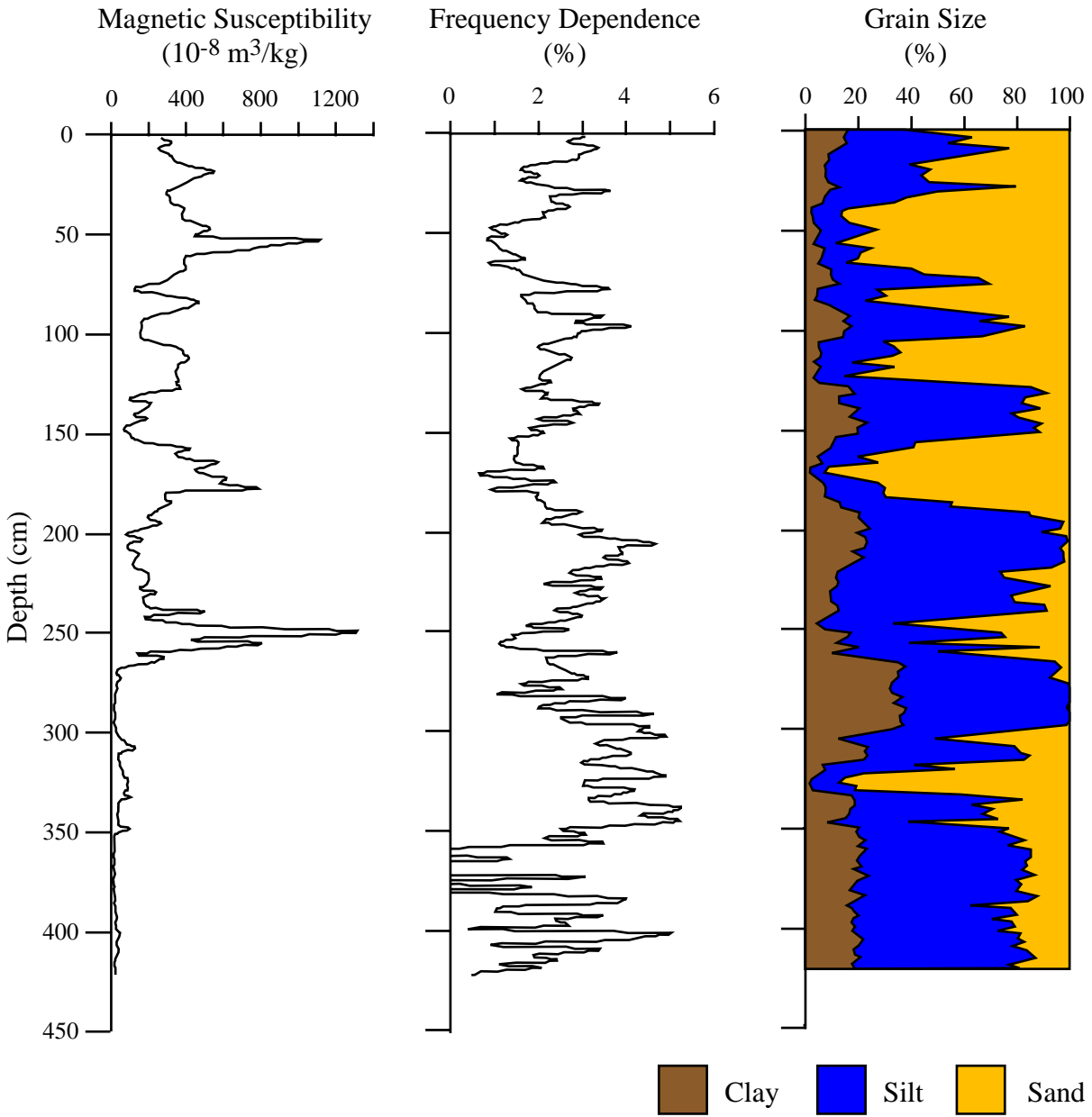
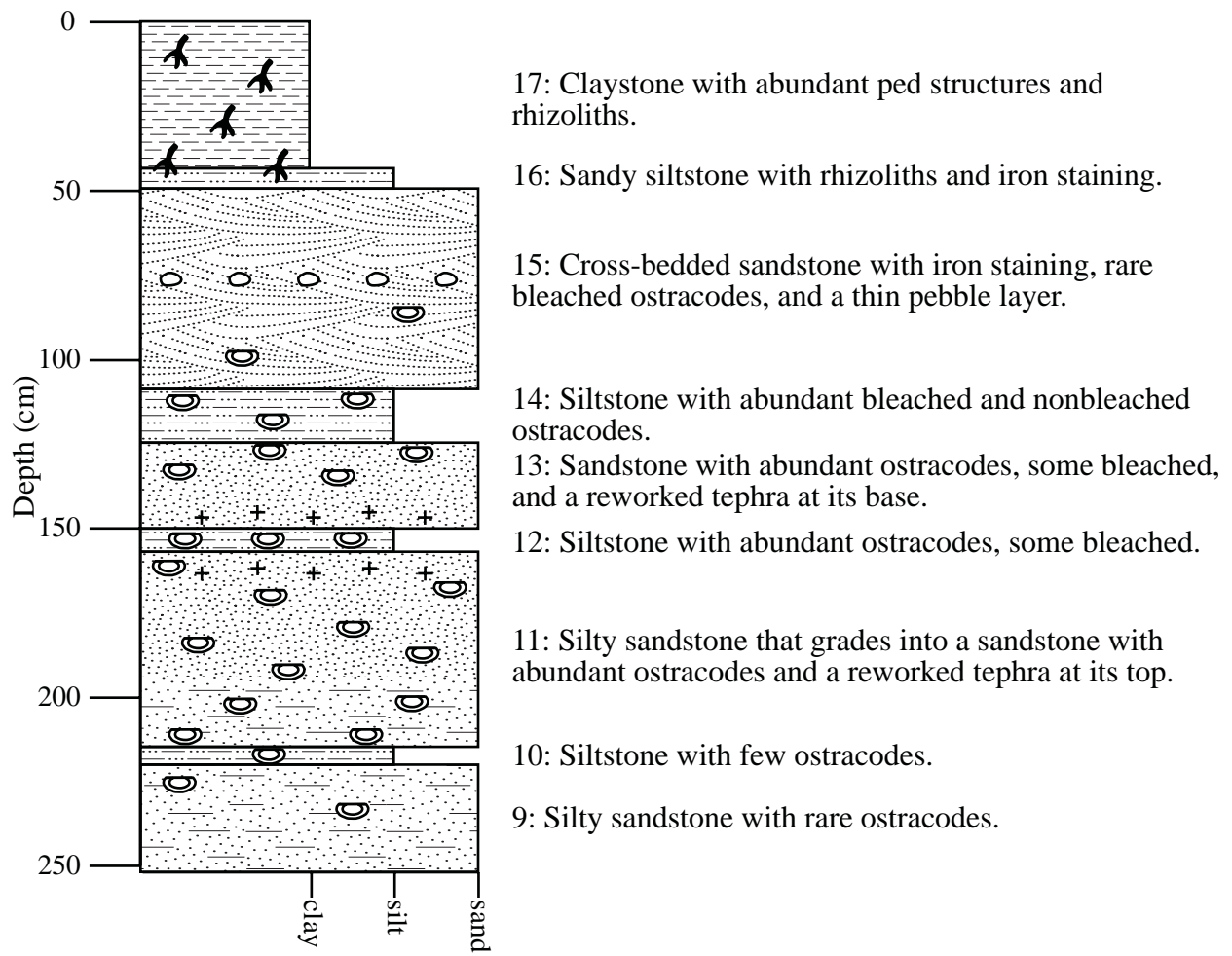


Fig. 6. Magnetic susceptibility, frequency dependence percentages and grain size percentages for core 5.



Key for all lithostratigraphic figures

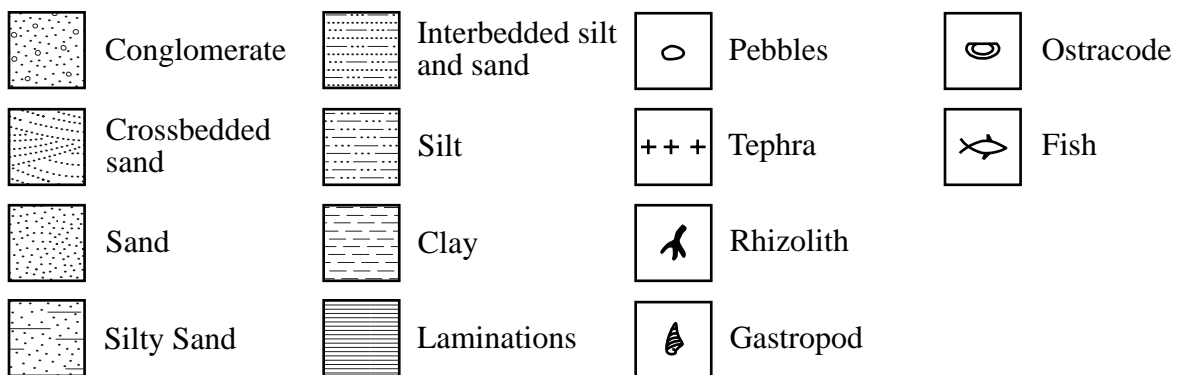


Fig. 7. Lithostratigraphy of core 1.

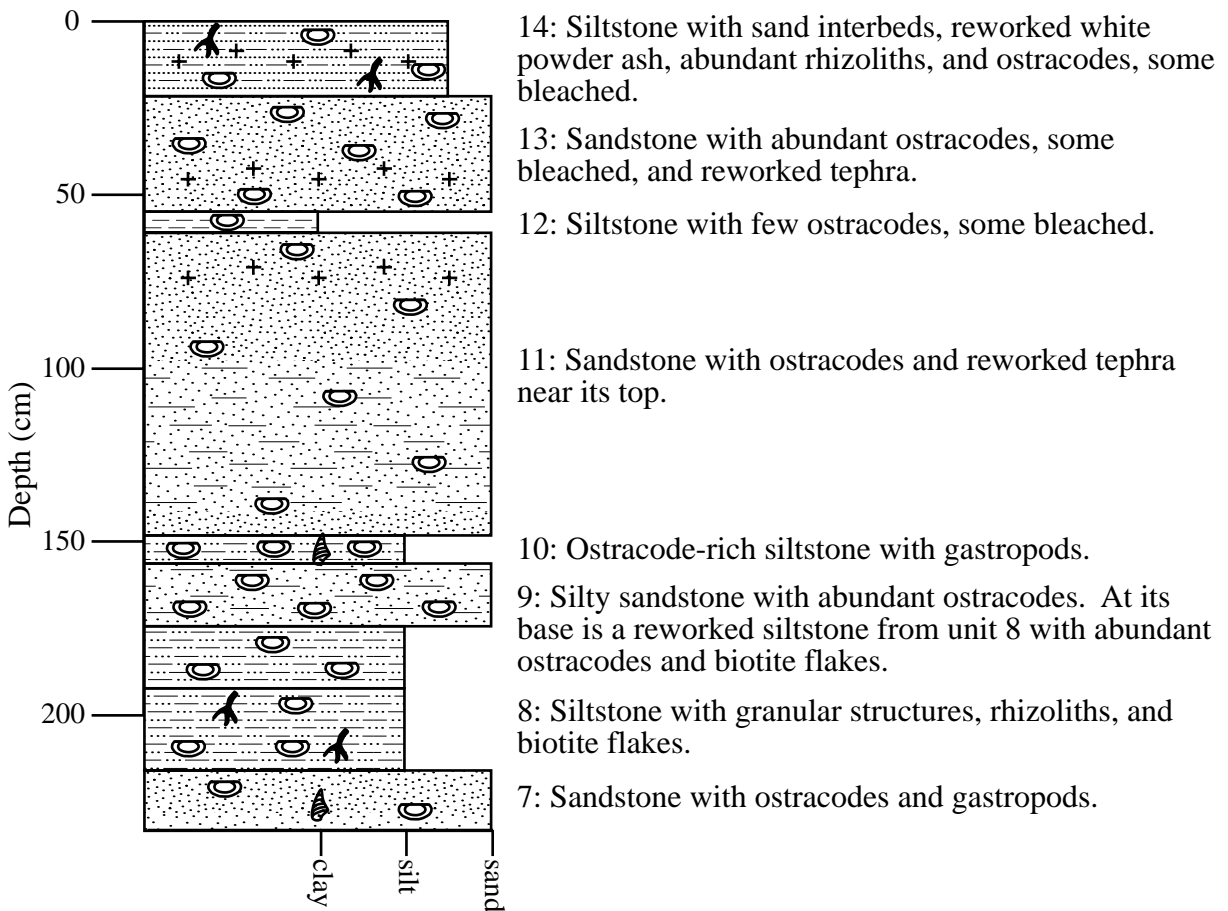


Fig. 8. Lithostratigraphy of core 2. See Fig. 7 for key to symbols.

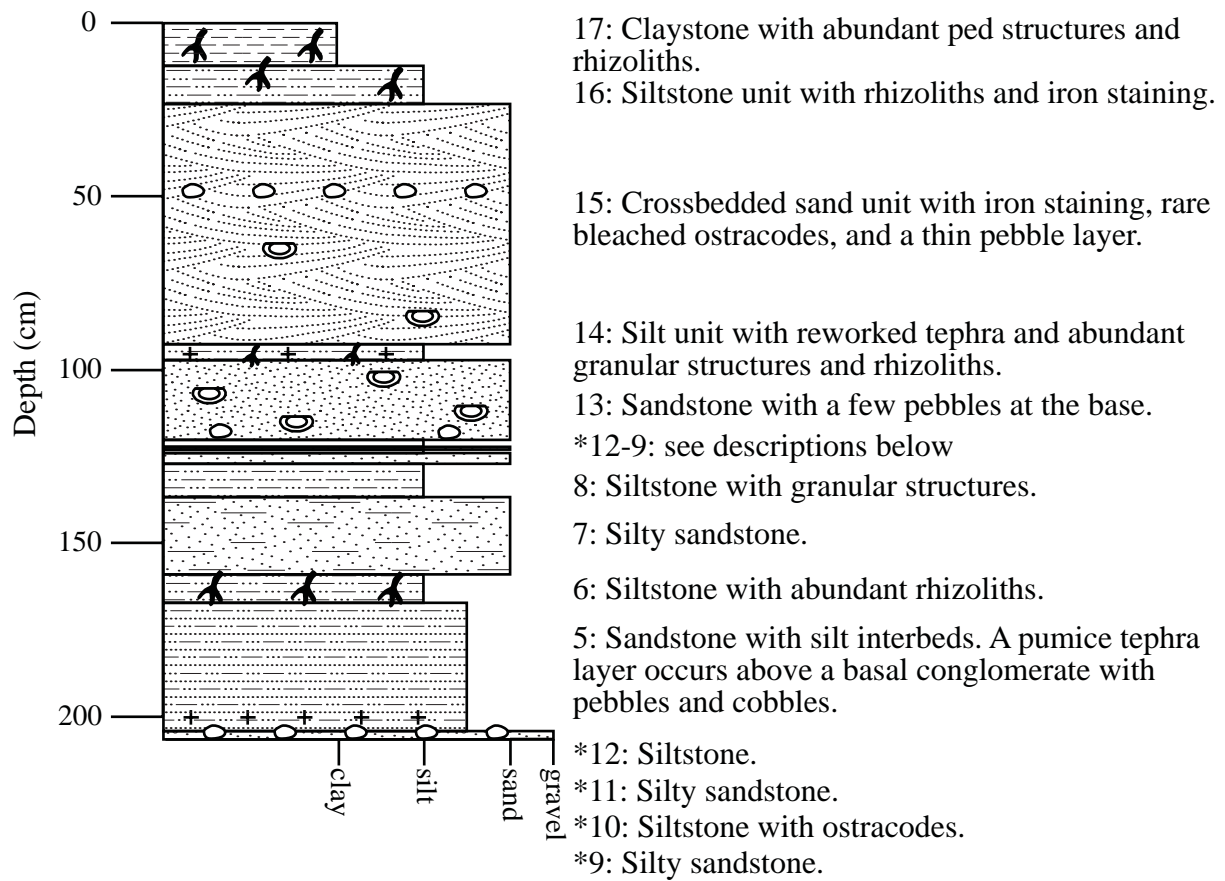


Fig. 9. Lithostratigraphy of core 3. See Fig. 7 for key to symbols.

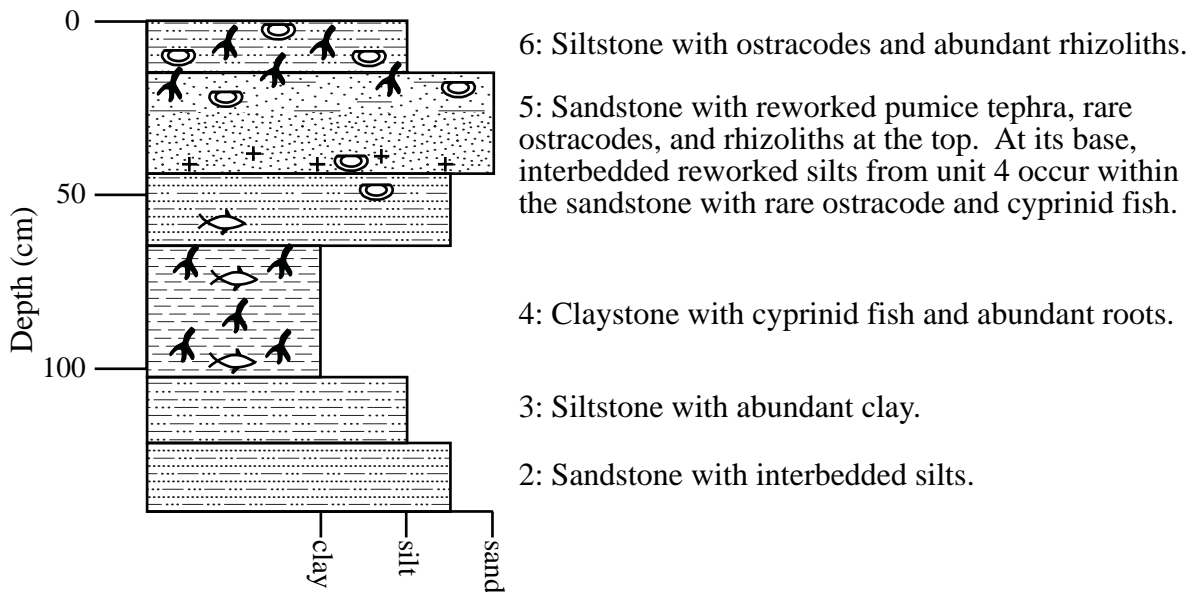


Fig. 10. Lithostratigraphy of core 4. See Fig. 7 for key to symbols.

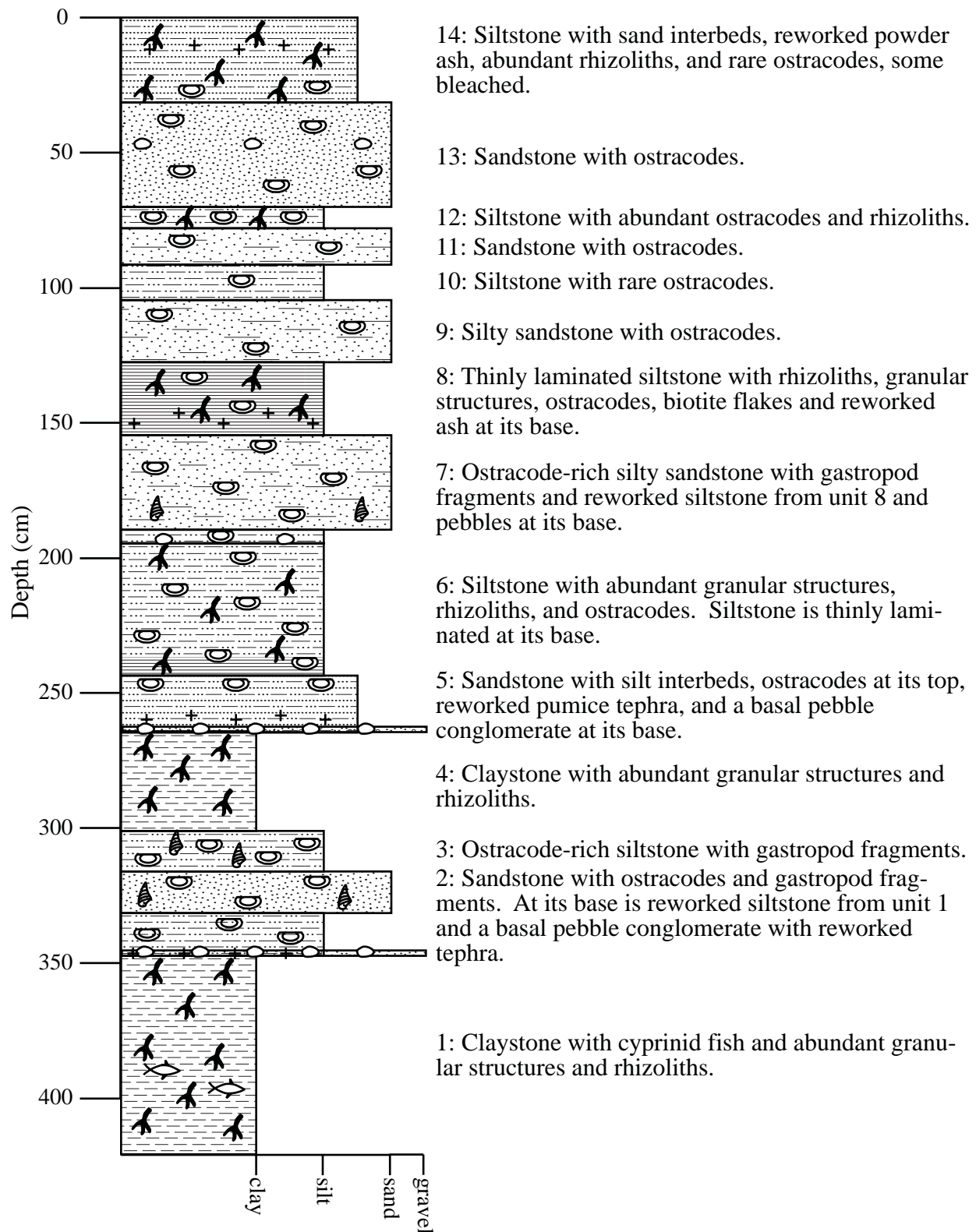


Fig. 11. Lithostratigraphy of core 5. See Fig. 7 for key to symbols.

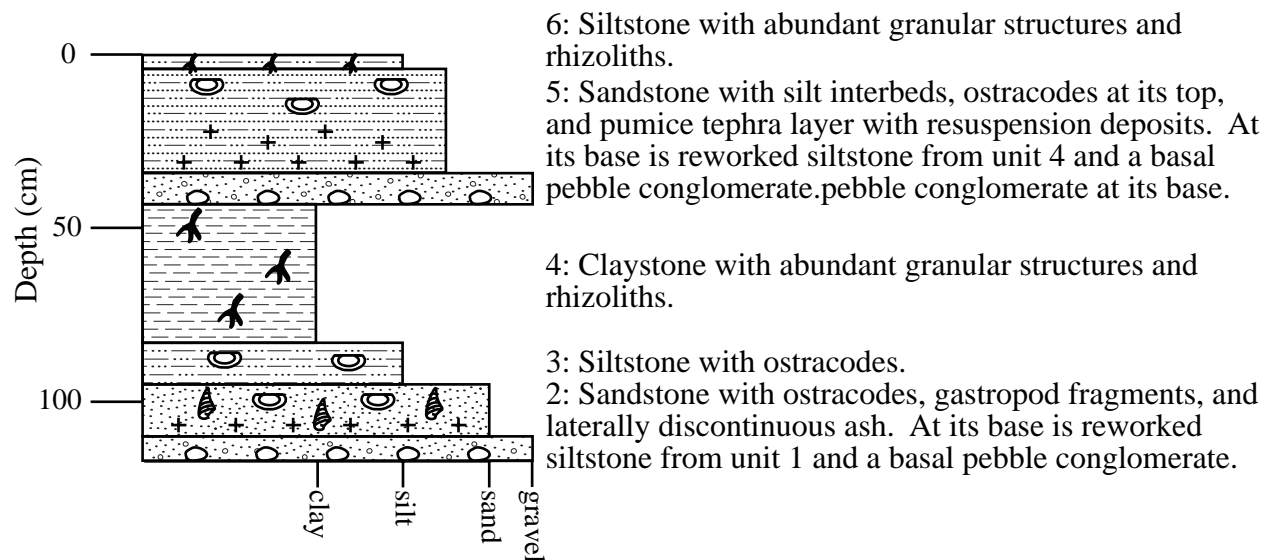


Fig. 12. Lithostratigraphy of trench 1. See Fig. 7 for key to symbols.

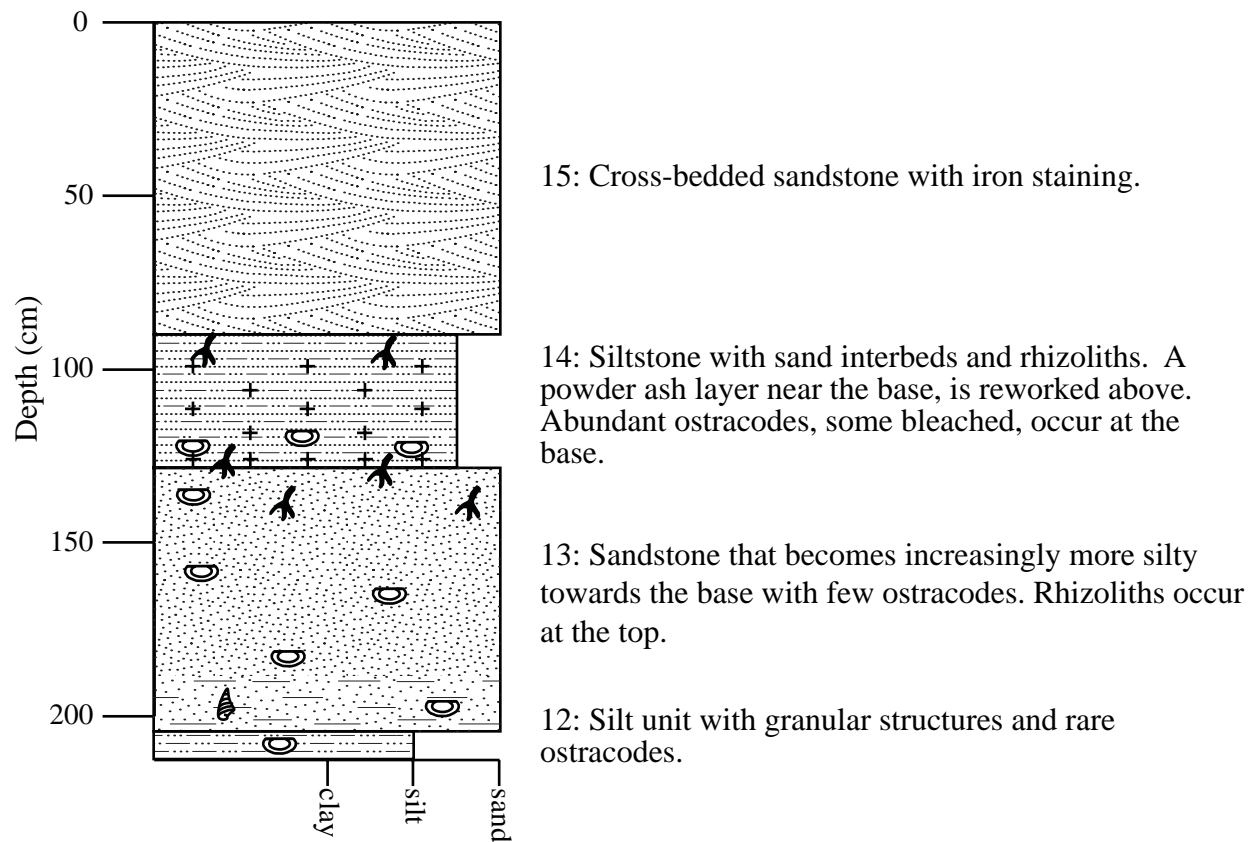


Fig. 13. Lithostratigraphy of trench 2. See Fig. 7 for key to symbols.

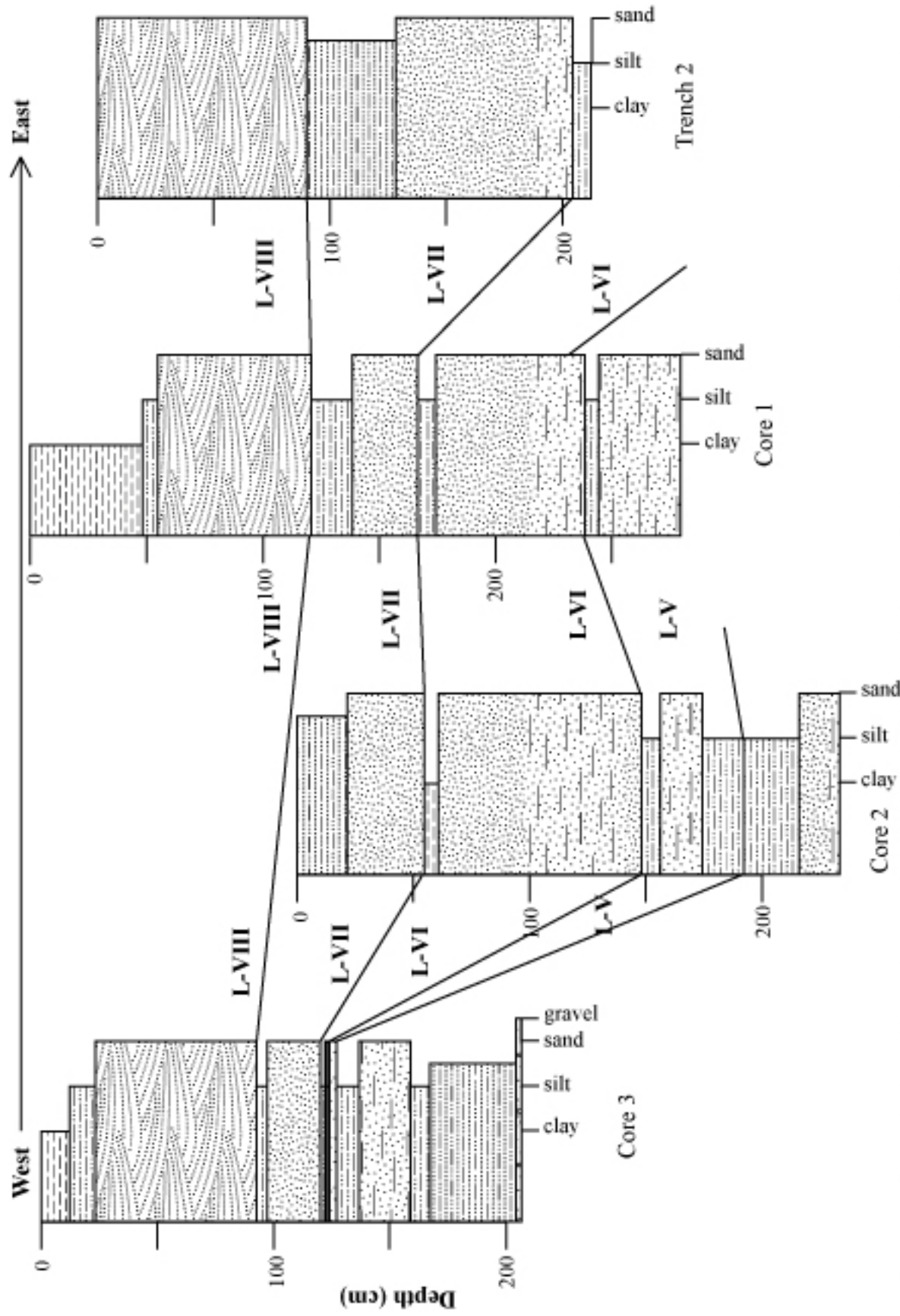


Fig. 14. Lithostratigraphy cross-sections in a west-east transect through the northern part of Fossil Lake Basin. See Fig. 7 for key to symbols.

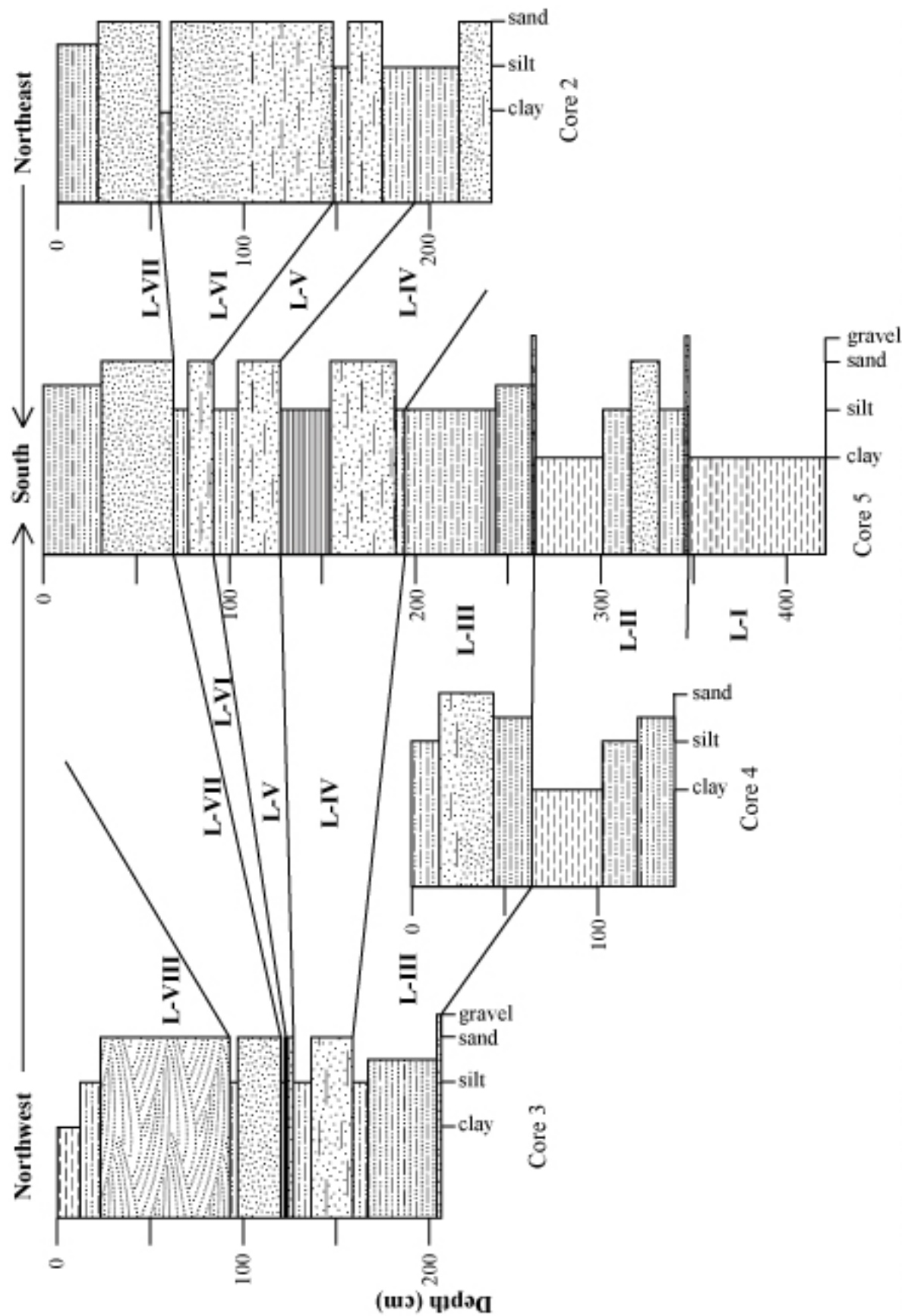


Fig. 15. Lithostratigraphy cross-sections in a northwest-south-northeast transect through the western part of Fossil Lake Basin. See Fig. 7 for key symbols.

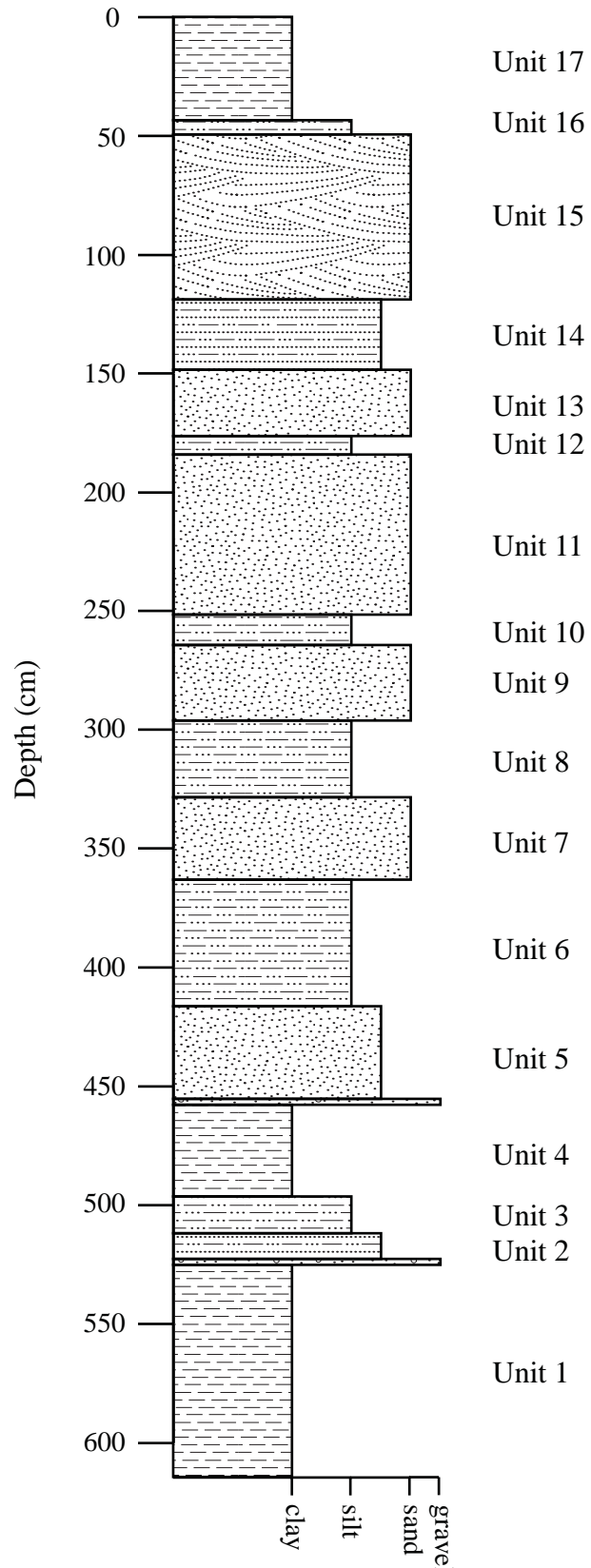


Fig. 16. Composite lithostratigraphic section of Fossil Lake. See Fig. 7 for key to symbols.

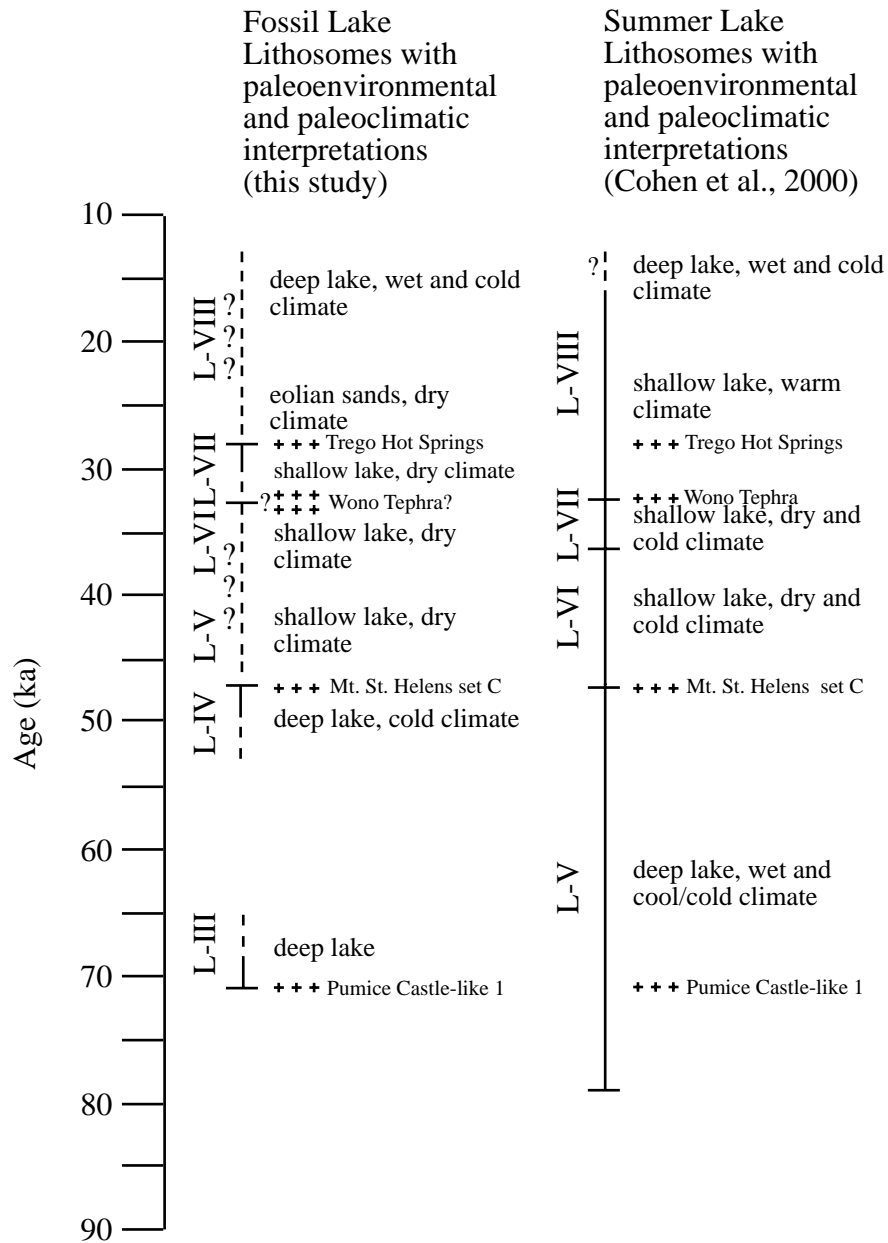


Fig. 17. Comparison of Fossil Lake and Summer Lake (Cohen et al., 2000) lithosomes (L) with paleoenvironmental and paleoclimatic interpretations. Correlations based on tephra marker beds (cross symbols).

CHAPTER 3

FOSSIL LAKE OSTRACODE FAUNAL ASSEMBLAGES

Introduction

Ostracodes are bivalved, aquatic microcrustaceans with carapaces composed of low-magnesium calcite. The valves of ostracodes are commonly preserved in lacustrine or paludal sediments. Modern lacustrine ostracode species can be highly sensitive to environmental change because their life cycle—egg hatching, growth, and reproduction—is coupled to specific environmental conditions. Modern studies of lacustrine ostracode species have found that their presence, absence, and abundance in lacustrine environments of an individual species are controlled primarily by their tolerances for dissolved ion content and total dissolved solids (TDS) (Delorme, 1969; Forester, 1983; 1986; 1991a), and water temperature (Delorme and Zoltari, 1984; DeDeckker and Forester, 1988; Foster, 1991a). For example, *Mytilocypris henricae* ostracode populations take between 4 and 5 months to reach maturity during the winter but only take between 2 and 2.5 months during the summer. The eggs of this *Mytilocypris henricae* will not hatch below certain temperatures (Martens et al., 1985).

By studying modern ostracode assemblages from lakes with various hydrochemical properties in the northern Midwest, Smith (1993) found that distinct ostracode assemblages are associated with certain hydrochemical lake types. Since lake temperature and chemistry are linked to regional climate, ostracode distribution can also be linked to regional climate, allowing fossil ostracodes to be used as a proxy in paleoclimate and paleohydrochemical reconstructions (Forester, 1991b), assuming that the hydrochemical and environmental tolerance of ostracode species have not significantly changed in the recent past. The purpose of this investigation is to

reconstruct the paleohydrology and paleoclimate of Fossil Lake, Oregon, for the past ~71 ka from fossil ostracode faunal assemblages.

Methods

The samples used in this investigation were taken from core 5, Lithosomes III-VII, and core 1, Lithosome VIII, representing ~ 71–13 ka. Cores were sampled with 8 cc paleomagnetic cubes, approximately every 2.5 cm. From each cube, 1.0-g subsamples were processed for ostracodes. The subsamples were screened through 425 μm , 250 μm , and 180 μm sieves to remove silts and clays. Each sieve residue was analyzed under a Bausch and Lomb StereoZoom 4 (zoom range 0.7–3X) stereoscopic microscope. Ostracode valves and carapaces were picked from the residue using a 20/0 paintbrush. All ostracodes were identified by A. J. Smith at Kent State University. Ostracode valves were counted for each sample and the percentage of each species and the adult:juvenile ratios were calculated. Taphonomic features were also recorded, including fragmentation, recrystallization (including steinkerns), oxidation staining, bleaching, and coatings. Taphonomic percent averages and standard deviation for each lithosome were calculated from samples that contained more than 20 ostracode valves. Representative specimens were examined and photographed at the University of Akron using an FEI Quanta 200 Environmental Scanning Electron Microscope (ESEM). An attached energy dispersive X-ray analyzer (EDX) was used to determine elemental composition of ostracode coatings.

Results

A total of four species of ostracodes, *Candona patzcuaro*, *Fabaeformiscandona caudata*, *Limnocythere ceriotuberosa*, and *L. platyforma*, occur in Fossil Lake sediments for the past ~ 71

ka (Plate 1). Ostracode abundance is highly variable (Fig. 1 and 2). Low abundance was generally associated with samples that contained evidence of pedogenesis or abundant tephra grains. *Limnocythere ceriotuberosa* and *C. patzcuaro* were common throughout all the lithosomes.

Photomicrographs and EDX maps of the ostracode coatings indicated two different types of coatings. The most common type of ostracode coating observed was a white coating dominated by silica (Si), oxygen (O), and aluminum (Al) with lesser amounts of calcium (Ca), sodium (Na), iron (Fe) and magnesium (Mg) (Fig. 3). This aluminosilicate coating varied in thickness and coverage. Thin coats generally did not cover the entire valve, but were observed along the edges of the valves or filling in the reticulate ornamentation of *Limnocythere* species. Thicker coats mostly or entirely covered the valve. Crystal size was too small to determine mineralogy of the coating.

The second type of ostracode coating is composed calcium carbonate (CaCO_3). The carbonate coatings are thicker generally than the aluminosilicate coatings and cover the entire ostracode valve. Under ESEM some specimens were observed with an aluminosilicate coating on top of a carbonate coating (Fig. 4).

In Lithosome III (~ 71 ka), ostracode abundance is highly variable, 0–794 ostracodes g^{-1} (n= 29). Ostracodes are rare at the base of the lithosome, associated with a tephra deposit. Ostracodes are moderately fragmented, $18.3 \pm 11.6\%$ (n=13), rarely stained, $2.3 \pm 3.3\%$, rarely bleached, $1.5 \pm 2.3\%$, and rarely recrystallized, < 1 valves g^{-1} . Ostracode coatings are variable in this lithosome, $71.4 \pm 45.6\%$. Thin coatings are rare at the base of this lithosome and abundant at the top. Whole carapaces are common. The fauna is dominated by *L. ceriotuberosa* and *C.*

patzcuaro with rare occurrences of *L. platyforma*. At the top of the lithosome, ostracode abundance significantly decreases as a result of pedogenesis, and only *C. patzcuaro* are present.

In Lithosome IV (~ 47 ka), ostracode abundance is highly variable, 22–378 ostracodes g⁻¹ (n= 27). Ostracodes are moderately fragmented, 20.8 ± 8.7% (n=27), rarely stained, 4.7 ± 8.7%, and abundantly coated, 92.7 ± 13.4%. Ostracode coatings are generally very thin.

Recrystallized carapaces and valves are most common in the basal sandstone unit, 39.6 ± 27.9 valves g⁻¹, of this lithosome, but are rare in the upper siltstone, 2.4 ± 7.2 valves g⁻¹. Whole carapaces are common. The fauna is dominated by *L. ceriotuberosa* with common occurrences of *C. patzcuaro* and minor occurrences of *L. platyforma*. *Fabaeformiscandona caudata* appears in the middle of the lithosome and becomes abundant near the top of the lithosome. A low percentage of adults was observed in *C. patzcuaro*, 1.7 ± 2.5%, and *F. caudata*, 3.0 ± 4.9%.

In Lithosome V, ostracode abundance is low, 7–181 ostracodes g⁻¹ (n= 14). Ostracodes are moderately fragmented, 21.0 ± 12.8% (n=12), moderately stained, 14.7 ± 6.1%, rarely recrystallized, 8.8 ± 5.9 valves g⁻¹, and abundantly coated, 98.0 ± 2.3%. Thin ostracode coatings occur in the basal sandstone, while thicker coatings occur in the upper siltstone. The fauna is dominated by *L. ceriotuberosa* with common occurrences of *C. patzcuaro* and *L. platyforma* and minor occurrences of *F. caudata*. A low percentage of adults was observed in *L. platyforma*, 1.9 ± 4.0%, and no adults of *F. caudata* were observed.

In Lithosome VI, ostracode abundance is low in the basal sandstone, 4–96 ostracodes g⁻¹ (n= 4), but moderately abundant in the upper siltstone, 226–551 ostracodes g⁻¹ (n= 4). Ostracodes are moderately fragmented, 25.5 ± 7.7% (n=6), moderately stained, 17.7 ± 16.9%, low to moderately recrystallized, 13.8 ± 14.0 valves g⁻¹, and abundantly coated, 88.5 ± 11.9%. Thick ostracode coatings occur in the basal sandstone, while thinner coatings occur in the upper

siltstone. The fauna is dominated by *L. ceriotuberosa* with minor occurrences of *C. patzcuaro*, *L. platyforma*, and *F. caudata*. A low percentage of adults were observed in *L. platyforma*, $2.1 \pm 2.4\%$, and only one *F. caudata* adult was observed.

In Lithosome VII (~27 ka), ostracode abundance is low, 0–117 ostracodes g^{-1} (n= 27). Ostracodes are highly fragmented, $27.6 \pm 9.9\%$ (n=13), highly stained, $47.6 \pm 31.8\%$, moderately recrystallized, 16.3 ± 10.6 valves g^{-1} , rarely bleached, <1%, and abundantly coated, $93.2 \pm 10.9\%$. Ostracode coatings are generally thick. In the basal sandstone, the fauna is dominated by *L. ceriotuberosa* and *L. platyforma* with minor occurrences of *C. patzcuaro*. In the upper siltstone, the fauna is dominated by *C. patzcuaro* with minor occurrences of *L. ceriotuberosa*.

In Lithosome VIII (~15.4 ka), ostracodes were extremely rare, 0–12 ostracodes g^{-1} (n=53), and were only found in the sandstone unit. A total of 44 ostracodes were observed in this lithosome from 13 samples. All of the ostracodes were bleached and stained, half were fragmented, and none were coated. The fauna was composed of *L. ceriotuberosa*, *C. patzcuaro*, and *L. platyforma*.

Discussion

Ostracodes of Fossil Lake

All of the ostracode species present in the Fossil Lake sediments were common in Great Basin pluvial lakes during the Pleistocene and can still be found in modern lacustrine environments. The most common species, *Limnocythere ceriotuberosa*, is euryhaline and eurythermic. It typically lives in alkaline waters that have strong seasonality in volume and associated chemistry (Bradbury and Forester, 2002) and salinities that range from ~ 500–25,000

ppm (Forester, 1987), however, it can tolerate higher salinities in Cl⁻ dominated waters (Forester, 1986). Today, *L. ceriotuberosa*, is found living in deep or shallow to ephemeral lakes above the frost line in the Great Basin, central prairies, and Canada (Delorme, 1971; Forester, 1985; 1987).

Candona patzcuaro prefers to live in freshwater environments, but can tolerate higher salinities. Today, *C. patzcuaro* lives in deep or shallow to ephemeral lakes in North America. The length of the life cycle for *C. patzcuaro* is temperature dependent and generally requires three to six months of standing water (Markgraf and Lennon, 1986; Palacios-Fest, 1994), but it can survive desiccation events through torpidity (Horne, 1993).

Today *Fabaeformiscandona caudata* lives in freshwater lakes at considerable depths and in streams (Delorme, 1970). Like *L. ceriotuberosa*, *F. caudata* is a eurythermic species that is only found living above the frostline, suggesting that their life cycle may require cold temperatures (Forester, 1991b). *Limnocythere platyforma* typically lives in relatively freshwater, cold, alkaline lakes (Palacios-Fest et al., 2002).

Paleoclimate and Paleohydrology Interpretation

Using modern ostracode assemblages and their modern environmental tolerances, we can hypothesize a paleoclimatic and paleohydrologic history for Fossil Lake for the past ~ 71 ka (Fig. 4). Unconformities at the base of each lithosome suggest that at least six periods of oscillations between wet and dry conditions existed. The major unconformity at the base of Lithosome III, indicates that the basin was arid prior to flooding at ~ 71 ka. As the basin began to fill, rare *Limnocythere ceriotuberosa* and *Candona patzcuaro* are preserved in the sediment. The rarity of ostracodes at the initiation of flooding is likely the result of a high energy flooding event, as indicated by the cobble/pebble conglomerate layer. Above the conglomerate,

ostracodes continue to be rarely preserved, the result of the pumice tephra depositional layer. Above the tephra layer, ostracode abundance increases but is highly variable, suggesting fluctuating water depths or water conditions or changes in clastic sedimentation. The ostracodes were observed with moderate fragmentation, rare oxidation staining, and frequently as whole carapaces, indicating deposition in a relatively deep and calm environment. The co-dominance of *L. ceriotuberosa* and *C. patzcuaro* suggest a slightly saline, alkaline lake. While rare, *Limnocythere platyforma* is present for a short period of time in this lithosome, suggesting a brief period of decreased salinity and cooler temperatures, possibly the result of seasonality or increased precipitation or stream flow into the basin. Salinity remained too high for the presence of the freshwater species *Fabaeformiscandona caudata*. Increases in the ostracode fragmentation, coatings, and bleaching near the top of the lithosome are consistent with shallow lake levels. Rare ostracodes are preserved at the top of Lithosome III, likely the result of pedogenetic acidification.

After another period of aridity, wetter conditions returned and the basin began to refill at the base of Lithosome IV. The ostracode fauna at the base of Lithosome IV is dominated by *L. ceriotuberosa* indicating a saline and alkaline environment. Minor occurrences of *L. platyforma* suggest seasonal dilution and cool to cold water temperatures. Increased fragmentation in ostracode valves at the base suggests shallow water conditions. Near the top of the lithosome, ~ 47 ka, *F. caudata* appears and quickly becomes common in the sediment indicating a relatively freshwater, deep lake formed from wetter conditions. Abundant whole carapaces, moderate fragmentation, and rare oxidation staining also suggest a calm, deep lake. The co-occurrence of *L. ceriotuberosa* and *F. caudata* suggests seasonal precipitation and evaporation resulting in cycles of dilution and solute concentration (Forester, 1991b). The dearth of adult fossils of *C.*

patzcuaro and *F. caudata* may suggest either an “end product” assemblage from a low energy transport of juveniles from an original death assemblage (Whatley, 1983) or the result of fragmentation. The large size of adult specimens of *C. patzcuaro* and *F. caudata* made them more susceptible to breakage and the similar carapace features make species identification difficult to determine from fragmented carapaces. A shallow lake ostracode assemblage was not observed at the top of Lithosome IV suggesting that desiccation of the lake was very rapid or part of the record was eroded by deflation.

Throughout most of Lithosomes V–VII, ostracode valves are moderately to highly fragmented, moderately stained, and highly coated suggesting deposition in an agitated shallow water environment. Unconformities at the top of each of these lithosomes suggest fluctuating wet and dry periods. Lithosomes V and VI have similar ostracode assemblages, dominated by *L. ceriotuberosa* with minor to common occurrences of *C. patzcuaro* and *L. platyforma*, indicating a cold, saline and alkaline lake with fluctuating salinities from increased precipitation or stream inflow or increased seasonal dilution cycles. *Fabaeformiscandona caudata* is present, but in low numbers in Lithosomes V and VI, suggesting a seasonal dilution cycle or that they were transported in from freshwater streams. At the top of Lithosome VI, ostracode abundance increases significantly and the number of oxidation stained valves decreases, suggesting increasing water depths. The dearth of adult fossils of *L. platyforma* and *F. caudata* in Lithosome V and VI suggest favorable environmental conditions existed for their eggs to hatch but conditions became unfavorable, likely because of increases in salinity, before many individuals could reach adulthood. In the basal unit of Lithosome VII, *L. platyforma* becomes co-dominant with *L. ceriotuberosa*, indicating a cold, relatively freshwater lake with increased alkalinity. The absence of *F. caudata* in the basal unit of Lithosome VII is likely the result of

increased alkalinity or shallow water conditions, not from higher salinities. In the top siltstone unit of Lithosome VII (~ 27 ka), the ostracode fauna is dominated by *C. patzcuaro*, suggesting freshwater conditions, but the low abundance of ostracodes throughout the upper unit limits additional paleoenvironmental interpretations. Rare ostracodes are preserved at the top of Lithosome VII, likely the result of pedogenic dissolution.

At the base of the Lithosome VIII, rare *L. ceriotuberosa* and *C. patzcuaro* fossils are preserved in eolian sandstone. All of the ostracodes were bleached from subaerial exposure and only half of the ostracodes were broken, suggesting a relatively short transportation distance. These transported ostracodes in the eolian sands may be from either a nearby time-equivalent shallow lake or playa environment, or represents older fossil ostracodes that were exposed and transported during deflation and deposition of eolian dunes. No ostracodes are preserved in the lacustrine sediments at the top of Lithosome VIII, likely the result of pedogenic dissolution.

The aluminosilicate ostracode coatings likely are either aluminum phyllosilicate clay or a zeolitic coating. Volcanic glass can alter rapidly in saline, alkaline lakes to produce various authigenic clay and zeolite minerals (Sheppard and Gude, 1968; 1973). Ostracodes coatings are very common throughout Lithosomes III–VII, corroborating that Fossil Lake was alkaline and saline or seasonally saline.

Another paleohydrologic reconstruction study was conducted by Martin et al. (2005) using rare earth element (REE) analysis of vertebrate bones to determine changes in salinity and alkalinity. REEs in fossil bones reflect the water composition (lake or groundwater) during fossilization. Modern lakes with low alkalinity and near-neutral pH produced flat REE signatures, whereas highly saline, alkaline lakes produced signatures that are high REE (HREE) enriched and with positive Ce anomalies (Martin et al., 2005). One to seven fossil bones from

each unit were analyzed. Fossil bones from Lithosomes (Martin et al.'s packages) III, IV, V, and the basal unit of VII exhibited flat REE signatures while bones from Lithosome VI, the upper unit of VII, and VIII exhibited positive Ce anomalies. From the REE signatures, Martin et al. (2005) reconstructed a low-resolution paleoenvironment history for Fossil Lake. Lithosome III, IV, and VI represented a low salinity, low alkalinity lake system. Alkaline conditions continued but with increasing salinities throughout the deposition of Lithosome V, VI and the basal unit of VII. The upper unit of Lithosome VII indicated low salinities. Lithosome VIII represented a return to high salinities.

The paleohydrologic reconstruction from fossil ostracode faunal assemblages is mostly in agreement with that of Martin et al. (2005), suggesting that vertebrate bones fossilized relatively soon after death. The main difference between the REE and ostracode faunal assemblage reconstructions occurs in Lithosome V and the basal unit of Lithosome VII. Both fossil ostracode faunal assemblages and REE signatures indicate low salinities, alkaline conditions for Lithosome III and IV, however, REE signatures suggest low salinities continue through Lithosome V while fossil ostracode faunal assemblages suggest an increase in salinity. Both reconstructions agree with increased salinity and alkaline conditions in Lithosome VI. REE signatures suggest high salinities in the basal unit of Lithosome VII and low salinities in the upper unit, whereas fossil ostracode faunal assemblages suggest a low salinity for the all of Lithosome VII. The dearth of ostracodes in Lithosome VIII makes it impossible to infer its paleohydrochemical conditions; however, if the ostracodes preserved in the eolian sandstone were transported from a time-equivalent saline playa system, the fossil ostracode faunal assemblages would agree with the high salinity REE signature for the basal eolian sand unit. Discrepancies between the two reconstructions are likely the result of offset in the timing of

fossilization, ostracodes calcify new carapaces from the lake geochemistry over the period of a few hours (Turpen and Angell, 1971) to a few days (Roca and Wansard, 1997). Discrepancies could also be the result of fossil reworking or heterogeneous REE signatures resulting from complex diagenetic fossilization (Suarez et al., 2010).

Conclusions

Four species of ostracodes were recovered from cores at Fossil Lake spanning ~ 71–13 ka. The species of ostracodes included *Limnocythere ceriotuberosa*, *Candona patzcuaro*, *Limnocythere platyforma*, and *Fabaeformiscandona caudata*. Climatic variability in Fossil Lake can be inferred from the fossil ostracode assemblages, whereas taphonomic variables, including fragmentation, oxidation staining, bleaching, and whole carapaces, can be used to delineate lake levels. Six unconformity surfaces are observed in association with Lithosome III–VIII, suggesting repeated oscillations between wet and dry conditions. The basin was arid, marked by an unconformity, before wetter conditions began to refill the basin at ~ 71 ka. This lake stand, Lithosome III, is slightly saline, alkaline, and reaches relatively deep depths before drier conditions returned and the lake desiccated. The next lake stand, Lithosome IV, was initially cool to cold, saline, and alkaline but became increasingly fresher and deeper, with increased seasonality, during wetter conditions, marked by the appearance of *F. caudata* at ~ 47 ka. Dry conditions set in again and the lake desiccated. Lake stands during Lithosome V and VI were shallow, cold, saline and alkaline, however, salinities fluctuated from seasonal dilution cycles. The lake stand of Lithosome VII was cold and shallow with low salinities. Ostracodes were extremely rare in Lithosome VIII were only recovered from the basal eolian sandstone,

suggesting ostracodes were transported from a nearby time-equivalent shallow lake or playa environment or from older sediments during deflation.

The paleohydrological and paleoclimatic reconstruction from Fossil ostracode fauna assemblages generally supports the low resolution reconstruction from vertebrate fossil bone REE signatures proposed by Martin et al. (2005). Inferred salinity differs between the two reconstruction models for Lithosome V and the basal unit of Lithosome VII. Disagreement between the ostracode fauna assemblages and REE signatures of vertebrates is likely the result of offset in the timing of fossilization.

References

- Bradbury, J.P., Forester, R.M., 2002. Environment and paleolimnology of Owens Lake, California: A record of climate and hydrology for the past 50,000 years. In: Hershler, R., Madsen, D.B., Currey, D.R. (Eds.), *Smithsonian Contributions to the Earth Sciences* 33, Great Basin Aquatic Systems History. Smithsonian Institution Press, Washington D. C., pp. 145–174.
- DeDeckker, P., Forester, R.M., 1988. The use of ostracods to reconstruct continental palaeoenvironmental records. In: DeDeckker, P., Colin, J.P., Peypouquet, J.P. (Eds.), *Ostracoda in the Earth Sciences*. Elsevier, New York, NY, pp. 175–199.
- Delorme, L.D., 1969. Ostracodes as Quaternary paleoecological indicators. *Canadian Journal of Earth Sciences* 49, 43–64.
- Delorme, L.D., 1970. Freshwater ostracodes of Canada. Part III. Family Candonidae. *Canadian Journal of Zoology* 48, 1099–1127.

- Delorme, L.D., 1971. Freshwater ostracodes of Canada. Part V. Families Lymnocytheridae, Loxoconchidae. *Canadian Journal of Zoology* 49, 43–64.
- Delorme, L.D., Zoltai, S.C., 1984. Distribution of an arctic ostracode fauna in space and time. *Quaternary Research* 21, 65–73.
- Forester, R.M., 1983. Relationship of two lacustrine ostracode species to solute and composition and salinity: implications for paleohydrochemistry. *Geology* 11, 435–438.
- Forester, R.M., 1985. *Limnocythere bradburyi* n. sp.; A modern ostracode from central Mexico and a possible Quaternary paleoclimate indicator. *Journal of Paleontology* 59, 8–20.
- Forester, R.M., 1986. Determination of the dissolved anion composition of ancient lakes from fossil ostracodes. *Geology* 14, 796–798.
- Forester, R.M., 1987. Late Quaternary paleoclimate records from lacustrine ostracodes. In: Ruddiman, W.F., Wright, H.E. (Eds.), *The Geology of North America K-3, North America and Adjacent Oceans During the Last Glaciation*. The Geological Society of America, pp. 261–276.
- Forester, R.M., 1991a. Ostracode assemblages from springs in the western United States: implications for paleohydrology. *Memoirs of the Entomological Society of Canada* 155, 181–201.
- Forester, R.M., 1991b. Pliocene-climate history of the western United States derived from lacustrine ostracodes. *Quaternary Science Reviews* 10, 133–146.
- Horne, F.R., 1993. Survival strategy to escape desiccation in a freshwater ostracode. *Crustaceana* 65, 53–61.

- Markgraf, V., Lennon, T., 1986. Paleoenvironmental History of the Last 13,000 Years of the Eastern Powder River Basin, Wyoming, and its Implications for Prehistoric Cultural Patterns. *Plains Anthropologist* 31, 1–12.
- Martens, K., DeDeckker, P., Marples, T.G., 1985. Life history of *Mytilocypris henricae* (Chapman) (Crustacea: Ostracoda) in Lake Bathurst, New South Wales. *Australian Journal of Marine and Freshwater Research* 36, 807–819.
- Martin, J.E., Patrick, D., Kihm, A.J., Foit Jr., F.F., Grandstaff, D.E., 2005. Lithostratigraphy, tephrochronology, and rare earth element geochemistry of fossils at the classical Pleistocene Fossil Lake Area, South Central Oregon. *Journal of Geology* 113, 139–155.
- Palacios-Fest, M.R., 1994. Nonmarine ostracode shell chemistry from ancient hohokam irrigation canals in central Arizona: A paleohydrochemical tool for the interpretation of prehistoric human occupation in the North American Southwest. *Geoarchaeology* 9, 1-29.
- Palacios-Fest, M.R., Carreño, A.L., Ortega-Ramírez J.R., Alvarado-Valdéz, G., 2002. A paleoenvironmental reconstruction of Laguna Babícora, Chihuahua, Mexico based on ostracode paleoecology and trace element shell chemistry. *Journal of Paleolimnology* 27, 185-206.
- Roca, J.R., Wansard, G., 1997. Temperature influence on development and calcification of *Heterocypris brevicaudata* Kaufmann, 1900 (Crustacea: Ostracoda) under experimental conditions. *Hydrobiologia* 347, 91–95.
- Sheppard, R.A., Gude, A.J., 1968. Distribution and genesis of authigenic silicate minerals in tuffs of Pleistocene Lake Tecopa, Inyo County, California. U. S. Geological Survey Professional Paper 597, pp 38.

- Sheppard, R.A., Gude, A.J., 1973. Zeolites and associated authigenic silicate minerals in tuffaceous rocks of Big Sandy Formation, Mohave County, Arizona. U. S. Geological Survey Professional Paper 830, pp 36.
- Smith, A.J., 1993. Lacustrine ostracodes as hydrochemical indicators in lakes of the north-central United States. *Journal of Paleolimnology* 8, 121–134.
- Suarez, C.A., Macpherson, G.L., González, L.A., Grandstaff, D.E., 2010. Heterogeneous rare earth element (REE) patterns and concentrations in a fossil bone: Implications for the use of REE in vertebrate taphonomy and fossilization history. *Geochimica et Cosmochimica Acta* 74, 2970-2988.
- Turpen, J.B., Angell, R.W., 1971. Aspects of molting and calcification in the ostracod *Heterocypris*. *The Biological Bulletin* 140, 331–338.
- Whatley, R., 1983. The application of Ostracoda to palaeoenvironmental analysis. In: Maddocks, R.F. (Ed.), *Applications of Ostracoda: Proceedings of the Eighth International Symposium on Ostracoda*. Department of Geosciences University of Houston–University Park, Houston, TX, pp. 51–77.

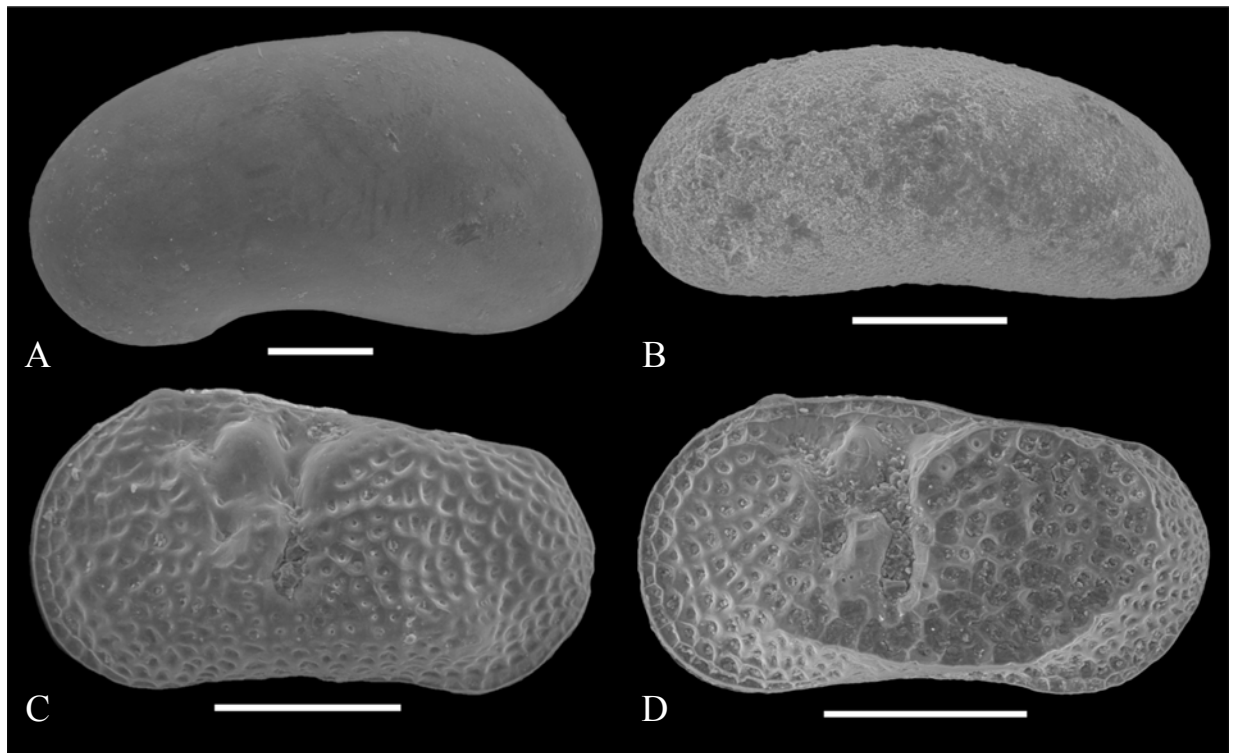


Plate 1. Plate indicating typical examples of Fossil Lake ostracodes. (A) Left valve of *Candona patzcuaro* from core 2, 35.2–38.1 cm. (B) Right valve of *Fabaeformiscandona caudata* with carbonate coating from trench 2, 79–81 cm. (C) Left valve of *Limnocythere ceriotuberosa* from core 5, 50.9–52.5 cm. (D) Left valve of *Limnocythere platyforma* from core 5, 112.7–114.7 cm. Scale bars are 200 μm .

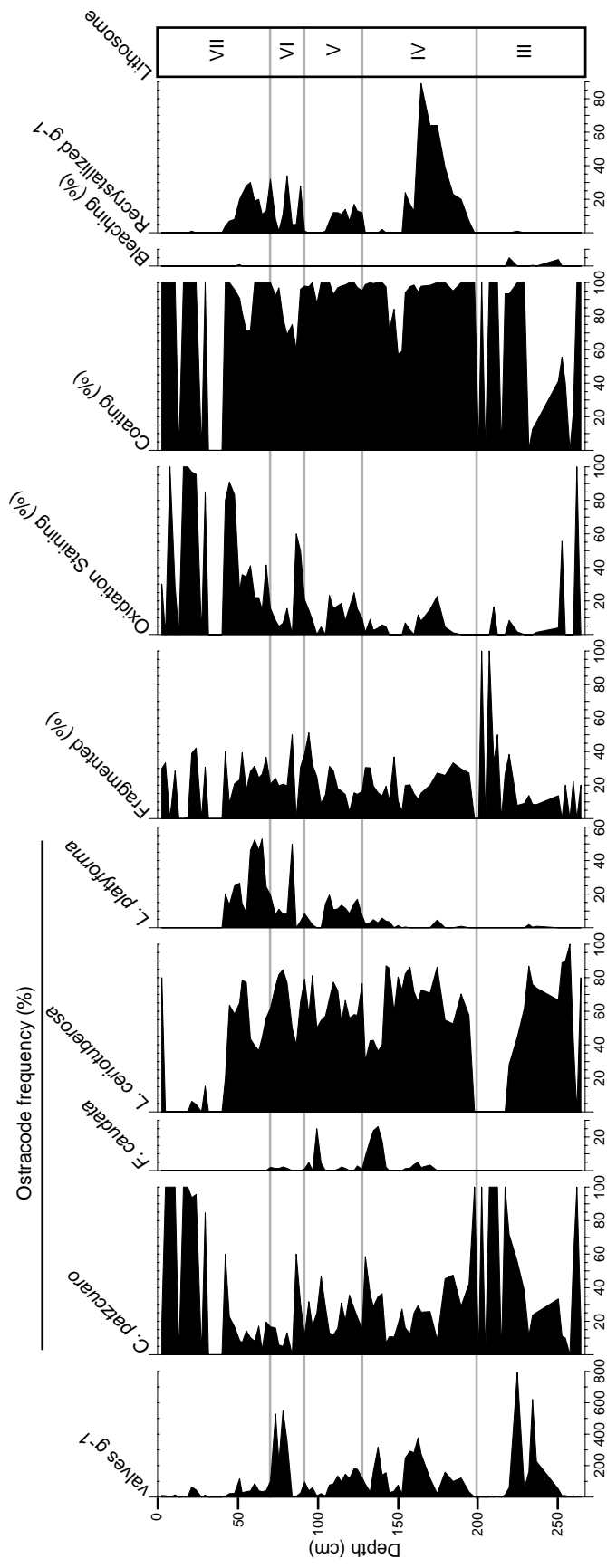


Fig 1. Distribution of ostracode abundance, taxa, and taphonomic variables throughout Lithosome III–VII of core 5. Recrystallized g-1 includes both recrystallized valves and steinkerns. Gray lines indicate the boundaries of lithosomes.

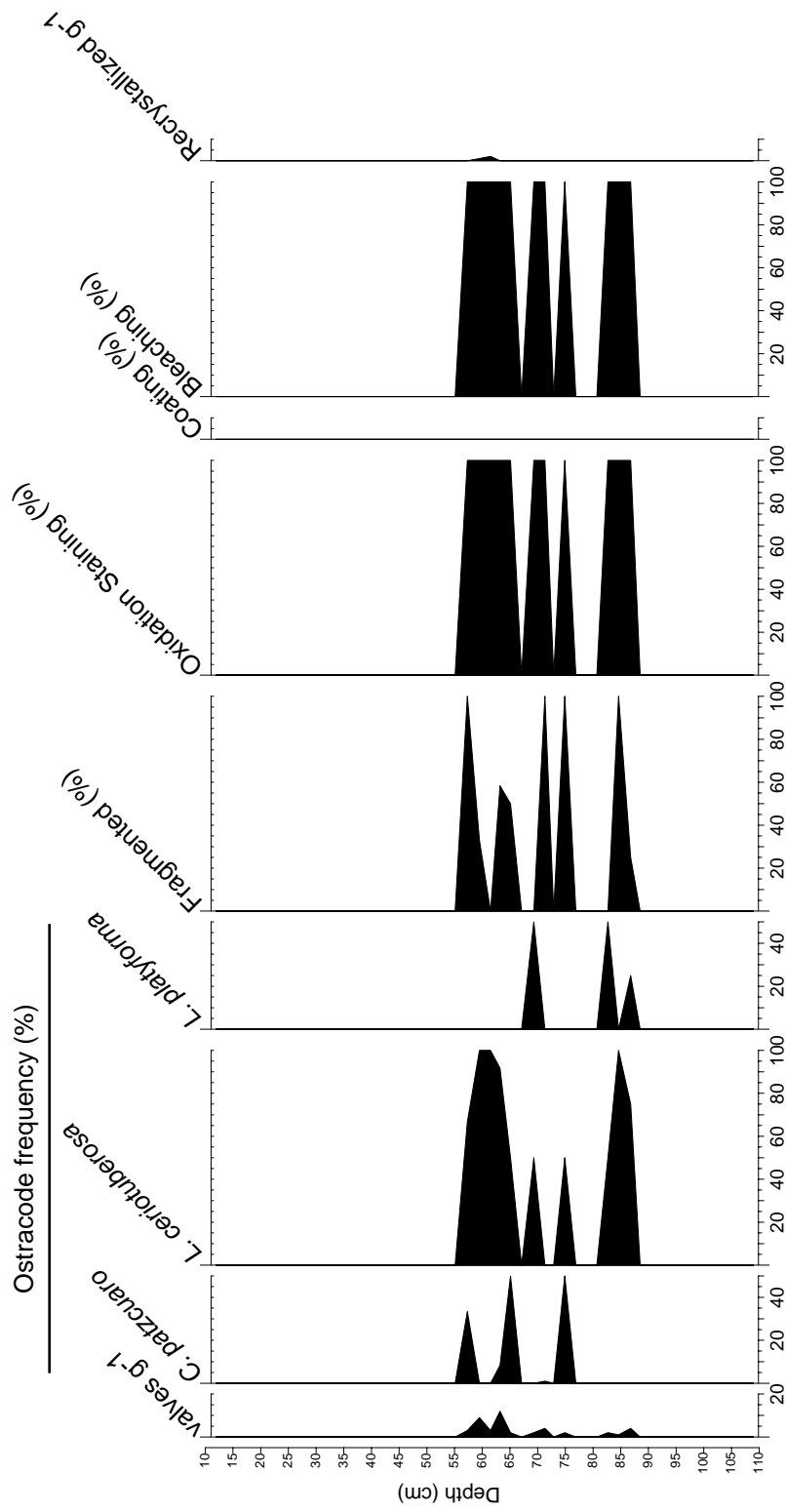


Fig 2. Distribution of ostracode abundance, taxa, and taphonomic variables throughout Lithosome VIII of core 1. Recrystallized g⁻¹ includes both recrystallized valves and steinkerns.

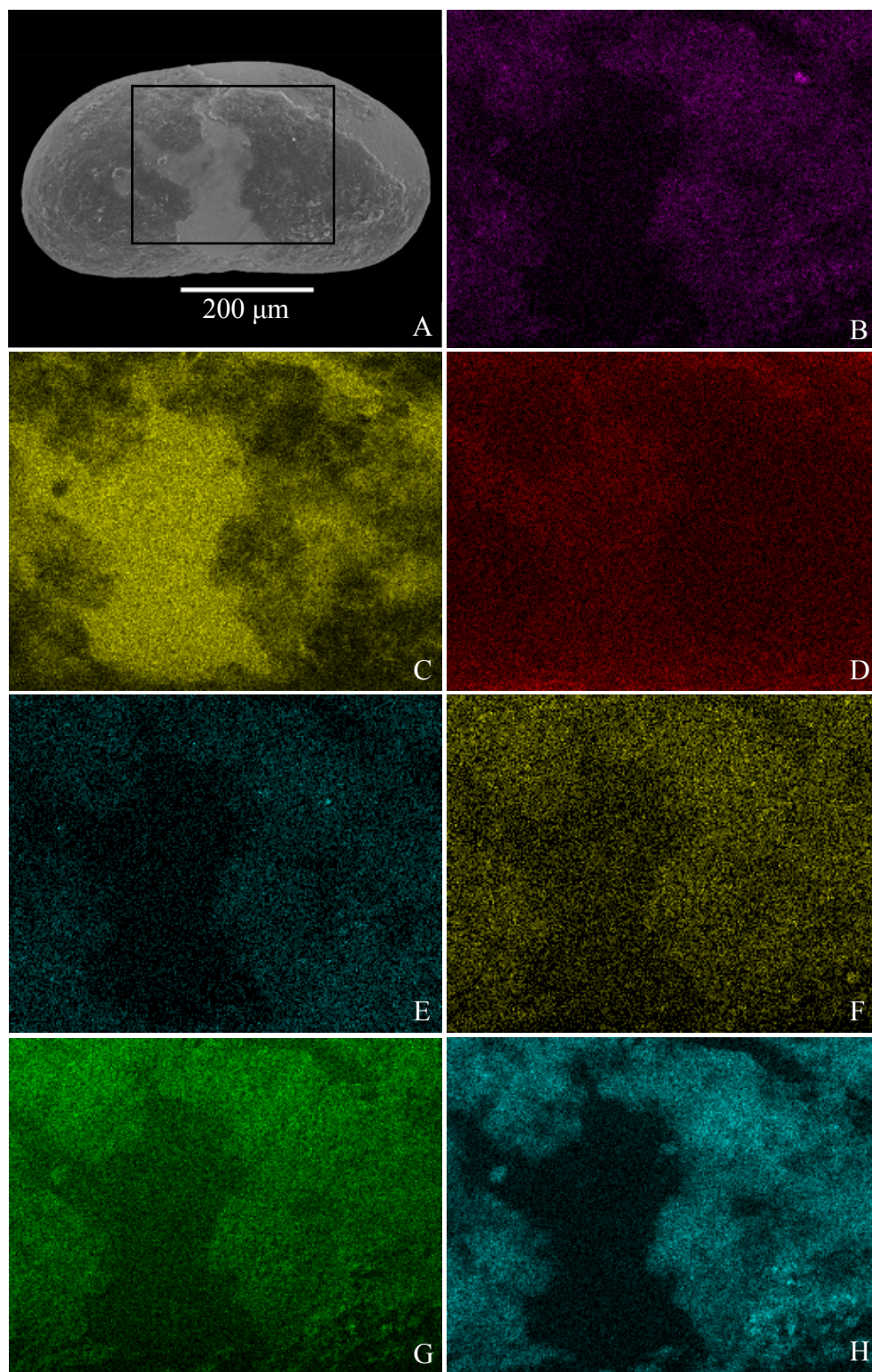


Fig. 3. EDX maps of thin aluminosilicate coating on a calcite ostracode valve. (A) Scanning electron microscope image of a left valve of *Candona patzcuaro* from core 5, 112.7–114.7 cm. The box outlines the area of EDX maps for aluminum (B), calcium (C), carbon (D), iron (E), magnesium (F), oxygen (G), and silica (H).

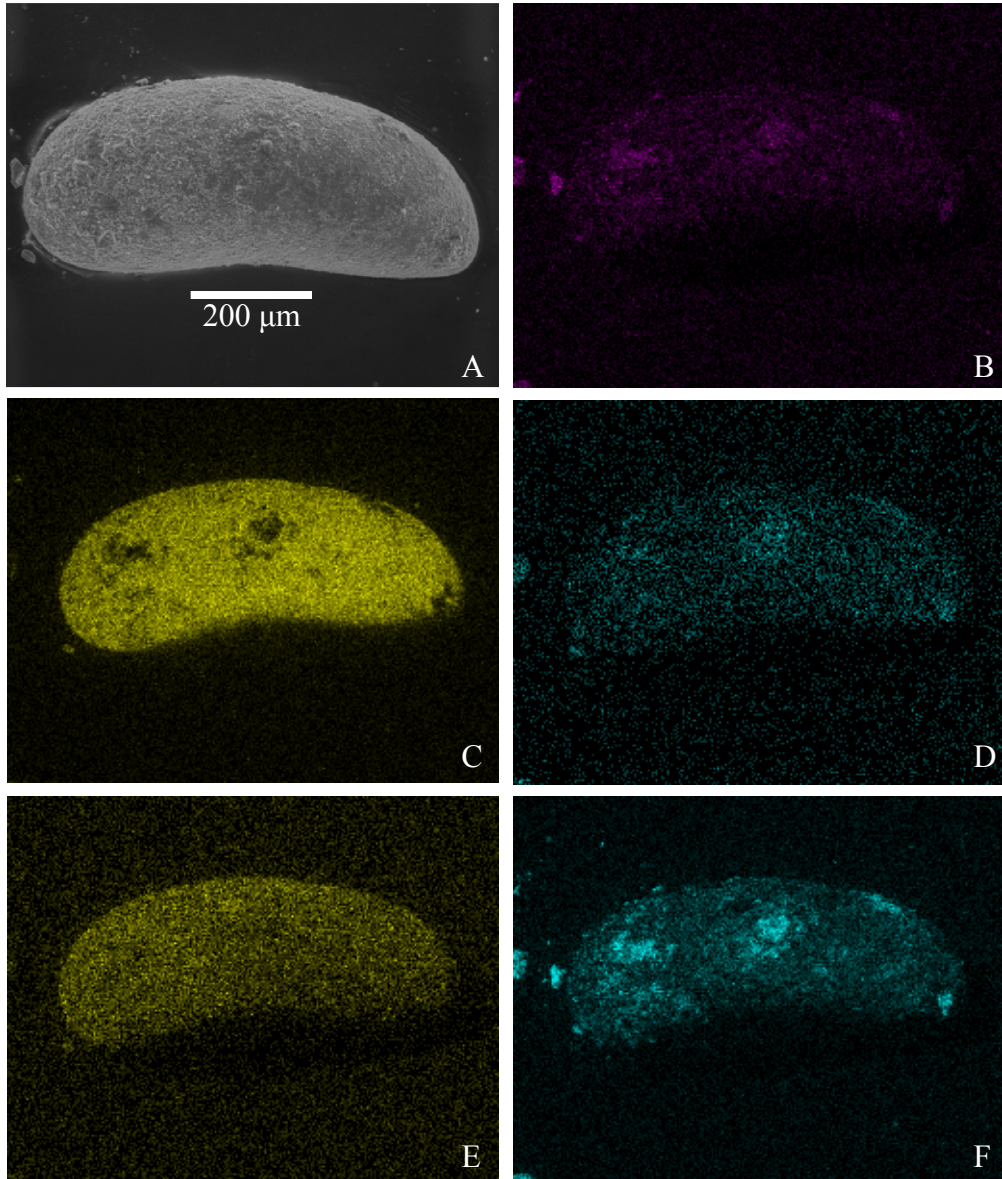


Fig. 4. EDX maps of calcium carbonate coating (with some aluminosilicate coating) on an ostracode valve. (A) Scanning electron microscope image of a left valve of *Fabaeformiscandona caudata* from trench 2, 79–81 cm. The box outlines the area of EDX maps for aluminum (B), calcium (C), iron (D), magnesium (E), and silica (F).

CHAPTER 4

CARBON AND OXYGEN STABLE ISOTOPES OF FOSSIL LAKE OSTRACODES

Introduction

The oxygen and carbon stable isotope signal in lake waters has been shown to respond to changes in local temperature, precipitation, groundwater inputs and biological activity (Kelts and Hsü, 1978) and is incorporated into authigenic and biogenic carbonates during calcification. Although stable isotope geochemistry of authigenic carbonates is useful for paleolimnologic studies, the use of ostracode biogenic carbonate geochemistry may be preferable. Ostracodes calcify new carapaces from the lake geochemistry over the period of a few hours (Turpen and Angell, 1971) to a few days (Roca and Wansard, 1997) and represent a time- and space-specific record of water conditions, which avoids the possibility of inclusion of detrital carbonate (Holmes, 1996). Modern laboratory cultures and field experiments, however, have found that calcification of carapace may not always occur in isotopic equilibrium with the host water and total dissolved inorganic carbon (TDIC) (Durazzi, 1977; Xia et al., 1997; van Grafenstein et al., 1999; Keating et al., 2002). This vital effect of ostracodes can produce offsets in $\delta^{18}\text{O}$ of as much as + 3 ‰ than expected for equilibrium precipitation (Keating et al., 2002). Despite the vital effect, stable isotopic geochemistry of ostracodes has been used extensively in paleoenvironmental reconstructions (e.g., Palacios-Fest et al., 1993; Bridgwater et al., 1999), and when compared to other lacustrine proxies, has produced similar paleoclimatic and paleoenvironmental interpretations (e.g., Cohen et al., 2005; Bright et al., 2006).

In this investigation I use the oxygen and carbon isotopes from ostracode calcite to reconstruct paleoenvironmental and paleohydrologic changes at Fossil Lake.

Methods

Stable isotope analysis was carried out on ostracode samples from cores 1 and 2 in the northern part of the basin and core 5 in the southern part of the basin. In particular I examine isotopic changes between ~ 71–25 ka, Lithosome III through VII, where *Limnocythere ceriotuberosa* and *Candona patzcuaro* fossils were common. Neither core 1 (Lithosomes V–VII) nor core 2 (Lithosome VI–VII) recovered a complete record for this time slice. Ostracode valves from all of core 1 and from Lithosome VI and V of core 2 were used to produce a representative composite section for the northern part of the basin. Cores were sampled with 8 cc paleomagnetic cubes, approximately every 2.5 cm. The sediment in the paleomagnetic cubes, ranging in weight from 2.46–11.56 g, was generally loose and unconsolidated which allowed for samples to be dry sieved to prevent the potential for isotopic offset as a result of sample preparation treatments (Mischke et al., 2008). Sediment was screened through 425 µm and 250 µm sieves. Well-preserved adult *L. ceriotuberosa* and *C. patzcuaro* valves and recrystallized valves or steinkerns representing diagenetic carbonate were picked from each residue using a 20/0 paintbrush under a Bausch and Lomb StereoZoom 4 (zoom range 0.7–3X) binocular microscope. The valves were thoroughly brushed and cleaned with ultrapure water to remove adhered sediment using a 20/0 paintbrush. A minimum of 25 µg was required for each ostracode stable isotope analysis. This minimum weight generally required one *C. patzcuaro* valve, two to three *L. ceriotuberosa* valves, and only one recrystallized valve or steinkern. Up to three samples from each paleomagnetic cube were analyzed for each species of ostracode and recrystallized valve or steinkern. Recrystallized valves and steinkern were analyzed to determine isotope values for diagenetic carbonate in each sedimentary unit. All samples were analyzed at the W.M. Keck Paleoenvironmental and Environmental Stable Isotope Lab at the University of

Kansas. Samples were vacuum roasted at 200°C for one hour to remove volatile contaminants and analyzed using phosphoric acid digestion at 75° C on a ThermoFinnigan Kiel III single sample acid dosing system connected to a ThermoFinnigan MAT 253 isotope ratio mass spectrometer. Precision was monitored by daily analysis of NBS-18 and NBS-19 and is better than 0.1 ‰ for both carbon and oxygen. All carbonate data are reported relative to VPDB (Vienna Pee Dee Belemnite). Confidence ellipses were generated using PAST (paleontological statistics software version 1.79; Hammer et al., 2008). Ostracode specimens with coating were not excluded from analysis since many to most of the ostracodes in the cores were coated however, specimens without coating, when present, were preferentially chosen for analysis over specimens with coatings.

Results

The carbon isotope record for *L. ceriotuberosa* and *C. patzcuaro* ranged from -2.41 to +15.33 ‰ and -1.55 to +16.99 ‰, respectively (Table 1 and 2). The average $\delta^{13}\text{C}$ variability within each 2-cm sample was 2.22 ± 1.72 ‰ and 2.81 ± 1.43 ‰ for *L. ceriotuberosa* and *C. patzcuaro*, respectively. $\delta^{13}\text{C}$ values were generally more depleted in *L. ceriotuberosa* than in *C. patzcuaro* (Fig. 1 and 2). Distinct temporal (depth) trends are recorded in each lithosome and both species generally showed similar $\delta^{13}\text{C}$ trends (Fig. 3). At the base of Lithosome III, both *L. ceriotuberosa* and *C. patzcuaro* record $\delta^{13}\text{C}$ depletions of ~ 4 ‰ and ~ 3 ‰, respectively. *Candona patzcuaro* also records a $\delta^{13}\text{C}$ increase of ~ 3 ‰ near the top of the lithosome. Lithosome IV records a large $\delta^{13}\text{C}$ enrichment spike; $\delta^{13}\text{C}$ values increased ~ 15 ‰ and ~ 14‰ for *L. ceriotuberosa* and *C. patzcuaro*, respectively. Throughout Lithosome V, $\delta^{13}\text{C}$ values decreased ~ 6 ‰ and ~ 2‰ for *L. ceriotuberosa* and *C. patzcuaro*, respectively. At the base of

Lithosome VI, $\delta^{13}\text{C}$ values for *L. ceriotuberosa* and *C. patzcuaro* record opposite trends. At the top of Lithosome VI, *L. ceriotuberosa* records $\delta^{13}\text{C}$ depletions of ~ 3 ‰. Values of $\delta^{13}\text{C}$ from *L. ceriotuberosa* and *C. patzcuaro* also decreased ~ 3 ‰ in Lithosome VII.

The oxygen isotope record for *Limnocythere ceriotuberosa* and *Candona patzcuaro* ranged from -6.43 to +2.36 ‰ and -7.40 to +2.75 ‰, respectively (Table 1 and 2). The average $\delta^{18}\text{O}$ variability within each 2-cm sample was 2.02 ± 1.30 ‰ and 2.32 ± 1.76 ‰ for *L. ceriotuberosa* and *C. patzcuaro*, respectively. Values of $\delta^{18}\text{O}$ generally were more depleted, by $\sim 2 - 3$ ‰, in *L. ceriotuberosa* than in *C. patzcuaro* (Fig. 1 and 2). Exceptions occur at the base of Lithosome IV and near the base of Lithosome VI, where $\delta^{18}\text{O}$ values of the two species overlapped. Distinct temporal $\delta^{18}\text{O}$ trends are visible in most of the lithosomes and both species generally showed similar $\delta^{18}\text{O}$ trends (Fig. 3). In Lithosome III there are no distinct $\delta^{18}\text{O}$ trends with depth and both ostracode species show fluctuating $\delta^{18}\text{O}$ values within the range of sample variability. In Lithosome IV, $\delta^{18}\text{O}$ values decrease $\sim 2 - 4$ ‰ in both *L. ceriotuberosa* and *C. patzcuaro* after inundation of the basin. Depleted $\delta^{18}\text{O}$ values are recorded for *L. ceriotuberosa* throughout the remainder of the lithosome, but $\delta^{18}\text{O}$ values for *C. patzcuaro* increased $\sim 4 - 6$ ‰ from 309–346 cm, which corresponds to a $\delta^{13}\text{C}$ enrichment spike, and decreased ~ 2 ‰ from 298–311 cm. The only visible $\delta^{18}\text{O}$ trend in Lithosome V, occurs at the top of the lithosome in *C. patzcuaro*, $\delta^{18}\text{O}$ values decreased ~ 3 ‰ near the top of the lithosome. The most depleted $\delta^{18}\text{O}$ value, -7.40 ‰, occurs at the top of Lithosome V. In Lithosome VI, $\delta^{18}\text{O}$ values for *L. ceriotuberosa* and *C. patzcuaro* increased ~ 3 ‰ at the base of the lithosome. At the top of Lithosome VI, $\delta^{18}\text{O}$ values for *L. ceriotuberosa* are depleted in relationship to $\delta^{18}\text{O}$ values on the base of the lithosome. In Lithosome VII, $\delta^{18}\text{O}$ values for *L. ceriotuberosa* and *C. patzcuaro*

decreased ~ 3.5 ‰ and ~ 5 ‰, respectively, from base to top. The only offset between cores was recorded at the base of Lithosome VII.

Cross plots of $\delta^{13}\text{C}$ and $\delta^{18}\text{O}$ values for *L. ceriotuberosa* and *C. patzcuaro* show weak covariant trends for Lithosome VI ($R^2 = 0.39\text{--}0.46$) and Lithosome VII ($R^2 = 0.15\text{--}0.18$) (Fig. 3). In Lithosome IV, *C. patzcuaro* shows a weak covariant trend ($R^2 = 0.26$), but *L. ceriotuberosa* does not show covariant trend ($R^2 = 0$). Lithosome III and V do not show covariant trends ($R^2 < 0.10$).

Diagenetic carbonates, recrystallized valves and steinkerns, recorded $\delta^{13}\text{C}$ and $\delta^{18}\text{O}$ values that ranged from $+3.11$ to $+15.12$ ‰ and -4.27 to -1.46 ‰, respectively, with calculated means of $+10.41 \pm 2.63$ ‰ and -1.27 ± 1.01 ‰, respectively. The $\delta^{13}\text{C}$ values of diagenetic carbonates were more enriched than those values from ostracodes except during the $\delta^{13}\text{C}$ enrichment spike in Lithosome IV. Diagenetic carbonate $\delta^{18}\text{O}$ values fall within the standard deviation of ostracode $\delta^{18}\text{O}$ values.

In samples that contained both aluminosilicate coated and noncoated ostracode valves, the $\delta^{13}\text{C}$ and $\delta^{18}\text{O}$ values of coated ostracodes was within ± 2.0 ‰ of the isotopic values of noncoated ostracodes, and was within the range of sample variability. Thicker aluminosilicate coatings were observed completely intact in the residual acid after analysis. Only one coated ostracode specimen resulted in isotopic values consistent with those of the diagenetic carbonate, and was removed from the data set.

Discussion

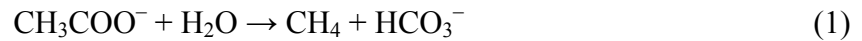
Carbon stable isotopes

The isotopic composition of dissolved inorganic carbon (DIC) in continental aquatic environments is dependent upon several factors: 1) rock-water and soil-water interactions; 2) CO₂ exchange with the atmosphere; 3) photosynthetic consumption of ¹³C-depleted CO₂; 4) degradation and recycling of aquatic and terrestrial organic matter; and 5) microbial processes, such as methanogenesis, in the water column (Durazzi, 1977; McKenzie, 1985; Kelts and Talbot, 1990; Chivas et al., 1993; Heaton et al., 1995). Generally, enriched δ¹³C values as high as +5 - +6 ‰ in lakes are associated with high levels of primary productivity (Stiller and Kaufman, 1985). Values of δ¹³C ranging from -10 to +2 ‰ are generally attributed to the degradation and recycling of δ¹³C-depleted aquatic and terrestrial organic matter (McKenzie, 1985; Curry et al., 1997).

In Fossil Lake sediments, changes in δ¹³C values of benthic ostracodes are likely a function of primary productivity and water depth (Fig. 4). Ostracode enriched δ¹³C values are associated with high primary productivity (McKenzie, 1985) and suggest either shallow water conditions or a well-mixed lake. Primary producers preferentially uptake ¹²C over ¹³C, resulting in an enrichment of δ¹³C_{DIC}, which is incorporated into ostracode carapaces. In deep or deeper portions of lakes, benthic environments are influenced less by primary productivity and more by the degradation and recycling of isotopically depleted organic matter. Many of the lithosomes in Fossil Lake show an upward temporal trend of depleting δ¹³C values (Fig 2). This trend is consistent with shallow water conditions represented by the enriched δ¹³C values resulting from high primary productivity, and deepening of the lake represented by depleted δ¹³C values with

increasing degradation and recycling of organic matter. Lithosome III and VII ostracodes record enriched $\delta^{13}\text{C}$ values at their top, indicating a return to shallower conditions (Fig. 4).

The extreme $\delta^{13}\text{C}$ positive spike in Lithosome IV, can not be attributed to primary productivity, but is likely the result of methanogenesis. Methanogenesis occurs when anoxic conditions occur at or just below the sediment-water interface and is the result of either acetate cleavage (1) or CO_2 reduction (2).



Both the production of HCO_3^- (1) and consumption of CO_2 (2) result in an increase in calcite saturation, favoring the preservation of ostracode carbonate valves (Curry et al., 1997) and may have contributed to the abundance of steinkerns and recrystallized valves in Lithosome IV.

The carbon isotopic composition of methane from lake sediments resulting from the acetate pathways range from -50 to -60‰, whereas CO_2 reduction is > -60 ‰ (Whiticar, 1999). CO_2 reduction causes an enrichment of the $\delta^{13}\text{C}_{\text{DIC}}$ reservoir in the lake water that is incorporated into ostracode carbonate during calcification of carapaces. Acetate cleavage is a common pathway of methanogenesis in freshwater environments (Whiticar, 1999), however, the extremely positive ostracode $\delta^{13}\text{C}$ values recorded indicate CO_2 reduction was the dominant pathway at Fossil Lake. The extremely positive $\delta^{13}\text{C}$ values also suggest most of the CH_4 produced during methanogenesis was lost to the atmosphere before the CH_4 could be oxidized, resulting in the diffusion of isotopically-depleted dissolved CO_2 into the sediment for methanogenesis and producing an enrichment of $\delta^{13}\text{C}_{\text{DIC}}$ in the water column. Curry et al. (1997) discussed two methods under which methanogenic CO_2 reduction pathway can occur in the sediment without the oxidation of CH_4 and any detrimental effects to benthic ostracode survival

or preservation. One method is the near complete loss of methane by ebullition, and the other is emission through the stems of such aquatic macrophytes as cattails. Ebullition occurs when the concentration of methane dissolved in the sediment porewaters exceeds the hydrostatic pressure of the overlying water, allowing bubbles of gas to form and escape into the atmosphere (Schlesinger, 1997).

Methane emission rates are the highest when sediment temperatures exceed $\sim 15^{\circ}\text{C}$ (Zeikus and Winfrey 1976). Increased sediment temperatures from methanogenesis may have slightly increased the lake bottom water temperatures and could explain the rarity and absence of the cold-water ostracode species, *Limnocythere platyforma*, during the methanogenic $\delta^{13}\text{C}$ enrichment spike.

Near the top of Lithosome IV, $\delta^{13}\text{C}$ values start to deplete. The return to pre-methanogenic $\delta^{13}\text{C}$ values probably reflects increasing water depths which would have lowered overall sediment temperatures, lower rates of methanogenesis, and produced a larger DIC reservoir that can buffer the isotopic effects of methanogenesis (Curry et al., 1997).

Oxygen stable isotopes

Values of $\delta^{18}\text{O}$ in water and carbonates precipitated in continental aquatic environments are affected by several factors including: 1) the oxygen isotopic composition of precipitation falling on the basin and watershed; 2) humidity; 3) the balance between evaporation and precipitation; 4) the temperature during carbonate precipitation; 5) the mineralogy of the precipitated carbonate phases; and 6) the hydrology of the basin (Dansgaard, 1964; Kelts & Talbot, 1989; Krabbenhoft et al., 1990). All of these factors undergo seasonal changes. The high variability of $\delta^{18}\text{O}$ values recorded by the ostracodes in a single sample or within a

lithosome is probably the result of time-averaging of short-term variability in P/E ratios within the basin. The temporal trends of $\delta^{18}\text{O}$ are assumed to be the result of long-term change in precipitation/evaporation (P/E) ratios influenced by climatic changes. In Lithosome IV and VI, depleted $\delta^{18}\text{O}$ during the inundation of the basin indicate wet conditions with increased precipitation and inflow. After inundation, $\delta^{18}\text{O}$ values become more enriched for an extended period of time in Lithosome IV and VI, indicating dry conditions with increased evaporation or decreased precipitation. Wet conditions returned at the top of Lithosome IV and VI, as indicated by the depletion $\delta^{18}\text{O}$ (Fig. 4). The depleted $\delta^{18}\text{O}$ values near the base of Lithosome VII correspond with an increase in abundance of *L. platyforma* (Chapter 3), suggesting cold, wet conditions.

The $\delta^{18}\text{O}$ offset between *L. ceriotuberosa* and *C. patzcuaro* may be the result of differing species vital effects or maturing during different seasons. The inferred $\delta^{18}\text{O}$ vital offset for Candoninae species is 2.2 ± 0.15 ‰ when compared with an equilibrium calcite (von Grafenstein et al., 1999). From the same study, von Grafenstein et al. (1999) reported a $\delta^{18}\text{O}$ vital offset of 0.78 ± 0.20 ‰ for *Limnocythere inopinata*, but no other studies have investigated *Limnocythere* species. *Candona patzcuaro* takes three to six months to mature and usually reaches maturity in the summer (Markgraf and Lennon, 1986; Palaios-Fest, 1994) when lakes are warmer, melt water influx is diminished, and evaporation is more prominent, resulting in $\delta^{18}\text{O}$ enrichment of lake waters. *L. ceriotuberosa* probably reaches adulthood in four to six weeks during the spring, like many temperate ostracodes in the North America (Forester, 1985) when lakes are generally receiving an influx of isotopically depleted cold spring melt waters.

The two species of ostracodes have overlapping of $\delta^{18}\text{O}$ values at the base of Lithosome IV, prior to the onset of methanogenesis, and may be the result of low sample size and poor

temporal resolution of the data or a change in timing of maturity of one or both species. During the methanogenic $\delta^{13}\text{C}$ enrichment, the two ostracodes show different temporal trends, $\delta^{18}\text{O}$ values of *L. ceriotuberosa* remained depleted while the $\delta^{18}\text{O}$ values of *C. patzcuaro* become enriched. One explanation for the differing $\delta^{18}\text{O}$ temporal trends may be that *L. ceriotuberosa* reached optimal temperatures for hatching and maturity earlier in the spring (isotopically depleted $\delta^{18}\text{O}$ waters) as a result of methanogenesis producing slightly warmer bottom waters. The slight warming associated with methanogenesis, however, would have little to no effect on *C. patzcuaro* because of its longer life cycle, the result of maturation during the warm summer months.

Cross Plots

Patterns of long-term covariance in $\delta^{13}\text{C}$ and $\delta^{18}\text{O}$ have been recognized in authigenic carbonates from modern hydrologically closed basins, whereas hydrologically open basins show little to no $\delta^{13}\text{C}$ and $\delta^{18}\text{O}$ covariance (Talbot, 1990). The weak covariant trends observed in Lithosome VI and VII suggest a relatively closed basin, where evaporation influenced values of $\delta^{18}\text{O}$. The lack of $\delta^{13}\text{C}$ and $\delta^{18}\text{O}$ covariance in Lithosomes III and V indicate an open and balanced basin. In Lithosome IV, the methanogenic influence overwhelms the isotopic signal so covariance trends can not be determined.

Conclusions

The carbon and oxygen isotopic composition of *Limnocythere ceriotuberosa* and *Candona patzcuaro* valves from Fossil Lake basin record distinct temporal trends relating to changes in P/E ratios ($\delta^{18}\text{O}$) and primary productivity associated with water depth ($\delta^{13}\text{C}$). Both

ostracode species generally showed similar $\delta^{18}\text{O}$ temporal trends, suggesting the two species respond congruently to environmental and climatic changes. A large $\delta^{13}\text{C}$ positive spike, with $\delta^{13}\text{C}$ values reaching $\sim +17\text{‰}$, is attributed to methanogenesis with near complete removal of methane by ebullition or emission through the stems of aquatic vegetation.

The base of each lake stand begins with a relatively shallow lake environment with high primary productivity that gradually deepens over time with increasing P/E ratios. Only Lithosomes III and VII return to shallower lake environments with increasing primary productivity, recorded by enriched $\delta^{13}\text{C}$ values. High variability of $\delta^{18}\text{O}$ values was recorded in all lithosome resulting from time-averaging of short-term variability in P/E ratios within the basin.

References

- Bridgwater, N.D., Heaton, T.H.E., O'Hara, S.L., 1999. A late Holocene palaeolimnological record from central Mexico, based on faunal and stable-isotope analysis of ostracod shells. *Journal of Paleolimnology* 22, 383–397.
- Bright, J., Kaufman, D.S., Forester, R.M., Dean, W.E., 2006. A continuous 250,000 yr record of oxygen and carbon isotopes in ostracode and bulk-sediment carbonate from Bear Lake, Utah-Idaho. *Quaternary Science Reviews* 25, 2258–2270.
- Chivas, A.R., DeDeckker, P., Cali, J.A., Chapman, A., Kiss, E., Shelley, J.M.G., 1993. Coupled stable-isotope and trace-element measurements of lacustrine carbonates as paleoclimatic indicators. In: Swart, P.K., Kohmann, K.C. McKenzie, M., Savin, S. (Eds.), *Geophysical Monograph 78: Climate Change in Continental Isotope Records*. American Geophysical Union, Washington D. C., pp. 113–121.

- Cohen, A.S., Palacios-Fest, M.R., Negrini, R.M., Wigand, P.E., Erbes, D.B., 2000. A paleoclimate record for the past 250,000 years from Summer Lake, Oregon, USA: II. Sedimentology, paleontology, and geochemistry. *Journal of Paleolimnology* 24, 151–182.
- Curry, B.B., Anderson, T.F., Lohmann, K.C., 1997. Unusual carbon and oxygen isotopic ratios of ostracodal calcite from last interglacial (Sangamon episode) lacustrine sediment in Raymond Basin, Illinois, USA. *Journal of Paleolimnology* 17, 421–435.
- Durazzi, J.T., 1977. Stable isotopes in ostracod shell: A preliminary study. *Geochimica et Cosmochimica Acta* 41, 1168–1170.
- Dansgaard, W., 1964. Stable isotopes in precipitation. *Tellus* 16, 436–468.
- Forester, R.M., 1985. *Limnocythere bradburyi* n. sp.: A modern ostracode from central Mexico and a possible Quaternary paleoclimatic indicator. *Journal of Paleontology* 59, 8–20.
- Hammer, Ø., Harper, D. A. T., and Ryan, P. D., 2008, PAST-Paleontological Statistics, version 1.79.
- Heaton, T.H.E., Holmes, J.A., Bridgwater, N.D., 1995. Carbon and oxygen isotope variations among lacustrine ostracods: Implications for paleoclimatic studies. *The Holocene* 5, 428–434.
- Holmes, J.A., 1996. Trace-element and stable isotope geochemistry of non-marine ostracod shells in Quaternary paleoenvironmental reconstruction. *Journal of Paleolimnology* 15, 223–235.
- Keating, K.W., Heaton, T.H.E., Holmes, J.A., 2002. Carbon and oxygen isotope fractionation in non-marine ostracods: Results from a “natural culture” environment. *Geochimica et Cosmochimica Acta* 66, 1701–1711.

- Kelts, K., Talbot, M.R., 1989. Lacustrine carbonates as geochemical archives of environmental change and biotic-abiotic interactions. In: Tilzer, M.M., Serruya, C. (Eds.), *Ecological Structure and Function in Large Lakes*. Science and Technology Publishers, Madison, WI, pp. 290–317.
- Kelts, K., Talbot, M.R., 1990. Lacustrine carbonates as geochemical archives of environmental change of biotic/abiotic interactions. In: Tilzer, M.M., Serruya, C., (Eds.), *Large Lakes: Ecological Structure and Function*. Science and Technology Publishers, Madison, WI, pp. 288–315.
- Krabbenhoft, D.P., Bowser, C.J., Anderson, M.P., Valley J.W., 1990. Estimating groundwater exchange with lakes: 1. The stable isotope mass balance method. *Water Resources Research* 26, 2445–2453.
- Markgraf, V., Lennon, T., 1986. Paleoenvironmental History of the Last 13,000 Years of the Eastern Powder River Basin, Wyoming, and its Implications for Prehistoric Cultural Patterns. *Plains Anthropologist* 31, 1–12.
- McKenzie, J., 1985. Carbon isotopes and productivity in the lacustrine and marine environment. In: Stumm, W. (Ed.), *Chemical Processes in Lakes*. J. Wiley, New York: 99–118.
- Mischke, S., Zhang, C., Börner, A., 2008. Bias of ostracod stable isotope data caused by drying of sieve residues from water. *Journal of Paleolimnology* 40, 567–575.
- Palacios-Fest, M.R., Carreño, A.L., Ortega-Ramírez J.R., Alvarado-Valdéz, G., 2002. A paleoenvironmental reconstruction of Laguna Babícora, Chihuahua, Mexico based on ostracode paleoecology and trace element shell chemistry. *Journal of Paleolimnology* 27, 185-206.

- Palacios-Fest, M.R., Cohen, A.S., Ruiz, J., Blank, B., 1993. Comparative paleoclimatic interpretations of from nonmarine ostracodes from faunal assemblages, trace elements shell chemistry and stable isotope data. In: Swart, P.K., Kohmann, K.C. McKenzie, M., Savin, S. (Eds.), Geophysical Monograph 78: Climate Change in Continental Isotope Records. American Geophysical Union, Washington D. C., pp. 179–190.
- Roca, J.R., Wansard, G., 1997. Temperature influence on development and calcification of *Heterocypris brevicaudata* Kaufmann, 1900 (Crustacea: Ostracoda) under experimental conditions. *Hydrobiologia* 347, 91–95.
- Schlesinger, W.H., 1997. Biogeochemistry: An analysis of global change, 2nd ed. Academic Press, New York, pp. 588.
- Stiller, M., Kaufman, A., 1985. Paleoclimatic trends revealed by the isotopic composition of carbonates in Lake Kinneret. *Zeitschrift für Gletscherkunde und Glazialgeologie* 21, 79–87.
- Talbot, M.R., 1990. A review of the paleohydrological interpretation of carbon and oxygen ratios in primary lacustrine carbonates. *Chemical Geology* 80, 261–279.
- Turpen, J.B., Angell, R.W., 1971. Aspects of molting and calcification in the ostracod *Heterocypris*. *The Biological Bulletin* 140, 331–338.
- van Grafenstein, U., Erlenkeuser, H., Trimborn, P., 1997. Oxygen and carbon isotopes in modern fresh-water ostracod valves: assessing vital offsets and autecological effects of interest for paleoclimate studies. *Palaeogeography, Palaeoclimatology, Palaeoecology* 148, 133–152.
- Whiticar, M.J., 1999. Carbon and hydrogen isotope systematics of bacterial formation and oxidation of methane. *Chemical Geology* 161, 291–314.

Xia, J., Engstrom, D.R., Ito, E., 1997. Geochemistry of ostracode calcite: 1. an experimental determination of oxygen isotopes fractionation. *Geochimica et Cosmochimica Acta* 61, 377–382.

Zeikus, J.G., Winfrey, M.R., 1976. Temperature limitation of methanogenesis in aquatic sediments. *Applied and Environmental Microbiology* 31, 99–107.

Table 1. Statistics on stable isotope data for adult ostracode valves from the north core. Species designations include *Limnocythere ceriotuberosa* (LIMC) and *Candona patzcuaro* (CANP).

Lithosome	Depth (cm)		$\delta^{13}\text{C}$		$\delta^{18}\text{O}$	
			LIMC	CANP	LIMC	CANP
VII	111.4– 150.2	max	+3.84	+4.14	+2.18	+2.24
		min	-2.41	-1.47	-6.27	-4.31
	mean	-0.17	+2.06	-3.49	-0.41	
	std. dev.	1.38	1.99	2.12	2.49	
	sample no.	31	10	31	10	
VI	150.2– 214.9	max	+3.03	+6.73	+0.15	+2.13
		min	-1.73	+0.51	-6.43	-2.04
	mean	+0.05	+3.04	-2.52	+0.13	
	std. dev.	1.17	1.93	1.82	1.23	
	sample no.	35	10	35	10	
V	214.9– 252.0	max	+6.35	+2.52	-0.61	+0.51
		min	-0.76	+0.78	-4.33	-0.47
	mean	+2.70	+1.65	-2.29	+0.02	
	std. dev.	2.25	1.23	1.02	0.69	
	sample no.	25	2	25	2	
IV	252.0– 293.1	max	+14.05	–	-0.60	–
		min	+2.63	–	-4.59	–
	mean	+8.84	3.98	-2.71	-5.26	
	std. dev.	2.96	–	1.15	–	
	sample no.	18	1	18	1	

Table 2. Statistics on stable isotope data for adult ostracode valves from the south core. Species designations include *Limnocythere ceriotuberosa* (LIMC) and *Candona patzcuaro* (CANP).

Lithosome	Depth (cm)		$\delta^{13}\text{C}$		$\delta^{18}\text{O}$	
			LIMC	CANP	LIMC	CANP
VII	0–70.2	max	+4.53	+4.54	+0.89	+2.75
		min	-1.21	-1.55	-5.00	-5.48
		mean	+0.47	+1.80	-2.05	-0.54
		std. dev.	1.10	2.00	1.55	2.67
		sample no.	34	16	34	16
VI	70.2– 91.6	max	+2.52	+5.49	+1.39	+2.65
		min	-1.83	+0.82	-3.75	-5.14
		mean	+0.33	+2.56	-1.49	-0.72
		std. dev.	1.04	1.25	1.53	2.39
		sample no.	21	16	21	16
V	91.6– 127.7	max	+8.80	+6.40	-0.13	+2.15
		min	-2.06	0.00	-5.65	-7.40
		mean	+1.69	+2.59	-2.77	-0.41
		std. dev.	2.75	1.49	1.23	1.91
		sample no.	28	31	28	31
IV	127.7– 194.7	max	+15.33	+16.99	+2.36	+2.40
		min	-1.29	-0.23	-4.69	-4.66
		mean	+5.41	+6.85	-2.34	-0.86
		std. dev.	4.67	5.05	1.42	1.78
		sample no.	81	45	81	45
III	194.7– 264.8	max	+4.54	+8.41	-1.09	+3.22
		min	-1.85	-0.6	-5.66	-3.41
		mean	+1.73	+4.26	-3.49	-0.16
		std. dev.	1.90	1.94	1.00	1.64
		sample no.	41	43	41	43

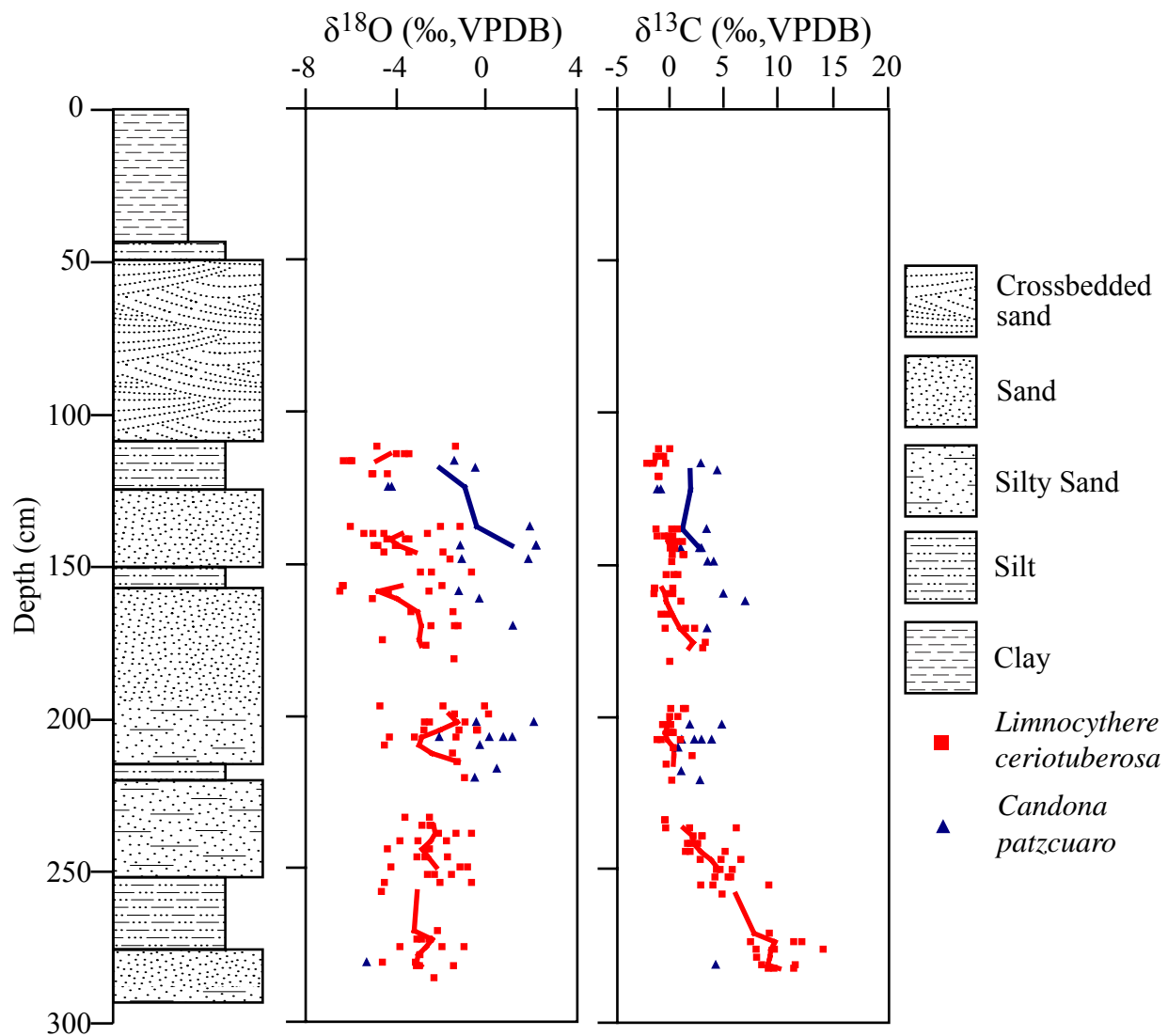


Fig. 1. North core stable isotope $\delta^{13}\text{C}$ and $\delta^{18}\text{O}$ profiles of *Candona patzcuaro* (blue) and *Limnocythere ceriotuberosa* (red). Lines indicate three-point running average.

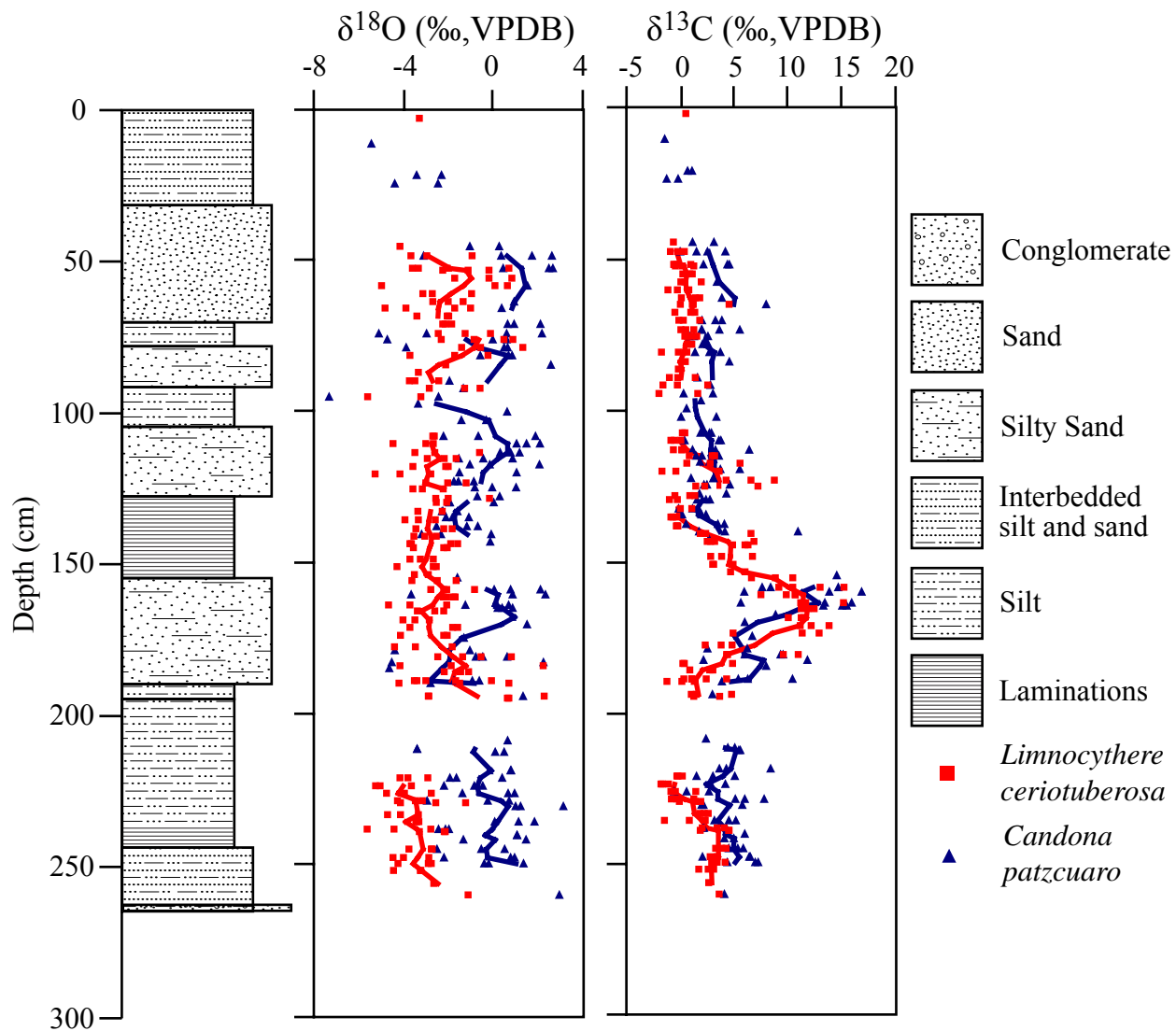


Fig. 2. South core stable isotope $\delta^{13}\text{C}$ and $\delta^{18}\text{O}$ profiles of *Candona patzcuaro* (blue) and *Limnocythere ceriotuberosa* (red). Lines indicate three-point running average.

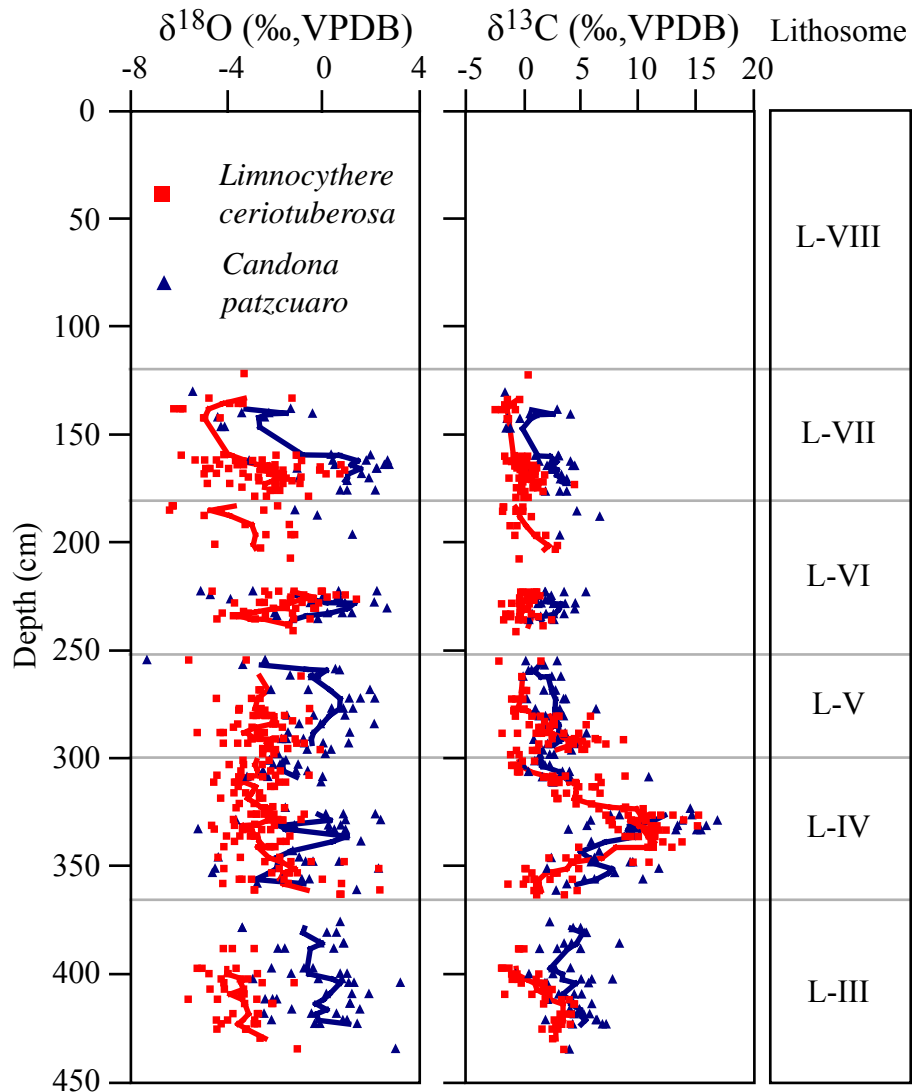


Fig. 3. Composite core stable isotope $\delta^{13}\text{C}$ and $\delta^{18}\text{O}$ profiles of *Candona patzcuaro* (blue) and *Limnocythere ceriotuberosa* (red). Colored lines indicate three-point running average. Gray lines indicate lithosome boundaries.

$\delta^{18}\text{O}$ (‰, VPDB)

C. patzcuaro

L. ceriotuberosa

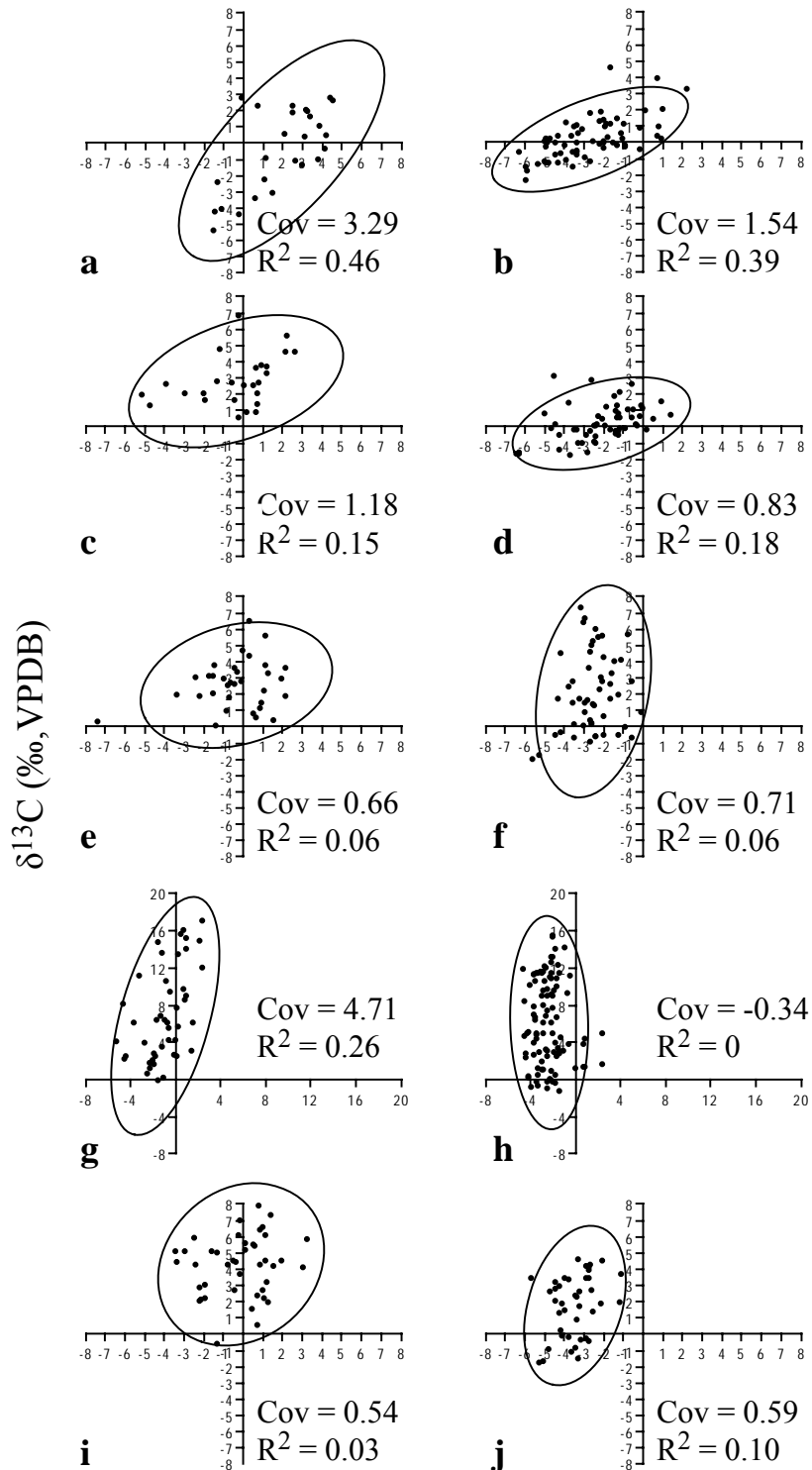


Fig. 4. *Candona patzcuaro* (left column) and *Limnocythere ceriotuberosa* (right column) $\delta^{13}\text{C}$ vs. $\delta^{18}\text{O}$ cross plots for Lithosome VII (a–b), VI (c–d), V (e–f), IV (g–h), and III (i–j).

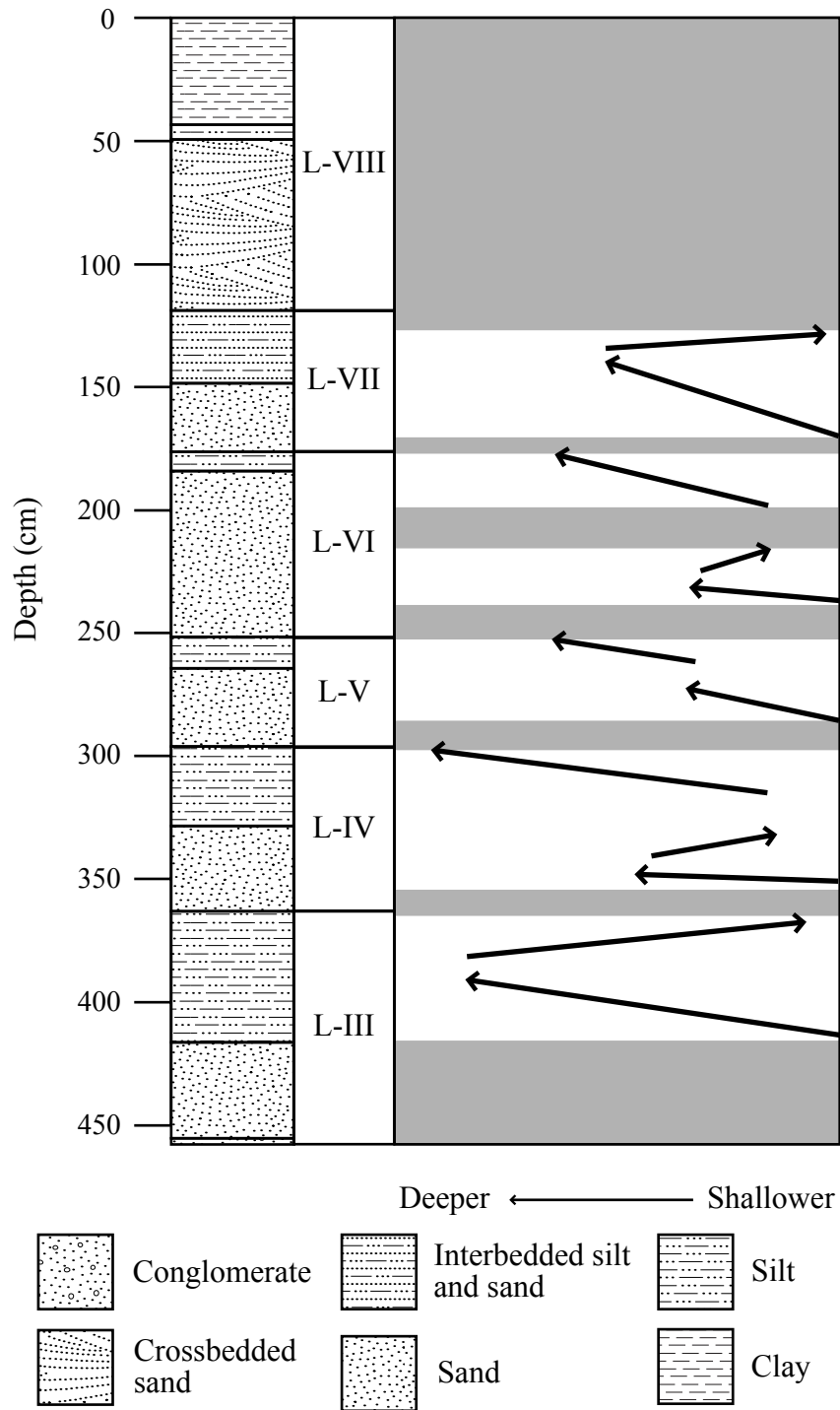


Fig. 5. Generalized water depth changes based on ostracode stable isotope $\delta^{13}\text{C}$ and $\delta^{18}\text{O}$. Gray areas indicate areas of no record.

CHAPTER 5

**MULTIPROXY PALEOCLIMATIC AND PALEOHYDROCHEMICAL
RECONSTRUCTION OF FOSSIL LAKE, OREGON, AND COMPARISON TO
PLEISTOCENE GLOBAL CLIMATE PATTERNS AND GREAT BASIN PALEOLAKE
RECORDS**

Introduction

The Fossil Lake record does not have the temporal resolution to infer fine-scale (decadal or centennial level) environmental changes, but does provide valuable insight into the broader scale changes. Each lake stand records fining-upward lithostratigraphic sequences indicating gradual transition from nearshore to deeper offshore environments. These lithostratigraphic sequences provide strong evidence for fluctuating lake levels, and by extension, changes in regional paleohydrology and paleoclimate. By comparing physical, chemical, and biological records from multiple lakes in the Great Basin, regional climate changes and localized variations can be interpreted.

The purpose of this chapter is to: 1) present a combined paleoenvironmental, paleohydrochemical, and paleoclimatic reconstruction for Fossil Lake, Oregon, from lithostratigraphy, fossil ostracode faunal assemblages, and ostracode stable isotope geochemistry records, and 2) compare reconstructions from Fossil Lake to other Great Basin paleolake records and to climate patterns of the Pleistocene, specifically, global ice volume record and marine oxygen isotope stages (MIS) (Lisiecki and Raymo, 2005).

Lithosome Interpretations

Lithosome I and II (~ 646–610 ka)

Paleoenvironmental interpretations for these two lithosome are based solely on lithostratigraphy, since ostracode fossils were not recovered from Lithosome I; ostracodes were found at the base of Lithosome II, but the faunal assemblage was dominated by the extinct species *Elkocythereis bramletti*. Unlike the other lithosomes at Fossil Lake, Lithosome I does not have a fining-upward lithologic sequence, but may represent the upper unit of one of these sequences. The lithology of Lithosome I is dominated by claystone. A thick, fining-upward layer of Rye Patch Dam tephra (~ 646 ka) is observed in the field, but was not seen in core. The claystone and tephra layer indicate deposition below storm-wave base in a relatively deep lacustrine environment. A paleosol with rhizoliths and blocky ped structures occurs at the top of the lithosome, suggesting the basin was subaerially exposed for an extended period of time. Lithosome II fines upward into massive claystone indicating a gradual transition from a nearshore to relatively deep offshore lacustrine environment. Near the base of Lithosome II is a laterally discontinuous layer of Dibekeluwe ash (610 ± 20 ka). Another paleosol with rhizoliths and blocky ped structures occurs at the top of Lithosome II.

The high stand of Lithosome I was deposited during MIS 16 based on the presence of the Rye Patch Dam tephra (Fig 1). MIS 16 represents extensive global ice coverage (Fig. 1) and one of the largest deviations toward glacial pluvial conditions (Morrison, 1991). The unconformity between Lithosome I and II likely coincides with a glacial termination at the end of MIS 16. The age of this glacial termination is at ~ 621 ka (Lisiecki and Raymo, (2005). The lake stand of Lithosome II was deposited during MIS 15, an interglacial period, based on the presence of the

Dibekeluwe ash. Increased lake depths during Lithosome II correspond to global ice volume increases during MIS 15.

The presence of the Rye Patch Dam tephra and the Dibekeluwe ash in Lake Lahontan basins allows for correlation of Lithosome I and II to the lacustrine deposits of the Rye Patch Alloformation of the Lake Lahontan Allogroup. The Rye Patch Alloformation is made up of two principal deep lake cycles, separated by an unconformity representing a lake recession (Morrison, 1991). The Paiute-Cocoon interlacustral overlies the Dibekeluwe ash in Lake Lahontan basins (Morrison, 1991). This interlacustral is represented by basins that were dry or held small, shallow ephemeral lakes. Moderate to well-developed paleosols are also common during the interlacustral. Lake Jonathan and Lake Pine, paleolakes in western Nevada, also record very high stands shortly after the deposition of the Rye Patch Dam tephra (Reheis, 1999; Reheis et al., 2002). In Lake Bonneville, Utah, deep lake marl deposits lie just below a tephra layer dated at ~ 620 ka (Oviatt et al., 1999).

Lithosome III (~ 71 ka)

Lithology and magnetic susceptibility and $\delta^{13}\text{C}$ temporal trends from Lithosome III show evidence of transitioning from shallow to a relatively deep open lake. $\delta^{13}\text{C}$ temporal trends also suggest the return of shallow-water conditions at the top of the lithosome. Ostracode faunal assemblages were dominated by *Limnocythere ceriotuberosa* and *Candona patzcuaro*, indicating the lake was alkaline and slightly saline, and the rare occurrence of *L. platyforma* suggests water temperatures were cool to cold. High variability in $\delta^{18}\text{O}$ values suggests short-term variability of precipitation/evaporation (P/E) ratios. A paleosol with rhizoliths and blocky ped structures

occurs at the top of the lithosome, suggesting the basin was subaerially exposed. The base of the lithosome contains a layer of Lao Rock Pumice Castle-like 1 tephra (~ 71 ka).

Lithosome III corresponds to MIS 4, a glacial expansion period lasting ~ 10 ka (Fig. 2). Summer Lake, a pluvial lake just south of Fossil Lake, records deep saline lake conditions with cool to cold temperature and moist climates from lithology, ostracode, and pollen evidence during MIS 4 (Cohen et al, 2000). Lake Bonneville also records offshore saline lake conditions (Balch et al., 2005). Death Valley, however, is dry and dominated by mudflats. Fluid inclusion studies suggest that Death Valley was generally cool (Lowenstein, 2002).

Lithosome IV–VII (~ 47–27.8 ka)

Much of Lithosome IV is dominated by the ostracode *L. ceriotuberosa*, suggesting saline, alkaline waters and rare *L. platyforma* valves suggests water temperatures were cool to cold. After inundation of the basin in Lithosome IV, lake levels dropped, indicated by $\delta^{18}\text{O}$ enrichment of *C. patzcuaro* and the increase in oxidation staining of ostracode valves. Decreasing lake levels also corresponded to increased rates of methanogenesis in the sediment, indicated by a positive spike in $\delta^{13}\text{C}$. Wet conditions returned and gradually lake levels rose while rates of methanogenesis decreased. Near the top of Lithosome IV, the ostracode *Fabaeformiscandona caudata* became abundant, indicating a relatively fresh, deep lake environment, with seasonal precipitation and evaporation resulting in cycles of dilution and solute concentration. The Marble Bluff Mt. St. Helens set C ash (~ 47 ka) was deposited near the top of the lithosome. A paleosol with rhizoliths and blocky ped structures occurs at the top of the lithosome, suggesting the basin was subaerially exposed.

The lithology, low ostracode abundances, and moderate number of fragmented and oxidation-stained ostracode valves of Lithosomes V–VII suggest deposition in shallow lake environments. The ostracode faunal assemblages in Lithosome V and VI are dominated by *L. ceriotuberosa* with rare *L. platyforma* and *F. caudata* indicating a cool to cold alkaline lake with moderate salinity that likely fluctuated with seasonal dilution cycles. In the basal unit of Lithosome VII, the abundance of *L. platyforma* increased so that it dominates with *L. ceriotuberosa*, indicating a switch to a cold, relatively fresh alkaline lake environment with seasonal dilution cycles. The top of Lithosome VI is dominated by *C. patzcuaro*, suggesting a relatively freshwater environment, but the dearth of ostracode does not allow for further interpretation of the paleohydrology. Lithosome V–VII generally remained shallow but each lithosome recorded increases in water depth, indicated by fining-up lithostratigraphic sequences and decreases in $\delta^{18}\text{O}$ and $\delta^{13}\text{C}$ values. A reworked coarse-grained tephra was observed at the top of Lithosome VI and at the base of Lithosome VII and may correlate to the Wono tephra (~ 32.6 ka) deposit at Summer Lake. At the top of Lithosome VII is a thick layer of Trego Hot Springs Tephra (~ 27.8 ka). The top of Lithosome V and VI are generally scoured throughout the basin but a poorly developed paleosol has been observed at the top of Lithosome VI. A paleosol with rhizoliths and blocky ped structures occurs at the top of the lithosome, suggesting the basin was subaerially exposed.

Lithosomes IV–VII were deposited during MIS 3, a relatively warm interstitial period prior to last glacial maximum. Summer Lake shows a very similar paleoclimate and paleohydrologic history as Fossil Lake during MIS 3. A high lake stand with cold moist climate conditions remained until ~ 47 ka, and then cold and drier, shallow lake environment were prevalent throughout the remainder of MIS 3 (Cohen et al., 2005). Shallow lake environments

are also observed at Pyramid Lake basin in Lake Lahontan from ~ 34–23 ka (Benson et al, 1997) and Lake Bonneville for most of MIS 3 (Balch et al, 2005). Low to moderate lake levels are observed in most of Lake Lahontan during MIS 3 (Bradbury, 1991). Searles Lake, California, went through six major lake cycles of expansion and contraction between 34 and 26 ka (Phillips et al., 1994). Death Valley was cold and dry and contained shallow saline lakes from ~ 60–35 ka and was cold and wet with a perennial saline lake for the rest of MIS 3 (Lowenstein, 2002). Owens Lake, California, was wet and cold with high lake levels from ~ 50–10 ka (Bradbury and Forester, 2002).

Lithosome VIII (~ 27.8–13 ka)

Dry conditions are recorded at the base of Lithosome VIII with the deposition of eolian sands. The presence of bleached, unbroken ostracodes in the sandstone suggests transport from either a nearby time-equivalent shallow lake or playa environment or represents older fossil ostracodes that were exposed and transported during deflation and deposition of eolian dunes. Deposited above the eolian sands is a thick claystone with abundant salmonid fossils, indicating a deep, cold lake. A number of wave cut terraces and caves in the Fort Rock basin indicate a basin-wide lake that reached depths up to 58 m (Allison, 1979; Friedel, 1993). A radiocarbon date of ~ 15.4 ka was reported from charcoal in a wave-cut cave when the lake was 38 m deep (Bedwell, 1970). A paleosol with rhizoliths and blocky ped structures occurs at the top of the lithosome, suggesting the basin was subaerially exposed for an extended period of time.

The eolian sand unit of Lithosome VIII was likely deposited at the end of MIS 3 and the lacustrine clay unit during the last glacial maximum in MIS 2. The age of the last glacial termination is at ~ 14 ka (Lisiecki and Raymo, 2005). Kelso Dunes, California, record a major

dune construction episode from 26–15 ka (Clarke, 1994). Very high lake stands are recorded during MIS 2 in Summer Lake (Cohen et al., 2000), Lake Bonneville (Balch et al, 2005), and Owens Lake (Bradbury and Forester, 2002). Death Valley was also wet with a perennial lake (Lowenstein, 2002)

Conclusions

Both conceptual and General Circulation Models (GCM) have predicted changes in P/E ratios in the Great Basin are the result from a southward diversion of the jet stream during glacial maxima (COHMAP, 1988; Thompson et al., 1993). Changes in the position of the jet stream induced by changing configurations of the Laurentide ice sheet could affect both precipitation and temperature in the western United States. Global circulation models show that the ice sheet induces splitting of the jet stream, and the movement of the two branches and their associated storm tracks appears to account for pluvial lake fluctuations in the Great Basin during the late Pleistocene (e.g., Thompson et al., 1993). Changes in lake level and inferred paleoclimate for Fossil Lake are in general agreement with other records from Great Basin paleolakes and changes in global ice volume, suggesting that climate forcing has played a major role in the lake level fluctuations. Over all, high and very high stands coincide with glacial cycles in MIS 16, 4, and 2. The high stand in Lithosome II coincides with an interglacial period in MIS 15, but increases in lake level are likely associated with the expansion of glaciers.

References

Allison, I.S., 1979. Pluvial Fort Rock Lake, Lake County, Oregon. State of Oregon Department of Geology and Mineral Industries Special Paper 7, pp. 72.

- Balch, D.P., Cohen, A.S., Schnurrenberger, D.W., Haskell, B.J., Valero Garces, B.L., Beck, J.W., Cheng, H., Edwards, R.L., 2005. Ecosystem and paleohydrological response to Quaternary climate change in the Bonneville Basin, Utah. *Palaeogeography, Palaeoclimatology, Palaeoecology* 221, 99–122.
- Bedwell, S.F., 1970. Prehistory and environment of the Pluvial Fort Rock Lake area of south central Oregon. Ph.D. Thesis, University of Oregon.
- Benson, L.V., Smoot, J.P., Kashgarian, M., Sarna-Wojcicki, A., Burdett, J.W., 1997. Radiocarbon ages and environments of deposition of the Wono and Trego Hot Springs Tephra layers in the Pyramid Lake Subbasin, Nevada. *Quaternary Research* 47, 251–260.
- Bradbury, J.P., 1991. The Late Cenozoic Diatom Stratigraphy and Paleolimnology of Tulelake, Siskiyou Co., California. *Journal of Paleolimnology* 6, 205–255.
- Bradbury, J.P., Forester, R.M., 2002. Environment and paleolimnology of Owens Lake, California: A record of climate and hydrology for the past 50,000 years. In: Hershler, R., Madsen, D.B., Currey, D.R. (Eds.), *Smithsonian Contributions to the Earth Sciences* 33, Great Basin Aquatic Systems History. Smithsonian Institution Press, Washington D. C., pp. 145–174.
- Clarke, M.L., 1994. Infra-red stimulated luminescence ages from aeolian sand and alluvial fan deposits from the eastern Mojave Desert, California. *Quaternary Science Reviews* 13, 533–538.
- Cohen, A.S., Palacios-Fest, M.R., Negrini, R.M., Wigand, P.E., Erbes, D.B., 2000. A paleoclimate record for the past 250,000 years from Summer Lake, Oregon, USA: II. Sedimentology, paleontology, and geochemistry. *Journal of Paleolimnology* 24, 151–182.

- COHMAP, 1988. Climate changes in the last 18,000 years: Observations and simulations. *Science* 241, 1043–1052.
- Friedel, D.E., 1993. Chronology and climatic controls of late Quaternary lake-level fluctuations in Chewaucan, Fort Rock, and Alkali basins, south-central Oregon. Ph.D. Thesis, University of Oregon.
- Lisiecki, L.E., Raymo, M.E., 2005. A Pliocene-Pleistocene stack of 57 globally distributed benthic $\delta^{18}\text{O}$ records. *Paleoceanography* 20, PA1003, doi:10.1029/2004PA001071.
- Lowenstein, T.K., 2002. Pleistocene lakes and Paleoclimates (0 to 200 Ka) in Death Valley, California. In: Hershler, R., Madsen, D.B., Currey, D.R. (Eds.), *Smithsonian Contributions to the Earth Sciences* 33, Great Basin Aquatic Systems History. Smithsonian Institution Press, Washington D. C., pp. 109–120.
- Morrison, R.B., 1991. Quaternary stratigraphy, hydrologic, and climatic history of the Great Basin, with emphasis on Lakes Lahontan, Bonneville, and Tecopa. In: Morrison, R.B. (Ed.), *The Geology of North America K-2, Quaternary nonglacial geology: Conterminous U.S.* The Geological Society of America, Boulder, Colorado, pp. 283–320.
- Oviatt, C.G., Thompson, R.S., Kaufman, D.S., Bright, J., Forester, R.M., 1999. Reinterpretation of the Burmester core, Bonneville Basin, Utah. *Quaternary Research* 52, 180–184.
- Phillips, F.M., Campbell, A.R., Smith, G.I., Bischoff, J.L., 1994. Interstadial climatic cycles: a link between western North America and Greenland?. *Geology* 22, 1115–1118.
- Reheis, M.C., 1999. Highest pluvial-lake shorelines and Pleistocene climate of the western Great Basin. *Quaternary Research* 52, 196–205.

Reheis, M.C., Sarna-Wojcicki, A.M., Reynold, R.L., Repenning, C.A., Mifflin, M.D., 2002.

Pliocene to middle Pleistocene lakes in the western Great Basin: Ages and connections.

In: Hershler, R., Madsen, D.B., Currey, D.R. (Eds.), *Smithsonian Contributions to the Earth Sciences 33, Great Basin Aquatic Systems History*. Smithsonian Institution Press, Washington D. C., pp. 53–108.

Thompson, R.S., Whitlock, C., Bartlein, P.J., Harrison, S.P., Spaulding, W.G., 1993. Climatic changes in the western United States since 18,000 yr B.P. In: Wright Jr., H.E., Kutzbach, J.E., Webb, T.I., Ruddiman, W.T., Street-Perrott, F.A., Bartlein, P.J. (Eds.), *Global Climates Since the Last Glacial Maximum*. University of Minnesota, Minneapolis, pp. 468–513.

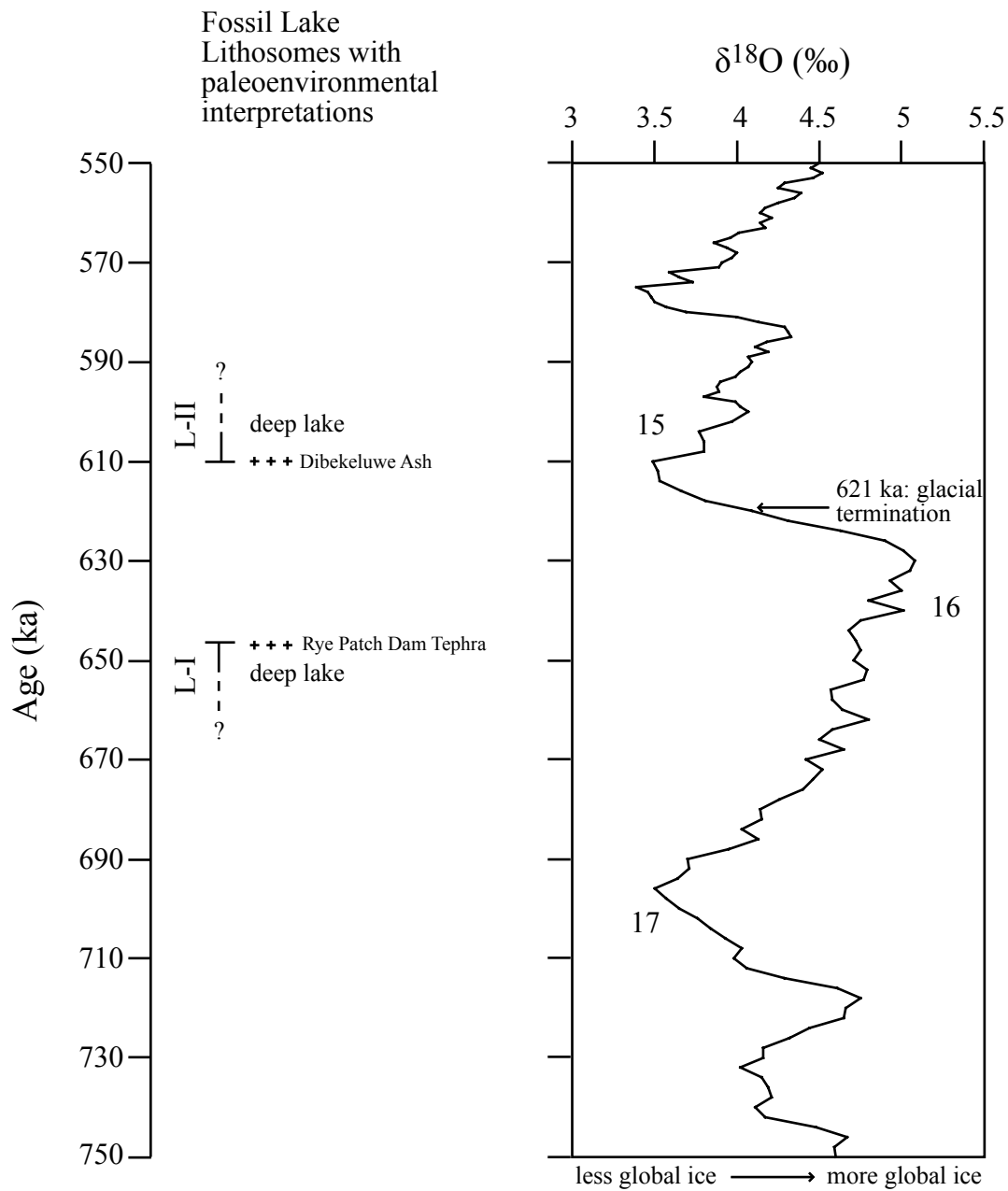


Fig. 1. Comparison of Fossil Lake paleoenvironmental interpretations of Lithosomes (L) I and II with middle Pleistocene marine oxygen isotope stages 15–17 (Lisiecki and Raymo, 2005). Correlations based on ages of tephra marker beds (cross symbols).

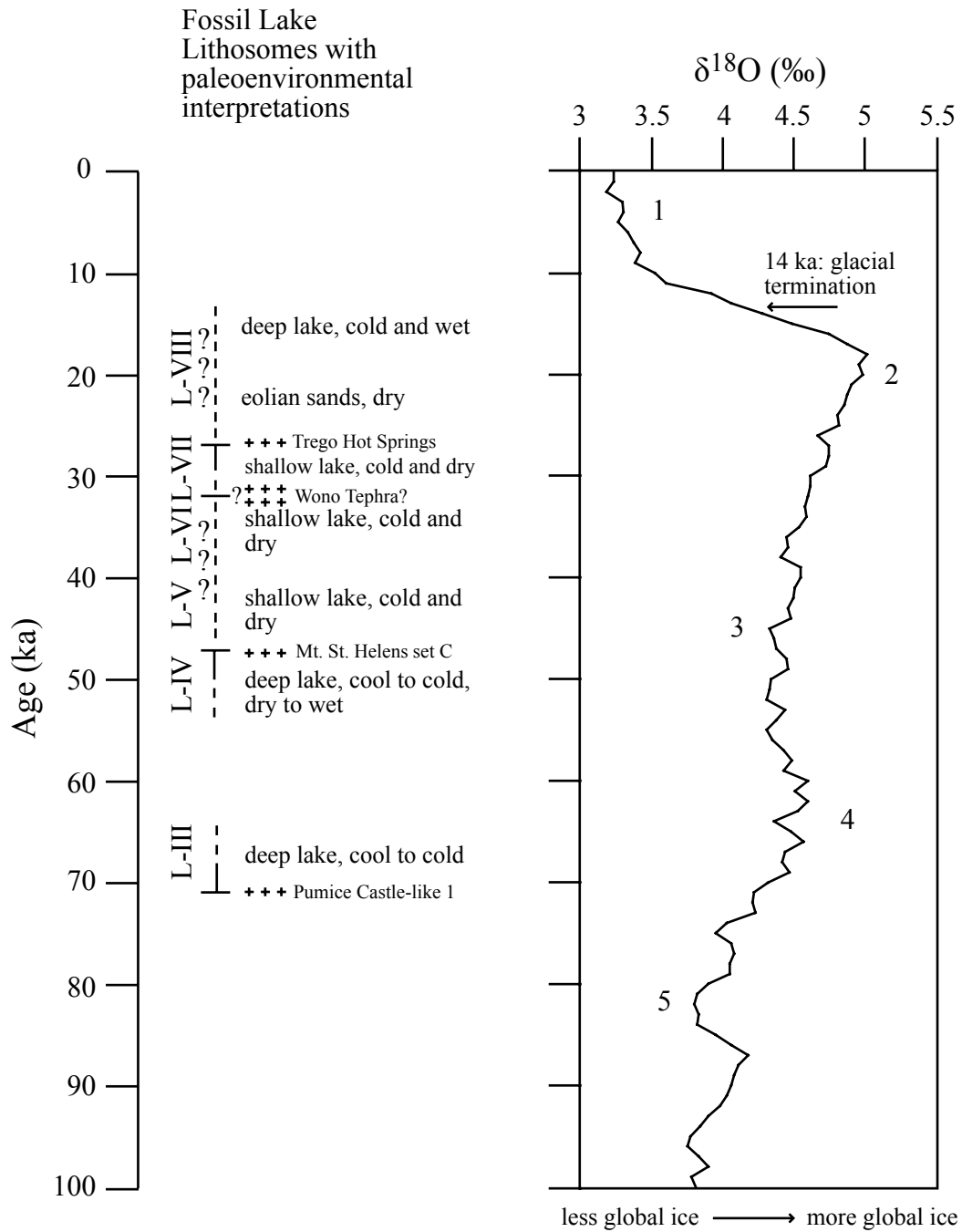


Fig. 2. Comparison of Fossil Lake paleoenvironmental interpretations of Lithosomes (L) III–VIII with late Pleistocene marine oxygen isotope stages 1–5 (Lisiecki and Raymo, 2005). Correlations based on ages of tephra marker beds (cross symbols).

CHAPTER 6
NEOICHOLOGICAL EXPERIMENTS WITH THE FRESHWATER OSTRACODE
***HETEROCYPRIS INCONGRUENS*: IMPLICATIONS FOR RECONSTRUCTING**
AQUATIC SETTINGS

ABSTRACT

Neoichnological experiments with freshwater ostracodes allow documentation and description of different morphological types of traces, their associated behavior in a variety of water depths and media (=substrates) in controlled microcosms, and the potential for their identification in the fossil record. In uncompacted, very fine-grained to medium-grained sand media the nektobenthic freshwater ostracode *Heterocypris incongruens* produced seven types of traces: three crawling trails, a swimming trail, a resting trace, a burrow, and a self-righting trace. The most common crawling trails, Type 1, are randomly sinuous with infrequent looping. The other two crawling trails are observed infrequently and are self-looping, Type 2, and zigzagging, Type 7. Swimming trails, Type 3, are straight to sinuous and are composed of parallel set of appendage scratch marks. Crawling and swimming trails likely indicate exploratory or foraging behaviors associated with locomotion. Oval-shaped depressions, Type 4, commonly occur and represent a resting behavior. Burrowing produced asymmetrical U-shaped burrows, Type 5, and represents hiding from a stimulus or a foraging behavior. A fan-shaped trace of appendage scratches, Type 6, was produced when *H. incongruens* needed to self-right itself after landing in the sediment upside down. No traces were observed in media composed of coarse or very coarse sand, but ostracodes were observed pushing and toppling sand grains. The preservation potential of ostracode traces in freshwater environments is likely poor. Traces were observed to degrade

and fill in with sediment within 24–48 hours after formation or were destroyed immediately in water currents that disrupt the sediment surface. Ostracode traces are likely preserved best when formed below storm wave-base and buried rapidly, or prior to desiccation in an ephemeral environment. After desiccation, only gross morphology of the traces can be observed and desiccation cracks tend to follow crawling trails.

INTRODUCTION

The purpose of this investigation is to document and describe the different types of traces produced by the freshwater ostracode *Heterocypris incongruens* in various sediment types in a laboratory setting and provide insight into the preservation potential of these traces in such aquatic settings as lakes (lacustrine) and swamps (palustrine). Neoichnological experiments using marine organisms have assisted in the ecological, biological, and environmental significance of marine trace fossils (e.g., Frey et al., 1978, 1984; Savrda, 1995; Gingras et al., 2002; 2004). Few neoichnological studies, however, have documented the traces of lacustrine organisms (e.g., Silvey, 1936; Fisher et al., 1980; Duck, 1986; Hasiotis and Mitchell, 1993; Gingras et al., 2007; Hamer and Sheldon, 2010; Hasiotis et al., 2010). Detailed studies of modern lacustrine tracemakers may allow for better understanding of lacustrine ichnology more accurate interpretation and reconstruction of paleoenvironments, sedimentation rates, paleohydrology, and paleoecology of ancient lacustrine environments.

Ostracodes are small bivalved crustaceans that inhabit all types of waters, often in large numbers. Many species of nektic, nektobenthic, and benthic ostracodes have been observed burrowing or crawling on media (=substrates) using their appendages (e.g., Kornicker and Wise, 1960; Voight and Hartman, 1970; Reichholf, 1983; Sohn, 1987; Abe and Vannier, 1991), but

only a few studies have examined the behaviors associated with these traces (Delorme and Donald, 1969; Roca and Danielopol, 1991; Vannier and Abe, 1993).

THE ORGANISM

Heterocypris incongruens Ramdohr (Podocopida: Podocopina: Cypridacea) is a nektobenthic species (Fig. 1) that prefers to live just above the sediment surface, but can also be found swimming in the water column or on macroalgae or macrophytes (Rossi and Menozzi, 1990). They have a worldwide distribution and can tolerate a wide range of environmental conditions (Sars, 1928). *Heterocypris incongruens* is omnivorous and feeds on algae, bacteria, and organic detritus. In rare cases, they prey on small organisms like *Daphnia* (Fryer, 1997), or scavenge carcasses (Reichholf, 1983). Reproduction is by parthenogenesis and eggs are cemented to any suitable firm media, like vegetation stems (Angell and Hancock, 1989). *Heterocypris incongruens* range from 0.2 mm long after hatching to 1 mm long in adults. There is no evidence that *H. incongruens* undergoes estivation or hibernation during periods of drying or freezing (R.M. Forester, personal communications in Angell and Hancock, 1989).

Swimming in ostracodes is accomplished when the first pair of antennae extends upward and back, while the second pair of antennae move downward and back (Van Morkhoven, 1962). Septae on the first pair of antennae may also assist with swimming, crawling, or digging (Maddocks, 2000). The claws on the second pair of antennae (Dole-Oliver et al., 2000) and the furca (Vannier and Abe, 1993) can also be used for digging. Crawling in *H. incongruens* is accomplished by using the second pair of antennae and the first pair of thoracic legs, both of which end in claws (Fryer, 1997).

METHODS

Thirteen runs were conducted in plastic Petri dishes (9.0 cm diameter x 1.5 cm height) with various numbers of ostracodes, sediment type and compaction, water depth, and food availability (Table 1). All of the ostracodes were descendant from a single female *Heterocypris incongruens* collected from the Baker wetlands in Lawrence, Kansas. Both juvenile and adult ostracodes were used in the experiments. The use of shallow Petri dishes allowed for easier viewing and photographing of ostracode movements and behaviors under a Nikon SMZ1000 stereoscopic microscope without having to focus through lots of water. To provide reference points for recording the position of traces, Petri dishes were subdivided into four quadrants by marking the sides. Three sediment types were used in the experiments: 1) crushed kaolinite sieved to particle sizes $< 177 \mu\text{m}$ (9 runs); 2) a heterogeneous very fine- to medium-grained sand produced from crushing metamorphic rocks in the rock crushing lab at the University of Kansas (2 runs); and 3) a heterogeneous medium- to very coarse-grained sand collected from eolian dunes at Fossil Lake, Oregon (2 runs). To get a uniform sediment base, the sediment was first mixed with distilled water in a beaker and poured into the Petri dishes to a water depth of 4 mm. The sediment was allowed to settle for 24–48 hours before ostracodes were introduced into the experiment. Final sediment thicknesses ranged from 1–3 mm. In the compacted kaolinite runs, the clay was compacted with a glass beaker bottom. Food was added only to one experimental run.

After the sediment settled, an ostracode(s) was pipetted into each Petri dish. The ostracodes were observed immediately and all traces and behaviors were recorded with digital photographs and hand-drawn sketches. Illustrations of each trace were recorded with respect to the four quadrants so additional observation of the traces could be made throughout the

experiment. Eight observations per experimental run were made over a two-day period, recording the addition or disappearance of traces. Macroalgae, multiple ostracodes, and agitation were introduced into some experiments (Table 1) to determine if and how ostracode tracemaking behavior changed. In the agitation experiments, water currents were produced by gently shaking the Petri dishes by hand. Small-scale agitation is defined as that which produced motion visible in the water column, while large-scale agitation is here defined as that which produced visible movement of both the water column and the top of sediment. Most trials were allowed to completely desiccate after two days to observe any changes in the morphology of the traces. Digital photographs using a Nikon DXM1200 digital microscope camera and a Nikon D100 with a zoom macro-lens were taken before, during, and after each experimental trial. Digital short movies of various behaviors and traces were produced by stringing together digital photographs taken at ~ 1 second interval (see supplemental data).

EXPERIMENTAL RESULTS

Heterocypris incongruens produced a variety of traces in the neoichnological experiments. A total of seven distinct ostracode traces were observed: three types of crawling trails, one type of trace associated with swimming, burrowing, resting, and self-righting (Table 2). Sediment grain size, presence of food, number of ostracodes, water agitation, and water depth produced different varieties and abundances of traces.

Experiment 1: Crushed Kaolinite Sediment

Ostracodes started making traces almost immediately after they were introduced into the Petri dish. A total of six distinct ostracode traces were observed from the 1-mm, 4-mm, and 50-

mm water depths experiments. Traces ranged from short to long, discontinuous to continuous and crosscutting and generally have well-defined morphologic characteristics.

The most common trace was a randomly sinuous, infrequent looping and crosscutting trail (Type 1), created when the ostracode crawled through the sediment using its appendages to excavate sediment from anterior to posterior (Fig. 2A–B; see supplementary data). The trail width was ≤ 0.5 mm, and was < 0.25 mm deep. Trails were generally wider and deeper at the 1-mm water depth than at 4- or 50-mm water depths. Trail length varied from 5 mm to > 50 mm. Ostracodes had an average crawling speed of 60 cm min^{-1} .

Two distinct morphologies of this trace were observed. In cross-section, the basic morphology of the sinuous trace had a U-shape, with sediment piled up along the outside edges. The second morphology in cross-section had a W-shape, with a medial ridge in the trail. The medial ridge was observed to degrade through time (24–48 hours) into the U-shaped cross-section. The U-shaped cross-section was more common in water depths > 4 mm but the medial ridge morphology was more common in 1-mm water depth.

A less commonly observed crawling trace was a frequently self-looping, overlapping trail (Type 2), created similarly to the Type 1 trails (Fig. 2C–D). Type 2 locomotion trails were always associated with Type 1 trails, as well as with similar dimensions and cross-sectional morphologies. The diameter of the loops typically ranged from 5 to 10 mm. Type 2 traces were more common in water depths of 1- and 4-mm than at 50-mm water depth.

Only one swimming trace was observed, a straight to sinuous trail composed of parallel sets of antenna scratch marks (Type 3) created as the ostracode swam just above the sediment surface (Fig. 2E–F). Some trail curves only record one set of antenna scratch marks. The width of this locomotion trace was approximate the width of the ostracode, ≤ 0.5 mm, and barely

penetrated the surface, < 0.1 mm deep. The length of Type 3 trails varied from 5 mm to > 40 mm. Observation of some trails showed repeated switching between the swimming and sinuous crawling trace that produced interconnected Type 1 and Type 3 trails. Type 3 traces were common and only observed at 1- and 4-mm water depths.

Oval-shaped traces (Type 4) were produced when the ostracode rested in the sediment (Fig. 3A–B). The ostracodes always rested with their appendages in the sediment. Resting traces were the width of the ostracode, ≤ 0.5 mm, and varied in depth from ~ 0.25 – 0.5 mm. Occasionally a Type 1 trail was observed leaving a Type 4 trace. Resting traces are very common at water depths > 4 mm and rare at 1-mm water depth.

Ostracodes were also observed burrowing into the sediment. An asymmetrical U-shaped burrow (Type 5) was produced as the ostracode entered the sediment at a steep angle, nearly vertical, and exits at a very gradual angle, leaving behind a pair of circular openings (Fig. 3C-D; see supplementary data). Displaced sediment from the burrow was left near the entrance and exit openings. The duration of time the ostracode remained in the burrow was variable, but generally less two minutes. The diameters of the openings were the diameter of the ostracode, ≤ 0.5 mm, and the distance between the two burrow openings was generally < 2 mm. The depth of the burrow was shallow, ~ 1 mm. Type 5 traces were frequent and only observed at 4 and 50 mm water depth.

No changes in trace types or behavior were observed in the runs with the addition of macroalgae, multiple ostracode, or compacted sediment. In the run with macroalgae, traces were more concentrated around the macroalgae. Bioturbation was greater in runs with multiple ostracodes. In the compacted runs, only Type 1 traces were observed and they were only found

along disruptions in the compacted sediment where the ostracode could penetrate into the sediment. Otherwise the sediment surface was too firm to penetrate.

Agitation produced varying results. Small-scale agitation did not affect the ostracode or its behavior. Large-scale agitation caused disruption in ostracode swimming and forced it to retreat to the bottom of the Petri dish. Occasionally the ostracode would burrow into the sediment producing a U-shaped burrow (Type 5). Agitation was stopped when the ostracode began to burrow in order to document the burrowing process. Burrowing into the sediment was rapid, < 30 seconds. The ostracode remained in the burrow for < 2 minutes before exiting. In general, large-scale agitation partially or completely erased surface and subsurface traces constructed previously.

As a result of the large-scale agitation, ostracodes were sometimes flipped upside down (posterior side) onto the sediment. The ostracode righted itself by using its first pair of antennae, and possibly the second pair, to push away from the sediment and flip over, rotating on its distal end. A fan-shaped trace (Type 6) was produced from this behavior (Fig. 3E–F). The width of the fan-shaped trace is approximately the width of the ostracode, ≤ 0.5 mm, and barely penetrated the sediment surface, < 0.1 mm. Occasionally a small, oval depression, similar to the resting trace, but shallower, was created where the ostracode was stuck in the sediment (Type 4). A Type 1 trail was observed often leaving the fan-shaped self-righting trace.

Summary.—Noticeable differences were observed between experiments with 1-mm water depth and those conducted with 4-mm and 50-mm water depth (Fig. 4). At 1-mm water depth, the sediment was highly bioturbated and dominated by long, continuous Type 1 traces, frequently with medial ridges. Type 1 trails were > 20 mm long. Type 3 trails were common while Type 2 and 4 traces were rare at 1-mm water depth. The sediment in the 4-mm and 50-mm

water depth experiments was poorly (50-mm) to moderately (4-mm) bioturbated and dominated by short, discontinuous Type 1 traces with occasional medial ridges. Type 1 trails were < 20 mm long. Type 4 and 5 traces were common and Type 2 trails were rare at 4-mm and 50-mm water depths.

Experiment 2: Heterogeneous very fine- to medium-grained sand

Four types of traces were observed in this experiment: Type 1, Type 4, and Type 5. A third type of crawling trace—a zigzag pattern (Type 7)—was also observed, but was rare. The Type 7 locomotion trace is similar to the Type 1, but differs by its sharp ~ 90° turns (Fig. 5A–B). A medial ridge was never observed with this locomotion trace. The width of this trace was approximate the width of the ostracode, ≤ 0.5 mm, and < 0.25 mm deep. Trails were < 5 mm long, discontinuous, and lacked appendage scratch marks.

Experiment 3: Heterogeneous medium- to very coarse-grained sand

No traces were produced in these experiments. The sand grains were often larger than the ostracode itself and too heavy between which to crawl or burrow. Occasionally, ostracodes were able to use their appendages to push and topple grains. When pore space between sand grains was large enough, ostracodes would swim through the interstitial spaces, but they always remained close to the sediment surface.

Trace Morphology After Sediment Desiccation

Types 1–7 became less well defined as the Petri dishes were allowed to desiccate (Fig. 6). Sediment surrounding the traces began to infill the trails, depressions, and burrows, and fine

morphological details of the traces degraded. After desiccation was complete, all except the parallel appendage scratch marks of Type 3 and Type 6 traces were still visible on the sediment surface. All medial ridge morphologies in Type 1 and Type 2 traces were erased. Desiccation cracks developed and followed the Type 1 and Type 2 traces (Fig. 6C).

DISCUSSION

Trace Behaviors

After introduction, *Heterocypris incongruens* preferred to stay relatively close to the sediment surface, swimming or crawling along the surface. In the 50-mm water depth experimental runs, ostracodes initially remained within 10 mm of the sediment surface. Type 1 and Type 3 traces were the most abundant in the experiments and were always the first traces produced after the introduction. Type 3 trails were observed at 1- and 4-mm water depths, however, it is likely they were present in the 50 mm water depth experimental run but were not visible as a result of their shallow nature and distortion from the water column. In the heterogeneous coarse sand experiment, ostracodes were also observed swimming near the sediment surface and within the sediment interstices. Similar interstices swimming by the freshwater ostracode *Cypridopsis vidua* was also observed by Roca and Danielopol (1991), without a food stimuli. These observations suggest that swimming and crawling traces (including Type 2 and Type 7) represent an exploratory behavior, at least initially. The rapid speed of crawling and the random sinuosity and looping nature of crawling traces also supports an exploratory behavior. The crawling speeds we observed in our experiments with *Heterocypris incongruens*, $\sim 60 \text{ cm min}^{-1}$, were slower than those observed by Abe and Vannier (1991) with marine ostracodes, $70\text{--}80 \text{ cm min}^{-1}$. The crawling traces may also represent foraging behavior if

the ostracodes became hungry during the experiment. Since food was absent in most experiments (see Table 1), ostracodes would have been forced to forage through the sediment for detritus.

Exploratory behaviors have been observed previously in ostracodes. Uiblein et al. (1996) observed exploratory swimming behaviors in laboratory aquarium experiments using *Cypridopsis vidua*, which did not result in any traces. This ostracode initially stayed near the sediment surface exploring the surroundings before eventually swimming higher in the water column in search of food. Swimming close to the sediment surface reduces predation risk and generally offered additional shelter opportunities in vegetation, which may explain the Type 1 and Type 3 trail patterns in this study and the concentration of Type 1 trails near the macroalgae.

The presence of a medial ridge in Type 1 and Type 2 traces does not appear to be controlled by behavior, but instead is a result of water depth and media type and cohesiveness. Extremely shallow water depths, < 1 mm, produced wider trails because the ostracode was forced further into the sediment because of the lack of water column. The medial ridge is likely the result of crawling deeper into the sediment which caused the open valves and appendages to be pulled through the sediment. Alternately, the presence of medial ridge may be a function of clay flocculation. A medial ridge is never observed in the heterogeneous fine-grained sand experimental run, resulting from heterogeneity and the lack of sediment cohesiveness or the inability to penetrate deeply into the sediment. The short, discontinuous nature of Type 1 and Type 7 traces in the heterogeneous fine-grained sand is likely the result of increased difficulty crawling in a sandy medium that caused the ostracode to cease crawling and return to active swimming or find a new path by performing sharp $\sim 90^\circ$ turns (Type 7).

Ostracode burrowing is the result of several different stimuli and behavior. Delorme and Donald (1969) observed the freshwater ostracode *Candona rawsoni* burrowing into mud to survive desiccation conditions. The ostracodes burrowed to depths sufficient to keep themselves moist, up to 5 mm, and survived in a torpid state for short periods of drought or freezing, up to 2 days. Vannier and Abe (1993) observe the marine ostracode *Vargula hilgendorffii* burrowing less than a few millimeters in the sediment as a response to both predation and light stimuli. This paper also provided illustrations of ostracode burrowing (Vannier and Abe, 1993, fig. 11). The freshwater ostracode, *Darwinula stevensoni*, can not swim and has been observed burrowing where plant debris was abundant (Robinson, 1980), suggesting a foraging or grazing behavior. Kornicker and Wise (1960) studied the burrowing time of two marine ostracodes, *Sarsiella zostericola* and *Hemicythere conradi*. They found both species generally spent less than 100 seconds burrowing in silty sands but in oolitic sands burrow times ranged from ~ 50–1000 seconds.

In our study, burrowing by *Heterocypris incongruens* was observed during simulated water currents but also during calm conditions. Burrowing resulting from water currents suggests a hiding behavior to prevent getting swept away in a strong current. Once the agitation was removed, the ostracode emerged from its burrow. During calm conditions, burrowing is likely the result of the sensitivity to the bright lights that were used to view the experiments under the stereomicroscope or as a result of foraging for detritus. Burrowing times were generally < 120 seconds and are similar to the burrowing times of marine ostracodes in silty sands observed by Kornicker and Wise (1960). *Heterocypris incongruens* did not burrow during desiccation and died on the sediment surface, confirming that *H. incongruens* does not undergo any form of torpidity during periods of drying.

The oval-shaped traces, Type 4, are the result of resting behaviors. *Heterocypris incongruens* were occasionally observed sitting in the depressions during observation checkpoints, but they were never observed coming to rest in the sediment. The ostracodes were always active while the bright observation lights were on. It is unclear if the ostracode digs a depression to rest in to provide some protection, or if they passively settle into the sediment. It is also unclear the duration of ostracode resting, but the creation of > 10 resting traces in 24 hours suggests multiple resting periods per day.

The fan-shaped appendage scratch mark trace, Type 6, is the result of a self-righting behavior that allows an upside down ostracode to flip over and resume swimming or crawling.

Preservation Potential

Ostracodes usually occur in large numbers in palustrine and lacustrine environments and, while this occurrence should increase their preservation potential, their very shallow traces have poor preservation potential as a result of degradation through time and destruction by water currents. Ostracode traces may also be overprinted by larger tracemakers (e.g., Hasiotis et al., 2010). The ostracode traces produced in the koalinite just prior to desiccation, however, were preserved and recognizable after the sediment was completely dry. Only the gross morphology of these traces was preserved, and some of the crawling traces were masked by desiccation cracks that formed inside after desiccation (Fig. 6C). Trusheim (1931) also observed sinuous crawling traces of ostracodes on the muddy margins of a desiccated pond. The crawling traces all led towards an area where hundreds of ostracode carapaces were found, indicating the location of the last remaining water before the pond desiccated. Ostracode traces could also be

preserved if they were formed below wave-base level and then buried rapidly by nonerosive depositional processes. Rapid burial may also potentially preserved fine morphological details.

Paleontological Significance

The oldest freshwater ostracode fossils belonged to the Family Darwinulidae and are first reported from the Devonian, ~ 400–370 Ma (Marten and Horne, 2009). Even with the long geologic record, there have been only two reports of trace fossils attributed to freshwater ostracodes from (Jarzembowski, 1989; Garvey and Hasiotis, 2008). Jarzembowski (1989) first reported ostracode traces from an Upper Carboniferous lacustrine environment in England. These traces were later described by Pollard and Hardy (1991). Both locomotion and resting traces were observed in fissile siltstone and were so abundant that it gave the bedding plane a wrinkled appearance. The locomotion traces were mostly irregular sinuous trails with rare loops. In cross section, trails were V-shaped grooves (epichnia) or ridges (hypichnia) measuring ~ 0.25–0.5 mm wide and up to 40 mm long. Loops associated with the locomotion trails had an average diameter of 5 mm. The resting traces were ovoid depressions (epichnia), ~ 0.5 mm x 1.0 mm. Some locomotion trails are connected to the resting depressions. Pollard and Hardy (1991) did not assign an ichnotaxon for the traces but stated the locomotion traces closely resembled the ichnotaxon *Mermia* isp., but without the distinctive looping. The dimensions and patterns of these traces closely resemble the modern traces described within this paper.

The second report of ostracode trace fossils is from the Lower Carboniferous of Australia. Garvey and Hasiotis (2008) described slightly bilobate to elongate arrow-shaped resting traces in red shale that are 3 to 5 mm long, and 1 to 3 mm wide. These resting traces are

assigned to the ichnospecies *Sagittichnus linki*. The dimensions of these traces are two to three times greater than the resting traces dimension produced by *Heterocypris incongruens*.

We can compare the traces produced by *H. incongruens* in our experiments with similar ichnotaxa (e.g., Häntzschel, 1975; Pemberton et al., 2001; Hasiotis, 2002) to provide further insights to their use for interpreting the paleoenvironment, ethology, and tracemaker (Table 2). The gross morphology of Type 1 and Type 2 traces are similar to *Gordia marina* and *Haplotichnus indianensis*, and with overlapping loops it closely resembles the ichnotaxon *Mermia mermia*. When a medial ridge is present in the trails and loops, both are similar to the ichnotaxon *Cruziana problematica*. Type 7 traces are similar to *Treptichnus bifurcus*, whereas Type 3 traces are similar to the ichnotaxon *Harpepus* isp. and *Mesichnium* isp. Type 4 traces closely resemble the ichnotaxon *Sagittichnus lincki*. Type 5 traces are similar to the ichnotaxon *Phycodes circinnatum*. There is no comparable ichnotaxon for the Type 6 traces.

The assemblage of ostracodes traces and their abundance can offer insight to the water depth in which they were formed and preserved. Long continuous sinuous crawling traces with or without medial ridges, > 20 mm, are formed in extremely shallow water conditions, just prior to desiccation. The sediment would also be highly bioturbated. In our study, resting traces were rare, however, only one ostracode was used in the experiments and usually the only resting trace was associated with the death location. In an ephemeral pond or lake, ostracodes would be more abundant and resting traces may be common. The presence of desiccation cracks inside the crawling traces indicates subaerial exposure shortly after trace formation. In shallow water, high-energy conditions, water currents would likely destroy all ostracode traces. Shallow water, low-energy conditions and sediments below storm wave base might preserve assemblages dominated by short, discontinuous ostracode crawling traces, < 20 mm, resting traces, and

occasional burrows. The sediment would be poorly to moderately bioturbated. Unfortunately, water depth cannot be determined from this trace assemblage because similar assemblages were observed at 4-mm and 50-mm water depths lacking water current. No traces would be found in lacustrine profundal settings that are meromictic and have anoxic bottom water (Brinkhurst, 1974; Hasiotis et al., 2010).

While no traces were recorded in the coarse sand experiments, the act of pushing and toppling sand grains by ostracodes may displace enough grains to produce the ghosting effect or cryptobioturbation in lacustrine laminated sediments. Other meiofauna organisms similar in size to ostracodes have been observed to cryptobioturbate foreshore marine sediments (Pemberton et al., 2001).

CONCLUSION

Ostracode neoichnological experiments produced a number of different traces. The most common of these traces is a randomly sinuous locomotion trail (Type 1), occasionally preserved with a medial ridge. The other locomotion traces, overlapping loops (Type 2), zigzag (Type 7), and parallel appendage scratch mark trails (Type 3) were observed less frequently. Types 1, 2, and 7 are likely associated with exploratory behavior to foraging for detritus. Type 3 traces were produced as the ostracode swam over the sediment surface. Commonly associated with Types 1 trails, are small oval resting depressions (Types 4). Rare fan-shaped self-righting traces (Types 6) were formed after an ostracode was flipped upside down into the sediment during water agitation that affected the bottom sediment. Asymmetrical U-shaped burrows (Type 5) were produced during period of calm and agitated waters, suggesting they are formed by multiple behaviors. During agitation, burrowing was initiated by hiding behaviors to prevent getting

swept up in the current. During calm conditions burrowing resulted from either foraging or hiding from a light stimuli.

Ostracode trace assemblages can aid in paleoenvironment interpretations. Highly bioturbated sediments containing long continuous crawling traces with occasional resting traces represent very shallow water and desiccation conditions. Desiccation cracks form in crawling traces after they are subaerially exposed. Poor to moderately bioturbated sediments containing short, discontinuous crawling traces, resting traces, and occasional burrow represent an environment below wave-base level. The preservation potential of ostracode traces is poor but may be preserved if made just prior to desiccation or below wave-base level and quickly buried.

REFERENCES

- ABE, K., and VANNIER, J., 1991, Mating behavior in the Podocopid ostracode *Bicornucythere bisanensis* (Okubo, 1975): Rotation of a female by a male with asymmetric fifth limbs: *Journal of Crustacean Biology*, v. 11, p. 250–260.
- ANGELL, R.W., and HANCOCK, J.W., 1989, Response of eggs of *Heterocypris incongruens* (Ostracoda) to experimental stress: *Journal of Crustacean Biology*, v. 9, p. 381–386.
- BRINKHURST, R.O., 1974, *The benthos of lakes*: Macmillan Press, London, 190 p.
- DELORME, L.D., and DONALD, D., 1969, Torpidity of freshwater ostracodes: *Canadian Journal of Zoology*, v. 47, p. 997–999.
- DOLE-OLIVER, M.-J., GALASSI, D.M.P., MARMONIER, P., and CREUZÉ DES CHÂTELLIERS, M., 2000, The biology and ecology of lotic microcrustaceans: *Freshwater Biology*, v. 44, p. 63–91.

- DUCK, R.W., 1986, Traces made by the amphipod *Gammrus* in subaerially-exposed marginal sediments of a freshwater lake: *Boreas*, v. 15, p. 19–23.
- FISHER, J.B., LICK, W., MCCALL, P.L., and ROBBINS, J.A., 1980, Vertical mixing of lake sediment by tubificid oligochaetes: *Journal of Geophysical Research*, v. 85, p. 3997–4006.
- FREY, R.W., CYRRAN, H.A., and PEMBERTON, S.G., 1984, Tracemaking activities of crabs and their environmental significance: The ichnogenus *Psilonichnus*: *Journal of Paleontology*, v. 58, p. 333–350.
- FREY, R.W., HOWARD, J.D., and PRYOR, W.A., 1978, *Ophiomorpha*: Its morphologic, taxonomic, and environmental significance: *Palaeogeography, Palaeoclimatology, Palaeoecology*, v. 23, p. 199–229.
- FRYER, G., 1997, The horse-trough ostracod *Heterocypris incongruens*: *The Naturalist*, v. 122, p. 121–135.
- GINGRAS, M.K., MACEachern, J.A., and PICKERILL, R.K., 2004, Modern perspectives on the *Teredolites* ichnofacies: Observations from Willapa Bay, Washington: *PALAIOS*, v. 19, p. 79–88.
- GINGRAS, M.K., PICKERILL, R., and PEMBERTON, S.G., 2002, Resin cast of modern burrows provides analogs for composite trace fossils: *PALAIOS*, v. 17, p. 206–211.
- GINGRAS, M.K., LALOND, S.V., AMSKOLD, L., and KONHAUSER, K.O., 2007, Wintering chironomids mine oxygen: *PALAIOS*, v. 22, p. 433–438.
- GARVEY, J.M., and HASIOTIS, S.T., 2008, An ichnofossil assemblage from the Lower Carboniferous Snowy Plains Formation, Mansfield Basin, Australia: *Palaeogeography, Palaeoclimatology, Palaeoecology*, v. 258, p. 257–276.

- HAMER, J.M.M., and SHELDON, N.D., 2010, Neoichnology at lake margins: Implications for paleo-lake systems: *Sedimentary Geology*, v. 228, p. 319–327.
- HÄNTZSCHEL, W., 1975. Trace fossils and Problematica, *in* Moore, R.C., Ed., *Treatise on Invertebrate Paleontology. Part W, Miscellanea, Supplement 1: Geological Society of America and the University of Kansas Press, Boulder, Colorado and Lawrence, Kansas*, p. W1-W269.
- HASIOTIS, S.T., 2002, Continental Trace Fossils: SEPM Short Course Notes Number 51, Tulsa, Oklahoma, 130 p.
- HASIOTIS, S.T., and MITCHELL, C.E., 1993, A comparison of crayfish burrow morphologies: Triassic and Holocene fossil, paleo- and neo-ichnological evidence, and the identification of their burrowing signatures: *Ichnos*, v. 2, p. 291–314.
- HASIOTIS, S.T., PLATT, B.F., REILLY, M., AMOS, K., LANG, S., KENNEDY, D., TODD, J.A., and MICHEL, E., 2010, Actualistic studies of the spatial and temporal distributions of terrestrial and aquatic organism traces in continental environments to differentiate lacustrine from fluvial, eolian, and marine deposits in the geologic record, *in* Baganz, O.W., Bartov, Y., Bohacs, K., and Nummendal, D., eds., *Lacustrine sandstone reservoirs and hydrocarbon systems: AAPG Memoir 95*, p. 1–56.
- JARZEMBOWSKI, E.A., 1989, Writhlington Geological Nature Reserve: Proceedings of the Geologists Association, v. 100, p. 219–234.
- KORNICKER, L.S., and WISE, C.D., 1960, Some environmental boundaries of a marine ostracode: *Micropaleontology*, v. 6, p. 393–398.
- MADDOCKS, R.F., 2000, The antennule in Podocopid Ostracoda: Chaetotaxy, Ontogeny, and Morphometrics: *Micropaleontology*, v. 46, supp. 2, p.1–72.



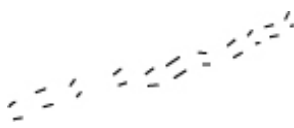




- MARTEN, K., and HORNE, D.J., 2009, Ostracoda, *in* Likkens, G., ed., *Encyclopedia of Inland Waters*: Elsevier Publishing, Boston, p. 405–415.
- PEMBERTON, S.G., SPILA, M., PULHAM, A.J., SAUNDERS, T., MACEACHERN, J.A., ROBBINS, D., and SINCLAIR, I.K., 2001, Ichnology and sedimentology of shallow to marginal marine systems: Ben Nevis and Avalon Reservoirs, Jeanne d’Arc Basin: Geological Association of Canada, St. John’s Newfoundland, Short Course Notes 15, 353 p.
- POLLARD, J.E., and HARDY, P.G., 1991, Trace fossils from the Westphalian D of Writhlington Geological Nature Reserve, nr. Radstock, Avon: Proceedings to the Geological Association, v. 102, p. 169–178.
- REICHHOLF, V.J., 1983, Ökologie und Verhalten des Muschelkrebses *Heterocypris incongruens* Claus, 1892 (Ostracoda): *Spixiana*, v. 6, p. 205–210.
- ROBINSON, J.E., 1980, The Ostracod Fauna of the Interglacial Deposits at Sugworth, Oxfordshire: *Philosophical Transactions of the Royal Society of London. Series B, Biological Sciences*, v. 289, p. 99–106.
- ROCA, J.R., and DANIELOPOL, D.L., 1991, Exploration of the interstitial habitats by the phytophilous ostracod *Cypridopsis vidua* (O. F. Müller): Experimental evidence, *Annales de Limnologie*, v. 27, p. 243–252.
- ROSSI, V., and MENOZZI, P., 1990, The Clonal Ecology of *Heterocypris incongruens* (Ostracoda): *Oikos*, v. 57, p. 388–398.
- SARS, G.O., 1928, *An account of the Crustacea of Norway. Volume IX*: Bergen Museum, Oslo, Norway, 277 p.
- SAVRDA, C.E., 1995, Ichnologic applications in paleoceanographic, paleoclimatic, and sea-level studies: *PALAIOS*, v. 10, p. 565–577.

- SILVEY, J.K.G., 1936, An investigation of the burrowing inner-beach insects of some fresh-water lakes: Michigan Academy of Science, Arts, and Letters, v. 21, p. 655–696.
- SOHN, I.G., 1987, The Ubiquitous Ostracode *Darwinula stevensoni* (Brady and Robertson, 1870), Redescription of the Species and Lectotype Designation: Micropaleontology, v. 33, p. 150–163.
- TRUSHEIM, V.F., 1931, Aktuo-paläontologische Beobachtungen an *Triops cancriformis* Schaeffer (Crust. Phyll.): Senckenbergiana, v. 13, p. 234–243.
- UIBLEIN, F., ROCA, J.R., BALTANÁS, A., and DANIELOPOL, D.L., 1996, Tradeoff between forging and antipredator behaviour in a macrophyte dwelling ostracod: Archiv für Hydrobiologie, v. 137, p. 119–133.
- VOIGT, E., and HARTMANN, G., 1970, Über rezente vergipste Ostracodenfährten, Senckenbergiana maritime, v. 2, p. 103–118.
- VAN MORKHOVEN, F.P.C.M., 1962, Post-Paleozoic Ostracoda, their morphology, taxonomy, and economic use: Elsevier, New York, 196 p.
- VANNIER, J., and ABE, K., 1993, Functional morphology and behavior of *Vargula hilgendorfi* (Ostracoda: Myodocopida) from Japan, and discussion of its crustacean ectoparasites: Preliminary results from video recordings: Journal of Crustacean Biology, v. 13, p. 51–76

Table 1. Summary of conditions for 13 experimental runs that examined *Heterocypris incongruens* traces.

Run No.	Sediment Type			Water depth (mm)			No. of Ostracodes		Types of Additions		
	Clay	Fine Sand	Coarse Sand	1	4	50	1	3-5	Food	Sediment compaction	Water Agitation
1	X			X			X				
2	X				X		X				
3	X				X		X		X		
4	X				X		X			X	
5	X				X		X				X
6	X				X			X			
7	X				X			X		X	
8	X					X	X				
9	X					X		X			
10		X			X		X				
11		X			X			X			
12			X		X		X				
13			X		X			X			

Table 2. Types of modern *Heterocypris incongruens* traces.

Type	Morphology	Comparable Ichnotaxon	Representative drawing
1	randomly sinuous, infrequent looping and crosscutting crawling trail	<i>Gordia marina</i> , <i>Haplotichnus indianensis</i> , <i>Cruziana problematica</i>	
2	frequently self-looping, overlapping crawling trail	<i>Mermia mermia</i> , <i>Cruziana problematica</i>	
3	straight to sinuous swimming trail composed of parallel sets of antenna scratch marks	<i>Harpepus</i> isp., <i>Mesichnium</i> isp.	
4	oval-shaped resting depression	<i>Sagittichnus lincki</i>	
5	asymmetrical U-shaped burrow	<i>Phycodes circinnatum</i>	
6	fan-shaped self-righting trace	none	
7	zigzag crawling trail	<i>Treptichnus bifurcus</i>	

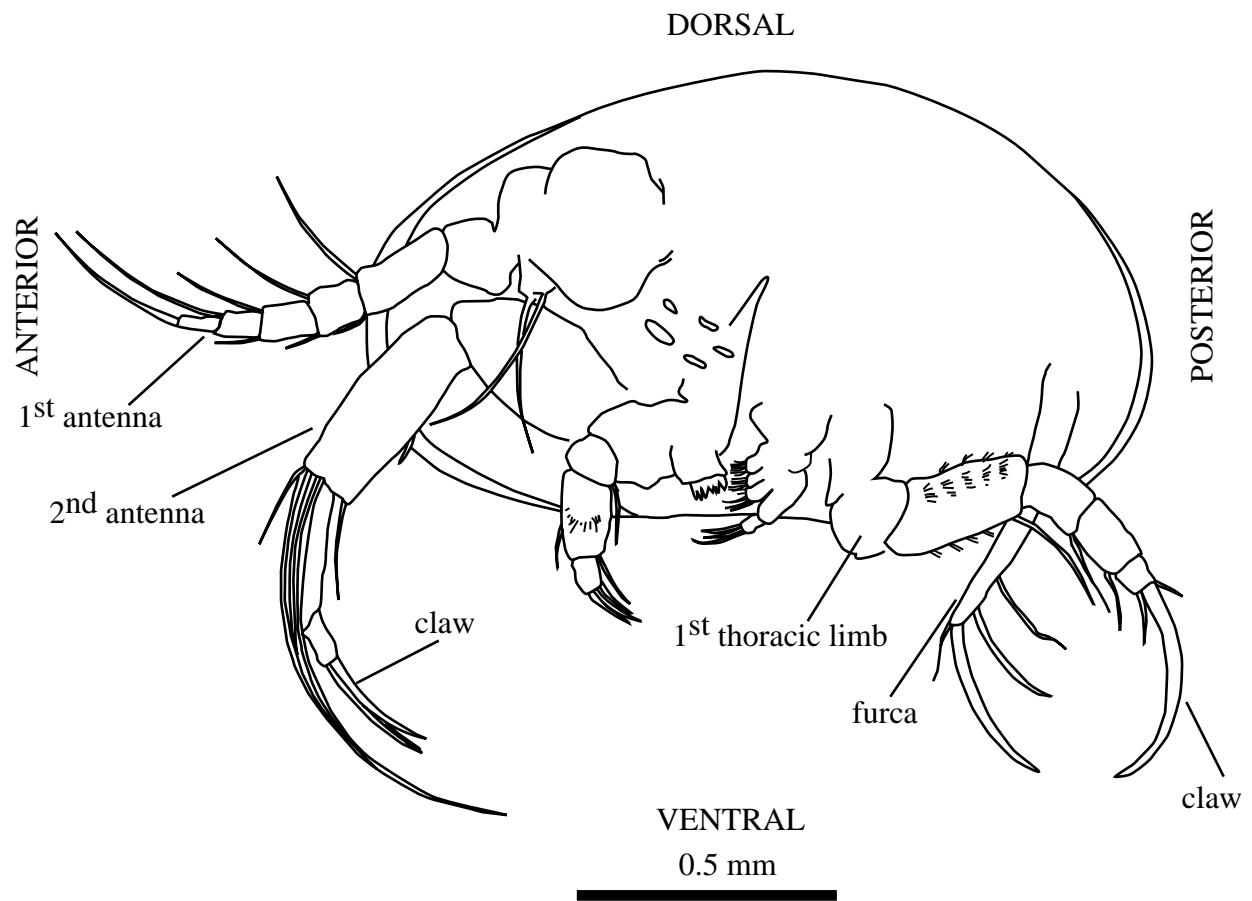


FIGURE 1—Interior view of a single valve of a generalized *Heterocypris incongruens*. Modified from Rossi and Menozzi (1990).

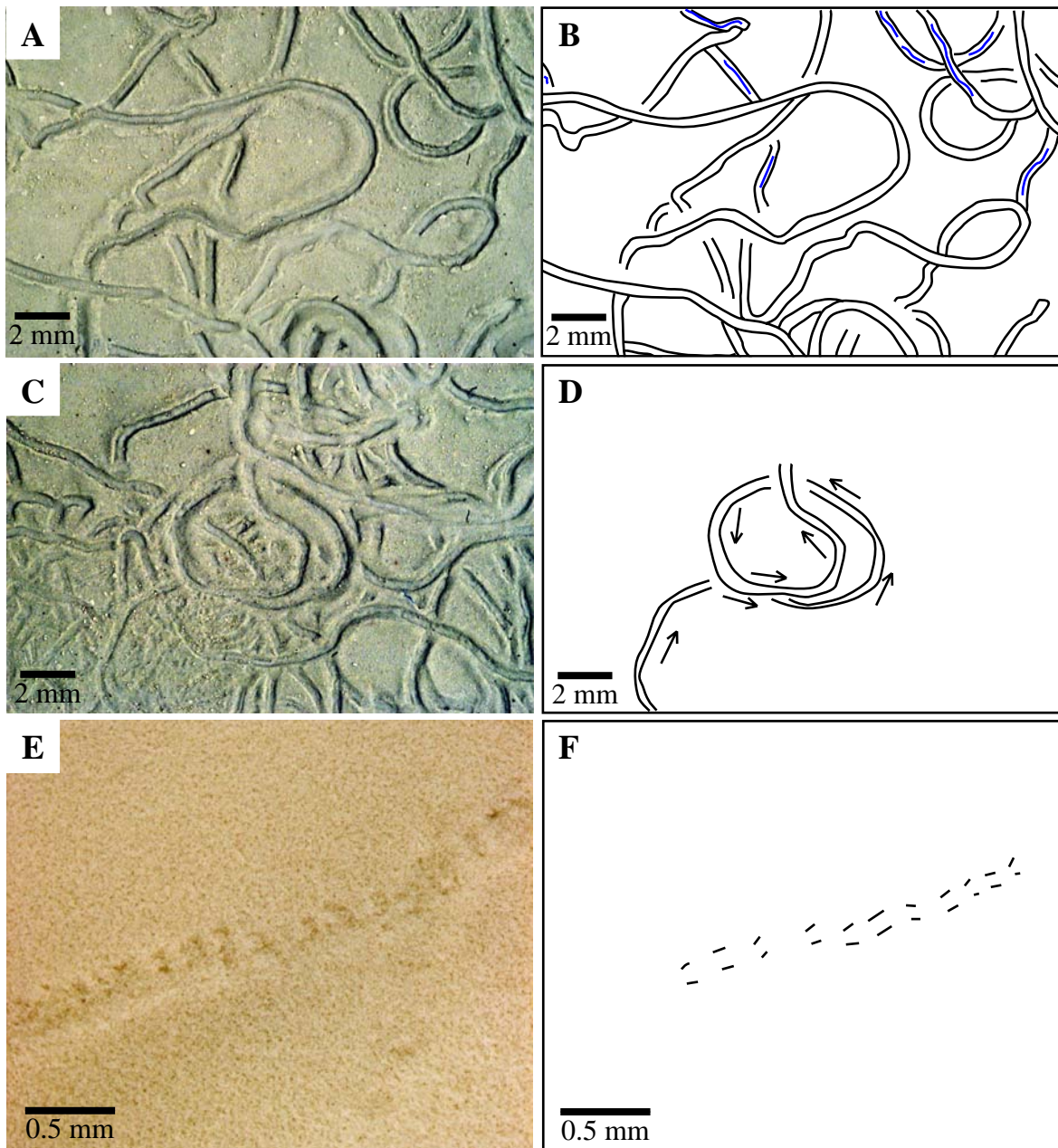


FIGURE 2—Traces produced by *Heterocypris incongruens* in kaolinite sediment. A) Type 1 crawling trails, some with medial ridges, in 1-mm water depth and B) the outline of the trails. Blue lines indicate the location of medial ridges. C) Type 2 crawling trail (center) in 1-mm water depth and D) the outline of the trail. Arrows indicate direction of ostracode movement. E) Type 3 swimming trail in 1-mm water depth and F) the outline of the trail.

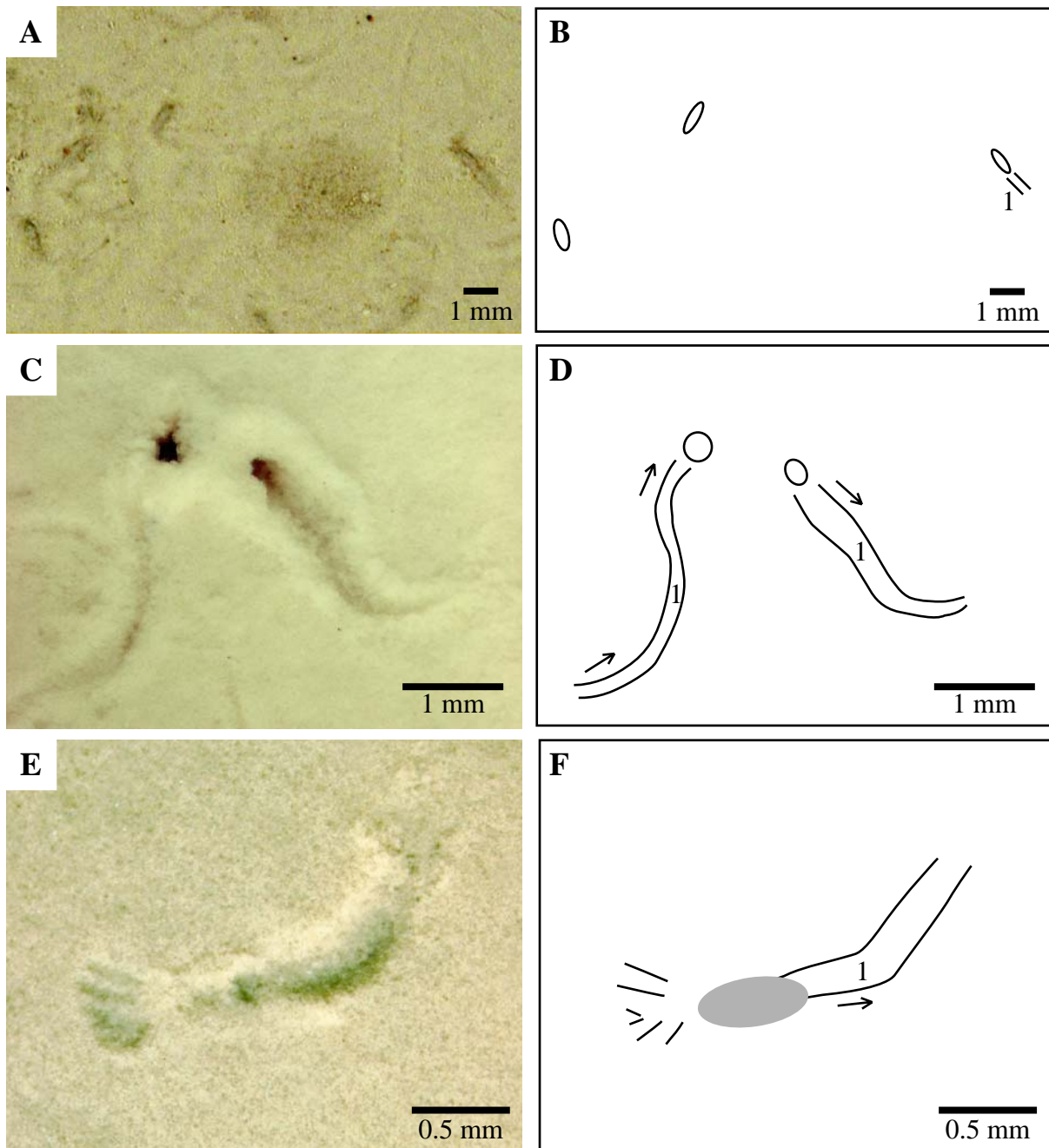


FIGURE 3—Traces produced by *Heterocypris incongruens* in kaolinite sediment. A) Type 4 resting depression in 4-mm water depth and B) the outline of the depressions. Type 1 trail (1) is seen leaving the depression on the right. C) Type 5 asymmetrical burrow entrance and exit opening in 4-mm water depth with Type 1 trails (1) leading to and from the burrow and D) the outline of the burrow openings and Type 1 trails. E) Type 6 self-righting trace in 1-mm water depth with exiting Type 1 trail and F) the outline of the trail. The gray circle indicates the location where the ostracode was stuck upside down in the sediment. Arrows indicate direction of ostracode movement.

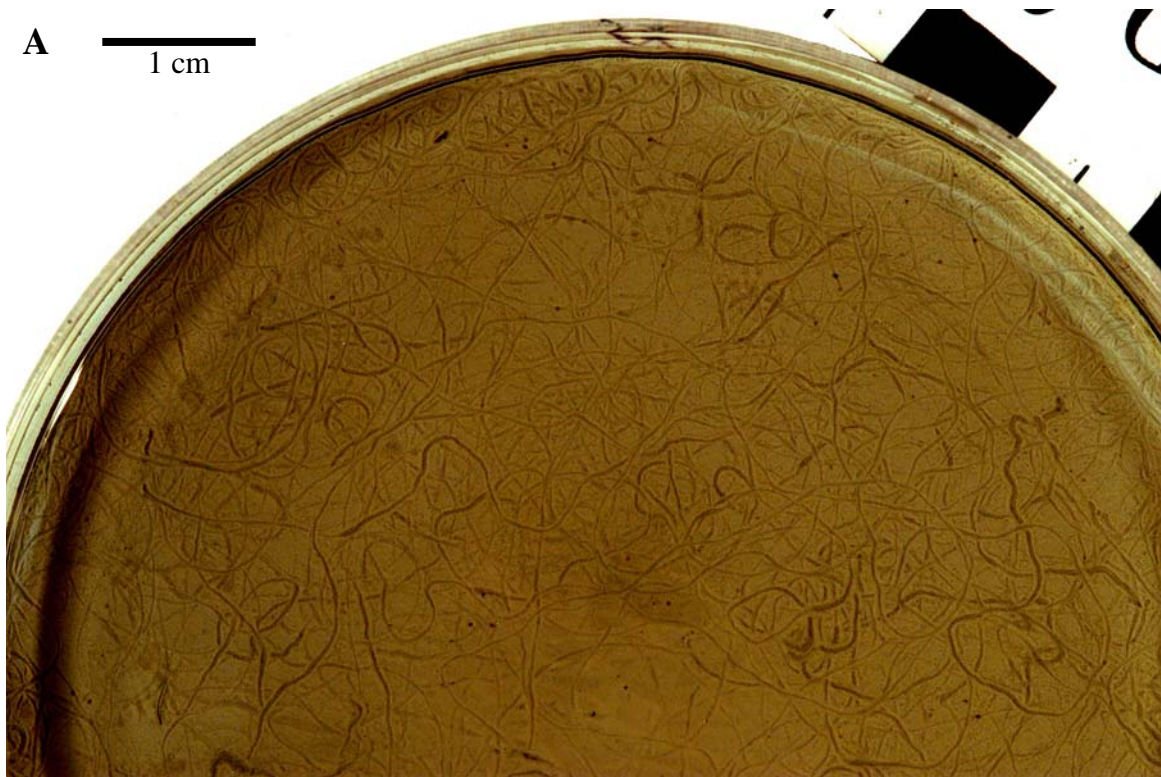


FIGURE 4—*Heterocypris incongruens* traces in kaolinite substrate at 1-mm water depth (A) and 4-mm water depth (B).

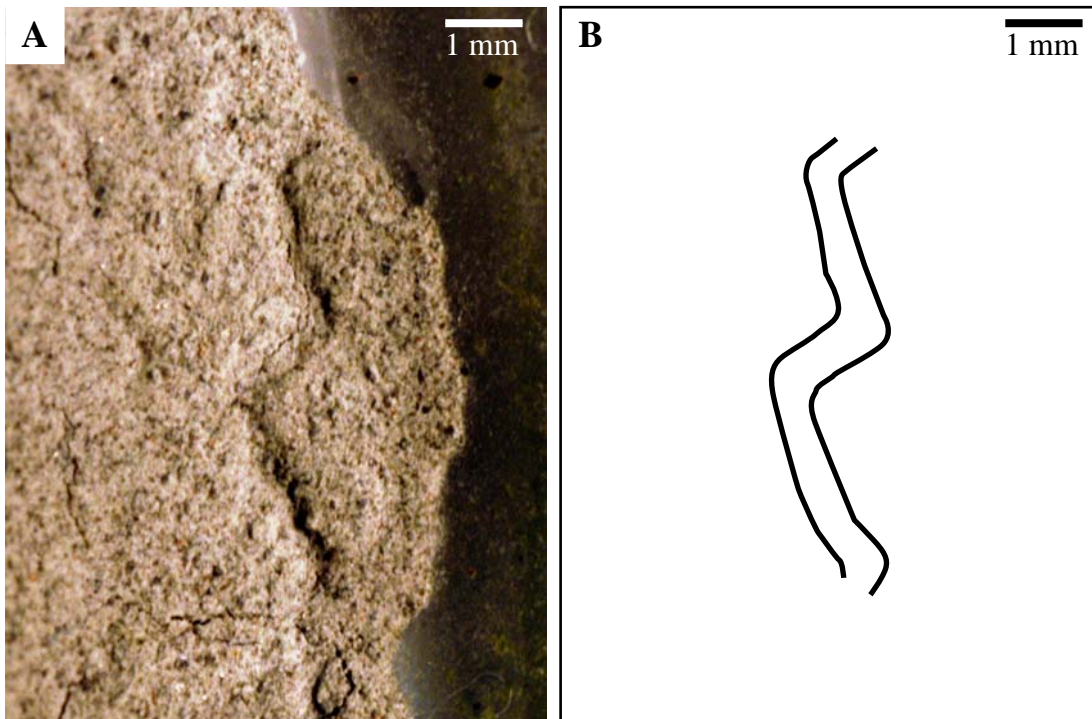


FIGURE 5—Trail produced by *Heterocypris incongruens* in heterogeneous very fine- to medium-grained sand. A) Type 7 crawling trail in 4-mm water depth and B) the outline of the trail.

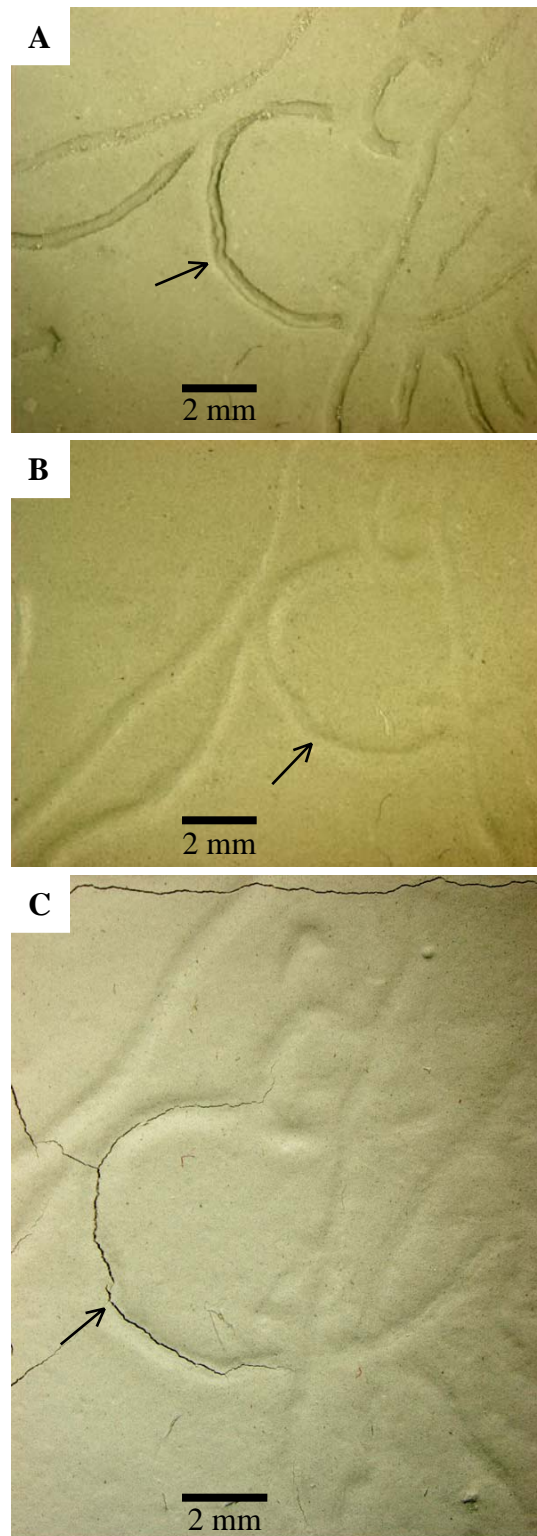


FIGURE 6—Preservation of Type 1 trails during desiccation. Arrows point to the same location in each photo. A) Trails immediately after formation in 1-mm water depth. Trails are detailed, some with medial ridges. B) Trails one day after formation, sediment is moist but there is no water column. Trails lack fine details. C) Trails two days after formation, sediment is completely desiccated. Desiccation cracks occasionally form along trails.

CHAPTER 7

CONCLUSIONS

The repetitive cycles of flooding, lake stand, and desiccation indicate that Fossil Lake was highly susceptible to changes in precipitation (P) and evaporation (E) and preserve a record of local climate change. This study presents high-resolution, multi-proxy records from core but the poor temporal resolution makes it difficult to determine the timing and duration of paleoclimate and paleohydrologic changes. Using lithostratigraphy, fossil ostracode faunal assemblages, and ostracode stable isotopes, changes in paleoenvironment, paleoclimate, and paleohydrochemistry were interpreted for the eight individual lake stands (lithosomes). Each lithosome, except Lithosome I, records a fining-upward depositional sequence that represents transition from nearshore, shallow water to offshore environments and capped by an unconformity surface. The unconformity and facies histories indicate that the lake basin underwent several major lake-level excursions suggesting that climate forcing played a major role in the lake level fluctuations. The high and very high lake stands coincide with glacial cycles in MIS 16, 4, and 2.

Lithosome I and II, ~ 646–610 ka, record deep lake environments deposited during wet conditions that were subsequently subaerially exposed and pedogenically modified during drier conditions. A major unconformity exists above Lithosome II, ~ 610–71 ka. Both Lithosome III and IV, ~ 71–47 ka, were deposited during wet conditions with short-term variability of P/E ratios and record deep lake that were alkaline with salinities ranging from slightly saline to freshwater and water temperatures that were cool to cold. Lithosome V, VI, and VII were deposited during relatively dry conditions and record shallow cold, alkaline and saline lake with fluctuating salinities from increased precipitation or stream inflow or increased

seasonal dilution cycles. Lithosome VII, records a relatively freshwater alkaline lake. Dry conditions persisted at the base of Lithosome VIII with the deposition of eolian sands. Wet conditions returned and a deep, cold lake was recorded at the top of Lithosome VIII. The paleoenvironmental and paleohydrochemical reconstruction of this study generally agrees with a similar reconstruction from rare earth element (REE) analysis by Martin et al. (2005).

Even with the poor temporal resolution, the long record from Fossil Lake will provide insight into the paleoecology, paleohydrology, and paleoclimate of the Great Basin. This long record will provide additional insights into the paleohydrology and paleoclimate of middle Pleistocene pluvial lake systems in the Great Basin, where only a few records have been studied. The Fossil Lake reconstructions may also aid our understanding of links between hydrochemistry and climatic change with biotic changes of the diverse vertebrate faunal assemblage preserved at Fossil Lake.

Reference

Martin, J.E., Patrick, D., Kihm, A.J., Foit Jr., F.F., Grandstaff, D.E., 2005. Lithostratigraphy, tephrochronology, and rare earth element geochemistry of fossils at the classical Pleistocene Fossil Lake Area, South Central Oregon. *Journal of Geology* 113, 139–155.

APPENDIX A

GRAIN SIZE DISTRIBUTION DATA AND SHEPARD CLASSIFICATIONS

- 1) Table A1. Grain size distribution and Shepard classification for core 1 samples. Key to abbreviations: $d_{0.1} (\mu\text{m}) = 10^{\text{th}}$ percentile of grain size distribution; $d_{0.5} (\mu\text{m}) = 50^{\text{th}}$ percentile of grain size distribution; $d_{0.9} (\mu\text{m}) = 90^{\text{th}}$ percentile of grain size distribution.
- 2) Table A2. Grain size distribution and Shepard classification for core 2 samples. Key to abbreviations: $d_{0.1} (\mu\text{m}) = 10^{\text{th}}$ percentile of grain size distribution; $d_{0.5} (\mu\text{m}) = 50^{\text{th}}$ percentile of grain size distribution; $d_{0.9} (\mu\text{m}) = 90^{\text{th}}$ percentile of grain size distribution.
- 3) Table A3. Grain size distribution and Shepard classification for core 3 samples. Key to abbreviations: $d_{0.1} (\mu\text{m}) = 10^{\text{th}}$ percentile of grain size distribution; $d_{0.5} (\mu\text{m}) = 50^{\text{th}}$ percentile of grain size distribution; $d_{0.9} (\mu\text{m}) = 90^{\text{th}}$ percentile of grain size distribution.
- 4) Table A4. Grain size distribution and Shepard classification for core 4 samples. Key to abbreviations: $d_{0.1} (\mu\text{m}) = 10^{\text{th}}$ percentile of grain size distribution; $d_{0.5} (\mu\text{m}) = 50^{\text{th}}$ percentile of grain size distribution; $d_{0.9} (\mu\text{m}) = 90^{\text{th}}$ percentile of grain size distribution.
- 5) Table A5. Grain size distribution and Shepard classification for core 5 samples. Key to abbreviations: $d_{0.1} (\mu\text{m}) = 10^{\text{th}}$ percentile of grain size distribution; $d_{0.5} (\mu\text{m}) = 50^{\text{th}}$ percentile of grain size distribution; $d_{0.9} (\mu\text{m}) = 90^{\text{th}}$ percentile of grain size distribution.

Table A1. Grain size distribution and Shepard classification for core 1 samples. Key to abbreviations: d 0.1 (μm) = 10th percentile of grain size distribution; d 0.5 (μm) = 50th percentile of grain size distribution; d 0.9 (μm) = 90th percentile of grain size distribution.

Sample ID	Depth (cm)	Lithosome	Unit	d 0.1 (μm)	d 0.5 (μm)	d 0.9 (μm)	% Clay	% Silt	% Sand	Shepard Class
601	12.0	VIII	17	3.957	28.248	85.311	20.666	62.587	16.747	CLAYEY SILT
602	14.0	VIII	17	4.245	26.906	77.329	19.955	66.554	13.491	CLAYEY SILT
603	16.0	VIII	17	3.748	26.350	82.405	21.672	63.084	15.243	CLAYEY SILT
604	18.0	VIII	17	3.055	22.130	80.448	25.912	60.677	13.411	CLAYEY SILT
605	19.6	VIII	17	3.495	24.193	74.683	23.567	64.187	12.246	CLAYEY SILT
606	21.2	VIII	17	3.508	24.992	76.417	23.435	63.667	12.899	CLAYEY SILT
607	23.1	VIII	17	3.383	23.637	70.328	24.297	65.220	10.483	CLAYEY SILT
608	25.1	VIII	17	3.869	24.982	69.193	21.908	68.087	10.004	CLAYEY SILT
609	27.0	VIII	17	4.155	27.435	81.386	20.415	64.798	14.787	CLAYEY SILT
610	28.7	VIII	17	3.979	25.177	77.122	21.560	65.758	12.682	CLAYEY SILT
611	31.4	VIII	17	4.478	27.670	72.555	19.066	69.388	11.545	CLAYEY SILT
612	33.8	VIII	17	4.396	24.736	65.937	20.068	71.337	8.595	CLAYEY SILT
613	35.8	VIII	17	3.781	25.387	67.056	21.677	69.284	9.039	CLAYEY SILT
614	37.5	VIII	17	3.740	26.380	79.755	22.001	64.129	13.870	CLAYEY SILT
615	39.2	VIII	17	3.771	27.393	74.493	21.536	66.156	12.308	CLAYEY SILT
616	41.6	VIII	17	3.675	26.931	71.112	21.485	67.656	10.860	CLAYEY SILT
617	43.5	VIII	17	3.739	26.330	77.295	21.804	65.182	13.014	CLAYEY SILT
618	45.1	VIII	16	4.870	39.259	99.743	16.245	59.617	24.138	SANDY SILT
619	47.3	VIII	16	3.991	34.554	86.744	18.989	62.451	18.560	CLAYEY SILT
620	49.5	VIII	16	7.321	53.826	122.150	11.480	51.804	36.716	SANDY SILT
621	51.7	VIII	15	29.398	156.387	322.929	3.540	15.929	80.531	SAND
622	53.4	VIII	15	99.336	177.894	310.673	0.000	2.429	97.571	SAND
623	55.1	VIII	15	103.880	193.164	350.323	0.000	1.866	98.134	SAND
624	57.3	VIII	15	97.612	173.902	301.909	0.000	2.580	97.420	SAND
625	59.5	VIII	15	92.408	183.515	353.460	0.353	3.468	96.178	SAND

Sample ID	Depth (cm)	Lithosome	Unit	d 0.1 (µm)	d 0.5 (µm)	d 0.9 (µm)	% Clay	% Silt	% Sand	Shepard Class
626	61.5	VIII	15	110.116	212.650	392.349	0.775	1.977	97.248	SAND
627	63.2	VIII	15	100.436	206.671	396.730	1.005	3.162	95.833	SAND
628	65.1	VIII	15	83.175	148.588	254.671	1.004	4.126	94.870	SAND
629	67.1	VIII	15	90.437	163.638	281.221	1.120	3.136	95.744	SAND
630	69.3	VIII	15	101.374	186.609	329.317	0.825	2.179	96.996	SAND
631	71.3	VIII	15	99.190	182.417	319.669	1.009	2.471	96.520	SAND
632	72.9	VIII	15	94.590	171.550	294.325	0.992	2.781	96.226	SAND
633	74.9	VIII	15	99.966	180.456	310.819	1.166	2.443	96.391	SAND
634	76.9	VIII	15	70.075	128.317	222.442	1.510	8.077	90.414	SAND
635	78.5	VIII	15	94.957	172.013	297.339	0.927	2.539	96.533	SAND
636	80.7	VIII	15	96.379	203.321	389.047	1.042	3.555	95.403	SAND
637	82.7	VIII	15	98.697	183.849	323.805	1.094	2.528	96.378	SAND
638	84.6	VIII	15	97.368	184.702	330.560	1.292	2.906	95.802	SAND
639	86.8	VIII	15	98.934	181.102	311.475	1.188	2.634	96.178	SAND
640	88.5	VIII	15	98.621	197.943	364.687	1.062	3.092	95.845	SAND
641	90.9	VIII	15	87.837	192.756	382.970	1.319	4.661	94.020	SAND
642	92.8	VIII	15	99.600	226.576	462.365	1.011	3.513	95.475	SAND
643	94.7	VIII	15	95.381	226.227	459.509	1.218	4.279	94.502	SAND
644	96.4	VIII	15	94.365	223.331	461.721	0.830	3.900	95.270	SAND
645	98.8	VIII	15	86.204	177.786	335.264	1.223	4.493	94.284	SAND
646	100.7	VIII	15	76.141	151.754	284.161	1.124	6.401	92.475	SAND
647	102.7	VIII	15	81.577	153.232	276.327	1.290	4.610	94.100	SAND
648	104.3	VIII	15	81.031	158.321	278.842	1.821	5.124	93.055	SAND
652	106.1	VIII	15	56.738	133.072	269.547	2.183	12.801	85.017	SAND
653	108.9	VIII	15	54.269	113.048	274.305	1.592	17.770	80.638	SAND
654	111.4	VII	14	5.110	33.530	108.307	15.100	61.311	23.589	SANDY SILT
655	113.9	VII	14	5.410	29.931	99.215	15.276	65.570	19.155	SANDY SILT

Sample ID	Depth (cm)	Lithosome	Unit	d 0.1 (µm)	d 0.5 (µm)	d 0.9 (µm)	% Clay	% Silt	% Sand	Shepard Class
656	116.2	VII	14	10.695	66.216	160.819	8.337	43.495	48.168	SILTY SAND
657	118.5	VII	14	4.967	32.414	107.358	16.306	60.969	22.725	SANDY SILT
658	120.4	VII	14	7.493	57.958	158.875	11.469	44.837	43.694	SANDY SILT
659	122.7	VII	14	5.541	39.234	125.199	15.102	54.793	30.105	SANDY SILT
660	124.8	VII	14	4.085	25.487	76.749	19.752	67.882	12.366	CLAYEY SILT
661	127.1	VII	13	24.592	105.233	230.592	3.549	25.213	71.237	SILTY SAND
662	129.0	VII	13	34.116	136.122	336.648	2.597	17.548	79.854	SAND
663	131.3	VII	13	18.020	105.043	270.926	4.714	29.349	65.937	SILTY SAND
664	133.2	VII	13	57.855	156.913	353.557	1.454	11.663	86.883	SAND
665	135.7	VII	13	32.807	166.939	404.951	2.739	15.374	81.887	SAND
666	137.8	VII	13	21.786	167.479	402.463	4.272	19.860	75.867	SAND
667	140.1	VII	13	37.700	153.008	360.199	2.777	13.189	84.033	SAND
668	141.9	VII	13	53.524	158.495	412.254	1.944	11.915	86.141	SAND
669	144.0	VII	13	67.219	148.543	349.199	1.036	9.728	89.236	SAND
670	146.1	VII	13	73.424	147.203	325.744	0.127	7.994	91.879	SAND
671	148.4	VII	13	72.642	153.284	340.461	0.794	7.793	91.414	SAND
672	150.2	VII	13	69.315	150.961	328.115	1.075	8.875	90.050	SAND
673	152.7	VI	12	13.108	127.548	366.063	7.157	20.805	72.038	SILTY SAND
674	155.0	VI	12	8.274	43.169	266.445	10.461	55.342	34.196	SANDY SILT
675	157.1	VI	12	4.405	33.675	128.060	17.460	56.860	25.680	SANDY SILT
676	159.0	VI	11	52.598	135.750	300.429	2.247	13.427	84.326	SAND
677	161.5	VI	11	74.187	171.951	417.799	1.325	7.049	91.626	SAND
678	163.6	VI	11	56.365	119.280	229.099	2.726	13.652	83.622	SAND
679	165.7	VI	11	69.876	160.217	419.766	1.261	8.498	90.242	SAND
680	167.8	VI	11	61.359	153.299	344.707	3.042	9.082	87.876	SAND
681	170.3	VI	11	49.418	148.374	354.409	3.548	10.883	85.569	SAND
682	172.4	VI	11	90.055	170.092	298.308	1.623	3.556	94.821	SAND

Sample ID	Depth (cm)	Lithosome	Unit	d 0.1 (µm)	d 0.5 (µm)	d 0.9 (µm)	% Clay	% Silt	% Sand	Shepard Class
723	243.6	V	9	5.503	82.368	237.548	15.379	30.636	53.985	SILTY SAND
724	246.2	V	9	5.442	64.859	199.605	15.139	36.558	48.303	SILTY SAND
725	249.4	V	9	8.335	120.183	321.723	10.409	25.060	64.531	SILTY SAND
726	252.0	V	9	10.063	142.591	432.012	8.801	20.851	70.348	SILTY SAND

Table A2. Grain size distribution and Shepard classification for core 2 samples. Key to abbreviations: d 0.1 (μm) = 10th percentile of grain size distribution; d 0.5 (μm) = 50th percentile of grain size distribution; d 0.9 (μm) = 90th percentile of grain size distribution.

Sample ID	Depth (cm)	Lithosome	Unit	d 0.1 (μm)	d 0.5 (μm)	d 0.9 (μm)	% Clay	% Silt	% Sand	Shepard Class
1	2.5	VII	14	18.112	97.455	230.759	4.679	28.256	67.066	SILTY SAND
2	5.2	VII	14	12.034	61.804	164.742	6.985	47.706	45.309	SANDY SILT
3	7.9	VII	14	11.170	67.857	218.735	7.806	42.840	49.354	SILTY SAND
4	11.5	VII	14	8.907	45.999	155.046	9.777	55.265	34.959	SANDY SILT
5	14.2	VII	14	22.119	82.949	203.688	4.546	35.751	59.703	SILTY SAND
6	17.1	VII	14	10.122	64.212	194.612	8.632	44.027	47.342	SILTY SAND
7	21.6	VII	14	8.493	39.253	96.558	10.235	68.014	21.752	SANDY SILT
8	23.6	VII	13	25.518	115.158	306.379	3.373	25.704	70.924	SILTY SAND
9	26.5	VII	13	33.076	152.355	385.802	2.702	16.356	80.942	SAND
10	29.2	VII	13	75.713	176.747	381.730	1.254	7.040	91.707	SAND
11	32.3	VII	13	39.255	199.529	444.775	2.284	12.475	85.240	SAND
12	35.2	VII	13	49.518	209.638	502.702	2.534	9.885	87.581	SAND
13	38.1	VII	13	77.912	178.732	426.480	1.261	6.243	92.496	SAND
14	40.8	VII	13	74.348	185.638	529.805	1.582	7.109	91.309	SAND
15	43.7	VII	13	71.105	168.721	403.092	1.654	7.765	90.581	SAND
16	46.6	VII	13	66.950	144.355	337.868	1.249	9.722	89.029	SAND
17	49.3	VII	13	75.418	165.669	368.564	1.003	6.866	92.131	SAND
18	52.2	VII	13	76.621	186.350	417.014	1.728	6.382	91.890	SAND
19	54.9	VII	13	19.378	131.247	367.090	5.203	16.094	78.703	SAND
20	58.0	VI	12	3.027	22.052	69.756	23.817	66.020	10.163	CLAYEY SILT
21	61.0	VI	12	15.943	101.042	278.399	5.801	28.795	65.404	SILTY SAND
22	63.8	VI	11	62.475	140.991	327.184	1.367	11.421	87.212	SAND
23	66.5	VI	11	69.853	152.408	361.170	1.349	8.398	90.253	SAND
24	69.2	VI	11	79.237	211.649	528.179	1.629	5.963	92.408	SAND
25	72.1	VI	11	61.313	172.935	431.661	2.948	8.833	88.219	SAND

Sample ID	Depth (cm)	Lithosome	Unit	d 0.1 (µm)	d 0.5 (µm)	d 0.9 (µm)	% Clay	% Silt	% Sand	Shepard Class
26	75.0	VI	11	64.161	195.550	475.154	2.980	7.903	89.117	SAND
27	77.9	VI	11	73.400	230.531	494.990	2.633	6.882	90.485	SAND
28	80.6	VI	11	64.976	149.689	367.153	2.279	9.109	88.612	SAND
29	83.3	VI	11	65.227	178.269	448.164	2.326	8.564	89.110	SAND
30	86.2	VI	11	53.988	184.598	530.070	2.353	11.410	86.238	SAND
31	89.1	VI	11	50.504	183.151	443.684	2.288	11.548	86.163	SAND
32	92.0	VI	11	7.573	118.630	303.139	11.277	23.508	65.215	SILTY SAND
33	94.9	VI	11	14.911	148.390	325.427	6.464	14.352	79.184	SAND
34	97.8	VI	11	20.224	149.215	333.569	4.612	14.446	80.943	SAND
35	100.5	VI	11	15.059	102.887	296.735	6.296	30.566	63.138	SILTY SAND
36	103.6	VI	11	13.766	77.856	268.802	7.006	38.884	54.110	SILTY SAND
37	106.5	VI	11	13.637	102.307	301.266	6.861	29.590	63.550	SILTY SAND
38	109.4	VI	11	12.743	101.357	310.173	7.323	29.687	62.991	SILTY SAND
39	112.1	VI	11	11.054	128.530	394.382	7.863	26.051	66.085	SILTY SAND
40	115.0	VI	11	7.008	86.375	235.773	11.967	31.459	56.574	SILTY SAND
41	117.9	VI	11	20.180	118.214	244.854	4.894	19.108	75.998	SAND
42	120.6	VI	11	13.896	112.264	238.246	6.724	21.286	71.990	SILTY SAND
43	123.5	VI	11	8.037	78.008	187.683	10.751	34.734	54.515	SILTY SAND
44	126.4	VI	11	5.326	48.952	170.868	15.865	43.273	40.863	SANDY SILT
45	127.5	VI	11	5.846	60.012	179.517	14.320	39.881	45.799	SILTY SAND
50	130.4	VI	11	7.822	75.669	164.822	10.854	34.853	54.292	SILTY SAND
51	133.3	VI	11	7.738	91.357	242.726	11.041	30.468	58.491	SILTY SAND
52	136.0	VI	11	10.995	148.986	331.997	8.228	18.062	73.710	SILTY SAND
53	137.9	VI	11	6.895	53.365	217.276	12.298	43.735	43.967	SILTY SAND
54	141.4	VI	11	9.876	118.290	307.965	8.905	26.902	64.193	SILTY SAND
55	144.1	VI	11	23.680	136.657	294.506	4.293	18.026	77.681	SAND
56	146.2	VI	11	22.336	149.628	375.404	4.498	17.791	77.711	SAND

Sample ID	Depth (cm)	Lithosome	Unit	d 0.1 (µm)	d 0.5 (µm)	d 0.9 (µm)	% Clay	% Silt	% Sand	Shepard Class
57	148.3	VI	11	32.159	122.946	279.479	3.576	18.563	77.861	SAND
58	151.4	V	10	7.001	50.121	143.669	12.046	51.997	35.957	SANDY SILT
59	154.3	V	10	6.502	51.342	141.865	12.961	49.805	37.234	SANDY SILT
60	156.4	V	10	8.931	56.437	264.191	9.759	46.242	43.999	SANDY SILT
61	158.7	V	9	23.151	85.940	280.319	3.956	36.084	59.960	SILTY SAND
62	161.2	V	9	17.353	68.083	277.981	5.386	45.314	49.300	SILTY SAND
63	164.3	V	9	15.140	55.397	200.980	6.678	54.592	38.730	SANDY SILT
64	166.6	V	9	14.891	83.632	314.524	6.286	37.552	56.162	SILTY SAND
65	169.1	V	9	6.526	55.732	226.705	12.838	43.370	43.791	SILTY SAND
66	171.4	V	9	23.967	194.671	465.257	3.978	19.752	76.270	SAND
67	174.5	V	9	20.126	70.542	184.445	6.096	42.846	51.058	SILTY SAND
68	177.0	V	9	11.548	49.722	141.475	8.427	59.026	32.547	SANDY SILT
69	179.5	V	9	10.288	48.981	153.520	8.828	57.465	33.707	SANDY SILT
70	182.4	V	9	10.611	47.903	161.491	8.636	57.660	33.703	SANDY SILT
71	184.9	V	9	10.322	48.250	157.924	8.766	55.865	35.369	SANDY SILT
72	187.6	V	9	11.499	58.008	246.919	7.598	47.867	44.536	SANDY SILT
73	189.9	V	9	7.386	53.309	235.123	11.653	44.905	43.442	SANDY SILT
74	192.4	V	9	11.028	113.394	306.629	8.125	27.129	64.746	SILTY SAND
75	194.9	IV	8	4.815	33.728	169.687	16.889	57.598	25.514	SANDY SILT
76	198.0	IV	8	4.425	26.350	84.005	18.491	68.131	13.378	CLAYEY SILT
77	200.3	IV	8	4.920	24.196	57.281	16.920	77.002	6.078	SILT
78	203.2	IV	8	5.287	26.393	68.746	15.709	74.426	9.865	CLAYEY SILT
79	205.5	IV	8	5.002	26.855	65.509	16.421	74.992	8.587	CLAYEY SILT
80	207.4	IV	8	3.043	24.682	69.865	24.212	65.533	10.255	CLAYEY SILT
81	210.7	IV	8	3.984	36.082	92.319	18.782	61.376	19.842	SANDY SILT
82	213.6	IV	8	5.009	39.860	113.750	15.338	57.744	26.918	SANDY SILT
83	216.1	IV	8	3.715	32.198	106.111	20.226	57.527	22.247	SAND SILT CLAY

Sample ID	Depth (cm)	Lithosome	Unit	d 0.1 (µm)	d 0.5 (µm)	d 0.9 (µm)	% Clay	% Silt	% Sand	Shepard Class
84	218.6	IV	7	30.348	185.868	409.438	3.296	13.678	83.026	SAND
85	221.1	IV	7	92.733	212.706	423.870	1.317	4.693	93.990	SAND
86	222.3	IV	7	101.144	225.334	455.648	0.899	3.331	95.770	SAND
87	226.2	IV	7	84.742	225.923	474.464	1.269	5.807	92.924	SAND
88	228.3	IV	7	12.169	101.948	391.522	7.456	29.131	63.413	SILTY SAND
89	231.4	IV	7	13.559	96.921	214.866	6.675	26.944	66.381	SILTY SAND
90	233.5	IV	7	7.489	81.199	282.346	11.437	34.436	54.127	SILTY SAND

Table A3. Grain size distribution and Shepard classification for core 3 samples. Key to abbreviations: d 0.1 (μm) = 10th percentile of grain size distribution; d 0.5 (μm) = 50th percentile of grain size distribution; d 0.9 (μm) = 90th percentile of grain size distribution.

Sample ID	Depth (cm)	Lithosome	Unit	d 0.1 (μm)	d 0.5 (μm)	d 0.9 (μm)	% Clay	% Silt	% Sand	Shepard Class
801	3.8	VIII	17	4.858	31.428	79.803	17.406	67.470	15.124	CLAYEY SILT
802	5.9	VIII	17	4.562	29.852	79.029	18.641	66.791	14.568	CLAYEY SILT
803	8.5	VIII	17	5.310	33.649	83.814	16.232	66.501	17.268	SANDY SILT
804	10.2	VIII	17	4.671	28.876	76.713	18.439	68.122	13.439	CLAYEY SILT
805	12.3	VIII	17	3.951	26.603	72.200	21.535	67.111	11.354	CLAYEY SILT
806	14.8	VIII	16	5.283	36.998	92.572	15.520	63.454	21.025	SANDY SILT
807	17.0	VIII	16	6.355	42.353	103.985	13.172	60.404	26.425	SANDY SILT
808	19.1	VIII	16	6.236	40.192	98.801	13.427	62.797	23.775	SANDY SILT
809	21.2	VIII	16	7.020	44.497	124.975	12.120	57.121	30.759	SANDY SILT
810	23.3	VIII	16	13.686	107.628	271.965	6.652	29.263	64.084	SILTY SAND
811	25.4	VIII	15	41.073	164.694	323.767	2.160	12.285	85.555	SAND
812	27.5	VIII	15	94.596	170.226	302.800	0.000	2.792	97.208	SAND
813	29.6	VIII	15	85.811	166.197	317.204	0.000	4.416	95.584	SAND
814	31.7	VIII	15	89.433	179.769	316.652	2.208	4.572	93.221	SAND
815	33.8	VIII	15	91.848	177.173	308.321	1.878	3.912	94.210	SAND
816	35.8	VIII	15	82.364	165.707	292.317	2.252	5.052	92.696	SAND
817	38.0	VIII	15	85.653	157.065	270.554	1.553	3.798	94.649	SAND
818	40.0	VIII	15	86.747	174.952	315.283	2.041	4.543	93.416	SAND
819	42.2	VIII	15	83.193	154.625	263.208	1.977	4.281	93.743	SAND
820	44.3	VIII	15	79.026	157.786	278.881	2.317	5.377	92.306	SAND
821	46.4	VIII	15	80.711	157.058	280.503	2.147	4.829	93.024	SAND
822	48.5	VIII	15	81.195	212.492	459.519	2.497	5.878	91.625	SAND
823	50.6	VIII	15	77.141	196.180	393.464	2.753	6.246	91.000	SAND
824	52.7	VIII	15	87.974	180.104	320.777	2.236	4.661	93.104	SAND
825	54.8	VIII	15	86.331	177.227	310.449	2.329	4.948	92.723	SAND

Sample ID	Depth (cm)	Lithosome	Unit	d0.1 (µm)	d0.5 (µm)	d0.9 (µm)	% Clay	% Silt	% Sand	Shepard Class
826	56.9	VIII	15	97.352	200.945	349.432	2.214	4.727	93.061	SAND
827	59.0	VIII	15	90.034	178.480	317.168	1.473	4.120	94.407	SAND
828	61.1	VIII	15	85.504	173.389	302.073	2.151	4.983	92.866	SAND
829	63.2	VIII	15	95.577	181.312	314.694	1.348	3.353	95.299	SAND
830	65.4	VIII	15	71.527	140.168	259.523	1.907	7.221	90.871	SAND
831	67.4	VIII	15	82.031	189.239	395.782	1.582	5.414	93.004	SAND
832	69.5	VIII	15	88.055	206.331	409.698	2.123	4.761	93.116	SAND
833	71.6	VIII	15	67.664	146.186	293.136	2.492	8.026	89.483	SAND
834	73.7	VIII	15	82.899	191.788	389.988	2.280	5.292	92.428	SAND
835	75.8	VIII	15	78.961	174.533	336.519	2.373	5.713	91.914	SAND
836	77.9	VIII	15	73.764	159.740	315.863	2.102	6.649	91.249	SAND
837	80.0	VIII	15	74.270	153.489	292.802	1.790	6.632	91.577	SAND
838	82.1	VIII	15	50.698	158.452	334.512	3.344	9.823	86.833	SAND
839	84.2	VIII	15	23.416	147.402	324.215	4.655	13.856	81.489	SAND
840	85.9	VIII	15	17.081	152.301	359.602	6.203	14.925	78.872	SAND
855	88.2	VIII	15	3.855	32.458	165.610	21.032	46.239	32.730	SAND SILT CLAY
856	90.5	VIII	15	15.336	147.725	294.050	6.922	11.864	81.214	SAND
857	92.8	VIII	15	22.220	162.206	321.571	5.410	9.296	85.294	SAND
858	95.1	VII	14	5.906	38.572	105.170	14.545	60.635	24.820	SANDY SILT
859	97.4	VII	14	5.125	33.788	99.827	16.810	61.640	21.550	SANDY SILT
860	99.7	VII	13	8.998	94.972	223.372	9.744	27.820	62.436	SILTY SAND
861	102.0	VII	13	50.298	122.060	246.669	2.761	14.551	82.689	SAND
862	104.3	VII	13	68.349	135.958	284.171	0.896	9.497	89.607	SAND
863	106.6	VII	13	68.638	145.232	340.588	0.893	9.344	89.765	SAND
864	108.9	VII	13	73.358	197.656	466.894	1.174	7.647	91.179	SAND
865	111.2	VII	13	64.630	173.674	353.622	2.405	8.453	89.142	SAND
866	113.5	VII	13	82.070	201.338	420.728	1.852	5.824	92.324	SAND

Sample ID	Depth (cm)	Lithosome	Unit	d0.1 (µm)	d0.5 (µm)	d0.9 (µm)	% Clay	% Silt	% Sand	Shepard Class
867	115.8	VII	13	58.529	541.370	1356.349	2.301	9.444	88.256	SAND
868	118.1	VII	13	47.255	241.900	675.133	2.776	9.722	87.502	SAND
869	120.4	VII	13	47.948	162.099	445.995	2.697	11.913	85.390	SAND
870	122.7	VI	12/11	14.224	79.412	309.473	6.645	39.018	54.338	SILTY SAND
871	125.0	V	10/9	25.479	114.770	364.038	3.121	31.195	65.684	SILTY SAND
872	127.3	V/IV	9/8	6.490	73.413	290.800	12.307	35.885	51.808	SILTY SAND
873	129.6	IV	8	5.514	54.130	246.455	14.434	43.988	41.579	SANDY SILT
874	131.9	IV	8	3.537	30.873	102.296	21.984	57.208	20.808	SAND SILT CLAY
875	134.2	IV	8	3.926	39.060	135.307	19.393	52.331	28.275	SANDY SILT
876	136.9	IV	8	5.022	45.110	228.688	16.025	47.535	36.440	SANDY SILT
877	139.6	IV	7	10.210	162.300	477.008	8.709	25.881	65.410	SILTY SAND
879	146.1	IV	7	10.526	232.303	516.629	8.439	21.801	69.760	SILTY SAND
880	148.7	IV	7	9.353	125.277	421.335	9.447	22.702	67.852	SILTY SAND
881	151.5	IV	7	8.530	110.065	344.490	10.166	24.644	65.190	SILTY SAND
882	154.2	IV	7	10.306	121.971	324.118	8.776	21.889	69.335	SILTY SAND
883	156.5	IV	7	6.044	111.315	301.129	13.227	25.140	61.632	SILTY SAND
884	159.2	IV	7	5.614	75.876	244.613	14.429	33.471	52.100	SILTY SAND
885	161.5	III	6	7.007	80.588	260.846	11.984	34.126	53.890	SILTY SAND
886	164.1	III	6	5.818	42.128	152.642	14.506	53.370	32.124	SANDY SILT
887	167.4	III	6	6.795	44.872	146.312	12.701	54.442	32.857	SANDY SILT
888	169.8	III	5	8.342	109.167	275.507	10.348	26.962	62.690	SILTY SAND
889	172.2	III	5	6.937	111.163	299.845	11.972	26.809	61.219	SILTY SAND
890	174.6	III	5	6.610	103.828	300.159	12.454	27.930	59.616	SILTY SAND
891	177.0	III	5	6.932	90.924	381.510	12.202	33.340	54.458	SILTY SAND
892	179.4	III	5	4.939	33.850	310.475	16.572	45.052	38.376	SANDY SILT
893	181.8	III	5	23.212	229.065	499.091	4.856	13.904	81.239	SAND
894	184.2	III	5	13.804	174.398	446.590	6.925	18.830	74.245	SILTY SAND

Sample ID	Depth (cm)	Lithosome	Unit	d0.1 (µm)	d0.5 (µm)	d0.9 (µm)	% Clay	% Silt	% Sand	Shepard Class
895	186.6	III	5	19.173	228.933	527.273	5.445	17.450	77.105	SAND
896	189.0	III	5	10.966	117.270	515.307	8.221	28.995	62.784	SILTY SAND
897	191.4	III	5	12.016	90.672	439.346	7.675	34.485	57.840	SILTY SAND
898	193.8	III	5	4.552	37.241	390.707	18.094	44.320	37.586	SANDY SILT
899	196.4	III	5	6.500	250.133	768.793	13.349	25.649	61.002	SILTY SAND
900	198.9	III	5	8.383	371.132	897.890	10.386	20.577	69.038	SILTY SAND
901	201.5	III	5	6.937	85.721	649.475	12.305	32.603	55.093	SILTY SAND
902	204.4	III	5	5.966	55.035	812.446	14.553	39.390	46.057	SILTY SAND

Table A4. Grain size distribution and Shepard classification for core 4 samples. Key to abbreviations: d 0.1 (μm) = 10th percentile of grain size distribution; d 0.5 (μm) = 50th percentile of grain size distribution; d 0.9 (μm) = 90th percentile of grain size distribution.

Sample ID	Depth (cm)	Lithosome	Unit	d 0.1 (μm)	d 0.5 (μm)	d 0.9 (μm)	% Clay	% Silt	% Sand	Shepard Class
201	1.0	III	6	3.464	27.433	82.574	21.343	64.010	14.647	CLAYEY SILT
202	4.1	III	6	3.476	26.768	82.592	22.010	63.358	14.633	CLAYEY SILT
203	7.2	III	6	3.153	23.123	69.988	23.056	66.707	10.238	CLAYEY SILT
204	10.3	III	6	3.292	26.330	97.689	22.486	61.322	16.192	CLAYEY SILT
205	12.4	III	6	3.127	24.431	65.350	23.286	68.248	8.466	CLAYEY SILT
206	15.0	III	6	3.461	27.327	76.368	21.752	65.386	12.862	CLAYEY SILT
207	18.1	III	5	8.140	68.077	264.591	10.577	39.993	49.430	SILTY SAND
208	20.7	III	5	13.371	107.200	434.932	6.616	32.165	61.219	SILTY SAND
209	23.3	III	5	13.071	122.174	361.769	7.131	27.957	64.912	SILTY SAND
210	26.4	III	5	20.455	133.345	493.853	4.746	26.850	68.404	SILTY SAND
211	28.5	III	5	30.064	287.579	586.684	3.273	15.212	81.514	SAND
212	31.1	III	5	38.120	282.713	605.263	2.792	14.256	82.952	SAND
213	33.7	III	5	56.876	247.241	508.188	2.197	10.470	87.333	SAND
214	36.3	III	5	35.172	282.125	680.549	3.790	14.903	81.306	SAND
215	39.4	III	5	81.768	240.842	769.492	1.324	5.955	92.721	SAND
216	41.5	III	5	24.630	160.762	643.930	3.892	16.173	79.935	SAND
217	44.1	III	5	44.668	237.224	773.794	2.640	10.473	86.887	SAND
218	46.7	III	5	37.762	122.260	286.079	3.188	17.063	79.748	SAND
219	49.8	III	5	25.833	109.083	277.120	3.902	22.230	73.868	SILTY SAND
220	51.9	III	5	4.781	31.358	103.208	16.714	63.413	19.873	SANDY SILT
221	54.5	III	5	5.440	65.624	158.032	14.426	37.839	47.735	SILTY SAND
222	57.1	III	5	5.736	69.195	166.834	13.846	36.147	50.007	SILTY SAND
223	59.4	III	5	5.978	64.583	144.693	13.439	39.799	46.762	SILTY SAND
224	62.3	III	5	3.032	31.606	114.521	24.860	49.911	25.229	SAND SILT CLAY
225	64.9	III	5	3.314	29.322	95.322	24.013	55.323	20.664	SAND SILT CLAY

Sample ID	Depth (cm)	Lithosome	Unit	d 0.1 (µm)	d 0.5 (µm)	d 0.9 (µm)	% Clay	% Silt	% Sand	Shepard Class
226	67.0	II	4	3.218	17.459	57.178	28.739	64.984	6.276	CLAYEY SILT
227	69.6	II	4	3.138	22.332	81.789	26.784	58.697	14.519	CLAYEY SILT
228	72.7	II	4	2.859	23.047	80.285	28.173	57.443	14.384	CLAYEY SILT
229	74.8	II	4	3.094	24.471	86.254	26.381	57.256	16.363	CLAYEY SILT
230	77.4	II	4	2.845	22.034	83.341	28.184	56.425	15.391	CLAYEY SILT
231	80.0	II	4	3.090	21.999	83.835	27.394	57.340	15.266	CLAYEY SILT
232	83.1	II	4	3.478	24.084	84.206	24.298	60.354	15.348	CLAYEY SILT
233	85.2	II	4	3.106	21.826	75.145	27.204	60.714	12.082	CLAYEY SILT
234	87.8	II	4	3.019	22.327	86.318	27.478	56.646	15.876	CLAYEY SILT
235	90.4	II	4	2.962	27.926	91.545	25.504	55.517	18.979	CLAYEY SILT
236	93.5	II	4	2.647	23.097	74.908	28.662	59.015	12.322	CLAYEY SILT
237	96.1	II	4	2.896	22.075	71.358	27.811	61.316	10.873	CLAYEY SILT
238	98.7	II	4	3.464	28.433	91.021	23.425	57.739	18.836	CLAYEY SILT
239	102.8	II	4	3.068	25.326	85.698	26.215	57.130	16.655	CLAYEY SILT
240	103.8	II	3	2.620	23.944	107.227	29.309	49.580	21.112	SAND SILT CLAY
245	107.4	II	3	2.665	22.419	87.776	28.903	55.346	15.750	CLAYEY SILT
246	109.2	II	3	2.707	23.120	84.758	28.377	56.138	15.485	CLAYEY SILT
247	111.9	II	3	2.795	25.661	94.098	27.361	53.992	18.647	CLAYEY SILT
248	114.6	II	3	2.743	23.709	85.247	28.177	56.052	15.771	CLAYEY SILT
249	116.4	II	3	2.830	25.683	92.305	26.938	54.876	18.186	CLAYEY SILT
250	119.1	II	3	2.926	27.333	99.223	26.167	53.925	19.907	CLAYEY SILT
251	121.8	II	3	2.862	26.053	95.402	26.988	53.734	19.279	CLAYEY SILT
252	123.6	II	2	2.700	27.122	103.468	27.943	50.103	21.954	SAND SILT CLAY
253	126.3	II	2	2.652	26.221	98.344	28.383	50.746	20.870	SAND SILT CLAY
254	128.1	II	2	3.199	38.070	125.635	23.057	45.837	31.106	SAND SILT CLAY
255	130.8	II	2	3.562	36.893	128.204	21.492	48.617	29.891	SAND SILT CLAY
256	132.6	II	2	5.376	75.839	196.645	14.654	32.219	53.127	SILTY SAND

Sample ID	Depth (cm)	Lithosome	Unit	d 0.1 (µm)	d 0.5 (µm)	d 0.9 (µm)	% Clay	% Silt	% Sand	Shepard Class
257	135.3	II	2	3.751	45.132	131.373	20.057	44.727	35.217	SAND SILT CLAY
258	137.1	II	2	5.090	69.929	211.965	15.475	34.220	50.305	SILTY SAND
259	139.8	II	2	3.861	48.885	131.473	19.281	43.827	36.892	SANDY SILT
260	141.6	II	2	4.924	67.828	194.300	15.659	34.998	49.342	SILTY SAND

Table A5. Grain size distribution and Shepard classification for core 5 samples. Key to abbreviations: d 0.1 (μm) = 10th percentile of grain size distribution; d 0.5 (μm) = 50th percentile of grain size distribution; d 0.9 (μm) = 90th percentile of grain size distribution.

Sample ID	Depth (cm)	Lithosome	Unit	d 0.1 (μm)	d 0.5 (μm)	d 0.9 (μm)	% Clay	% Silt	% Sand	Shepard Class
401	2.1	VII	14	4.143	94.720	205.684	16.005	21.617	62.379	SILTY SAND
402	4.4	VII	14	5.386	46.954	170.599	14.538	48.429	37.033	SANDY SILT
403	7.3	VII	14	4.641	55.942	305.890	15.611	38.422	45.967	SILTY SAND
404	10.5	VII	14	6.859	36.905	116.256	12.080	64.971	22.948	SANDY SILT
405	12.8	VII	14	10.535	43.125	133.202	8.685	61.969	29.346	SANDY SILT
406	15.7	VII	14	9.855	72.611	170.215	8.989	38.627	52.384	SILTY SAND
407	18.4	VII	14	12.460	88.579	238.641	7.339	32.030	60.631	SILTY SAND
408	20.9	VII	14	11.664	74.840	252.407	7.773	39.445	52.783	SILTY SAND
409	23.6	VII	14	12.162	80.029	209.472	7.571	36.183	56.246	SILTY SAND
410	27.0	VII	14	10.207	74.675	186.177	8.649	38.181	53.170	SILTY SAND
411	29.3	VII	14	6.785	30.454	123.089	12.840	66.726	20.434	SANDY SILT
412	31.4	VII	14	9.467	67.968	212.297	9.258	41.337	49.404	SILTY SAND
413	34.6	VII	13	12.375	95.251	267.142	7.352	30.844	61.804	SILTY SAND
414	37.2	VII	13	14.101	115.280	370.097	6.533	27.019	66.448	SILTY SAND
415	39.8	VII	13	49.932	144.191	350.251	2.390	13.809	83.800	SAND
416	41.9	VII	13	48.728	185.625	421.477	2.316	11.556	86.127	SAND
417	44.5	VII	13	54.154	168.651	398.123	2.760	10.800	86.440	SAND
418	47.7	VII	13	31.750	184.768	418.582	3.100	13.658	83.242	SAND
419	50.9	VII	13	15.230	166.785	395.465	5.886	21.089	73.025	SILTY SAND
420	52.5	VII	13	16.684	188.499	446.936	5.308	18.100	76.591	SAND
421	55.1	VII	13	23.226	186.760	426.618	4.212	13.015	82.773	SAND
422	57.7	VII	13	47.916	214.465	445.034	3.116	8.360	88.524	SAND
423	60.3	VII	13	12.693	151.860	371.901	7.272	17.667	75.061	SAND
424	62.9	VII	13	14.604	168.807	505.360	6.616	14.260	79.125	SAND
425	65.0	VII	13	15.651	171.603	390.471	6.067	13.831	80.103	SAND

Sample ID	Depth (cm)	Lithosome	Unit	d 0.1 (µm)	d 0.5 (µm)	d 0.9 (µm)	% Clay	% Silt	% Sand	Shepard Class
426	67.6	VII	13	21.947	194.292	417.004	4.921	10.563	84.516	SAND
427	70.2	VII	13	8.899	103.062	453.230	9.809	30.232	59.959	SILTY SAND
428	73.4	VI	12	9.024	82.594	282.033	9.686	35.623	54.691	SILTY SAND
429	75.5	VI	12	8.331	44.551	237.449	10.365	55.032	34.603	SANDY SILT
430	78.1	VI	12	6.367	38.954	269.448	12.880	56.695	30.425	SANDY SILT
431	80.7	VI	11	21.190	169.247	409.045	4.703	22.499	72.798	SILTY SAND
432	83.9	VI	11	21.419	109.910	266.143	4.462	26.033	69.505	SILTY SAND
433	86.4	VI	11	25.811	139.211	308.515	3.668	19.052	77.280	SAND
434	89.1	VI	11	9.679	102.146	224.340	9.076	25.822	65.102	SILTY SAND
435	91.6	VI	11	6.799	63.027	211.650	12.452	40.029	47.519	SILTY SAND
436	94.3	V	10	5.029	29.819	136.639	16.802	60.256	22.942	SANDY SILT
437	96.6	V	10	5.789	38.148	203.704	14.400	51.537	34.063	SANDY SILT
438	99.3	V	10	4.582	28.973	99.589	17.488	65.536	16.976	CLAYEY SILT
439	102.0	V	10	5.732	32.496	314.735	14.675	58.490	26.834	SANDY SILT
440	104.7	V	10	5.880	40.031	168.807	14.257	52.471	33.272	SANDY SILT
445	107.2	V	9	18.675	127.029	372.120	5.154	24.257	70.588	SILTY SAND
446	109.7	V	9	18.324	112.142	328.499	5.167	28.357	66.476	SILTY SAND
447	112.7	V	9	15.262	104.732	311.565	6.095	29.850	64.054	SILTY SAND
448	114.7	V	9	16.828	110.009	280.531	5.567	27.214	67.220	SILTY SAND
449	117.2	V	9	32.874	155.725	353.878	3.348	14.296	82.355	SAND
450	119.7	V	9	16.896	113.750	331.047	5.790	28.022	66.188	SILTY SAND
451	122.7	V	9	25.769	147.272	322.689	3.956	16.087	79.958	SAND
452	124.7	V	9	35.953	195.487	454.398	3.032	11.665	85.303	SAND
453	127.7	V	9	16.899	106.069	333.757	5.394	30.352	64.254	SILTY SAND
454	129.7	IV	8	4.728	32.953	81.674	16.225	68.995	14.780	CLAYEY SILT
455	132.7	IV	8	4.104	29.976	66.626	18.709	72.558	8.733	CLAYEY SILT
456	134.7	IV	8	6.429	34.609	86.810	12.802	70.380	16.818	SANDY SILT

Sample ID	Depth (cm)	Lithosome	Unit	d 0.1 (µm)	d 0.5 (µm)	d 0.9 (µm)	% Clay	% Silt	% Sand	Shepard Class
457	137.7	IV	8	6.585	34.228	92.247	12.828	69.018	18.155	SANDY SILT
458	140.2	IV	8	3.990	25.781	72.917	20.419	68.387	11.194	CLAYEY SILT
459	142.7	IV	8	4.494	31.146	110.342	17.854	60.179	21.967	SANDY SILT
460	144.7	IV	8	4.879	31.615	101.052	16.730	64.080	19.191	SANDY SILT
461	147.7	IV	8	3.277	23.855	71.153	23.399	65.912	10.689	CLAYEY SILT
462	150.2	IV	8	3.798	29.894	77.856	19.694	66.704	13.602	CLAYEY SILT
463	152.7	IV	8	3.983	27.649	72.660	19.815	68.747	11.438	CLAYEY SILT
464	154.7	IV	8	7.356	46.001	252.568	11.618	50.918	37.465	SANDY SILT
465	157.7	IV	7	8.093	109.630	330.152	10.686	30.962	58.351	SILTY SAND
466	160.2	IV	7	9.209	98.582	266.417	9.486	31.361	59.153	SILTY SAND
467	162.7	IV	7	14.160	142.428	328.325	6.439	21.022	72.539	SILTY SAND
468	164.7	IV	7	20.728	158.081	331.168	4.662	15.129	80.209	SAND
469	167.7	IV	7	14.174	135.292	327.497	6.514	21.191	72.295	SILTY SAND
470	170.2	IV	7	76.743	197.938	412.888	1.931	6.917	91.152	SAND
471	172.7	IV	7	93.405	230.435	446.616	1.694	5.522	92.784	SAND
472	174.7	IV	7	35.455	184.719	392.139	3.531	10.657	85.813	SAND
473	177.7	IV	7	14.044	131.840	344.263	6.808	20.460	72.732	SILTY SAND
474	179.7	IV	7	11.887	115.850	277.657	7.677	22.380	69.942	SILTY SAND
475	182.7	IV	7	12.004	120.890	315.449	7.620	21.864	70.516	SILTY SAND
476	184.7	IV	7	12.451	114.803	280.539	7.387	23.070	69.543	SILTY SAND
477	187.7	IV	7	6.465	58.942	219.172	13.039	42.395	44.566	SILTY SAND
478	189.7	IV	7	6.276	56.668	304.053	13.475	41.307	45.218	SILTY SAND
479	192.7	IV	7	4.036	24.908	150.887	20.504	64.038	15.458	CLAYEY SILT
480	194.7	IV	7	4.147	24.948	220.458	20.104	65.017	14.879	CLAYEY SILT
481	198.2	III	6	3.612	22.284	51.427	22.448	75.087	2.465	SILT
482	200.7	III	6	3.178	23.073	54.641	24.294	72.060	3.646	CLAYEY SILT
487	202.6	III	6	4.075	27.225	71.381	19.508	69.702	10.789	CLAYEY SILT

Sample ID	Depth (cm)	Lithosome	Unit	d 0.1 (µm)	d 0.5 (µm)	d 0.9 (µm)	% Clay	% Silt	% Sand	Shepard Class
488	204.9	III	6	3.864	21.457	48.918	22.637	75.955	1.409	SILT
489	207.4	III	6	3.771	20.998	47.210	23.310	75.875	0.815	SILT
490	210.2	III	6	3.569	23.922	55.170	22.358	73.990	3.652	CLAYEY SILT
491	212.5	III	6	4.746	23.828	52.022	17.814	79.745	2.441	SILT
492	215.0	III	6	3.736	22.901	52.297	22.119	75.459	2.422	SILT
493	217.3	III	6	4.429	23.271	51.090	18.892	79.003	2.105	SILT
494	219.8	III	6	5.511	27.231	62.797	15.093	77.545	7.363	SILT
495	222.5	III	6	6.787	39.291	128.050	12.212	61.445	26.344	SANDY SILT
496	225.0	III	6	7.263	38.951	122.463	11.600	63.574	24.826	SANDY SILT
497	227.5	III	6	6.613	37.453	89.961	12.493	68.607	18.899	SANDY SILT
498	229.4	III	6	7.056	30.136	63.486	11.996	80.761	7.243	SILT
499	232.2	III	6	9.527	35.218	75.502	9.298	77.553	13.149	SILT
500	234.5	III	6	9.155	38.580	106.303	9.603	68.218	22.179	SANDY SILT
501	237.0	III	6	8.855	37.567	99.664	9.856	69.319	20.825	SANDY SILT
502	238.9	III	6	7.018	32.064	68.579	12.083	78.217	9.700	SILT
503	241.6	III	6	6.769	29.734	66.465	12.647	78.567	8.786	SILT
504	243.7	III	6	9.557	43.972	279.590	9.177	58.894	31.929	SANDY SILT
505	246.5	III	5	14.102	74.504	461.708	6.412	41.329	52.259	SILTY SAND
506	248.4	III	5	21.570	166.898	488.978	4.295	28.881	66.823	SILTY SAND
507	250.7	III	5	12.050	118.838	553.350	7.380	35.185	57.435	SILTY SAND
508	253.0	III	5	5.063	27.527	380.957	17.242	56.728	26.030	SANDY SILT
509	255.1	III	5	5.378	28.242	353.710	15.859	59.685	24.455	SANDY SILT
510	257.9	III	5	7.337	222.948	567.253	11.785	27.489	60.727	SILTY SAND
511	260.0	III	5	4.236	23.374	73.473	20.140	68.536	11.324	CLAYEY SILT
512	262.3	III	5	8.663	68.596	490.998	10.053	40.125	49.822	SILTY SAND
513	264.8	III	5	5.074	34.760	345.321	16.843	47.861	35.296	SANDY SILT
514	267.5	II	4	2.678	13.228	44.605	34.998	59.136	5.867	CLAYEY SILT

Sample ID	Depth (cm)	Lithosome	Unit	d 0.1 (µm)	d 0.5 (µm)	d 0.9 (µm)	% Clay	% Silt	% Sand	Shepard Class
515	270.0	II	4	2.732	11.810	33.466	37.702	59.041	3.257	CLAYEY SILT
516	272.5	II	4	2.745	13.852	48.850	34.991	59.571	5.437	CLAYEY SILT
517	275.2	II	4	2.741	13.660	55.107	35.276	57.154	7.569	CLAYEY SILT
518	278.0	II	4	2.703	14.408	37.466	32.646	66.934	0.421	CLAYEY SILT
519	280.5	II	4	2.790	14.825	38.098	31.984	67.957	0.059	CLAYEY SILT
520	282.8	II	4	2.719	14.567	37.708	32.763	67.184	0.053	CLAYEY SILT
521	285.1	II	4	2.593	12.357	32.257	36.672	63.265	0.063	CLAYEY SILT
522	287.6	II	4	2.683	14.333	36.519	33.317	66.661	0.022	CLAYEY SILT
523	290.3	II	4	2.556	12.434	35.847	38.163	60.686	1.151	CLAYEY SILT
524	292.4	II	4	2.465	12.962	35.990	37.326	62.649	0.025	CLAYEY SILT
525	294.3	II	4	2.478	13.855	38.010	35.759	64.195	0.046	CLAYEY SILT
530	296.9	II	4	2.646	13.858	38.105	36.034	63.843	0.123	CLAYEY SILT
531	299.1	II	4	2.298	14.347	44.230	37.014	61.688	1.298	CLAYEY SILT
532	301.7	II	4	2.508	18.319	63.242	32.406	59.361	8.233	CLAYEY SILT
533	303.9	II	3	3.801	36.587	124.194	20.422	51.008	28.570	SAND SILT CLAY
534	305.7	II	3	6.600	71.202	240.817	12.537	36.495	50.967	SILTY SAND
535	307.9	II	3	4.317	40.943	118.716	18.152	52.031	29.817	SANDY SILT
536	310.1	II	3	3.326	29.570	102.632	23.784	55.222	20.994	SAND SILT CLAY
537	312.7	II	3	3.552	29.436	95.326	22.467	58.956	18.577	CLAYEY SILT
538	314.5	II	3	3.348	29.255	80.935	23.502	61.275	15.223	CLAYEY SILT
539	316.7	II	3	3.453	31.531	86.672	22.067	60.589	17.344	CLAYEY SILT
540	319.3	II	2	14.390	85.548	268.352	6.587	34.582	58.831	SILTY SAND
541	321.5	II	2	11.786	60.398	156.253	7.539	49.071	43.390	SANDY SILT
542	323.7	II	2	27.898	178.348	594.238	4.092	18.394	77.515	SAND
543	325.9	II	2	53.298	141.958	322.816	2.307	12.705	84.988	SAND
544	328.1	II	2	59.535	167.440	394.286	1.787	10.974	87.239	SAND
545	330.3	II	2	48.194	119.618	248.783	2.218	17.089	80.693	SAND

Sample ID	Depth (cm)	Lithosome	Unit	d 0.1 (µm)	d 0.5 (µm)	d 0.9 (µm)	% Clay	% Silt	% Sand	Shepard Class
546	332.1	II	2	41.612	144.004	385.949	2.877	15.878	81.245	SAND
547	334.3	II	2	4.474	43.732	171.368	17.469	47.017	35.514	SANDY SILT
548	336.5	II	2	4.064	32.751	89.840	18.612	63.588	17.800	CLAYEY SILT
549	339.1	II	2	4.186	45.129	196.206	18.683	44.144	37.173	SANDY SILT
550	341.3	II	2	4.623	41.294	128.085	16.990	53.883	29.128	SANDY SILT
551	343.5	II	2	4.784	44.808	146.616	16.581	50.479	32.940	SANDY SILT
552	346.1	II	2	5.212	40.844	115.281	15.182	57.744	27.074	SANDY SILT
553	347.9	II	2	11.075	94.188	285.134	8.230	30.735	61.036	SILTY SAND
554	350.5	I	1	3.903	33.683	106.458	20.265	56.778	22.957	SAND SILT CLAY
555	352.7	I	1	4.208	35.779	120.383	19.277	54.190	26.532	SANDY SILT
556	354.9	I	1	4.105	31.186	97.742	20.273	58.989	20.738	SAND SILT CLAY
557	356.7	I	1	3.672	27.650	87.340	22.635	60.238	17.127	CLAYEY SILT
558	359.3	I	1	4.157	32.964	108.883	19.845	56.689	23.466	SANDY SILT
559	361.5	I	1	3.599	26.324	80.667	23.163	62.159	14.678	CLAYEY SILT
560	363.3	I	1	3.834	27.744	80.405	21.672	63.614	14.714	CLAYEY SILT
561	365.5	I	1	4.171	29.114	79.575	20.323	64.931	14.746	CLAYEY SILT
562	367.7	I	1	4.433	30.016	85.278	19.417	63.595	16.988	CLAYEY SILT
563	369.9	I	1	4.031	28.120	83.914	21.322	62.484	16.194	CLAYEY SILT
564	371.7	I	1	4.756	31.699	87.908	18.248	63.698	18.054	CLAYEY SILT
565	374.3	I	1	3.507	25.481	76.721	23.907	62.862	13.232	CLAYEY SILT
566	376.9	I	1	4.295	31.317	97.801	19.563	60.096	20.341	SANDY SILT
567	378.7	I	1	4.549	32.115	88.345	18.382	63.287	18.331	CLAYEY SILT
572	382.2	I	1	5.069	34.907	91.422	16.758	62.988	20.254	SANDY SILT
573	384.8	I	1	3.612	27.229	74.126	22.563	65.191	12.245	CLAYEY SILT
574	387.1	I	1	4.238	29.851	82.283	19.823	64.410	15.767	CLAYEY SILT
575	389.4	I	1	5.291	46.201	720.030	15.655	46.721	37.624	SANDY SILT
576	390.9	I	1	4.789	35.175	98.859	17.588	59.972	22.440	SANDY SILT

Sample ID	Depth (cm)	Lithosome	Unit	d 0.1 (µm)	d 0.5 (µm)	d 0.9 (µm)	% Clay	% Silt	% Sand	Shepard Class
577	392.7	I	1	4.561	33.763	94.096	18.370	60.755	20.875	SANDY SILT
578	394.7	I	1	4.085	31.861	92.810	20.096	59.972	19.931	CLAYEY SILT
579	396.2	I	1	4.502	39.143	128.610	18.148	52.344	29.508	SANDY SILT
580	398.0	I	1	4.806	36.087	95.369	17.456	60.426	22.117	SANDY SILT
581	399.8	I	1	4.369	34.910	91.462	18.795	60.502	20.703	SANDY SILT
582	402.0	I	1	4.583	39.410	118.480	17.657	55.003	27.340	SANDY SILT
583	403.8	I	1	4.243	32.691	87.450	19.414	61.952	18.634	CLAYEY SILT
584	406.1	I	1	3.683	30.875	91.991	21.969	58.288	19.743	CLAYEY SILT
585	407.8	I	1	3.841	30.533	84.896	21.212	61.577	17.211	CLAYEY SILT
586	410.0	I	1	4.019	34.556	93.989	20.289	58.032	21.678	SAND SILT CLAY
587	411.8	I	1	4.686	31.882	82.870	18.224	65.246	16.530	CLAYEY SILT
588	413.8	I	1	4.639	29.564	80.002	18.774	66.420	14.806	CLAYEY SILT
589	415.6	I	1	4.133	27.082	75.992	20.940	66.091	12.969	CLAYEY SILT
590	417.6	I	1	4.430	32.007	101.329	19.260	59.593	21.146	SANDY SILT
591	419.4	I	1	4.824	34.742	102.439	17.680	59.315	23.005	SANDY SILT
592	421.4	I	1	4.524	31.083	86.632	19.117	63.036	17.847	CLAYEY SILT

APPENDIX B

MAGNETIC SUSCEPTIBILITY AND FREQUENCY DEPENDENCE DATA

- 1) Table B1. Magnetic susceptibility (MS) and frequency dependence (FD) percentages for core 1 samples.
- 2) Table B2. Magnetic susceptibility (MS) and frequency dependence (FD) percentages for core 2 samples.
- 3) Table B3. Magnetic susceptibility (MS) and frequency dependence (FD) percentages for core 3 samples.
- 4) Table B4. Magnetic susceptibility (MS) and frequency dependence (FD) percentages for core 4 samples.
- 5) Table B5. Magnetic susceptibility (MS) and frequency dependence (FD) percentages for core 5 samples.

Table B1. Magnetic susceptibility (MS) and frequency dependence (FD) percentages for core 1 samples.

Sample ID	Depth (cm)	Lithosome	Unit	Weight (g)	MS ($10^{-8} \text{ m}^3 \text{ kg}^{-1}$)	FD (%)
601	12.0	VIII	17	4.25	213.88	3.19
602	14.0	VIII	17	3.79	217.94	4.12
603	16.0	VIII	17	4.04	206.44	3.96
604	18.0	VIII	17	3.96	229.17	3.91
605	19.6	VIII	17	4.10	239.63	3.92
606	21.2	VIII	17	4.60	241.74	3.91
607	23.1	VIII	17	6.06	259.98	3.14
608	25.1	VIII	17	5.75	263.04	3.87
609	27.0	VIII	17	3.87	249.22	2.85
610	28.7	VIII	17	4.26	265.49	3.71
611	31.4	VIII	17	4.94	230.97	3.72
612	33.8	VIII	17	5.00	230.00	4.35
613	35.8	VIII	17	4.43	280.25	3.50
614	37.5	VIII	17	5.52	291.21	4.07
615	39.2	VIII	17	6.42	274.14	3.89
616	41.6	VIII	17	5.73	287.43	4.40
617	43.5	VIII	17	6.38	255.96	3.61
618	45.1	VIII	16	6.94	306.12	4.42
619	47.3	VIII	16	7.76	390.34	3.42
620	49.5	VIII	16	7.03	451.14	3.18
621	51.7	VIII	15	7.10	474.79	1.65
622	53.4	VIII	15	8.40	447.56	2.61
623	55.1	VIII	15	8.72	392.20	1.56
624	57.3	VIII	15	7.78	361.05	1.44
625	59.5	VIII	15	8.94	364.26	2.72
626	61.5	VIII	15	6.44	410.87	3.02
627	63.2	VIII	15	7.69	500.07	0.81
628	65.1	VIII	15	7.84	374.74	0.60
629	67.1	VIII	15	8.35	369.94	1.67
630	69.3	VIII	15	8.98	321.10	3.05
631	71.3	VIII	15	7.80	268.08	1.51
632	72.9	VIII	15	7.76	274.23	2.47
633	74.9	VIII	15	7.93	232.28	1.82
634	76.9	VIII	15	8.28	409.90	2.99
635	78.5	VIII	15	9.02	450.89	2.62
636	80.7	VIII	15	9.51	341.54	2.32
637	82.7	VIII	15	9.36	365.65	3.05

Sample ID	Depth (cm)	Lithosome	Unit	Weight (g)	MS ($10^{-8} \text{ m}^3 \text{ kg}^{-1}$)	FD (%)
638	84.6	VIII	15	8.96	295.37	1.70
639	86.8	VIII	15	8.62	279.06	2.41
640	88.5	VIII	15	9.03	301.94	3.10
641	90.9	VIII	15	9.06	346.69	2.61
642	92.8	VIII	15	10.04	330.68	0.41
643	94.7	VIII	15	9.61	373.10	1.69
644	96.4	VIII	15	8.91	345.85	1.72
645	98.8	VIII	15	9.25	347.41	2.66
646	100.7	VIII	15	8.74	369.28	2.28
647	102.7	VIII	15	8.79	408.42	3.26
648	104.3	VIII	15	8.50	291.35	3.63
652	106.1	VIII	15	8.65	300.92	2.54
653	108.9	VIII	15	7.29	375.86	2.32
654	111.4	VII	14	6.92	384.83	2.18
655	113.9	VII	14	7.08	339.05	2.52
656	116.2	VII	14	7.90	396.84	1.75
657	118.5	VII	14	6.07	366.64	1.73
658	120.4	VII	14	6.01	299.50	2.72
659	122.7	VII	14	5.19	248.75	5.00
660	124.8	VII	14	4.82	235.48	5.73
661	127.1	VII	13	6.15	347.64	4.07
662	129.0	VII	13	7.26	326.58	2.66
663	131.3	VII	13	7.21	302.77	2.70
664	133.2	VII	13	7.60	276.78	1.64
665	135.7	VII	13	7.12	252.25	2.90
666	137.8	VII	13	7.26	198.55	3.64
667	140.1	VII	13	6.43	244.17	3.18
668	141.9	VII	13	7.52	216.16	2.40
669	144.0	VII	13	7.34	262.74	3.24
670	146.1	VII	13	8.33	287.27	2.82
671	148.4	VII	13	8.28	293.06	2.64
672	150.2	VII	13	8.88	269.82	2.46
673	152.7	VI	12	7.57	227.87	2.87
674	155.0	VI	12	7.73	222.06	4.86
675	157.1	VI	12	7.05	211.99	4.65
676	159.0	VI	11	7.60	290.39	3.06
677	161.5	VI	11	7.40	241.22	4.01
678	163.6	VI	11	8.62	355.92	2.31
679	165.7	VI	11	8.36	274.46	3.20

Sample ID	Depth (cm)	Lithosome	Unit	Weight (g)	MS ($10^{-8} \text{ m}^3 \text{ kg}^{-1}$)	FD (%)
680	167.8	VI	11	8.53	270.69	1.56
681	170.3	VI	11	8.53	260.26	2.32
682	172.4	VI	11	9.83	303.20	2.40
683	174.9	VI	11	7.98	256.58	1.25
684	176.7	VI	11	7.56	289.81	1.41
685	178.5	VI	11	7.90	309.05	2.36
699	181.2	VI	11	9.08	338.11	1.87
700	183.7	VI	11	10.09	240.29	0.25
701	186.3	VI	11	10.63	276.72	0.02
702	188.9	VI	11	9.61	269.04	2.69
703	191.5	VI	11	10.21	232.91	0.25
704	194.1	VI	11	10.85	255.58	2.40
705	196.7	VI	11	10.25	260.20	0.34
706	199.3	VI	11	8.97	249.50	0.54
707	201.9	VI	11	9.34	308.08	0.57
708	204.5	VI	11	10.27	276.34	1.09
709	206.8	VI	11	10.04	249.75	2.05
710	209.5	VI	11	10.80	286.94	1.84
711	212.2	VI	11	10.35	288.50	1.88
712	214.9	VI	11	10.52	248.72	2.18
713	217.2	V	10	9.00	199.39	2.65
714	220.2	V	10	8.87	190.02	1.81
715	222.7	V	9	10.91	344.73	1.87
716	225.4	V	9	10.88	333.41	0.55
717	228.0	V	9	10.61	345.38	0.85
718	230.6	V	9	10.92	355.04	0.32
719	233.2	V	9	10.17	311.16	0.54
720	235.8	V	9	10.94	274.04	0.72
721	238.5	V	9	10.56	279.26	0.73
722	241.0	V	9	11.45	327.55	0.84
723	243.6	V	9	10.96	307.25	0.59
724	246.2	V	9	10.89	338.29	1.85
725	249.4	V	9	10.91	345.88	0.62
726	252.0	V	9	10.68	371.63	0.71

Table B2. Magnetic susceptibility (MS) and frequency dependence (FD) percentages for core 2 samples.

Sample ID	Depth (cm)	Lithosome	Unit	Weight (g)	MS ($10^{-8} \text{ m}^3 \text{ kg}^{-1}$)	FD (%)
1	2.5	VII	14	7.81	414.79	1.53
2	5.2	VII	14	7.71	378.08	2.37
3	7.9	VII	14	7.35	380.07	1.65
4	11.5	VII	14	7.75	333.42	2.75
5	14.2	VII	14	6.57	323.67	4.07
6	17.1	VII	14	6.60	299.24	3.19
7	21.6	VII	14	6.48	208.87	4.99
8	23.6	VII	13	8.18	387.71	2.59
9	26.5	VII	13	7.85	314.39	3.18
10	29.2	VII	13	8.03	263.95	4.22
11	32.3	VII	13	8.30	227.71	1.96
12	35.2	VII	13	6.99	204.86	3.53
13	38.1	VII	13	7.14	233.75	3.36
14	40.8	VII	13	6.99	222.25	1.90
15	43.7	VII	13	6.99	224.89	2.39
16	46.6	VII	13	7.83	278.99	1.85
17	49.3	VII	13	8.52	266.67	3.35
18	52.2	VII	13	9.18	267.21	2.69
19	54.9	VII	13	7.98	240.85	3.77
20	58.0	VI	12	8.10	216.60	3.90
21	61.0	VI	12	6.88	217.81	3.94
22	63.8	VI	11	8.69	357.02	1.56
23	66.5	VI	11	8.79	326.22	2.49
24	69.2	VI	11	9.37	259.55	1.64
25	72.1	VI	11	8.33	263.21	3.22
26	75.0	VI	11	9.84	342.17	1.34
27	77.9	VI	11	9.32	254.13	2.03
28	80.6	VI	11	9.03	339.26	1.42
29	83.3	VI	11	8.48	258.90	2.39
30	86.2	VI	11	8.51	272.86	2.28
31	89.1	VI	11	8.74	241.70	2.18
32	92.0	VI	11	9.79	195.25	2.12
33	94.9	VI	11	9.78	209.25	2.25
34	97.8	VI	11	10.08	285.62	2.00
35	100.5	VI	11	9.61	408.43	1.82
36	103.6	VI	11	7.85	307.96	1.76
37	106.5	VI	11	7.92	258.21	2.27

Sample ID	Depth (cm)	Lithosome	Unit	Weight (g)	MS ($10^{-8} \text{ m}^3 \text{ kg}^{-1}$)	FD (%)
38	109.4	VI	11	9.61	289.54	1.98
39	112.1	VI	11	10.30	318.88	1.00
40	115.0	VI	11	10.20	361.27	1.56
41	117.9	VI	11	10.08	340.48	1.15
42	120.6	VI	11	10.18	340.28	1.20
43	123.5	VI	11	9.76	271.82	1.83
44	126.4	VI	11	9.40	229.41	2.16
45	127.5	VI	11	6.49	255.93	1.23
50	130.4	VI	11	8.87	315.84	2.52
51	133.3	VI	11	10.60	371.32	1.41
52	136.0	VI	11	10.77	339.88	1.53
53	137.9	VI	11	10.03	261.12	1.89
54	141.4	VI	11	10.31	356.84	1.29
55	144.1	VI	11	9.71	331.77	3.12
56	146.2	VI	11	9.73	303.70	1.56
57	148.3	VI	11	8.96	251.67	2.86
58	151.4	V	10	8.41	269.80	2.51
59	154.3	V	10	8.72	307.63	3.06
60	156.4	V	10	9.17	289.04	2.57
61	158.7	V	9	9.01	375.75	2.72
62	161.2	V	9	10.15	398.97	2.21
63	164.3	V	9	9.31	356.28	2.67
64	166.6	V	9	9.14	363.35	2.41
65	169.1	V	9	9.79	382.38	1.46
66	171.4	V	9	10.10	408.12	2.26
67	174.5	V	9	9.44	235.75	1.71
68	177.0	V	9	8.67	192.33	1.86
69	179.5	V	9	8.87	202.31	1.87
70	182.4	V	9	8.01	190.20	1.44
71	184.9	V	9	7.85	184.52	2.11
72	187.6	V	9	8.62	211.60	1.18
73	189.9	V	9	8.34	193.65	2.11
74	192.4	V	9	7.77	315.83	2.93
75	194.9	IV	8	7.82	255.24	1.90
76	198.0	IV	8	7.25	167.38	2.27
77	200.3	IV	8	6.48	125.46	2.03
78	203.2	IV	8	6.01	116.06	2.15
79	205.5	IV	8	6.17	88.57	3.75
80	207.4	IV	8	6.84	93.20	3.61

Sample ID	Depth (cm)	Lithosome	Unit	Weight (g)	MS ($10^{-8} \text{ m}^3 \text{ kg}^{-1}$)	FD (%)
81	210.7	IV	8	6.28	111.70	2.07
82	213.6	IV	8	7.50	197.47	1.45
83	216.1	IV	8	7.56	184.46	1.65
84	218.6	IV	7	9.54	365.20	2.67
85	221.1	IV	7	10.45	421.67	1.38
86	222.3	IV	7	9.43	364.32	1.85
87	226.2	IV	7	10.99	422.79	2.15
88	228.3	IV	7	10.12	322.53	1.79
89	231.4	IV	7	9.42	298.51	1.55
90	233.5	IV	7	9.99	278.48	2.16

Table B3. Magnetic susceptibility (MS) and frequency dependence (FD) percentages for core 3 samples.

Sample ID	Depth (cm)	Lithosome	Unit	Weight (g)	MS ($10^{-8} \text{ m}^3 \text{ kg}^{-1}$)	FD (%)
801	3.8	VIII	17	6.59	230.85	2.87
802	5.9	VIII	17	6.10	210.87	4.13
803	8.5	VIII	17	6.54	209.58	3.55
804	10.2	VIII	17	6.04	202.92	3.74
805	12.3	VIII	17	7.03	260.34	3.98
806	14.8	VIII	16	6.90	252.95	2.28
807	17.0	VIII	16	7.96	312.65	3.19
808	19.1	VIII	16	7.30	344.93	3.42
809	21.2	VIII	16	8.59	394.63	1.89
810	23.3	VIII	16	9.37	411.65	2.78
811	25.4	VIII	15	9.27	604.30	6.47
812	27.5	VIII	15	9.73	509.20	3.66
813	29.6	VIII	15	9.83	599.10	4.20
814	31.7	VIII	15	9.58	294.02	3.40
815	33.8	VIII	15	9.44	300.76	2.92
816	35.8	VIII	15	8.97	325.08	4.06
817	38.0	VIII	15	9.54	337.30	4.05
818	40.0	VIII	15	9.67	320.85	3.34
819	42.2	VIII	15	9.78	371.83	2.80
820	44.3	VIII	15	9.42	372.59	2.79
821	46.4	VIII	15	9.20	419.87	2.97
822	48.5	VIII	15	9.54	317.47	3.37
823	50.6	VIII	15	10.43	316.76	3.09
824	52.7	VIII	15	9.71	315.79	1.96
825	54.8	VIII	15	9.78	353.63	2.18
826	56.9	VIII	15	9.23	264.68	1.81
827	59.0	VIII	15	10.46	455.59	1.97
828	61.1	VIII	15	10.17	417.70	3.17
829	63.2	VIII	15	11.56	562.72	2.61
830	65.4	VIII	15	9.22	470.59	3.05
831	67.4	VIII	15	9.14	307.73	2.16
832	69.5	VIII	15	8.86	239.16	4.20
833	71.6	VIII	15	9.25	305.17	3.66
834	73.7	VIII	15	7.96	211.47	6.12
835	75.8	VIII	15	7.86	185.31	4.23
836	77.9	VIII	15	7.84	208.48	3.97
837	80.0	VIII	15	8.45	207.34	4.09

Sample ID	Depth (cm)	Lithosome	Unit	Weight (g)	MS ($10^{-8} \text{ m}^3 \text{ kg}^{-1}$)	FD (%)
838	82.1	VIII	15	7.67	185.64	4.86
839	84.2	VIII	15	7.89	185.85	5.42
840	85.9	VIII	15	8.24	212.74	4.57
855	88.2	VIII	15	8.40	229.54	2.26
856	90.5	VIII	15	8.77	331.05	2.22
857	92.8	VIII	15	9.13	345.58	1.43
858	95.1	VII	14	6.17	224.20	3.66
859	97.4	VII	14	6.66	241.44	2.33
860	99.7	VII	13	9.29	295.71	2.88
861	102.0	VII	13	9.62	299.67	2.54
862	104.3	VII	13	9.90	291.80	2.00
863	106.6	VII	13	10.29	280.52	1.69
864	108.9	VII	13	10.72	326.10	1.98
865	111.2	VII	13	10.77	404.12	2.25
866	113.5	VII	13	10.11	258.65	3.00
867	115.8	VII	13	11.04	192.03	-1.10
868	118.1	VII	13	9.61	239.73	-0.69
869	120.4	VII	13	10.34	368.81	0.17
870	122.7	VI	12/11	9.91	328.71	0.86
871	125.0	V	10/9	10.02	222.80	0.84
872	127.3	V/IV	9/8	8.59	206.17	0.17
873	129.6	IV	8	8.22	198.54	0.92
874	131.9	IV	8	7.15	124.38	0.81
875	134.2	IV	8	8.28	127.42	0.52
876	136.9	IV	8	7.37	175.62	2.06
877	139.6	IV	7	10.08	311.87	1.88
879	146.1	IV	7	10.08	325.30	-0.11
880	148.7	IV	7	9.31	325.81	-0.59
881	151.5	IV	7	9.00	289.07	1.20
882	154.2	IV	7	9.53	312.92	1.94
883	156.5	IV	7	8.38	268.79	1.48
884	159.2	IV	7	7.43	247.51	2.60
885	161.5	III	6	7.33	274.40	4.11
886	164.1	III	6	7.55	256.27	2.95
887	167.4	III	6	7.80	288.74	2.32
888	169.8	III	5	8.16	313.93	1.64
889	172.2	III	5	8.79	318.22	2.59
890	174.6	III	5	9.12	261.28	2.75
891	177.0	III	5	9.35	268.52	1.35

Sample ID	Depth (cm)	Lithosome	Unit	Weight (g)	MS ($10^{-8} \text{ m}^3 \text{ kg}^{-1}$)	FD (%)
892	179.4	III	5	11.62	657.59	1.09
893	181.8	III	5	9.30	764.12	0.81
894	184.2	III	5	7.82	521.70	1.71
895	186.6	III	5	8.67	545.83	0.88
896	189.0	III	5	7.79	516.71	1.85
897	191.4	III	5	8.35	583.59	0.64
898	193.8	III	5	8.19	664.63	1.65
899	196.4	III	5	5.89	802.66	0.39
900	198.9	III	5	6.20	804.62	0.85
901	201.5	III	5	6.34	290.38	2.51
902	204.4	III	5	6.52	111.86	3.54

Table B4. Magnetic susceptibility (MS) and frequency dependence (FD) percentages for core 4 samples.

Sample ID	Depth (cm)	Lithosome	Unit	Weight (g)	MS ($10^{-8} \text{ m}^3 \text{ kg}^{-1}$)	FD (%)
201	1.0	III	6	6.70	197.69	1.32
202	4.1	III	6	8.16	199.75	3.31
203	7.2	III	6	7.74	198.13	3.16
204	10.3	III	6	6.97	221.31	3.44
205	12.4	III	6	6.31	210.30	3.28
206	15.0	III	6	5.78	205.71	2.86
207	18.1	III	5	6.70	317.16	2.19
208	20.7	III	5	7.16	467.04	2.09
209	23.3	III	5	8.61	1104.41	1.38
210	26.4	III	5	7.45	883.22	1.34
211	28.5	III	5	8.80	981.53	1.15
212	31.1	III	5	8.46	852.25	1.35
213	33.7	III	5	7.60	947.83	1.03
214	36.3	III	5	8.31	1163.12	0.15
215	39.4	III	5	7.18	358.77	2.31
216	41.5	III	5	7.76	436.08	1.68
217	44.1	III	5	8.65	556.88	1.12
218	46.7	III	5	8.16	98.04	4.50
219	49.8	III	5	8.47	76.45	3.86
220	51.9	III	5	8.51	56.23	4.70
221	54.5	III	5	8.17	69.28	4.77
222	57.1	III	5	8.76	70.43	5.43
223	59.4	III	5	8.62	66.53	4.97
224	62.3	III	5	8.53	52.34	4.93
225	64.9	III	5	7.92	51.89	4.62
226	67.0	II	4	5.56	25.54	4.58
227	69.6	II	4	6.66	38.36	6.65
228	72.7	II	4	7.19	49.72	5.17
229	74.8	II	4	7.38	48.58	5.30
230	77.4	II	4	7.21	44.66	4.97
231	80.0	II	4	6.48	43.06	5.38
232	83.1	II	4	7.51	43.81	5.93
233	85.2	II	4	6.33	40.92	7.34
234	87.8	II	4	6.24	44.39	5.42
235	90.4	II	4	7.57	40.75	5.02
236	93.5	II	4	7.44	40.12	5.36
237	96.1	II	4	8.02	40.15	5.28

Sample ID	Depth (cm)	Lithosome	Unit	Weight (g)	MS ($10^{-8} \text{ m}^3 \text{ kg}^{-1}$)	FD (%)
238	98.7	II	4	7.53	45.42	6.87
239	102.8	II	4	7.59	42.16	5.94
240	103.8	II	3	7.09	46.14	5.84
245	107.4	II	3	8.21	74.12	3.78
246	109.2	II	3	8.47	44.57	5.70
247	111.9	II	3	7.64	43.00	5.18
248	114.6	II	3	7.33	43.32	5.83
249	116.4	II	3	7.24	46.34	5.07
250	119.1	II	3	7.52	44.22	4.96
251	121.8	II	3	7.22	46.19	5.85
252	123.6	II	2	7.27	40.03	5.33
253	126.3	II	2	7.12	44.03	5.26
254	128.1	II	2	8.82	61.45	8.58
255	130.8	II	2	8.81	56.19	4.65
256	132.6	II	2	9.74	65.50	5.88
257	135.3	II	2	9.45	69.37	5.26
258	137.1	II	2	9.03	58.69	6.04
259	139.8	II	2	8.54	62.88	4.93
260	141.6	II	2	8.96	64.45	4.68

Table B5. Magnetic susceptibility (MS) and frequency dependence (FD) percentages for core 5 samples.

Sample ID	Depth (cm)	Lithosome	Unit	Weight (g)	MS ($10^{-8} \text{ m}^3 \text{ kg}^{-1}$)	FD (%)
401	2.1	VII	14	9.66	268.17	3.07
402	4.4	VII	14	8.73	321.31	2.67
403	7.3	VII	14	8.76	254.62	3.36
404	10.5	VII	14	8.89	323.85	2.94
405	12.8	VII	14	9.09	338.67	2.87
406	15.7	VII	14	9.61	414.62	1.83
407	18.4	VII	14	9.31	548.60	1.60
408	20.9	VII	14	9.04	474.45	2.03
409	23.6	VII	14	7.36	411.48	1.60
410	27.0	VII	14	9.31	336.41	2.49
411	29.3	VII	14	8.28	296.92	3.62
412	31.4	VII	14	8.52	316.14	2.26
413	34.6	VII	13	8.11	317.63	2.31
414	37.2	VII	13	8.96	391.35	2.71
415	39.8	VII	13	7.93	377.87	2.12
416	41.9	VII	13	9.53	383.42	2.15
417	44.5	VII	13	9.93	467.98	1.45
418	47.7	VII	13	11.56	528.85	0.91
419	50.9	VII	13	10.51	458.66	1.29
420	52.5	VII	13	11.45	1103.06	0.84
421	55.1	VII	13	11.33	875.86	1.04
422	57.7	VII	13	11.02	706.81	1.13
423	60.3	VII	13	10.75	396.93	1.44
424	62.9	VII	13	10.10	391.68	1.67
425	65.0	VII	13	11.25	389.29	0.88
426	67.6	VII	13	10.95	399.04	1.45
427	70.2	VII	13	10.17	335.55	1.66
428	73.4	VI	12	9.42	279.41	2.13
429	75.5	VI	12	8.41	174.97	2.75
430	78.1	VI	12	8.73	131.33	3.58
431	80.7	VI	11	9.42	317.14	1.64
432	83.9	VI	11	10.58	461.77	1.72
433	86.4	VI	11	10.39	426.95	1.89
434	89.1	VI	11	10.19	335.13	1.99
435	91.6	VI	11	10.20	211.57	3.43
436	94.3	V	10	9.81	160.65	2.86
437	96.6	V	10	8.78	163.38	4.11

Sample ID	Depth (cm)	Lithosome	Unit	Weight (g)	MS ($10^{-8} \text{ m}^3 \text{ kg}^{-1}$)	FD (%)
438	99.3	V	10	9.16	154.20	2.97
439	102.0	V	10	9.27	161.27	2.88
440	104.7	V	10	9.62	253.48	2.34
445	107.2	V	9	9.02	368.02	1.99
446	109.7	V	9	9.79	385.96	2.37
447	112.7	V	9	8.91	414.20	2.75
448	114.7	V	9	9.48	361.66	2.48
449	117.2	V	9	9.37	356.67	2.27
450	119.7	V	9	9.49	343.52	2.12
451	122.7	V	9	9.74	362.01	2.03
452	124.7	V	9	8.24	347.69	2.29
453	127.7	V	9	6.95	363.88	1.64
454	129.7	IV	8	6.67	158.85	2.22
455	132.7	IV	8	8.45	98.88	2.09
456	134.7	IV	8	7.03	203.41	3.36
457	137.7	IV	8	7.59	171.81	2.80
458	140.2	IV	8	7.91	121.11	2.92
459	142.7	IV	8	7.51	187.88	1.98
460	144.7	IV	8	7.06	117.00	2.78
461	147.7	IV	8	7.00	66.57	1.82
462	150.2	IV	8	7.18	101.18	2.13
463	152.7	IV	8	7.80	124.62	1.39
464	154.7	IV	8	8.69	201.09	1.55
465	157.7	IV	7	8.60	416.63	1.54
466	160.2	IV	7	8.93	342.33	1.54
467	162.7	IV	7	9.72	404.22	1.44
468	164.7	IV	7	9.13	571.91	1.49
469	167.7	IV	7	10.08	449.26	2.10
470	170.2	IV	7	10.46	517.35	0.67
471	172.7	IV	7	9.83	617.90	1.56
472	174.7	IV	7	9.30	587.53	2.39
473	177.7	IV	7	8.48	782.84	0.93
474	179.7	IV	7	8.71	295.35	1.98
475	182.7	IV	7	8.85	290.40	1.95
476	184.7	IV	7	7.40	318.11	2.15
477	187.7	IV	7	7.32	252.32	2.19
478	189.7	IV	7	7.84	221.36	2.97
479	192.7	IV	7	8.23	194.47	2.22
480	194.7	IV	7	5.67	264.73	2.13

Sample ID	Depth (cm)	Lithosome	Unit	Weight (g)	MS ($10^{-8} \text{ m}^3 \text{ kg}^{-1}$)	FD (%)
481	198.2	III	6	5.17	123.79	3.44
482	200.7	III	6	7.60	80.79	2.93
487	202.6	III	6	6.77	162.70	3.63
488	204.9	III	6	5.92	101.52	4.66
489	207.4	III	6	6.38	89.42	3.86
490	210.2	III	6	5.51	148.46	3.91
491	212.5	III	6	5.90	126.78	3.48
492	215.0	III	6	6.31	113.00	4.07
493	217.3	III	6	7.08	127.12	3.06
494	219.8	III	6	6.33	195.89	2.70
495	222.5	III	6	5.85	199.40	3.43
496	225.0	III	6	5.68	194.54	2.13
497	227.5	III	6	6.37	154.55	3.45
498	229.4	III	6	5.39	237.57	2.85
499	232.2	III	6	5.46	173.72	3.48
500	234.5	III	6	6.21	176.57	3.33
501	237.0	III	6	6.59	208.65	2.87
502	238.9	III	6	5.19	498.07	2.38
503	241.6	III	6	5.80	184.14	3.00
504	243.7	III	6	7.27	255.85	2.61
505	246.5	III	5	8.19	506.23	1.72
506	248.4	III	5	7.75	1303.87	2.69
507	250.7	III	5	6.06	1131.27	1.43
508	253.0	III	5	7.59	429.31	1.47
509	255.1	III	5	6.32	803.40	1.10
510	257.9	III	5	6.65	526.92	1.58
511	260.0	III	5	6.49	148.07	3.80
512	262.3	III	5	8.04	277.49	2.20
513	264.8	III	5	7.50	228.80	2.21
514	267.5	II	4	8.01	54.93	2.50
515	270.0	II	4	7.87	25.35	2.76
516	272.5	II	4	7.38	48.24	3.09
517	275.2	II	4	7.62	28.48	1.61
518	278.0	II	4	6.17	32.09	2.53
519	280.5	II	4	6.41	22.23	1.05
520	282.8	II	4	6.14	22.39	4.00
521	285.1	II	4	5.90	20.93	2.43
522	287.6	II	4	6.53	18.53	2.07
523	290.3	II	4	6.65	22.71	4.64

Sample ID	Depth (cm)	Lithosome	Unit	Weight (g)	MS ($10^{-8} \text{ m}^3 \text{ kg}^{-1}$)	FD (%)
524	292.4	II	4	6.02	23.01	2.53
525	294.3	II	4	10.04	12.90	2.70
530	296.9	II	4	7.20	24.65	4.51
531	299.1	II	4	7.32	23.98	4.27
532	301.7	II	4	7.90	36.08	4.91
533	303.9	II	3	8.41	69.20	3.61
534	305.7	II	3	8.34	85.01	3.31
535	307.9	II	3	6.28	123.96	3.85
536	310.1	II	3	6.32	40.59	4.09
537	312.7	II	3	6.72	35.79	3.53
538	314.5	II	3	6.87	46.29	2.99
539	316.7	II	3	7.58	47.03	3.65
540	319.3	II	2	7.24	63.74	4.55
541	321.5	II	2	7.16	66.20	4.85
542	323.7	II	2	7.39	87.35	3.10
543	325.9	II	2	7.34	83.11	3.03
544	328.1	II	2	6.92	88.58	4.16
545	330.3	II	2	7.36	68.07	3.79
546	332.1	II	2	6.54	99.54	3.15
547	334.3	II	2	6.42	41.51	3.19
548	336.5	II	2	6.43	37.17	5.23
549	339.1	II	2	6.20	38.63	5.01
550	341.3	II	2	6.67	34.63	4.33
551	343.5	II	2	6.78	36.80	5.21
552	346.1	II	2	7.63	36.17	3.80
553	347.9	II	2	5.20	97.98	2.55
554	350.5	I	1	5.13	19.01	3.08
555	352.7	I	1	4.99	18.64	2.15
556	354.9	I	1	4.60	18.80	3.47
557	356.7	I	1	4.55	16.59	0.66
558	359.3	I	1	4.33	16.63	0.00
559	361.5	I	1	4.67	14.56	0.00
560	363.3	I	1	4.67	15.85	1.35
561	365.5	I	1	4.15	18.07	0.00
562	367.7	I	1	4.27	14.40	0.00
563	369.9	I	1	4.15	16.51	0.00
564	371.7	I	1	4.38	14.95	3.05
565	374.3	I	1	4.69	14.39	0.00
566	376.9	I	1	4.80	16.98	1.84

Sample ID	Depth (cm)	Lithosome	Unit	Weight (g)	MS ($10^{-8} \text{ m}^3 \text{ kg}^{-1}$)	FD (%)
567	378.7	I	1	9.01	11.32	0.00
572	382.2	I	1	4.65	19.03	3.95
573	384.8	I	1	4.84	16.74	3.70
574	387.1	I	1	4.23	19.86	1.19
575	389.4	I	1	4.45	21.69	1.04
576	390.9	I	1	3.28	26.52	3.45
577	392.7	I	1	4.25	29.29	2.41
578	394.7	I	1	4.48	21.65	2.58
579	396.2	I	1	4.30	25.93	2.69
580	398.0	I	1	4.63	26.57	0.41
581	399.8	I	1	5.98	45.23	4.99
582	402.0	I	1	4.37	43.02	4.52
583	403.8	I	1	5.17	35.40	3.83
584	406.1	I	1	5.57	29.71	0.91
585	407.8	I	1	5.76	36.11	3.37
586	410.0	I	1	5.80	36.55	2.83
587	411.8	I	1	4.93	26.88	1.89
588	413.8	I	1	3.21	19.31	2.42
589	415.6	I	1	2.46	18.29	1.11
590	417.6	I	1	3.56	20.22	2.08
591	419.4	I	1	3.33	19.52	0.77
592	421.4	I	1	4.80	21.35	0.49

APPENDIX C

COMPOSITE DEPTHS USED IN LITHOSTRATIGRAPHIC SECTION AND STABLE ISOTOPE GEOCHEMISTRY

- 1) Table C1. Composite depths for core 1 samples.
- 2) Table C2. Composite depths for core 2 samples.
- 3) Table C3. Composite depths for core 3 samples. Composite depths were not calculated for samples that contained more than one unit.
- 4) Table C4. Composite depths for core 4 samples.
- 5) Table C5. Composite depths for core 5 samples.
- 6) Figure C1. Composite vertical magnetic susceptibility profile.

Table C1. Composite depths for core 1 samples.

Sample ID	Depth (cm)	Lithosome	Unit	Composite depth (cm)
601	12.0	VIII	17	12.0
602	14.0	VIII	17	14.0
603	16.0	VIII	17	16.0
604	18.0	VIII	17	18.0
605	19.6	VIII	17	19.6
606	21.2	VIII	17	21.2
607	23.1	VIII	17	23.1
608	25.1	VIII	17	25.1
609	27.0	VIII	17	27.0
610	28.7	VIII	17	28.7
611	31.4	VIII	17	31.4
612	33.8	VIII	17	33.8
613	35.8	VIII	17	35.8
614	37.5	VIII	17	37.5
615	39.2	VIII	17	39.2
616	41.6	VIII	17	41.6
617	43.5	VIII	17	43.5
618	45.1	VIII	16	45.1
619	47.3	VIII	16	47.3
620	49.5	VIII	16	49.5
621	51.7	VIII	15	55.8
622	53.4	VIII	15	57.5
623	55.1	VIII	15	59.2
624	57.3	VIII	15	61.4
625	59.5	VIII	15	63.6
626	61.5	VIII	15	65.6
627	63.2	VIII	15	67.3
628	65.1	VIII	15	69.2
629	67.1	VIII	15	71.2
630	69.3	VIII	15	73.4
631	71.3	VIII	15	75.4
632	72.9	VIII	15	77.0
633	74.9	VIII	15	79.0
634	76.9	VIII	15	81.0
635	78.5	VIII	15	82.6
636	80.7	VIII	15	84.8
637	82.7	VIII	15	86.8
638	84.6	VIII	15	88.7

Sample ID	Depth (cm)	Lithosome	Unit	Composite depth (cm)
639	86.8	VIII	15	90.9
640	88.5	VIII	15	92.6
641	90.9	VIII	15	95.0
642	92.8	VIII	15	96.9
643	94.7	VIII	15	98.8
644	96.4	VIII	15	100.5
645	98.8	VIII	15	102.9
646	100.7	VIII	15	104.8
647	102.7	VIII	15	106.8
648	104.3	VIII	15	108.4
652	106.1	VIII	15	110.0
653	108.9	VIII	15	112.5
654	111.4	VII	14	133.5
655	113.9	VII	14	136.0
656	116.2	VII	14	138.3
657	118.5	VII	14	140.6
658	120.4	VII	14	142.5
659	122.7	VII	14	144.8
660	124.8	VII	14	146.9
661	127.1	VII	13	149.2
662	129.0	VII	13	151.1
663	131.3	VII	13	153.4
664	133.2	VII	13	155.3
665	135.7	VII	13	157.8
666	137.8	VII	13	159.9
667	140.1	VII	13	162.2
668	141.9	VII	13	164.0
669	144.0	VII	13	166.1
670	146.1	VII	13	168.2
671	148.4	VII	13	170.5
672	150.2	VII	13	172.3
673	152.7	VI	12	179.0
674	155.0	VI	12	181.3
675	157.1	VI	12	183.4
676	159.0	VI	11	185.3
677	161.5	VI	11	187.8
678	163.6	VI	11	189.9
679	165.7	VI	11	192.0
680	167.8	VI	11	194.1

Sample ID	Depth (cm)	Lithosome	Unit	Composite depth (cm)
681	170.3	VI	11	196.6
682	172.4	VI	11	198.7
683	174.9	VI	11	201.2
684	176.7	VI	11	203.0
685	178.5	VI	11	204.8
699	181.2	VI	11	207.5
700	183.7	VI	11	210.0
701	186.3	VI	11	212.6
702	188.9	VI	11	215.2
703	191.5	VI	11	217.8
704	194.1	VI	11	220.4
705	196.7	VI	11	223.0
706	199.3	VI	11	225.6
707	201.9	VI	11	228.2
708	204.5	VI	11	230.8
709	206.8	VI	11	233.1
710	209.5	VI	11	235.8
711	212.2	VI	11	238.5
712	214.9	VI	11	241.2
713	217.2	V	10	259.1
714	220.2	V	10	262.1
715	222.7	V	9	264.6
716	225.4	V	9	268.1
717	228.0	V	9	271.5
718	230.6	V	9	274.9
719	233.2	V	9	277.5
720	235.8	V	9	280.1
721	238.5	V	9	282.8
722	241.0	V	9	285.3
723	243.6	V	9	287.9
724	246.2	V	9	290.5
725	249.4	V	9	293.7
726	252.0	V	9	296.3

Table C2. Composite depths for core 2 samples.

Sample ID	Depth (cm)	Lithosome	Unit	Composite depth (cm)
1	2.5	VII	14	133.5
2	5.2	VII	14	136.0
3	7.9	VII	14	138.3
4	11.5	VII	14	140.6
5	14.2	VII	14	142.5
6	17.1	VII	14	144.8
7	21.6	VII	14	146.9
8	23.6	VII	13	149.2
9	26.5	VII	13	151.9
10	29.2	VII	13	154.4
11	32.3	VII	13	157.3
12	35.2	VII	13	160.0
13	38.1	VII	13	162.1
14	40.8	VII	13	164.0
15	43.7	VII	13	166.1
16	46.6	VII	13	168.2
17	49.3	VII	13	170.9
18	52.2	VII	13	173.8
19	54.9	VII	13	176.5
20	58.0	VI	12	181.3
21	61.0	VI	12	184.3
22	63.8	VI	11	187.1
23	66.5	VI	11	189.8
24	69.2	VI	11	192.5
25	72.1	VI	11	195.4
26	75.0	VI	11	198.3
27	77.9	VI	11	201.2
28	80.6	VI	11	202.9
29	83.3	VI	11	204.6
30	86.2	VI	11	206.4
31	89.1	VI	11	208.2
32	92.0	VI	11	210.0
33	94.9	VI	11	211.6
34	97.8	VI	11	214.5
35	100.5	VI	11	214.7
36	103.6	VI	11	216.4
37	106.5	VI	11	218.0
38	109.4	VI	11	220.2

Sample ID	Depth (cm)	Lithosome	Unit	Composite depth (cm)
39	112.1	VI	11	222.2
40	115.0	VI	11	224.4
41	117.9	VI	11	226.6
42	120.6	VI	11	228.6
43	123.5	VI	11	230.8
44	126.4	VI	11	233.0
45	127.5	VI	11	233.8
50	130.4	VI	11	235.9
51	133.3	VI	11	238.0
52	136.0	VI	11	239.9
53	137.9	VI	11	241.3
54	141.4	VI	11	244.8
55	144.1	VI	11	247.5
56	146.2	VI	11	249.6
57	148.3	VI	11	251.7
58	151.4	V	10	254.8
59	154.3	V	10	257.7
60	156.4	V	10	259.8
61	158.7	V	9	262.1
62	161.2	V	9	264.6
63	164.3	V	9	267.7
64	166.6	V	9	270.0
65	169.1	V	9	272.5
66	171.4	V	9	274.8
67	174.5	V	9	277.9
68	177.0	V	9	280.4
69	179.5	V	9	282.9
70	182.4	V	9	285.8
71	184.9	V	9	288.3
72	187.6	V	9	291.0
73	189.9	V	9	293.3
74	192.4	V	9	295.8
75	194.9	IV	8	308.2
76	198.0	IV	8	311.3
77	200.3	IV	8	312.8
78	203.2	IV	8	314.7
79	205.5	IV	8	316.2
80	207.4	IV	8	318.6
81	210.7	IV	8	322.7

Sample ID	Depth (cm)	Lithosome	Unit	Composite depth (cm)
82	213.6	IV	8	326.3
83	216.1	IV	8	328.6
84	218.6	IV	7	330.9
85	221.1	IV	7	333.2
86	222.3	IV	7	336.3
87	226.2	IV	7	341.3
88	228.3	IV	7	343.0
89	231.4	IV	7	345.5
90	233.5	IV	7	347.2

Table C3. Composite depths for core 3 samples. Composite depths were not calculated for samples that contained more than one unit.

Sample ID	Depth (cm)	Lithosome	Unit	Composite depth (cm)
801	3.8	VIII	17	28.7
802	5.9	VIII	17	30.4
803	8.5	VIII	17	32.5
804	10.2	VIII	17	33.9
805	12.3	VIII	17	36.3
806	14.8	VIII	16	39.2
807	17.0	VIII	16	41.4
808	19.1	VIII	16	43.5
809	21.2	VIII	16	45.6
810	23.3	VIII	16	47.7
811	25.4	VIII	15	51.6
812	27.5	VIII	15	53.7
813	29.6	VIII	15	55.8
814	31.7	VIII	15	57.9
815	33.8	VIII	15	60.0
816	35.8	VIII	15	62.0
817	38.0	VIII	15	64.2
818	40.0	VIII	15	66.2
819	42.2	VIII	15	68.4
820	44.3	VIII	15	70.5
821	46.4	VIII	15	72.6
822	48.5	VIII	15	74.7
823	50.6	VIII	15	76.8
824	52.7	VIII	15	78.9
825	54.8	VIII	15	81.0
826	56.9	VIII	15	83.1
827	59.0	VIII	15	85.2
828	61.1	VIII	15	87.3
829	63.2	VIII	15	89.4
830	65.4	VIII	15	91.6
831	67.4	VIII	15	93.6
832	69.5	VIII	15	95.7
833	71.6	VIII	15	97.8
834	73.7	VIII	15	99.9
835	75.8	VIII	15	102.0
836	77.9	VIII	15	104.1
837	80.0	VIII	15	106.2

Sample ID	Depth (cm)	Lithosome	Unit	Composite depth (cm)
838	82.1	VIII	15	108.3
839	84.2	VIII	15	110.4
840	85.9	VIII	15	112.1
855	88.2	VIII	15	114.4
856	90.5	VIII	15	116.7
857	92.8	VIII	15	119.0
858	95.1	VII	14	144.8
859	97.4	VII	14	147.1
860	99.7	VII	13	149.4
861	102.0	VII	13	151.7
862	104.3	VII	13	154.0
863	106.6	VII	13	156.3
864	108.9	VII	13	158.6
865	111.2	VII	13	160.9
866	113.5	VII	13	163.2
867	115.8	VII	13	165.5
868	118.1	VII	13	167.8
869	120.4	VII	13	170.1
870	122.7	VI	12/11	not calculated
871	125.0	V	10/9	not calculated
872	127.3	V/IV	9/8	not calculated
873	129.6	IV	8	314.0
874	131.9	IV	8	316.3
875	134.2	IV	8	318.6
876	136.9	IV	8	321.3
877	139.6	IV	7	324.0
879	146.1	IV	7	330.5
880	148.7	IV	7	333.1
881	151.5	IV	7	335.9
882	154.2	IV	7	338.6
883	156.5	IV	7	340.9
884	159.2	IV	7	343.6
885	161.5	III	6	404.4
886	164.1	III	6	406.7
887	167.4	III	6	409.6
888	169.8	III	5	411.7
889	172.2	III	5	413.8
890	174.6	III	5	417.0
891	177.0	III	5	420.2

Sample ID	Depth (cm)	Lithosome	Unit	Composite depth (cm)
892	179.4	III	5	423.4
893	181.8	III	5	424.3
894	184.2	III	5	425.2
895	186.6	III	5	426.1
896	189.0	III	5	427.4
897	191.4	III	5	428.7
898	193.8	III	5	430.0
899	196.4	III	5	435.0
900	198.9	III	5	437.3
901	201.5	III	5	439.9
902	204.4	III	5	442.8

Table C4. Composite depths for core 4 samples.

Sample ID	Depth (cm)	Lithosome	Unit	Composite depth (cm)
201	1.0	III	6	404.6
202	4.1	III	6	407.7
203	7.2	III	6	410.8
204	10.3	III	6	413.9
205	12.4	III	6	415.1
206	15.0	III	6	416.6
207	18.1	III	5	419.1
208	20.7	III	5	421.2
209	23.3	III	5	423.3
210	26.4	III	5	424.9
211	28.5	III	5	426.0
212	31.1	III	5	427.4
213	33.7	III	5	428.8
214	36.3	III	5	430.2
215	39.4	III	5	435.0
216	41.5	III	5	436.0
217	44.1	III	5	437.3
218	46.7	III	5	439.9
219	49.8	III	5	443.0
220	51.9	III	5	445.1
221	54.5	III	5	447.7
222	57.1	III	5	450.3
223	59.4	III	5	452.6
224	62.3	III	5	455.5
225	64.9	III	5	458.1
226	67.0	II	4	463.4
227	69.6	II	4	465.8
228	72.7	II	4	468.7
229	74.8	II	4	470.7
230	77.4	II	4	473.1
231	80.0	II	4	475.5
232	83.1	II	4	478.4
233	85.2	II	4	480.4
234	87.8	II	4	482.8
235	90.4	II	4	485.2
236	93.5	II	4	488.1
237	96.1	II	4	490.5
238	98.7	II	4	492.9

Sample ID	Depth (cm)	Lithosome	Unit	Composite depth (cm)
239	102.8	II	4	496.7
240	103.8	II	3	497.6
245	107.4	II	3	501.0
246	109.2	II	3	502.4
247	111.9	II	3	504.5
248	114.6	II	3	506.6
249	116.4	II	3	508.0
250	119.1	II	3	510.1
251	121.8	II	3	512.2
252	123.6	II	2	513.6
253	126.3	II	2	515.7
254	128.1	II	2	517.1
255	130.8	II	2	520.3
256	132.6	II	2	522.4
257	135.3	II	2	525.6
258	137.1	II	2	527.7
259	139.8	II	2	530.4
260	141.6	II	2	532.2

Table C5. Composite depths for core 5 samples.

Sample ID	Depth (cm)	Lithosome	Unit	Composite depth (cm)
401	2.1	VII	14	122.0
402	4.4	VII	14	124.3
403	7.3	VII	14	127.2
404	10.5	VII	14	130.4
405	12.8	VII	14	132.7
406	15.7	VII	14	135.6
407	18.4	VII	14	138.3
408	20.9	VII	14	140.3
409	23.6	VII	14	142.4
410	27.0	VII	14	145.1
411	29.3	VII	14	146.9
412	31.4	VII	14	148.6
413	34.6	VII	13	151.3
414	37.2	VII	13	153.5
415	39.8	VII	13	155.7
416	41.9	VII	13	157.4
417	44.5	VII	13	159.6
418	47.7	VII	13	162.3
419	50.9	VII	13	164.3
420	52.5	VII	13	165.3
421	55.1	VII	13	166.9
422	57.7	VII	13	168.5
423	60.3	VII	13	170.1
424	62.9	VII	13	171.7
425	65.0	VII	13	173.0
426	67.6	VII	13	174.6
427	70.2	VII	13	176.2
428	73.4	VI	12	223.0
429	75.5	VI	12	224.6
430	78.1	VI	12	226.5
431	80.7	VI	11	228.4
432	83.9	VI	11	230.8
433	86.4	VI	11	232.4
434	89.1	VI	11	234.2
435	91.6	VI	11	235.8
436	94.3	V	10	254.8
437	96.6	V	10	257.0
438	99.3	V	10	259.5

Sample ID	Depth (cm)	Lithosome	Unit	Composite depth (cm)
439	102.0	V	10	262.0
440	104.7	V	10	264.5
445	107.2	V	9	268.5
446	109.7	V	9	272.5
447	112.7	V	9	277.3
448	114.7	V	9	280.5
449	117.2	V	9	284.4
450	119.7	V	9	288.3
451	122.7	V	9	291.3
452	124.7	V	9	293.3
453	127.7	V	9	296.3
454	129.7	IV	8	298.3
455	132.7	IV	8	301.3
456	134.7	IV	8	303.3
457	137.7	IV	8	306.3
458	140.2	IV	8	308.8
459	142.7	IV	8	311.3
460	144.7	IV	8	313.3
461	147.7	IV	8	316.3
462	150.2	IV	8	318.8
463	152.7	IV	8	321.3
464	154.7	IV	8	323.3
465	157.7	IV	7	326.3
466	160.2	IV	7	328.8
467	162.7	IV	7	331.3
468	164.7	IV	7	333.3
469	167.7	IV	7	336.3
470	170.2	IV	7	338.8
471	172.7	IV	7	341.3
472	174.7	IV	7	343.3
473	177.7	IV	7	346.3
474	179.7	IV	7	348.3
475	182.7	IV	7	351.3
476	184.7	IV	7	353.3
477	187.7	IV	7	356.3
478	189.7	IV	7	358.3
479	192.7	IV	7	361.3
480	194.7	IV	7	363.3
481	198.2	III	6	366.8

Sample ID	Depth (cm)	Lithosome	Unit	Composite depth (cm)
482	200.7	III	6	369.3
487	202.6	III	6	371.2
488	204.9	III	6	373.5
489	207.4	III	6	376.0
490	210.2	III	6	378.8
491	212.5	III	6	381.1
492	215.0	III	6	383.6
493	217.3	III	6	385.9
494	219.8	III	6	388.4
495	222.5	III	6	397.5
496	225.0	III	6	400.0
497	227.5	III	6	402.5
498	229.4	III	6	404.4
499	232.2	III	6	407.2
500	234.5	III	6	409.5
501	237.0	III	6	412.0
502	238.9	III	6	413.9
503	241.6	III	6	416.6
504	243.7	III	6	418.7
505	246.5	III	5	421.5
506	248.4	III	5	423.4
507	250.7	III	5	425.7
508	253.0	III	5	428.0
509	255.1	III	5	430.1
510	257.9	III	5	432.9
511	260.0	III	5	435.0
512	262.3	III	5	437.3
513	264.8	III	5	439.8
514	267.5	II	4	460.9
515	270.0	II	4	463.4
516	272.5	II	4	465.9
517	275.2	II	4	468.6
518	278.0	II	4	471.4
519	280.5	II	4	473.9
520	282.8	II	4	476.2
521	285.1	II	4	478.5
522	287.6	II	4	481.0
523	290.3	II	4	483.7
524	292.4	II	4	485.8

Sample ID	Depth (cm)	Lithosome	Unit	Composite depth (cm)
525	294.3	II	4	487.7
530	296.9	II	4	490.3
531	299.1	II	4	492.5
532	301.7	II	4	495.1
533	303.9	II	3	497.3
534	305.7	II	3	499.1
535	307.9	II	3	501.3
536	310.1	II	3	503.5
537	312.7	II	3	506.1
538	314.5	II	3	507.9
539	316.7	II	3	510.1
540	319.3	II	2	512.7
541	321.5	II	2	514.9
542	323.7	II	2	517.1
543	325.9	II	2	519.3
544	328.1	II	2	521.5
545	330.3	II	2	523.7
546	332.1	II	2	525.5
547	334.3	II	2	527.7
548	336.5	II	2	529.9
549	339.1	II	2	532.5
550	341.3	II	2	534.7
551	343.5	II	2	536.9
552	346.1	II	2	539.5
553	347.9	II	2	541.3
554	350.5	I	1	543.9
555	352.7	I	1	546.1
556	354.9	I	1	548.3
557	356.7	I	1	550.1
558	359.3	I	1	552.7
559	361.5	I	1	554.9
560	363.3	I	1	556.7
561	365.5	I	1	558.9
562	367.7	I	1	561.1
563	369.9	I	1	563.3
564	371.7	I	1	565.1
565	374.3	I	1	567.7
566	376.9	I	1	570.3
567	378.7	I	1	572.1

Sample ID	Depth (cm)	Lithosome	Unit	Composite depth (cm)
572	382.2	I	1	575.6
573	384.8	I	1	578.2
574	387.1	I	1	580.5
575	389.4	I	1	582.8
576	390.9	I	1	584.3
577	392.7	I	1	586.1
578	394.7	I	1	588.1
579	396.2	I	1	589.6
580	398.0	I	1	591.4
581	399.8	I	1	593.2
582	402.0	I	1	595.4
583	403.8	I	1	597.2
584	406.1	I	1	599.5
585	407.8	I	1	601.2
586	410.0	I	1	603.4
587	411.8	I	1	605.2
588	413.8	I	1	607.2
589	415.6	I	1	609.0
590	417.6	I	1	611.0
591	419.4	I	1	612.8
592	421.4	I	1	614.8

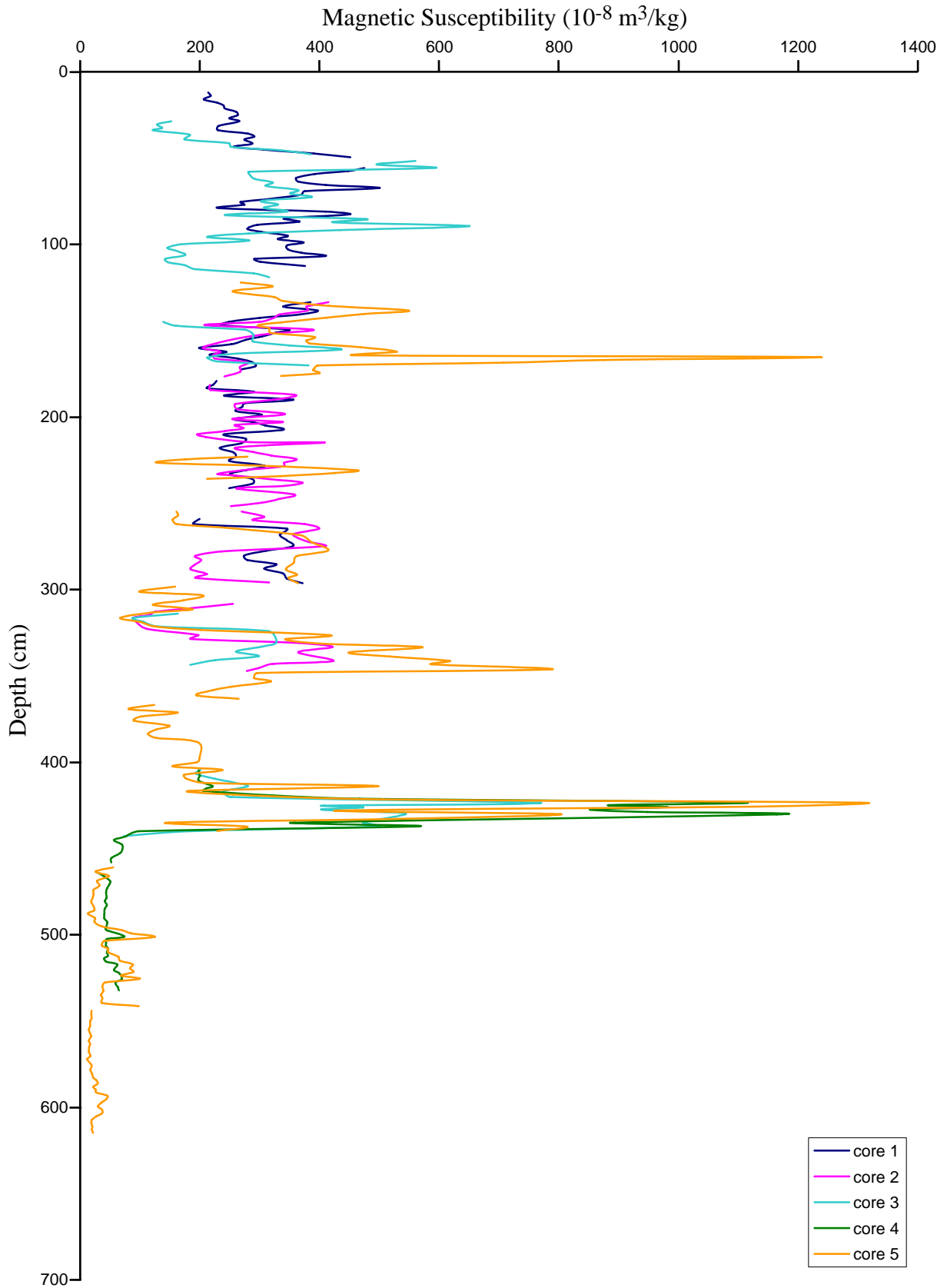


Fig. C1. Composite vertical magnetic susceptibility profile.

APPENDIX D

OSTRACODE SPECIES AND TAPHONOMIC FEATURE COUNTS

- 1) Table D1. *Candona patzcuaro* (CANP), *Fabaeformiscandona caudata* (FABC), *Limnocythere ceriotuberosa* (LIMC) and *Limnocythere platyforma* (LIMP) ostracode counts for core 1 samples from Lithosome VIII.
- 2) Table D2. Taphonomic feature counts for core 1 samples from Lithosome VIII.
- 3) Table D3. *Candona patzcuaro* (CANP), *Fabaeformiscandona caudata* (FABC), *Limnocythere ceriotuberosa* (LIMC) and *Limnocythere platyforma* (LIMP) ostracode counts for core 5 samples from Lithosome III–VII.
- 4) Table D4. Taphonomic feature counts for core 5 samples from Lithosome III–VII.

Table D1. *Candona patzcuaro* (CANP), *Fabaeformiscandona caudata* (FABC), *Limnocythere certiotuberosa* (LIMC) and *Limnocythere platyforma* (LIMP) ostracode counts for core 1 samples from Lithosome VIII.

Sample ID	Depth (cm)	Lithosome	Unit	CANP		FABC		LIMC		LIMP	
				Juvenile	Adult	Juvenile	Adult	Juvenile	Adult	Juvenile	Adult
601	12.0	VIII	17	0	0	0	0	0	0	0	0
602	14.0	VIII	17	0	0	0	0	0	0	0	0
603	16.0	VIII	17	0	0	0	0	0	0	0	0
604	18.0	VIII	17	0	0	0	0	0	0	0	0
605	19.6	VIII	17	0	0	0	0	0	0	0	0
606	21.2	VIII	17	0	0	0	0	0	0	0	0
607	23.1	VIII	17	0	0	0	0	0	0	0	0
608	25.1	VIII	17	0	0	0	0	0	0	0	0
609	27.0	VIII	17	0	0	0	0	0	0	0	0
610	28.7	VIII	17	0	0	0	0	0	0	0	0
611	31.4	VIII	17	0	0	0	0	0	0	0	0
612	33.8	VIII	17	0	0	0	0	0	0	0	0
613	35.8	VIII	17	0	0	0	0	0	0	0	0
614	37.5	VIII	17	0	0	0	0	0	0	0	0
615	39.2	VIII	17	0	0	0	0	0	0	0	0
616	41.6	VIII	17	0	0	0	0	0	0	0	0
617	43.5	VIII	17	0	0	0	0	0	0	0	0
618	45.1	VIII	16	0	0	0	0	0	0	0	0
619	47.3	VIII	16	0	0	0	0	0	0	0	0
620	49.5	VIII	16	0	0	0	0	0	0	0	0
621	51.7	VIII	15	0	0	0	0	0	0	0	0
622	53.4	VIII	15	0	0	0	0	0	0	0	0
623	55.1	VIII	15	0	0	0	0	0	0	0	0
624	57.3	VIII	15	1	0	0	0	2	0	0	0
625	59.5	VIII	15	0	0	0	0	5	4	0	0

Sample ID	Depth (cm)	Lithosome	Unit	CANP		FABC		LJMC		LIMP	
				Juvenile	Adult	Juvenile	Adult	Juvenile	Adult	Juvenile	Adult
626	61.5	VIII	15	0	0	0	0	3	0	0	0
627	63.2	VIII	15	1	0	0	0	9	2	0	0
628	65.1	VIII	15	1	0	0	0	1	0	0	0
629	67.1	VIII	15	0	0	0	0	0	0	0	0
630	69.3	VIII	15	0	0	0	0	1	0	0	1
631	71.3	VIII	15	4	0	0	0	0	0	0	0
632	72.9	VIII	15	0	0	0	0	0	0	0	0
633	74.9	VIII	15	1	0	0	0	1	0	0	0
634	76.9	VIII	15	0	0	0	0	0	0	0	0
635	78.5	VIII	15	0	0	0	0	0	0	0	0
636	80.7	VIII	15	0	0	0	0	0	0	0	0
637	82.7	VIII	15	0	0	0	0	1	0	0	0
638	84.6	VIII	15	0	0	0	0	0	1	0	0
639	86.8	VIII	15	0	0	0	0	2	1	0	0
640	88.5	VIII	15	0	0	0	0	0	0	0	0
641	90.9	VIII	15	0	0	0	0	0	0	0	0
642	92.8	VIII	15	0	0	0	0	0	0	0	0
643	94.7	VIII	15	0	0	0	0	0	0	0	0
644	96.4	VIII	15	0	0	0	0	0	0	0	0
645	98.8	VIII	15	0	0	0	0	0	0	0	0
646	100.7	VIII	15	0	0	0	0	0	0	0	0
647	102.7	VIII	15	0	0	0	0	0	0	0	0
648	104.3	VIII	15	0	0	0	0	0	0	0	0
652	106.1	VIII	15	0	0	0	0	0	0	0	0
653	108.9	VIII	15	0	0	0	0	0	0	0	0

Table D2. Taphonomic feature counts for core 1 samples from Lithosome VIII.

Sample ID	Depth (cm)	Lithosome	Unit	Fragmented	Oxidation staining	Coating	Bleaching	Recrystallization
601	12.0	VIII	17	0	0	0	0	0
602	14.0	VIII	17	0	0	0	0	0
603	16.0	VIII	17	0	0	0	0	0
604	18.0	VIII	17	0	0	0	0	0
605	19.6	VIII	17	0	0	0	0	0
606	21.2	VIII	17	0	0	0	0	0
607	23.1	VIII	17	0	0	0	0	0
608	25.1	VIII	17	0	0	0	0	0
609	27.0	VIII	17	0	0	0	0	0
610	28.7	VIII	17	0	0	0	0	0
611	31.4	VIII	17	0	0	0	0	0
612	33.8	VIII	17	0	0	0	0	0
613	35.8	VIII	17	0	0	0	0	0
614	37.5	VIII	17	0	0	0	0	0
615	39.2	VIII	17	0	0	0	0	0
616	41.6	VIII	17	0	0	0	0	0
617	43.5	VIII	17	0	0	0	0	0
618	45.1	VIII	16	0	0	0	0	0
619	47.3	VIII	16	0	0	0	0	0
620	49.5	VIII	16	0	0	0	0	0
621	51.7	VIII	15	0	0	0	0	0
622	53.4	VIII	15	0	0	0	0	0
623	55.1	VIII	15	0	0	0	0	0
624	57.3	VIII	15	3	3	0	3	0
625	59.5	VIII	15	3	10	0	9	1
626	61.5	VIII	15	0	5	0	3	2

Sample ID	Depth (cm)	Lithosome	Unit	Fragmented	Oxidation staining	Coating	Bleaching	Recrystallization
627	63.2	VIII	15	7	12	0	12	0
628	65.1	VIII	15	1	2	0	2	0
629	67.1	VIII	15	0	0	0	0	0
630	69.3	VIII	15	0	2	2	2	0
631	71.3	VIII	15	4	4	0	4	0
632	72.9	VIII	15	0	0	0	0	0
633	74.9	VIII	15	2	2	0	2	0
634	76.9	VIII	15	0	0	0	0	0
635	78.5	VIII	15	0	0	0	0	0
636	80.7	VIII	15	0	0	0	0	0
637	82.7	VIII	15	0	2	0	2	0
638	84.6	VIII	15	1	1	0	1	0
639	86.8	VIII	15	1	4	0	4	0
640	88.5	VIII	15	0	0	0	0	0
641	90.9	VIII	15	0	0	0	0	0
642	92.8	VIII	15	0	0	0	0	0
643	94.7	VIII	15	0	0	0	0	0
644	96.4	VIII	15	0	0	0	0	0
645	98.8	VIII	15	0	0	0	0	0
646	100.7	VIII	15	0	0	0	0	0
647	102.7	VIII	15	0	0	0	0	0
648	104.3	VIII	15	0	0	0	0	0
652	106.1	VIII	15	0	0	0	0	0
653	108.9	VIII	15	0	0	0	0	0

Table D3. *Candona patzcuaro* (CANP), *Fabaeformiscandona caudata* (FABC), *Limnocythere certiotuberosa* (LIMC) and *Limnocythere platyforma* (LIMP) ostracode counts for core 5 samples from Lithosome III–VII.

Sample ID	Depth (cm)	Lithosome	Unit	CANP		FABC		LIMC		LIMP	
				Juvenile	Adult	Juvenile	Adult	Juvenile	Adult	Juvenile	Adult
401	2.1	VII	14	2	0	0	0	8	0	0	0
402	4.4	VII	14	9	0	0	0	0	0	0	0
403	7.3	VII	14	1	0	0	0	0	0	0	0
404	10.5	VII	14	12	2	0	0	0	0	0	0
405	12.8	VII	14	0	0	0	0	0	0	0	0
406	15.7	VII	14	1	0	0	0	0	0	0	0
407	18.4	VII	14	3	0	0	0	0	0	0	0
408	20.9	VII	14	58	2	0	0	4	0	0	0
409	23.6	VII	14	42	1	0	0	2	0	0	0
410	27.0	VII	14	0	0	0	0	0	0	0	0
411	29.3	VII	14	11	0	0	0	2	0	0	0
412	31.4	VII	14	0	0	0	0	0	0	0	0
413	34.6	VII	13	0	0	0	0	0	0	0	0
414	37.2	VII	13	0	0	0	0	0	0	0	0
415	39.8	VII	13	0	0	0	0	0	0	0	0
416	41.9	VII	13	3	0	0	0	1	0	1	0
417	44.5	VII	13	4	1	0	0	13	1	3	0
418	47.7	VII	13	3	1	0	0	12	2	6	0
419	50.9	VII	13	7	3	0	0	58	18	28	3
420	52.5	VII	13	2	0	0	0	19	3	4	0
421	55.1	VII	13	5	0	0	0	27	0	3	0
422	57.7	VII	13	4	0	0	0	14	3	17	1
423	60.3	VII	13	7	0	0	0	32	2	44	1
424	62.9	VII	13	7	0	0	0	14	1	18	1
425	65.0	VII	13	1	0	0	0	13	2	18	0

Sample ID	Depth (cm)	Lithosome	Unit	CANP		FABC		LIMC		LIMP	
				Juvenile	Adult	Juvenile	Adult	Juvenile	Adult	Juvenile	Adult
426	67.6	VII	13	8	0	0	0	21	2	10	0
427	70.2	VII	13	15	2	0	0	44	19	20	0
428	73.4	VI	12	73	11	0	0	337	59	39	2
429	75.5	VI	12	10	3	1	1	149	36	24	1
430	78.1	VI	12	25	2	0	0	392	75	45	0
431	80.7	VI	11	46	1	0	0	259	16	29	1
432	83.9	VI	11	0	0	0	0	2	0	2	0
433	86.4	VI	11	3	0	0	0	2	0	0	0
434	89.1	VI	11	7	1	0	0	17	0	1	0
435	91.6	VI	11	10	1	0	0	71	5	8	0
436	94.3	V	10	12	1	0	0	21	3	2	0
437	96.6	V	10	10	0	0	0	45	3	1	0
438	99.3	V	10	2	0	0	0	3	1	0	0
439	102.0	V	10	9	0	0	0	10	2	0	0
440	104.7	V	10	2	0	0	0	3	1	1	0
445	107.2	V	9	8	2	0	0	47	5	15	0
446	109.7	V	9	8	2	0	0	60	5	9	0
447	112.7	V	9	19	2	0	0	85	12	15	0
448	114.7	V	9	26	4	0	0	45	7	13	0
449	117.2	V	9	28	2	0	0	79	18	16	1
450	119.7	V	9	39	3	0	0	51	15	9	1
451	122.7	V	9	48	2	0	0	94	11	26	0
452	124.7	V	9	37	3	0	0	90	12	30	0
453	127.7	V	9	19	0	0	0	82	12	9	0
454	129.7	IV	8	48	0	1	1	25	0	1	1
455	132.7	IV	8	12	0	0	0	12	2	1	0
456	134.7	IV	8	45	2	1	38	63	7	8	0

Sample ID	Depth (cm)	Lithosome	Unit	CANP		FABC		LIMC		LIMP	
				Juvenile	Adult	Juvenile	Adult	Juvenile	Adult	Juvenile	Adult
457	137.7	IV	8	103	7	78	5	91	24	9	0
458	140.2	IV	8	48	3	24	1	47	9	7	1
459	142.7	IV	8	11	0	3	0	115	20	6	0
460	144.7	IV	8	3	0	0	0	22	2	1	0
461	147.7	IV	8	4	0	0	0	29	5	0	0
462	150.2	IV	8	14	0	0	0	49	13	1	0
463	152.7	IV	8	6	0	0	0	13	3	0	0
464	154.7	IV	8	40	0	3	0	181	23	1	0
465	157.7	IV	7	34	2	4	0	224	28	0	0
466	160.2	IV	7	69	1	10	0	178	24	0	0
467	162.7	IV	7	108	3	18	1	209	39	0	0
468	164.7	IV	7	69	1	5	0	178	22	0	0
470	170.2	IV	7	31	0	4	0	75	10	0	0
472	174.7	IV	7	2	0	0	0	18	1	1	0
474	179.7	IV	7	68	4	0	0	76	11	0	0
476	184.7	IV	7	47	0	0	0	43	9	0	0
478	189.7	IV	7	35	0	0	0	84	1	1	0
480	194.7	IV	7	14	0	0	0	17	2	0	0
481	198.2	III	6	0	1	0	0	0	0	0	0
482	200.7	III	6	0	0	0	0	0	0	0	0
487	202.6	III	6	1	0	0	0	0	0	0	0
488	204.9	III	6	0	0	0	0	0	0	0	0
489	207.4	III	6	0	1	0	0	0	0	0	0
490	210.2	III	6	5	1	0	0	0	0	0	0
491	212.5	III	6	4	0	0	0	0	0	0	0
492	215.0	III	6	0	0	0	0	0	0	0	0
493	217.3	III	6	14	1	0	0	0	0	0	0

Sample ID	Depth (cm)	Lithosome	Unit	CANP		FABC		LIMC		LIMP	
				Juvenile	Adult	Juvenile	Adult	Juvenile	Adult	Juvenile	Adult
494	219.8	III	6	39	4	0	0	12	5	0	0
496	225.0	III	6	401	39	0	0	311	43	0	0
498	229.4	III	6	19	2	0	0	30	4	0	0
499	232.2	III	6	18	0	0	0	134	5	3	0
500	234.5	III	6	123	24	0	0	406	66	2	0
501	237.0	III	6	44	13	0	0	142	25	2	0
507	250.7	III	5	16	1	0	0	29	5	0	0
508	253.0	III	5	1	0	0	0	8	0	0	0
509	255.1	III	5	0	1	0	0	6	3	0	0
510	257.9	III	5	0	0	0	0	1	0	0	0
511	260.0	III	5	4	1	0	0	4	0	0	0
512	262.3	III	5	2	0	0	0	0	0	0	0
513	264.8	III	5	0	1	0	0	4	0	0	0

Table D4. Taphonomic feature counts for core 5 samples from Lithosome III–VII.

Sample ID	Depth (cm)	Lithosome	Unit	Fragmented	Oxidation		
					staining	Coating	Recrystallization
401	2.1	VII	14	3	10	0	0
402	4.4	VII	14	3	9	0	0
403	7.3	VII	14	0	1	0	0
404	10.5	VII	14	4	14	0	0
405	12.8	VII	14	0	0	0	0
406	15.7	VII	14	0	1	0	0
407	18.4	VII	14	1	3	0	0
408	20.9	VII	14	25	64	0	1
409	23.6	VII	14	19	45	0	0
410	27.0	VII	14	0	0	0	0
411	29.3	VII	14	4	13	0	0
412	31.4	VII	14	0	0	0	0
413	34.6	VII	13	0	0	0	0
414	37.2	VII	13	0	0	0	0
415	39.8	VII	13	0	0	0	0
416	41.9	VII	13	2	5	0	4
417	44.5	VII	13	2	22	0	7
418	47.7	VII	13	5	23	0	8
419	50.9	VII	13	27	106	1	20
420	52.5	VII	13	11	23	0	23
421	55.1	VII	13	6	25	0	28
422	57.7	VII	13	11	28	0	30
423	60.3	VII	13	27	86	0	19
424	62.9	VII	13	10	41	0	20
425	65.0	VII	13	9	34	0	11
426	67.6	VII	13	15	41	0	13

Sample ID	Depth (cm)	Lithosome	Unit	Fragmented	Oxidation			Recrystallization
					staining	Coating	Bleaching	
427	70.2	VII	13	21	16	102	0	32
428	73.4	VI	12	127	44	487	0	8
429	75.5	VI	12	44	11	219	0	1
430	78.1	VI	12	114	37	435	0	11
431	80.7	VI	11	70	56	246	0	34
432	83.9	VI	11	2	0	3	0	5
433	86.4	VI	11	0	3	3	0	5
434	89.1	VI	11	8	13	25	0	28
435	91.6	VI	11	37	20	94	0	1
436	94.3	V	10	21	6	40	0	0
437	96.6	V	10	19	5	59	0	0
438	99.3	V	10	2	0	7	0	0
439	102.0	V	10	2	1	22	0	0
440	104.7	V	10	1	0	7	0	1
445	107.2	V	9	24	18	77	0	7
446	109.7	V	9	24	13	78	0	12
447	112.7	V	9	24	23	130	0	12
448	114.7	V	9	16	18	95	0	11
449	117.2	V	9	21	12	144	0	14
450	119.7	V	9	5	19	118	0	7
451	122.7	V	9	28	45	181	0	17
452	124.7	V	9	26	27	172	0	13
453	127.7	V	9	20	12	117	0	12
454	129.7	IV	8	25	1	81	0	0
455	132.7	IV	8	10	3	33	0	0
456	134.7	IV	8	32	4	163	0	0
457	137.7	IV	8	49	12	317	0	0

Sample ID	Depth (cm)	Lithosome	Unit	Fragmented	Oxidation			Recrystallization
					staining	Coating	Bleaching	
458	140.2	IV	8	19	8	144	0	2
459	142.7	IV	8	30	7	151	0	0
460	144.7	IV	8	3	0	20	0	0
461	147.7	IV	8	14	0	32	0	0
462	150.2	IV	8	8	0	44	0	0
463	152.7	IV	8	1	0	13	0	0
464	154.7	IV	8	49	17	233	0	24
465	157.7	IV	7	59	8	285	0	17
466	160.2	IV	7	42	0	278	0	13
467	162.7	IV	7	44	44	356	0	60
468	164.7	IV	7	42	22	269	0	89
470	170.2	IV	7	24	18	118	0	64
472	174.7	IV	7	6	5	22	0	64
474	179.7	IV	7	41	7	159	0	39
476	184.7	IV	7	33	1	94	0	23
478	189.7	IV	7	36	0	121	0	20
480	194.7	IV	7	9	0	33	0	7
481	198.2	III	6	0	0	1	0	0
482	200.7	III	6	0	0	0	0	0
487	202.6	III	6	1	0	1	0	0
488	204.9	III	6	0	0	0	0	0
489	207.4	III	6	1	0	1	0	0
490	210.2	III	6	2	1	6	0	0
491	212.5	III	6	2	0	4	0	0
492	215.0	III	6	0	0	0	0	0
493	217.3	III	6	4	0	14	0	0
494	219.8	III	6	23	5	56	3	0

Sample ID	Depth (cm)	Lithosome	Unit	Fragmented	Oxidation staining	Coating	Bleaching	Recrystallization
496	225.0	III	6	63	12	794	0	1
498	229.4	III	6	5	0	55	0	0
499	232.2	III	6	22	0	1	0	0
500	234.5	III	6	53	0	79	3	0
501	237.0	III	6	19	3	38	0	0
507	250.7	III	5	7	2	21	2	0
508	253.0	III	5	0	5	5	0	0
509	255.1	III	5	2	0	4	0	0
510	257.9	III	5	0	0	0	0	0
511	260.0	III	5	2	0	2	0	0
512	262.3	III	5	0	2	2	0	0
513	264.8	III	5	1	0	5	0	0

APPENDIX E

EDX ELEMENTAL PROFILES FOR OSTRACODE COATINGS

- 1) Figure E1. EDX elemental composition profile for aluminosilicate ostracode coatings in chapter 3, figure 3.
- 2) Figure E2. EDX elemental composition profile for calcium carbonate ostracode coating in chapter 3, figure 4.

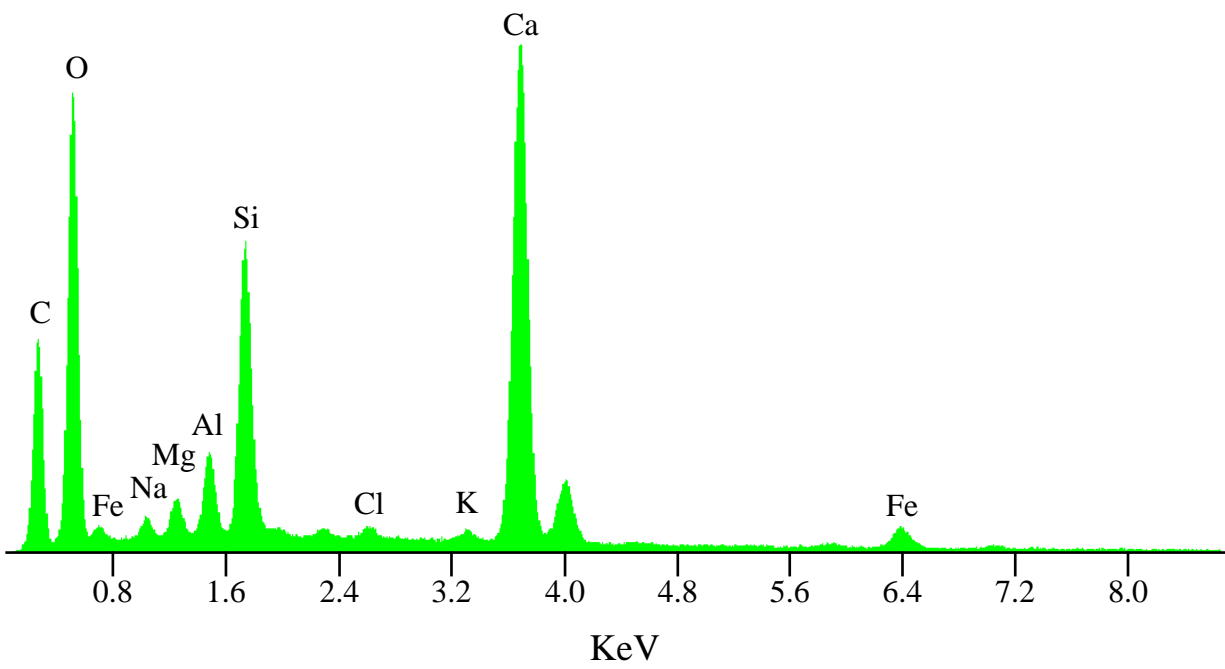


Fig. E1. EDX elemental composition profile for aluminosilicate ostracode coatings in chapter 3, figure 3.

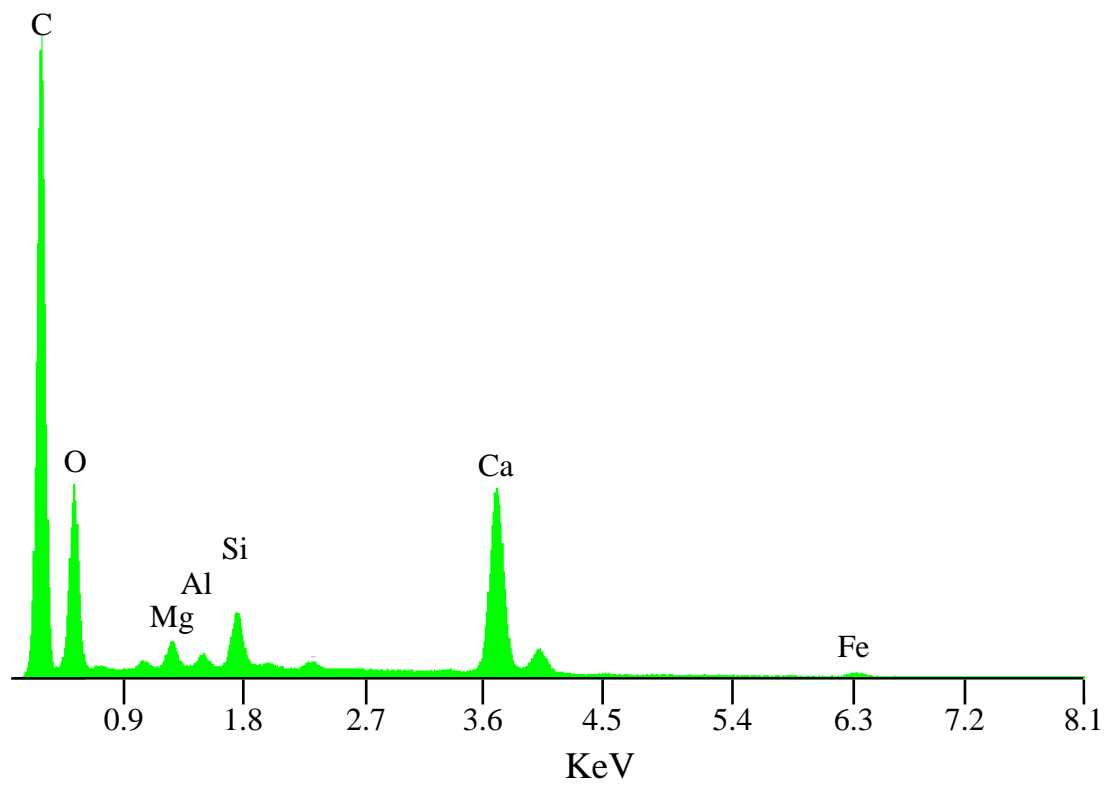


Fig. E2. EDX elemental composition profile for calcium carbonate ostracode coatings in chapter 3, figure 4.

APPENDIX F

OSTRACODE STABLE ISOTOPE DATA

- 1) Table F1. Stable carbon and oxygen isotopic compositions of *Candona patzcuaro* from the north core. All data is given relative to VPDB.
- 2) Table F2. Stable carbon and oxygen isotopic compositions of *Limnocythere ceriotuberosa* from the north core. All data is given relative to VPDB.
- 3) Table F3. Stable carbon and oxygen isotopic compositions of *Candona patzcuaro* from the south core. All data is given relative to VPDB.
- 4) Table F4. Stable carbon and oxygen isotopic compositions of *Limnocythere ceriotuberosa* from the south core. All data is given relative to VPDB.

Table F1. Stable carbon and oxygen isotopic compositions of *Candona patzcuaro* from the north core. All data is given relative to VPDB.

Sample ID	Depth (cm)	Composite depth (cm)	Lithosome	Unit	Run	$\delta^{13}\text{C}$ (‰)	$\delta^{18}\text{O}$ (‰)
656	116.2	138.3	VII	14	1	2.97	-1.39
657	118.5	140.6	VII	14	2	4.14	-0.45
660	124.8	146.9	VII	14	1	-1.47	-4.31
					2	-1.11	-4.15
666	137.8	159.9	VII	13	1	3.14	1.97
669	144.0	166.1	VII	13	1	2.50	2.24
					2	0.73	2.23
					3	2.65	-1.12
671	148.4	170.5	VII	13	1	3.25	1.90
					2	3.81	-1.05
676	159.0	185.3	VI	11	1	4.71	-1.19
677	161.5	187.8	VI	11	1	6.73	-0.26
681	170.3	196.6	VI	11	1	3.20	1.22
707	201.9	228.2	VI	11	1	1.60	-0.42
					2	4.55	2.13
709	206.8	233.1	VI	11	1	0.82	0.17
					2	2.66	0.79
					3	2.02	-2.04
					4	3.61	1.19
710	209.5	235.8	VI	11	1	0.51	-0.25
713	217.2	259.1	V	10	1	0.78	0.51
714	220.2	262.1	V	10	1	2.52	-0.47
85	280.7	333.2	IV	7	1	3.98	-5.26

Table F2. Stable carbon and oxygen isotopic compositions of *Limnocythere ceriotuberosa* from the north core. All data is given relative to VPDB.

Sample ID	Depth (cm)	Composite depth (cm)	Lithosome	Unit	Run	$\delta^{13}\text{C}$ (‰)	$\delta^{18}\text{O}$ (‰)
654	111.4	133.5	VII	14	1	-1.32	-4.79
					2	-0.27	-1.32
655	113.9	136.0	VII	14	1	-1.12	-3.92
					2	-0.82	-3.37
					3	-1.55	-3.56
656	116.2	138.3	VII	14	1	-0.63	-6.27
					2	-2.41	-5.99
					3	-1.85	-5.89
658	120.4	142.5	VII	14	1	-1.24	-5.01
					2	-1.35	-4.33
					3	-1.32	-4.96
666	137.8	159.9	VII	13	1	-1.55	-5.95
					2	-0.06	-1.98
					3	0.46	-1.12
667	140.1	162.2	VII	13	1	0.04	-2.55
					2	-0.80	-4.48
					3	-1.44	-5.36
					4	-0.36	-4.97
668	141.9	164.0	VII	13	1	0.92	-3.52
					2	0.33	-4.34
					3	-0.09	-3.37
669	144.0	166.1	VII	13	1	0.19	-4.74
					2	-0.23	-3.97
					3	0.18	-4.93
670	146.1	168.2	VII	13	1	0.95	-3.36
					2	1.08	-1.86
					3	-0.05	-4.49
671	148.4	170.5	VII	13	1	-0.09	-1.55
673	152.7	179.0	VI	12	1	0.10	-2.37
					2	0.49	-0.61
					3	-0.61	-2.87
675	157.1	183.4	VI	12	1	-1.70	-6.32
					2	-1.67	-6.27
					3	0.01	-1.92
676	159.0	185.3	VI	11	1	-1.73	-6.43
					2	-0.60	-4.28
					3	0.01	-2.49

Sample ID	Depth (cm)	Composite depth (cm)	Lithosome	Unit	Run	$\delta^{13}\text{C}$ (‰)	$\delta^{18}\text{O}$ (‰)
677	161.5	187.8	VI	11	1	0.78	-4.99
679	165.7	192.0	VI	11	1	-1.09	-3.28
					2	-0.48	-1.42
681	170.3	196.6	VI	11	1	2.04	-1.19
					2	1.22	-1.35
					3	-0.70	-2.41
683	174.9	201.2	VI	11	1	3.03	-4.55
684	176.7	203.0	VI	11	1	2.84	-2.62
699	181.2	207.5	VI	11	1	-0.29	-1.39
705	196.7	223.0	VI	11	1	1.04	-0.03
					2	1.19	-1.86
					3	-0.16	-4.66
706	199.3	225.6	VI	11	1	-0.26	0.15
					2	0.50	-1.36
707	201.9	228.2	VI	11	1	-0.95	-2.46
					2	-0.15	-0.89
					3	-0.31	-2.68
708	204.5	230.8	VI	11	2	0.07	-0.38
					3	-0.20	-1.16
					4	-0.02	-0.33
709	206.8	233.1	VI	11	1	-1.05	-3.13
					2	-1.47	-4.24
					3	0.74	-1.29
710	209.5	235.8	VI	11	1	0.09	-4.46
711	212.2	238.5	VI	11	1	1.81	-1.44
712	214.9	241.2	VI	11	1	-0.59	-1.25
714	220.2	262.1	V	10	1	-0.07	-0.92
67	174.5	277.9	V	9	1	-0.76	-3.54
					2	-0.70	-2.45
68	177.0	280.4	V	9	1	1.57	-2.81
					2	5.92	-2.45
					3	-0.65	-2.39
69	179.5	282.9	V	9	1	1.93	-1.29
					2	2.73	-0.61
					3	2.75	-2.07
70	182.4	285.8	V	9	1	1.66	-1.70
					2	2.36	-3.77
					3	1.41	-2.98
71	184.9	288.3	V	9	1	1.20	-2.47

Sample ID	Depth (cm)	Composite depth (cm)	Lithosome	Unit	Run	$\delta^{13}\text{C}$ (‰)	$\delta^{18}\text{O}$ (‰)
					2	1.63	-4.33
					3	4.92	-2.62
72	187.6	291.0	V	9	1	4.52	-2.66
					2	2.59	-1.67
					3	6.35	-3.02
73	189.9	293.3	V	9	1	4.07	-1.11
					2	4.42	-4.18
					3	5.57	-0.79
74	192.4	295.8	V	9	1	3.97	-1.48
					2	5.41	-2.25
					3	5.20	-2.55
75	254.5	308.2	IV	8	1	3.75	-0.60
					2	2.63	-4.46
					3	8.95	-1.99
76	257.6	311.3	IV	8	1	4.60	-4.59
81	270.3	322.7	IV	8	1	9.01	-2.12
82	273.2	326.3	IV	8	1	12.07	-2.81
					2	11.29	-3.02
					3	7.26	-2.48
83	275.7	328.6	IV	8	1	14.05	-0.93
					2	9.50	-1.92
					3	7.78	-3.76
84	278.2	330.9	IV	7	1	7.84	-2.88
85	280.7	333.2	IV	7	1	8.33	-4.56
					2	11.44	-3.09
86	281.9	336.3	IV	7	1	9.44	-2.90
					2	11.27	-1.40
					4	8.93	-3.05
87	285.8	341.3	IV	7	1	10.93	-2.27

Table F3. Stable carbon and oxygen isotopic compositions of *Candona patzcuaro* from the south core. All data is given relative to VPDB.

Sample ID	Depth (cm)	Composite depth (cm)	Lithosome	Unit	Run	$\delta^{13}\text{C}$ (‰)	$\delta^{18}\text{O}$ (‰)
404	10.5	130.4	VII	14	1	-1.55	-5.48
408	20.9	140.3	VII	14	1	1.03	-2.30
					2	0.60	-3.43
409	23.6	142.4	VII	14	1	-0.27	-4.42
					2	-1.36	-2.47
417	44.5	159.6	VII	13	1	1.09	-1.02
					2	3.09	0.32
418	47.7	162.3	VII	13	1	1.44	-3.11
					2	-0.09	2.70
					3	2.47	1.79
					4	4.17	0.40
419	50.9	164.3	VII	13	1	4.54	2.56
					2	4.36	2.75
					3	2.11	0.48
422	57.7	168.5	VII	13	1	3.35	1.58
424	62.9	171.7	VII	13	1	3.84	0.99
425	65.0	173.0	VII	13	1	7.98	0.42
427	70.2	176.2	VII	13	1	1.95	0.98
					2	3.20	2.18
					3	3.84	0.70
428	73.4	223.0	VI	12	1	1.90	-5.14
					2	5.49	2.24
					3	1.96	-2.97
					4	3.58	0.64
429	75.5	224.6	VI	12	1	0.82	0.64
					2	2.50	0.01
					3	1.22	-4.75
430	78.1	226.5	VI	12	1	1.99	0.70
					2	2.52	-3.90
					3	2.50	0.54
431	80.7	228.4	VI	11	1	1.32	0.73
					2	2.67	-0.55
					3	3.68	0.89
432	83.9	230.8	VI	11	1	4.52	2.65
434	89.1	234.2	VI	11	1	1.55	-1.95
435	91.6	235.8	VI	11	1	2.73	-1.31
436	94.3	254.8	V	10	1	2.97	-2.44

Sample ID	Depth (cm)	Composite depth (cm)	Lithosome	Unit	Run	$\delta^{13}\text{C}$ (‰)	$\delta^{18}\text{O}$ (‰)
					2	0.26	-7.40
437	96.6	257.0	V	10	1	1.88	-3.37
438	99.3	259.5	V	10	1	0.50	0.68
439	102.0	262.0	V	10	1	3.33	-0.28
					2	0.00	-1.40
445	107.2	268.5	V	9	1	2.66	-0.64
					2	2.87	1.96
					3	1.81	-2.21
446	109.7	272.5	V	9	1	0.34	1.55
					2	3.75	1.09
					3	3.56	2.15
447	112.7	277.3	V	9	1	1.08	0.83
					2	3.22	1.23
					3	6.40	0.34
448	114.7	280.5	V	9	1	1.40	0.91
					2	3.54	-0.41
					3	1.97	-1.52
449	117.2	284.4	V	9	1	2.69	-0.12
					2	1.80	2.13
					3	2.89	-1.02
450	119.7	288.3	V	9	1	3.68	-1.49
					3	5.53	1.10
451	122.7	291.3	V	9	1	0.93	-0.85
					2	3.04	-1.75
					3	3.03	-1.55
452	124.7	293.3	V	9	1	2.16	1.07
					2	4.60	-0.02
					3	2.44	-0.79
453	127.7	296.3	V	9	1	1.75	-0.69
					2	4.25	0.33
454	129.7	298.3	IV	8	1	1.49	-1.96
					2	2.35	0.07
					3	2.73	-1.92
455	132.7	301.3	IV	8	1	1.05	-2.24
					2	1.65	-2.28
					3	-0.23	-1.58
456	134.7	303.3	IV	8	1	2.34	-1.81
					2	1.90	-2.10
					3	0.09	-1.06

Sample ID	Depth (cm)	Composite depth (cm)	Lithosome	Unit	Run	$\delta^{13}\text{C}$ (‰)	$\delta^{18}\text{O}$ (‰)
457	137.7	306.3	IV	8	1	3.47	-1.15
					2	4.07	-0.66
					3	0.48	-2.53
458	140.2	308.8	IV	8	1	4.12	-0.04
					2	1.68	-2.33
					3	10.99	-3.22
459	142.7	311.3	IV	8	1	2.60	-0.10
464	154.7	323.3	IV	8	1	14.61	-1.59
465	157.7	326.3	IV	7	1	14.77	2.18
					2	8.42	0.83
					3	7.62	0.09
466	160.2	328.8	IV	7	1	13.90	0.91
					2	5.93	-3.68
					3	16.99	2.40
467	162.7	331.3	IV	7	1	5.60	0.22
					2	13.50	-1.22
					3	16.01	0.73
468	164.7	333.3	IV	7	1	13.37	0.23
					2	15.56	0.45
					3	15.15	0.92
469	167.7	336.3	IV	7	1	8.87	0.89
470	170.2	338.8	IV	7	1	5.97	1.57
472	174.7	343.3	IV	7	1	6.68	-1.29
473	177.7	346.3	IV	7	1	2.46	-4.42
					3	6.24	-1.02
474	179.7	348.3	IV	7	1	9.58	0.66
					2	9.34	-0.45
					3	5.96	-0.75
475	182.7	351.3	IV	7	1	2.10	-4.55
					2	11.86	2.31
476	184.7	353.3	IV	7	1	8.00	-4.66
477	187.7	356.3	IV	7	1	5.36	-0.59
					2	10.47	-0.90
					3	6.25	-1.73
478	189.7	358.3	IV	7	1	3.83	-2.79
479	192.7	361.3	IV	7	1	2.92	1.38
489	207.4	376.0	III	6	1	2.33	0.70
490	210.2	378.8	III	6	1	5.05	-3.41
					2	4.40	-3.40

Sample ID	Depth (cm)	Composite depth (cm)	Lithosome	Unit	Run	$\delta^{13}\text{C}$ (‰)	$\delta^{18}\text{O}$ (‰)
491	212.5	381.1	III	6	1	5.42	0.54
					2	5.55	0.13
493	217.3	385.9	III	6	1	3.60	-0.15
					2	4.24	0.85
					3	8.41	0.83
494	219.8	388.4	III	6	1	5.04	-1.62
					2	2.98	-1.92
					3	1.47	0.44
495	222.5	397.5	III	6	1	2.79	-2.19
					2	2.63	-0.43
					3	4.17	-0.81
496	225.0	400.0	III	6	1	-0.64	-1.35
					2	2.63	1.00
					3	0.52	0.70
497	227.5	402.5	III	6	1	5.99	-0.22
					2	7.82	0.76
					3	5.07	-2.96
498	229.4	404.4	III	6	1	2.12	1.06
					2	1.92	1.29
					3	5.74	3.22
500	234.5	409.5	III	6	1	5.12	0.11
					2	3.14	1.18
					3	4.47	1.91
501	237.0	412.0	III	6	1	4.23	-2.44
					2	2.07	-2.13
					3	2.14	-1.96
502	238.9	413.9	III	6	1	4.43	1.11
					2	6.00	1.12
503	241.6	416.6	III	6	1	4.95	-1.32
					2	4.09	1.53
504	243.7	418.7	III	6	1	5.32	0.55
					2	4.47	-0.50
					3	5.84	-2.50
505	246.5	421.5	III	5	1	1.99	-2.18
					2	6.38	0.82
					3	6.48	1.00
506	248.4	423.4	III	5	1	4.35	-0.37
					2	7.27	1.42
					3	6.95	-0.16

Sample ID	Depth (cm)	Composite depth (cm)	Lithosome	Unit	Run	$\delta^{13}\text{C}$ (‰)	$\delta^{18}\text{O}$ (‰)
511	260.0	435.0	III	5	1	4.07	3.02

Table F4. Stable carbon and oxygen isotopic compositions of *Limnocythere ceriotuberosa* from the south core. All data is given relative to VPDB.

Sample ID	Depth (cm)	Composite depth (cm)	Lithosome	Unit	Run	$\delta^{13}\text{C}$ (‰)	$\delta^{18}\text{O}$ (‰)
401	2.1	122.0	VII	14	1	0.47	-3.31
417	44.5	159.6	VII	13	1	-0.72	-4.16
418	47.7	162.3	VII	13	1	-0.97	-2.95
					2	0.35	-3.67
					3	-0.27	-0.91
419	50.9	164.3	VII	13	1	-0.65	-3.35
					2	-0.66	-3.60
					3	0.94	0.75
					4	-0.41	-2.03
420	52.5	165.3	VII	13	1	1.23	-2.24
					2	0.13	-1.08
					3	-0.49	-0.14
421	55.1	166.9	VII	13	1	0.17	0.89
					2	0.85	-0.14
					3	1.09	-1.69
422	57.7	168.5	VII	13	1	1.91	0.12
					2	-0.02	-5.00
					3	0.36	0.69
423	60.3	170.1	VII	13	1	-1.21	-2.70
					2	-0.33	-0.93
					3	0.76	-3.13
424	62.9	171.7	VII	13	1	0.02	-1.98
					2	1.37	-1.31
					3	1.77	-2.70
425	65.0	173.0	VII	13	1	-0.07	-4.86
					2	1.09	-0.97
					3	4.53	-1.69
					4	1.16	-3.91
426	67.6	174.6	VII	13	1	1.33	-2.03
					2	-0.55	-3.40
					3	0.92	-1.97
427	70.2	176.2	VII	13	1	-0.16	-2.23
					2	0.23	-1.83
					3	1.78	-2.12
428	73.4	223.0	VI	12	1	0.48	-1.22
					2	1.20	-0.09
					3	0.02	-2.44

Sample ID	Depth (cm)	Composite depth (cm)	Lithosome	Unit	Run	$\delta^{13}\text{C}$ (‰)	$\delta^{18}\text{O}$ (‰)
429	75.5	224.6	VI	12	1	0.99	-0.81
					2	0.39	0.54
					3	0.59	-2.30
					4	1.50	0.93
430	78.1	226.5	VI	12	1	0.91	-1.38
					2	0.63	1.39
					3	1.02	-0.52
431	80.7	228.4	VI	11	3	0.56	-0.19
					4	-1.83	-3.71
					5	-0.22	-1.69
432	83.9	230.8	VI	11	1	0.44	-2.10
433	86.4	232.4	VI	11	1	-0.23	-3.34
434	89.1	234.2	VI	11	1	-1.06	-2.42
					2	-0.27	-3.50
					3	1.37	-3.75
435	91.6	235.8	VI	11	1	-0.33	-1.24
					2	2.52	-0.55
					3	-1.67	-2.85
436	94.3	254.8	V	10	1	-2.06	-5.65
					2	1.61	-3.22
445	107.2	268.5	V	9	1	0.13	-2.62
					2	0.36	-2.68
446	109.7	272.5	V	9	1	-0.60	-4.48
					2	0.01	-3.00
					3	-0.95	-2.66
447	112.7	277.3	V	9	1	-0.71	-0.58
					2	0.10	-3.51
					3	0.11	-2.60
448	114.7	280.5	V	9	1	0.81	-2.93
					2	2.93	-2.16
					3	3.19	-1.63
449	117.2	284.4	V	9	1	5.55	-2.09
					2	2.76	-3.59
					4	0.56	-1.99
450	119.7	288.3	V	9	1	-1.80	-5.29
					2	3.58	-2.77
					3	-0.44	-4.18
451	122.7	291.3	V	9	1	8.80	-1.17
					2	4.24	-2.01

Sample ID	Depth (cm)	Composite depth (cm)	Lithosome	Unit	Run	$\delta^{13}\text{C}$ (‰)	$\delta^{18}\text{O}$ (‰)
452	124.7	293.3	V	9	3	6.57	-2.99
					1	7.27	-3.17
					2	2.24	-2.22
453	127.7	296.3	V	9	3	1.40	-3.58
					1	0.84	-0.13
					2	-0.56	-1.99
454	129.7	298.3	IV	8	3	1.29	-2.54
					2	-1.06	-2.53
					3	-0.31	-2.06
455	132.7	301.3	IV	8	1	1.04	-3.36
					2	-0.03	-2.26
456	134.7	303.3	IV	8	1	-0.75	-3.35
					2	-0.94	-3.95
					3	-0.37	-2.56
457	137.7	306.3	IV	8	1	-0.35	-3.45
					2	-0.44	-1.80
					3	-0.26	-2.20
458	140.2	308.8	IV	8	2	1.81	-3.04
					3	6.60	-3.54
					4	2.34	-2.54
					1	6.85	-3.66
459	142.7	311.3	IV	8	2	3.19	-1.57
					3	2.82	-1.87
					4	2.49	-3.73
					1	6.04	-2.20
460	144.7	313.3	IV	8	2	6.33	-3.56
					3	4.88	-2.04
					1	2.82	-3.26
461	147.7	316.3	IV	8	2	3.84	-3.73
					3	6.73	-2.66
					1	4.89	-4.30
462	150.2	318.8	IV	8	2	3.09	-2.67
					3	2.98	-2.53
					1	4.65	-3.52
463	152.7	321.3	IV	8	3	6.01	-2.88
					1	8.86	-2.48
464	154.7	323.3	IV	8	2	6.64	-1.63
					3	10.50	-3.64
					1	10.53	-2.79
465	157.7	326.3	IV	7	1	10.53	-2.79

Sample ID	Depth (cm)	Composite depth (cm)	Lithosome	Unit	Run	$\delta^{13}\text{C}$ (‰)	$\delta^{18}\text{O}$ (‰)
					2	9.22	-0.79
					3	15.33	-2.06
					4	13.11	-2.19
466	160.2	328.8	IV	7	1	7.53	-2.05
					2	9.92	-1.74
					3	10.75	-1.68
					4	10.75	-2.21
467	162.7	331.3	IV	7	1	15.26	-2.05
					2	11.72	-4.69
					3	11.24	-3.71
468	164.7	333.3	IV	7	1	12.53	-2.19
					2	11.32	-3.39
					3	11.91	-2.59
469	167.7	336.3	IV	7	2	11.55	-2.85
					3	10.08	-4.05
					4	11.30	-3.49
470	170.2	338.8	IV	7	1	13.92	-1.79
					2	11.22	-3.72
					3	12.23	-1.56
471	172.7	341.3	IV	7	1	13.01	-2.03
					2	4.92	-4.16
					3	11.40	-2.20
473	177.7	346.3	IV	7	1	4.81	-3.47
					2	3.79	-1.82
					3	2.30	-4.42
474	179.7	348.3	IV	7	1	9.62	-2.46
					2	4.31	0.87
					3	4.37	-1.35
					4	11.03	-0.50
475	182.7	351.3	IV	7	1	0.18	-4.16
					2	0.31	-1.85
					3	4.88	2.32
476	184.7	353.3	IV	7	1	3.01	-1.43
					2	3.00	-1.08
					3	0.82	-2.17
					4	2.72	-1.45
477	187.7	356.3	IV	7	1	2.39	-1.65
					2	1.02	-3.00
					3	1.04	-0.04

Sample ID	Depth (cm)	Composite depth (cm)	Lithosome	Unit	Run	$\delta^{13}\text{C}$ (‰)	$\delta^{18}\text{O}$ (‰)
					4	4.32	-3.51
					5	0.30	-3.40
478	189.7	358.3	IV	7	1	-1.29	-1.46
					2	1.24	0.76
					3	0.08	-4.21
479	192.7	361.3	IV	7	1	4.78	-2.87
					2	0.99	-2.88
					3	1.47	2.36
480	194.7	363.3	IV	7	1	1.22	0.69
					2	3.65	0.75
494	219.8	388.4	III	6	1	-0.37	-2.90
					2	0.13	-4.18
					3	-0.27	-3.81
495	222.5	397.5	III	6	1	-1.17	-3.66
					2	-1.85	-5.27
					3	-1.73	-5.07
496	225.0	400.0	III	6	1	-0.95	-4.78
					2	-0.49	-2.76
					3	1.43	-3.97
497	227.5	402.5	III	6	1	-0.91	-3.47
					2	-0.39	-3.15
					3	1.20	-4.28
498	229.4	404.4	III	6	1	1.34	-2.55
					2	-0.13	-4.15
					3	1.89	-1.21
499	232.2	407.2	III	6	1	1.80	-4.14
					2	2.20	-3.35
					3	2.58	-4.74
500	234.5	409.5	III	6	1	0.79	-3.40
					2	2.28	-3.46
					3	-1.54	-3.32
501	237.0	412.0	III	6	1	4.05	-2.78
					2	3.42	-5.66
					3	1.99	-4.43
502	238.9	413.9	III	6	1	4.47	-2.11
					3	1.82	-2.16
					4	4.54	-3.30
504	243.7	418.7	III	6	1	3.26	-3.78
					2	4.24	-2.72

Sample ID	Depth (cm)	Composite depth (cm)	Lithosome	Unit	Run	$\delta^{13}\text{C}$ (‰)	$\delta^{18}\text{O}$ (‰)
					3	3.84	-2.75
505	246.5	421.5	III	5	1	3.41	-2.88
					2	3.41	-4.01
					3	2.74	-4.48
506	248.4	423.4	III	5	1	2.92	-4.27
					2	3.42	-2.76
					3	4.16	-2.89
507	250.7	425.7	III	5	1	3.10	-4.46
					2	1.68	-3.25
					3	2.57	-3.22
509	255.1	430.1	III	5	1	2.60	-2.64
511	260.0	435.0	III	5	1	3.59	-1.09